

Fall 12-20-2019

The Vezo communities and fisheries of the coral reef ecosystem in the Bay of Ranobe, Madagascar

Shane Abeare
University of New Orleans, New Orleans, smabeare@gmail.com

Follow this and additional works at: <https://scholarworks.uno.edu/td>



Part of the [Aquaculture and Fisheries Commons](#), [Biodiversity Commons](#), [Marine Biology Commons](#), [Natural Resources and Conservation Commons](#), [Natural Resources Management and Policy Commons](#), and the [Oceanography Commons](#)

Recommended Citation

Abeare, Shane, "The Vezo communities and fisheries of the coral reef ecosystem in the Bay of Ranobe, Madagascar" (2019). *University of New Orleans Theses and Dissertations*. 2685.
<https://scholarworks.uno.edu/td/2685>

This Dissertation is protected by copyright and/or related rights. It has been brought to you by ScholarWorks@UNO with permission from the rights-holder(s). You are free to use this Dissertation in any way that is permitted by the copyright and related rights legislation that applies to your use. For other uses you need to obtain permission from the rights-holder(s) directly, unless additional rights are indicated by a Creative Commons license in the record and/or on the work itself.

This Dissertation has been accepted for inclusion in University of New Orleans Theses and Dissertations by an authorized administrator of ScholarWorks@UNO. For more information, please contact scholarworks@uno.edu.

The Vezo communities and fisheries of the coral reef ecosystem in the Bay of Ranobe,
Madagascar

A Dissertation

Submitted to the Graduate Faculty of the
University of New Orleans
in partial fulfillment of the
requirements for the degree of

Doctor of Philosophy
in
Engineering and Applied Science
Earth and Environmental Sciences

by

Shane M. Abeare

B.Sc. University of Michigan, USA, 1999
M.Sc. University of Pretoria, South Africa, 2004
M.Sc. Louisiana State University, USA, 2009

December, 2019

Acknowledgments

I would like to thank my advisor, Dr. Martin O'Connell, for his encouragement and support, the University of New Orleans Graduate School for the opportunity to pursue my interests in international conservation and fisheries management, and to my committee members, Drs. Eurico D'Sa, David Lyzenga, John McCorquodale, and Patrick Smith, for their thoughtful input. I would also like to recognize and express my appreciation for the financial and material support that I have received over the years from the University of New Orleans Graduate School, PADI Foundation, GeoEYE Foundation, and the ESRI Conservation Program.

A special thanks to the interns and volunteers of Reef Doctor for all the small contributions made by many to the data collection and data entry tasks, and also for all the great photos that were contributed to the archives over the years, particularly photos taken by Tanya Dodgen. Some of the unattributed photos used here in my dissertation were taken by people that passed through Ifaty over the last several years. In particular, I would like to thank some of the Reef Doctor staff that were involved in various aspects of my research, including Julien Floro and Emma Gibbons, and especially Pepin, François, and of course, Manjo.

A heartfelt-thanks to my family, especially, to my mother for her support, encouragement, and generosity in providing shelter in times of need. And lastly, to my wife, Christina, whose patience and support throughout the *many* years—from inception to conclusion—are what really have made it all possible.

Table of Contents

List of Figures	iv
List of Tables	xiii
Abstract	xvi
Part I. The Environment and the People: Communities of the Bay of Ranobe, Madagascar	
Chapter 1. Derivation of bathymetry and benthic habitat classification from multispectral satellite imagery	2
1.1 Introduction.....	2
1.2 Methodology	3
1.3 Results.....	43
1.4 Discussion	57
Works Cited	64
Appendix.....	72
Chapter 2. Vezo fishing communities: Small-area population estimates, demographics, and socioeconomics	88
2.1 Introduction.....	88
2.2 Methodology	100
2.3 Results & Discussion	112
Works Cited	128
Appendix.....	134
Part II. Artisanal Fisheries of the Vezo Communities of the Bay of Ranobe: Effort and catch dynamics	
Chapter 3. Vezo artisanal fisheries: fishing capacity, nominal effort, and spatio-temporal dynamics	137
3.1 Introduction.....	137
3.2 Methodology	147
3.3 Results.....	159
3.4 Discussion.....	184
Works cited	191
Appendix.....	198
Chapter 4. Vezo artisanal fisheries: Characterization of landings and economic valuation of the daytime, boat-based coral reef fisheries of the Bay of Ranobe	204
4.1 Introduction.....	204
4.2 Methodology	209
4.3 Results.....	215
4.4 Discussion.....	245
Works Cited	253
Appendix.....	260
Vita.....	292

List of Figures

Figure 1.1. a) Air temperature time series from on-site weather station for years 2011-2015; b) monthly means for all years combined; time series trends are Generalized Additive Model-smoothed with 95% confidence intervals 5

Figure 1.2. Monthly mean of on-site air temperature (red) for year 2014 compared to water temperature (blue) measured by HOBO pendant dataloggers at the Rose Garden Marine Reserve, Bay of Ranobe; time series trends are Generalized Additive Model-smoothed with 95% confidence intervals 6

Figure 1.3. Spiny forest floral species with village of Ifaty in background; dark haze over the village resembling smoke is actually a swarm of locusts 6

Figure 1.4. Bottom-right: Provinces of Madagascar with Toliara Province (shaded); Top-right magnified view of the coastline and the provincial capital, Toliara; Left: magnified view of the study area, Bay of Ranobe 7

Figure 1.5. World map of the dominance / intensity of the M2 tidal constituent; for areas where the white isolines converge, amphidromic points, little or no tide exists (Wikipedia image, https://en.wikipedia.org/wiki/Amphidromic_point) 9

Figure 1.6. Global Sea Level Observing System stations actively collecting data (GLOSS image, <https://www.psml.org>) 9

Figure 1.7. Manual collection of tide stage at the Port of Toliara (November 2012)..... 11

Figure 1.8. Comparison of tidal predictions for Toliara generated by WxTide32 (red line) and Mr. Tides (green line) software and observed tide levels (blue line) 11

Figure 1.9. Software-generated (Mr. Tides) tidal prediction fitted with 4th-order polynomial equation used to correct sonar data to LAT 13

Figure 1.10. IKONOS RGB image of the Bay of Ranobe, with sonar track point file overlay..... 14

Figure 1.11. Relationship of the coefficients of variation (CV) for recorded sonar depth and boat speed, with potential confounding effects of weather / sea state 16

Figure 1.12. IKONOS-2 and GEOEYE-1 images awarded by the GeoEye Foundation for full coverage of the Bay of Ranobe; image outlined in blue was selected for further research... 17

Figure 1.13. Workflow for the steps followed in the processing of the selected satellite image..... 18

Figure 1.14. Illustration from Jensen (2007) depicting the multiple potential pathways in which scattering and non-targeted reflectance, path radiance (L_P), may corrupt the signal received by the satellite sensor	23
Figure 1.15. Histogram of the IKONOS blue band image file calibrated to TOA radiance; right-shifting of histogram related to path radiance.....	23
Figure 1.16. IKONOS-2 image band files: (first row) a) red band, b) green band, and c) blue band with histogram equalization enhancement, (second row) d) identification of optically-deep region, and e) random sampling of the optically-deep region applied to all bands	27
Figure 1.17. Daily water vapor density (g/cm^2) measured on March 28-31, 2007 in Saint Denis, Reunion	30
Figure 1.18. Daily (top) and hourly (bottom) water vapor density (g/cm^2) measurements from March 2008 in Saint Denis, Reunion	31
Figure 1.19. Measurements of Aerosol Optical Depth (AOD), or Aerosol Optical Thickness (AOT), collected by MODIS (March 16, 2007) on southwest coast of Madagascar (top); AERONET measurement from March 28-31, 2007, Saint Denis, Reunion (bottom).....	33
Figure 1.20. RGB image of the Bay of Ranobe after water mask, clip, and spatial resampling.....	34
Figure 1.21. Beer-Lambert Law: Attenuation of incident light, I_0 , passing through a solution.....	36
Figure 1.22. Example of the log-transformed, $\text{DOS}_{1\%}$ -corrected RGB bands used as the independent variable in the statistical models	38
Figure 1.23. South pass in southern part of lagoon, with some of the sites targeted for benthic photo-quadrats marked with cross (+); examples of benthic habitat diversity: (clockwise) dense seagrass (<i>Thalassodendron ciliatum</i>), moderate density seagrass (<i>T. ciliatum</i>), coral thicket (<i>Acropora spp.</i>), and <i>Sargassum spp</i>	41
Figure 1.24. Aerial view of the Rose Garden marine reserve (top) – a patch reef dominated by the rose-like coral of the genus, <i>Montipora</i> ; located near sampling point #2 on the map in Figure 1.23.....	42
Figure 1.25. Regression term plots for the RGB DOS -corrected bands (top 3 plots) and RGB 6SV -corrected bands (bottom 3 plots)	45
Figure 1.26. Partial residual plots of the multiple linear regression model fitted with $\text{DOS}_{1\%}$ data; loess fit (pink line) and linear fit (dashed blue line)	46

Figure 1.27. Partial residual plots of the multiple linear regression model fitted with 6SV data; loess fit (pink line) and linear fit (dashed blue line)	47
Figure 1.28. Gradient boosting algorithm model-fitting process: iterative minimization of the loss function, residual deviance, as regression trees are added to the existing model; green line indicates the final number of trees (n = 1850), given model parameters (tree complexity = 1, learning rate = 0.1)	48
Figure 1.29. Visualization of relative influence scores	49
Figure 1.30. Functional relationships of the gradient boosting model fitted to log-transformed, DOS _{1%} data for each band: blue (top), green (middle) and red (bottom)	50
Figure 1.31. Functional relationships of the gradient boosting model fitted to log-transformed, 6SV data for each band: blue (top), green (middle) and red (bottom)	51
Figure 1.32. Model residuals plotted against water depth to illustrate biases resulting from each model type, MLR (top) versus GBM (bottom), particularly at depth extremes	53
Figure 1.33. Term plots of the final gradient boosting model for each model term: blue, green, and red (clockwise)	55
Figure 1.34. GBM final model residuals versus depth	56
Figure 1.35. Bathymetric map product created from the prediction of the final gradient boosting model	56
Figure 1.36. Benthic habitat classification for the Bay of Ranobe, with classes including: macroalgae, seagrass / macroalgae, seagrass, sand / silt, and sand (top); geomorphological zones of the Bay (bottom-left); example of cluster-busting classification of the intertidal zone	58
Figure 2.1. GDP per capita: Madagascar compared to other African countries: Ivory Coast (<i>Cote d'Ivoire</i>), Burkina Faso, Cameroon (<i>Cameroun</i>), Benin, and Sub-Saharan Africa (<i>Afrique subsaharienne</i>) as a whole (Source: Razafindrakoto <i>et al.</i> , 2017)	89
Figure 2.2. Percentage of population living in extreme poverty by country (Source: https://ourworldindata.org/extreme-poverty)	91
Figure 2.3. Madagascar administrative boundaries used for the aggregation of census data: province (<i>Faritany</i>), district (<i>Fivondronas</i>), and commune (<i>Firaisanas</i>) (Mistiaen <i>et al.</i> , 2002)	92
Figure 2.4. Madagascar human population distribution map at 100 m resolution (WorldPop, 2017)	95

Figure 2.5. IKONOS panchromatic image illustrates the fishing village of Ifaty (yellow polygon) separated by an area of salt flats from the herding village of Tsivinoe (red circle), with the outlying areas of land-use / deforestation	96
Figure 2.6. IKONOS high-resolution panchromatic image used to illustrate resolution required to conduct dwelling unit enumeration; inset demonstrates the typical resolution of LandSat products (30 m) and the loss of discernibility of dwelling units at reduced resolution	97
Figure 2.7. Photo illustrates roofing material and sized of typical village-style houses	97
Figure 2.8. a) The 21 villages of the Bay of Ranobe community (red circles, left); b) the 12 coastal Vezo villages (yellow polygons, right) and mangroves at the north-south extremes fo the Bay (green polygon)	102
Figure 2.9. a) 1-km buffer region created as boundary on landward side of the shore; b) 100 m grid divided into sections for export to Google Earth.....	104
Figure 2.10. 100-m grid shapefile imported into Google Earth, labeled with unique numbering system for individual grid cells, corresponding to dwelling-unit count (top); close-up view demonstrates clarity of image and resolution; note, individual boats, pirogues, visible on beach (bottom).....	105
Figure 2.11. Spatial distribution of household surveys conducted (red circles) in the villages of Ifaty, Mangily, Amboaboaka, Betsibaroka, Ambolomailaka, and Fitsitke, south to north	109
Figure 2.12. Village landing zones (LZ) divided into sub-zones (green, orange, and red) for surveying purposes: a) Andrevo (LZ = 785m), b) Ambolomailaka (LZ= 500m), c) Ifaty (LZ= 620m), and d) Beravy (LZ= 1025m)	111
Figure 2.13. Population distribution within 1 km of shore per 100 m grid cell; map legend symbology based on deciles of population count per grid cell.....	113
Figure 2.14. Number of dwelling units per 100 m grid cell (10,000 m ²) within 1 km of the coast for years 2004 (left) and 2016 (right)	118
Figure 2.15. Spatial representation of percent change in dwelling unit counts for the 3 time periods, T ₁ -T ₃ , studied here: 2004-2009, 2009-2012, 2012-2016	119
Figure 2.16. Short-lived periods of economic growth in Madagascar, GDP per capita (black line, primary y-axis), interrupted by political crises (<i>crise politique</i>), including the political crisis that occurred during the present study, 2009 – 2013; GDP growth rate (gray line, secondary y-axis (%)) (Source: Razafindrakoto <i>et al.</i> , 2017).....	122
Figure 3.1. Early movement of peoples from the Austronesian region to Madagascar (image reproduced from Chambers, 2001)	143

Figure 3.2. Drawing of the Vezo pirogue (image reproduced from Astuti, 1991)	143
Figure 3.3. Stages of construction of the Vezo pirogue (a-b); the apprenticeship of young Vezo boys, acquiring boating and navigation skills (c-e)	145
Figure 3.4. Women (n=13) collecting marine resources, intertidal gleaning	146
Figure 3.5. Fishermen returning with the day's catch, with collection and marketing activities commencing immediately upon landing	146
Figure 3.6. Village landing zones (LZ) divided into sub-zones (green, orange, and red) for surveying purposes: a) Andrevo (LZ = 785m), b) Ambolomailaka (LZ= 500m), c) Ifaty (LZ= 620m), and d) Beravy (LZ= 1025m)	152
Figure 3.7. Inactive pirogues on the beach mid-morning, latent capacity	153
Figure 3.8. A view of fishermen returning to shore in a loosely coordinated manner	153
Figure 3.9. Commonly-used fishing gears by the Vezo of the Bay of Ranobe: gillnets (a-b), harpoons (c), spearguns (d), small mesh nets / mosquito netting (e-f)	155
Figure 3.10. Aerial view of typical beach seine hauling operation in the BoR; mosquito net paneling often inserted into wings and/or cod-end	156
Figure 3.11. IKONOS image mosaic (black / white) with 500 m sampling grid overlay and the location of villages targeted for fisheries surveys (green polygon); insets illustrate the resolution of the IKONOS image (red border) and location (red square) and that for the Google Earth image (blue border) and the location within the BoR (blue square); note, image resolution allows for distinction of pirogue hull and smaller outrigger float	158
Figure 3.12. Smoothed histograms, or density profiles, of pirogue length data collected from the four targeted villages during Pirogue Registration campaign.....	161
Figure 3.13. Boxplots of the of pirogue length data collected from the four targeted villages during Pirogue Registration campaign; mean pirogue length for the village of Ambolomailaka is significantly different from the other villages	161
Figure 3.14. Generalized density profile for pirogue lengths of all pirogues recorded in the Pirogue Registration from the villages of Andrevo, Ambolomailaka, Ifaty, and Beravy ...	163
Figure 3.15. Regression plot of observed number of people versus pirogue length with fitted regression line, confidence interval (blue) and prediction interval (red dash) (top); Component plus residual plot with linear fit (dashed blue) and smooth fit (magenta)	165
Figure 3.16. Gear usage profiles: a) for all villages combined, b) Andrevo, c) Ambolomailaka, d) Ifaty, and e) Beravy (BS= boat seine, GN= gillnet, GN/MN= gillnet modified w/ mosquito net, HA= harpoon, HL= hook-line, MN= mosquito net, and SG= speargun)	168

Figure 3.17. Boxplot of pirogue length by gear type.....	170
Figure 3.18. Plot of scaled regression coefficients with 95% confidence intervals, indicating relative pirogue lengths associated with gear usage from shorter to longer pirogues (left to right).....	170
Figure 3.19. Daily average wind speeds color coded by year (\pm standard error in gray), with vertical lines representing the period covered by the fisheries catch and effort surveys (solid black) and the daily pirogue count survey (dashed black).....	172
Figure 3.20. Monthly averaged wind speeds (kph \pm se) for the morning and afternoon hours.....	172
Figure 3.21. Circular histogram of wind speed (m s^{-1}) according to wind direction Counts	173
Figure 3.22. Circular histogram for the departure (left) and return (right) times of fishermen recorded in the Fishing Effort dataset.....	173
Figure 3.23. Average monthly time (hours) spent fishing (blue line) \pm standard error (gray) as compared to monthly average wind speeds (kph; black line) \pm standard error (gray)	175
Figure 3.24. Component plus residual plot for the fitted GLM fishing time \sim wind speed) with linear fit (blue dash line) and smooth fit (magenta line) for comparison purposes	177
Figure 3.25. Changes in pirogue activity, percentage-use, relative to wind speed per targeted village.....	178
Figure 3.26. Monthly variations in pirogue activity, percentage of pirogues in-use, relative to the monthly changes in wind speed	180
Figure 3.27. Time-lagged model: GAM fit (red line) with 95% confidence intervals (blue dash) and model residuals (adjusted $R^2 = 0.0365$, deviance explained = 4.53%); rug plot – marks on axes indicate observed data values	181
Figure 3.28. Same-day model: GAM fit (red line) with 95% confidence intervals (blue dash) and model residuals (adjusted $R^2 = 0.109$, deviance explained = 12.7%); rug plot – marks on axes indicate observed data values.....	181
Figure 3.29. Spatial distribution of fishing effort based on the enumeration of pirogues at 500 m grid sampling resolution; colored grid cells indicate extent of image and intensity of effort for images from multiple dates and platforms: (left to right) IKONOS Pan image captured 16 March 2007 and Google Earth images from 17 February 2016, 8 March 2016, and 3 June 2018.....	185

Figure 3.30. Spatial distribution of fishing effort (pirogue-meters km ⁻²) within the Bay of Ranobe interpolated using the natural neighbor at 100m resolution, with villages indicated by orange-red polygons and arrows indicating the north-south passes (left); Voroni map representations of data: mean, median, and mode (right)	186
Figure 4.1. Village landing zones (LZ) divided into sub-zones (green, orange, and red) for surveying purposes: a) Andrevo (LZ = 785m), b) Ambolomailaka (LZ= 500m), c) Ifaty (LZ= 620m), and d) Beravy (LZ= 1025m)	214
Figure 4.2. Commonly-used fishing gears by the Vezo of the Bay of Ranobe: gillnets (a-b), harpoons (c), spearguns (d), small mesh nets / mosquito netting used in boat seining (e-f)	216
Figure 4.3. Landings time-series for the 4 most abundant fisheries groups: finfish, octopus, sea cucumber, and unknown, representing 91.9% of landings by weight	217
Figure 4.4. Relative abundance as a percentage of total surveyed finfish landings (24,426 kg) of the 50 most abundant groups ranked in descending order by a) family and b) species.....	219
Figure 4.5. Frequency of occurrence in daily landings: 50 most frequently occurring species in landing 296 sampling days.....	220
Figure 4.6. Relative abundance of species in landings w.r.t. village, with percentages calculated as a function of total landings per village: Ambolomailaka (8,161 kg), Andrevo (6,217 kg), Ifaty (5,237 kg), and Beravy (4,811 kg).....	221
Figure 4.7. Relative abundance as a percentage of total surveyed finfish landings (24,426 kg) of the 20 most abundant groups ranked in descending order by (a) northern and (b) southern villages; (c) of the 20 most abundant species in northern/southern, the relative abundance of the 10 species with overlapping distributions.....	222
Figure 4.8. Monthly average nCPUE for finfish (\pm se)	224
Figure 4.9. Comparison of log(nCPUE) values for villages of the north versus south	224
Figure 4.10. Pair-wise comparisons of log(nCPUE) between gear types; significant differences indicated by global ANOVA ($p < 0.001$) and between gear-type groups	226
Figure 4.11. Average monthly nCPUE by gear type	226
Figure 4.12. GLM regression coefficients from CPUE standardization models (Table 4.3) for species 1-5.....	230
Figure 4.13. GLM regression coefficients from CPUE standardization models (Table 4.3) for species 6-10.....	231

Figure 4.14. Species profile – *Siganus sutor*: image, total landings by month (top row), standardized CPUE year-index (gillnet), length frequency histogram (middle row), changes in average length over study period, and length by gear type (bottom row); length-at maturity, L_m = unknown, L_{max} = 45.0 cm SL (Froese and Pauly, 2019; FishBase)..... 232

Figure 4.15. Species profile – *Herklotsichthys quadrimaculatus*: image, total landings by month (top row), standardized CPUE year-index (gillnet), length frequency histogram (middle row), changes in average length over study period, and length by gear type (bottom row); L_m = 10.1 cm, L_{max} = 25.0 cm SL (Froese and Pauly, 2019; FishBase)..... 233

Figure 4.16. Clupeidae spp: Silver-stripe round herring, *Spratelloides gracilis* (middle row), and the Goldstripe sardinella, *Sardinella gibbosa* (bottom row); length-based analyses not performed due to insufficient data (grid squares = 10 cm) 234

Figure 4.17. Species profile – *Plotosus lineatus*: image, total landings by month (top row), standardized CPUE year-index (gillnet), length frequency histogram (middle row), changes in average length over study period, and length by gear type (bottom row); L_m = 14.0 cm, L_{max} = 32.0 cm TL (Froese and Pauly, 2019; FishBase)..... 235

Figure 4.18. Species profile – *Leptoscarus vaigiensis*: image, total landings by month (top row), standardized CPUE year-index (gillnet), length frequency histogram (middle row), changes in average length over study period, and length by gear type (bottom row); L_m = unknown, L_{max} = 35.0 cm TL (Froese and Pauly, 2019; FishBase)..... 236

Figure 4.19. Species profile – *Lethrinus harak*: image, total landings by month (top row), standardized CPUE year-index (gillnet), CPUE year-index (hook-line), length frequency histogram (middle row), changes in average length over study period, and length by gear type (bottom row); L_m = 19.5, L_{max} = 50.0 cm TL (Froese and Pauly, 2019; FishBase) 237

Figure 4.20. Species profile – *Caesio caerulea*: image, total landings by month (top row), standardized CPUE year-index (gillnet), length frequency histogram (middle row), changes in average length over study period, and length by gear type (bottom row); L_m = unknown, L_{max} = 35.0 cm TL (Froese and Pauly, 2019; FishBase)..... 238

Figure 4.21. Species profile – *Ostorhinchus cyanosoma*: image, total landings by month (top row), standardized CPUE year-index (gillnet), length frequency histogram (middle row), changes in average length over study period, and length by gear type (bottom row); L_m = unknown, L_{max} = 8.0 cm TL (Froese and Pauly, 2019; FishBase)..... 239

Figure 4.22. Species profile – *Scarus ghobban*: image, total landings by month (top row), standardized CPUE year-index (gillnet), length frequency histogram (middle row), changes in average length over study period, and length by gear type (bottom row); L_m = unknown, L_{max} = 75.0 cm TL (Froese and Pauly, 2019; FishBase)..... 240

Figure 4.23. Species profile – *Gerres longirostris*: image, total landings by month (top row), standardized CPUE year-index (gillnet), length frequency histogram (middle row), changes in average length over study period, and length by gear type (bottom row); $L_m = 20.6$ cm, $L_{max} = 44.5$ cm TL (Froese and Pauly, 2019; FishBase)..... 241

Figure 4.24. Distribution of coastal fishers; data collected by the Ministry of Fisheries (2011), *Ministère de la Pêche et des Ressources Halieutiques*; graphic reproduced from Le Manach *et al.* (2013b)..... 252

List of Tables

Table 1.1. Details of the satellite images used in the present study.....	16
Table 1.2. IKONOS-2 band description	17
Table 1.3. IKONOS Band-dependent Parameters	21
Table 1.4. Earth-Sun distance in Astronomical Units per Julian Day	21
Table 1.5. Calculated values for the parameters of the atmospheric correction	28
Table 1.6. 6SV Standard Atmospheric Models	29
Table 1.7. 6SV Standard Aerosol Models	29
Table 1.8. MLR-DOS regression results.....	44
Table 1.9. Relative influence scores for the gradient boosting models fitted to the 2 Datasets	49
Table 1.10. Comparison of relative influence scores for the final GBM, tree complexity=2, versus the scores for the GBM with tree complexity=1	55
Table 2.1. Details of the panchromatic images (Pan) used in the present study.....	104
Table 2.2. Selected image dates for each of the 12 Vezo villages.....	107
Table 2.3. Fractional year, Y , per time-step and village	107
Table 2.4. Population estimates per village based on projections of a global average population growth rate of 2.78% (2007 and 2016), values used by the government of Madagascar, and population estimates based on dwelling unit counts for 2004 and 2016	115
Table 2.5. Percent change in dwelling unit count for 3 time periods, T_1 - T_3 , spanning years 2004 – 2016.....	120
Table 2.6. Average ages and family size of fishermen per village	123
Table 2.7. Counts and percentages of fishing daytrip outcomes, kept versus sold, per village.....	125
Table 2.8. CPUE, total and average weights, and average sales prices of catch per village.....	125

Table 2.9. Species identified in the catch ranked by economic value in local currency, Malagasy Ariary (MGA)	126
Table 3.1. Total number of pirogues per the 12 villages of the Bay of Ranobe collected during the Annual Pirogue Count in 2013 and 2015, with targeted villages shaded	162
Table 3.2. Summary of pirogue lengths and counts per targeted village: counts of pirogues registered, and pirogue counts from census, Annual Pirogue Count 2013, and percent coverage of registration	163
Table 3.3. Pirogue counts for the 12 villages of the Bay of Ranobe, with total length in meters	164
Table 3.4. Results of simple linear regression of number of fishermen and pirogue length.....	164
Table 3.5. Pirogue counts, population estimates from 2013, and regression predictions of number of fishermen based on pirogue-length profiles, as percentage of total population per Village.....	167
Table 3.6. Summary of GLM results for model pirogue length ~ gear type	170
Table 3.7. Average daily time spent fishing per targeted village	174
Table 3.8. Average monthly time spent fishing for the four targeted villages combined...	175
Table 3.9. Summary of GLM results for the model: fishing time (hr) ~ wind speed (kph), with the same-day wind speeds (Date model) and wind speeds from the previous day (Date-1 model)	177
Table 3.10. Average activity, measured as percentage of pirogue-use, per targeted Village.....	178
Table 3.11. Monthly average activity, or pirogue-use, with data from all four targeted villages combined.....	180
Table 3.12. Percent change in village fleets from 2013-2015 from Annual Pirogue Count dataset, with villages ordered from north to south.....	183
Table 4.1. Landings by fisheries categories by total weight and percent	217
Table 4.2. Average nCPUE by village and by region, northern versus southern villages	224
Table 4.3. Average nCPUE per gear type and percentage of surveys reporting gear-type	225

Table 4.4. GLM results for the standardization of log(CPUE) for the 10 most abundant Species 228

Table 4.5. Expansion of surveyed landings to lagoon-wide estimates of annual yield per fisheries class..... 243

Table 4.6. Economic valuation of expanded landings per fisheries class..... 244

Table 4.7. Landings (tonnes year⁻¹) and value (USD year⁻¹) of fisheries products per village and per fishermen (USD day⁻¹)..... 245

Abstract

Madagascar, a country whose extraordinary levels of endemism and biodiversity are celebrated globally by scientists and laymen alike, yet historically has received surprisingly little research attention, is the setting of the present dissertation. Here, I contribute to the need for applied research by: 1) focusing on the most intensely fished section of the Toliara Barrier Reef, the Bay of Ranobe; 2) characterizing the marine environment, the human population, and the fisheries; and 3) collecting the longest known time-series of data on fisheries of Madagascar, thereby providing a useful baseline for future analyses. In Chapter 1, the bathymetry of the Bay was characterized following a unique application of the boosted regression tree classifier to the RGB bands of IKONOS imagery. Derivation of water depths, based on DOS-corrected images, following a generic, log-transformed multiple linear regression approach produced a predictive accuracy of 1.28 m, whereas model fitting performed using the boosted regression tree classifier, allowing for interaction effects (tree complexity= 2), provided increased accuracy (RMSE= 1.01 m). Estimates of human population abundance, distribution, and dynamics were obtained following a dwelling-unit enumeration approach, using IKONOS Panchromatic and Google Earth images. Results indicated, in 2016, 31,850 people lived within 1 km of the shore, and 28,046 people lived within the 12 coastal villages of the Bay. Localized population growth rates within the villages, where birth rates and migration are combined, ranged from 2.96% - 6.83%, greatly exceeding official estimates of 2.78%. Annual pirogue counts demonstrated a shift in fishing effort from south to the north. Gear and boat (*pirogue*) profiles were developed, and the theoretical maximum number of fishermen predicted ($n= 4,820$), in 2013, from a regression model based on pirogue lengths ($R^2= 0.49$). Spatial fishing effort distribution was mapped following a satellite-based enumeration of fishers-at-sea, resulting in a bay-wide estimate of intensity equaling 33.3 pirogue-meters km^{-2} . Landings and CPUE were characterized, with respect to finfish, by family, species, gear, and village. Expansion of landings to bay-wide fisheries yields indicated 1,885.8 mt year^{-1} of mixed fisheries productivity, with an estimated wholesale value of 1.64 million USD per annum.

Keywords: Madagascar, Bay of Ranobe, Coral reef fisheries, Fisheries productivity, Economic valuation, Remote sensing, Multispectral, Water depth, Bathymetry, Human population estimation

PART I

The Environment and the People:

Communities of the Bay of Ranobe, Madagascar



Caption: Young spear-fishermen with rabbitfish (top); village meeting (bottom); satellite image of the Southwest Coast of Madagascar and Toliara Barrier Reef Complex (right)

Derivation of bathymetry and benthic habitat classification from multispectral satellite imagery

1.1 Introduction

Advances in spatial visualization and analysis technologies, such as geographic information systems software (GIS), spatial statistics and the growing availability of remotely sensed data, have allowed for the characterization of large expanses of the globe with comparatively little effort. In many parts of the world, where ecological research is nearly non-existent, satellite archival imagery may be the only reliable historical datasets available. Use of spatial data in the fields of fisheries ecology and management is increasing, leading to improved accuracies in model predictions and giving birth to a new field, spatial fisheries ecology and management (Costello *et al.*, 2010; Lorenzen, 2010). Low-resolution, basin-wide satellite data products have been routinely used by fisheries oceanographers for several decades (Santos, 2000), for example: bathymetry (Bigelow, 1999), hydrodynamics (Klemas, 2009), sea-surface temperature (Wentz *et al.*, 2000), and primary productivity (Behrenfeld *et al.*, 2001; Beman *et al.*, 2005). However, in more recent years, high spatial- or spectral-resolution satellite imagery (*e.g.*, IKONOS, Sentinel-2, and WorldView 2-3 imagery) has proven to be useful in deriving bathymetry (Lyzenga, 1978; Strumpf and Holderied, 2003; Mishra *et al.*, 2004) and benthic habitat information for coral reef ecosystems, where clear, shallow water conditions often prevail (Lyzenga, 1981; Andrefouet *et al.*, 2003; Mumby and Edwards, 2002; Mumby *et al.*, 2004; Hedley *et al.*, 2012; Halls and Costin, 2016; Eugenio *et al.*, 2017, Colin *et al.*, 2017; Traganos and Reinartz, 2018; Traganos *et al.*, 2018). Products derived from high-resolution data sources allow for analyses to be conducted at finer scales, making these techniques much more amenable

to coral reef ecosystem studies and management applications, for example, in studies of habitat-use (Chassot, *et al.*, 2011 and references therein) and predictive modeling of species or habitats (*e.g.*, Pittman *et al.*, 2007; Walker, 2008; Pittman *et al.*, 2009; Knudby *et al.*, 2010; Yates *et al.*, 2016; Rees *et al.*, 2018; Roelfsema *et al.*, 2018).

Given the close species-habitat associations that exist in coral reef ecosystems, a prerequisite to any study in this environment is a firm understanding of local bathymetry (Beger and Possingham, 2008; Richards *et al.*, 2012) and the state, extent, and complexity of the benthic habitats (Pittman *et al.*, 2007; Walker, 2008; Pittman *et al.*, 2009; Knudby *et al.*, 2010). This information may then form the basis of any ecological survey design and sampling protocols.

In this chapter of my dissertation, the foundations are laid for present and future research into the coral reef ecosystem and fisheries of the Bay of Ranobe. Given the paucity of marine research in the region, it was necessary to begin with the quantification of some of the most basic metrics in nature, namely the weather and tides. From there, basic bathymetric and benthic habitat mapping products were created that are used in the chapters that follow, and that may be useful for future research.

1.2 Methodology

Study site

Unlike most tropical coral reef ecosystems in the world, the climate along the coast of the Toliara Barrier Reef Complex is semi-arid, with average annual rainfall of ca. 417 mm, falling over 43 days of the year. Mountains and plateaus along the tropical east side of the country capture most of the rain, creating a rain shadow that falls on the western and southern provinces. The austral summer of the Toliara region may be characterized by cloudless skies and scorching

sun for most months, with the likelihood of rain increasing during cyclone season, December - February. As winter approaches, the heat gives way to strong winds and highly- fluctuating daytime-nighttime air temperatures. On-site air temperature and weather data were collected throughout the study period, 2011-2015 (min = 10.1 °C, max = 39.3 °C, \bar{x} = 25.4 °C) (Figure 1.1a-b), while water temperature was monitored periodically, using HOBO pendant water temperature dataloggers, at selected sites (Figure 1.2).

In spite of the relatively harsh terrestrial environment, the Toliara region is home to the unique Spiny Forests of Madagascar, where 95% of the floral species are endemic (photos, Figure 1.3). Similarly, in the marine environment exists one of largest and least-known barrier reef systems, the Toliara Barrier Reef Complex, persisting at the southern extreme of the global coral reef distribution, bisected by the Tropic of Capricorn just 30 kms south of the study site, the Bay of Ranobe.

The Bay of Ranobe (23°05'S, 43°33'E) is a coastal lagoon situated along the southwestern coast of Madagascar, approximately 20 km northwest of the provincial capital city, Toliara. The Bay of Ranobe region may be geographically defined by the Manombo River and Fiherenana River that form the northern and southern borders, respectively. The lagoon system extends *ca.* 32 km along its southeast-northwest axis, measures *ca.* 8 km at the widest point, covering *ca.* 163 km² with maximum depths approaching 12 m within the lagoon. The lagoon experiences a semi-diurnal tidal regime with a spring tidal range of ± 2.3 m. The system is characterized by an inner reef flat composed of: patch reefs, sand, seagrass, macro-algae, and mangrove habitats, with a barrier reef forming the seaward boundary. The 32 km section of barrier reef that delimits the lagoon from the Mozambique Channel forms part of the greater Toliara Barrier Reef complex. Two reef passes divide the lagoon into three zones (Figure 1.4).

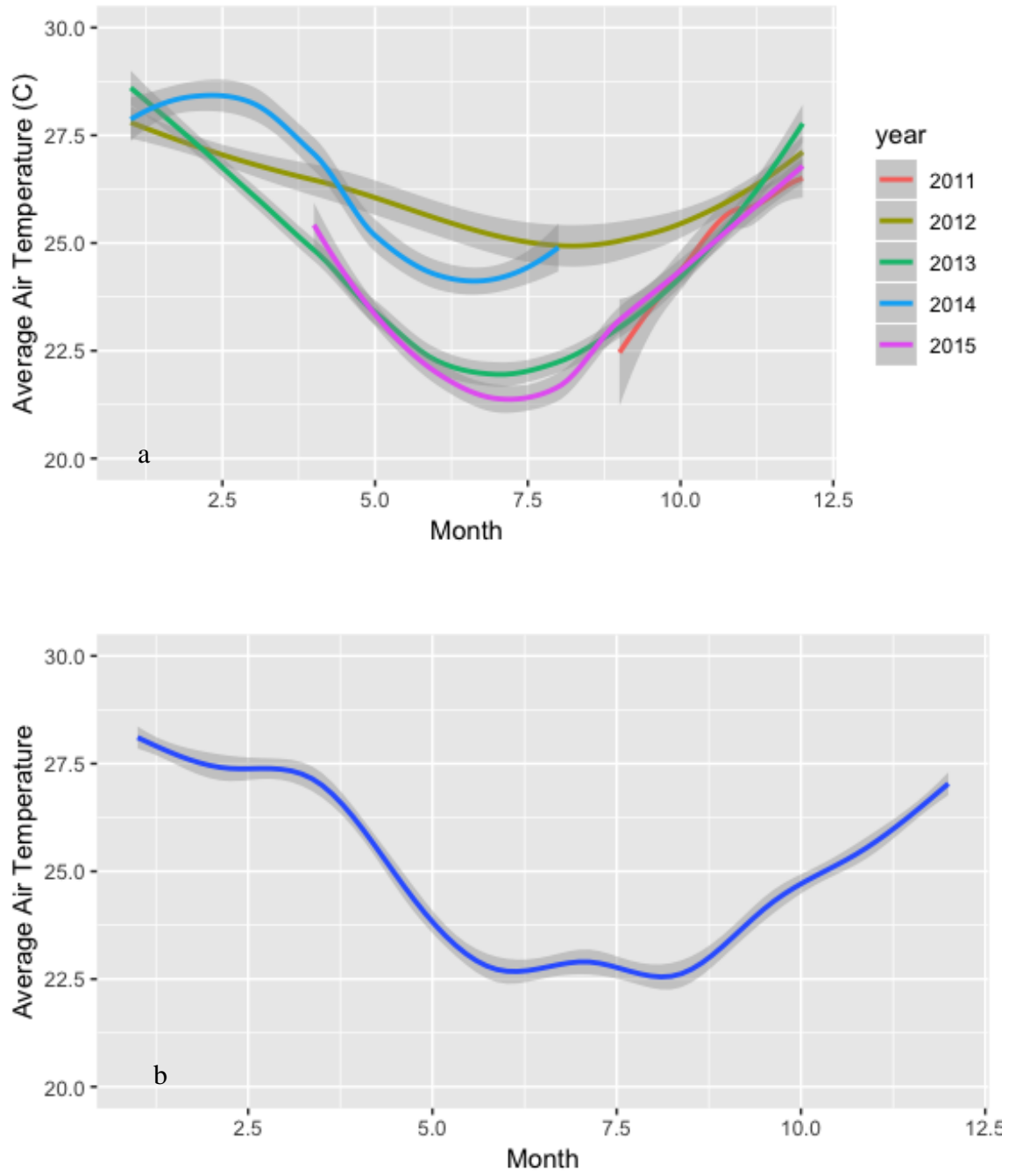


Figure 1.1. a) Air temperature time series from on-site weather station for years 2011-2015; b) monthly means for all years combined; time series trends are Generalized Additive Model-smoothed with 95% confidence intervals.

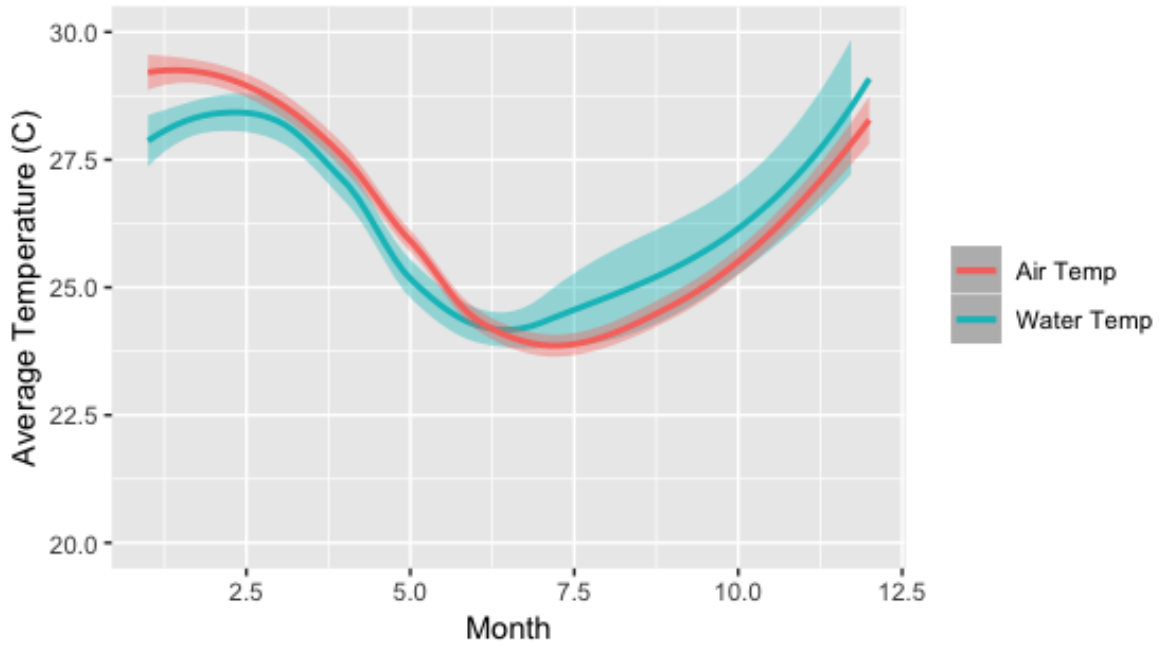


Figure 1.2. Monthly mean of on-site air temperature (red) for year 2014 compared to water temperature (blue) measured by HOBO pendant dataloggers at the Rose Garden Marine Reserve, Bay of Ranobe; time series trends are Generalized Additive Model-smoothed with 95% confidence intervals.



Figure 1.3. Spiny forest floral species with village of Ifaty in background; dark haze over the village resembling smoke is actually a swarm of locusts

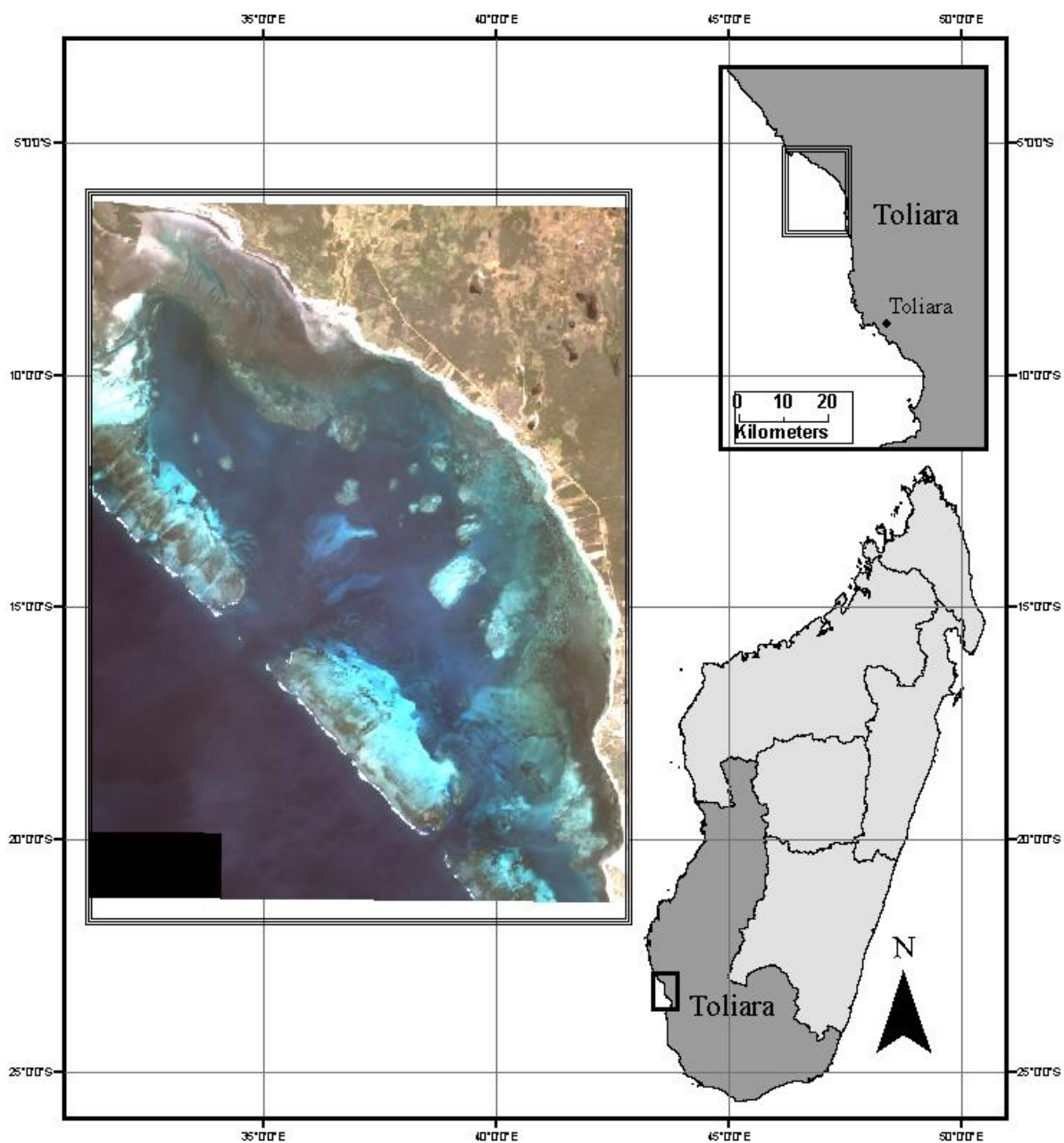


Figure 1.4. Bottom-right: Provinces of Madagascar with Toliara Province (shaded); Top-right magnified view of the coastline and the provincial capital, Toliara; Left: magnified view of the study area, Bay of Ranobe

Sonar data processing

Tidal correction

Tides are the harmonic expression of multiple constituent forces acting and interacting on seawater, including: astronomical, radiational, and geologic / topographic. For semi-diurnal tides, such as those expressed at the location of the present study, the principle harmonic constituents include: M_2 , the principal lunar semidiurnal constituent; S_2 , the principal solar semidiurnal constituent; and N_2 , the larger lunar elliptic semidiurnal constituent. Amongst these harmonic tidal constituents, the principal lunar semidiurnal constituent, M_2 , is the dominant constituent force. A global map of the expression of the M_2 tidal constituent, in terms of tidal range (Figure 1.5), indicates areas of the greatest tidal range (red area), while the white isolines converge on the areas of lowest tidal range (blue area), known as the amphidromic points. As can be seen in Figure 1.5, the coasts of Madagascar present a complex tidal environment, with extreme highs and lows occurring along its shores. Despite the tidal complexity surrounding this island nation, there are few functioning tide stations from which reliable tidal data may be obtained, with no tide stations operating within the region of the present study location (Figure 1.6; Map of the Global Sea Level Observing System, GLOSS).

In order to standardize depth data collected using sonar, which in turn will be used to create a bathymetric map of the study area, a tidal correction must be applied to the sonar data. After applying the tidal correction, depths standardized to a specific tidal datum may be achieved. Open-source tidal prediction software allow for the determination of tidal states at locations around the world, for example, WxTides32 and Mr. Tides for Windows and Mac operating systems, respectively. Tidal predictions generated by the software are based on “reference stations”, where functioning tide gauges exist. In the case of WxTides32, the

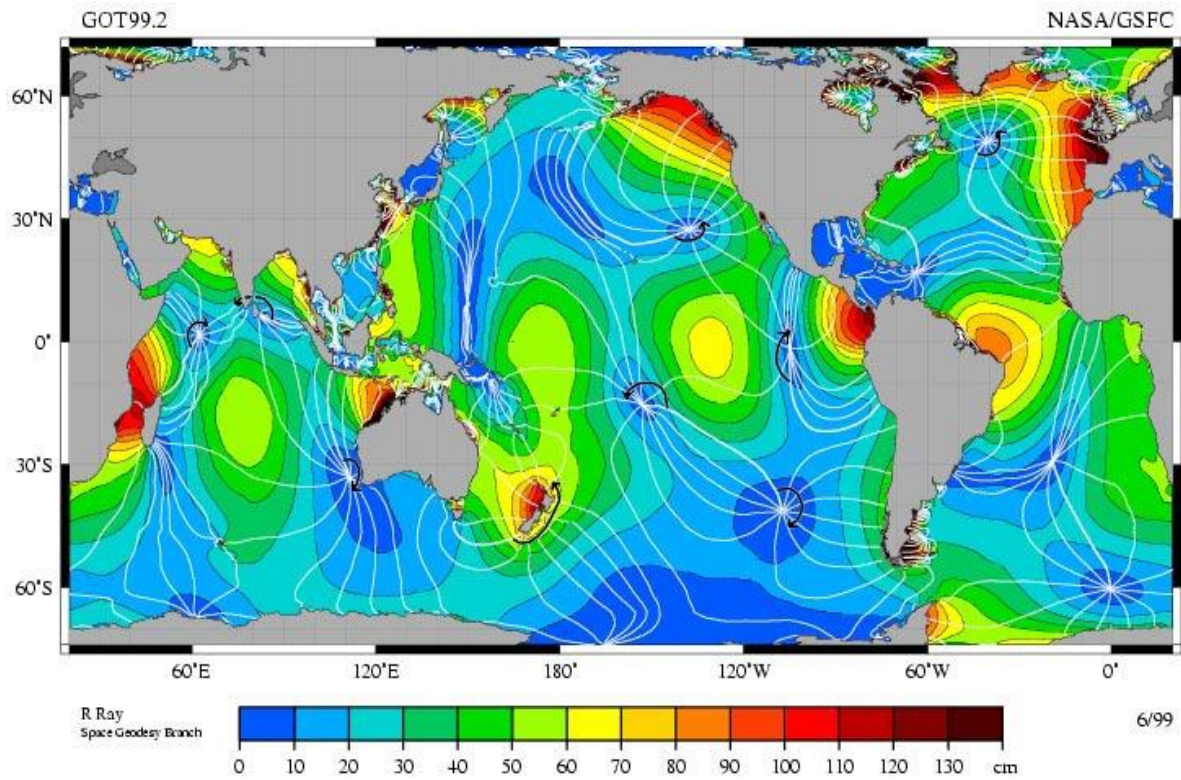


Figure 1.5. World map of the dominance / intensity of the M2 tidal constituent; for areas where the white isolines converge, amphidromic points, little or no tide exists (NASA – Goddard Space Flight Center, NASA-Jet Propulsion Laboratory, and Scientific Visualization Studio; <https://svs.gsfc.nasa.gov>)

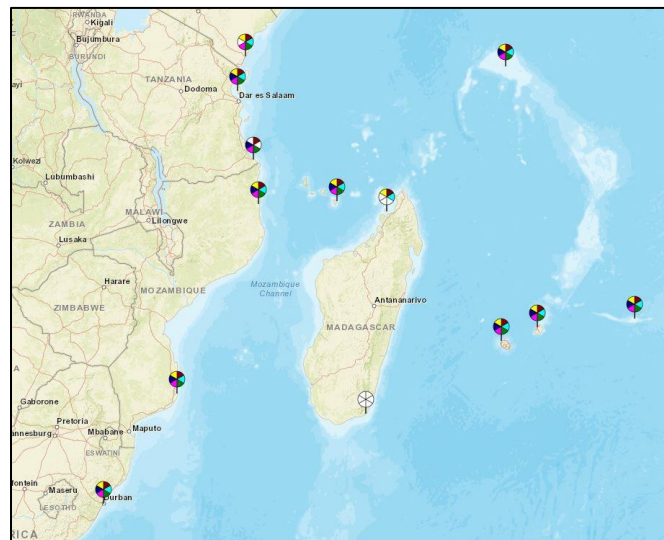


Figure 1.6. Global Sea Level Observing System stations actively collecting data (GLOSS image, <https://www.psmi.org>)

reference tidal station is in Dar es Salaam, Tanzania. “Subordinate stations” are locations where reliable historic tidal data have once been collected, where the data are then used to develop algorithms that allow for tidal predictions from the reference to subordinate location(s). In the case of WxTides32, the algorithm used is:

Dar Es Salaam, Tanzania + Corrections: High (+0:46 *0.77 +3.00) Low (+0:50 *0.77 +3.00)

To compare the accuracy of the WxTides32 and Mr. Tides tidal prediction algorithms, tidal data were collected manually at the Port of Toliara every 10 minutes from sunrise to sunset for 7 consecutive days, November 9-15, 2012 (Figure 1.7). A comparison of observed versus predicted tidal stages indicated the accuracy of the algorithms (Figure 1.8). While both algorithms appear to be in-phase with the observed waveform, the predicted amplitudes of the wave functions predicted by the Mr. Tides algorithm were clearly more accurate. Consequently, Mr. Tides tidal predictions were used for the correction of sonar survey data. Tidal predictions generated by Mr. Tides are based on the Lowest Astronomical Tide (LAT) tidal datum. Thus, corrections made to the recorded sonar depths, and the resultant bathymetric mapping products, adopted the LAT datum as reference (See Appendix 1.1 for a comparison of common tidal datums). The LAT is defined as:

...the lowest tide level which can be predicted to occur under average meteorological conditions and under any combination of astronomical conditions. (I.H.O., 2016)



Figure 1.7. Manual collection of tide stage at the Port of Toliara (November 2012)

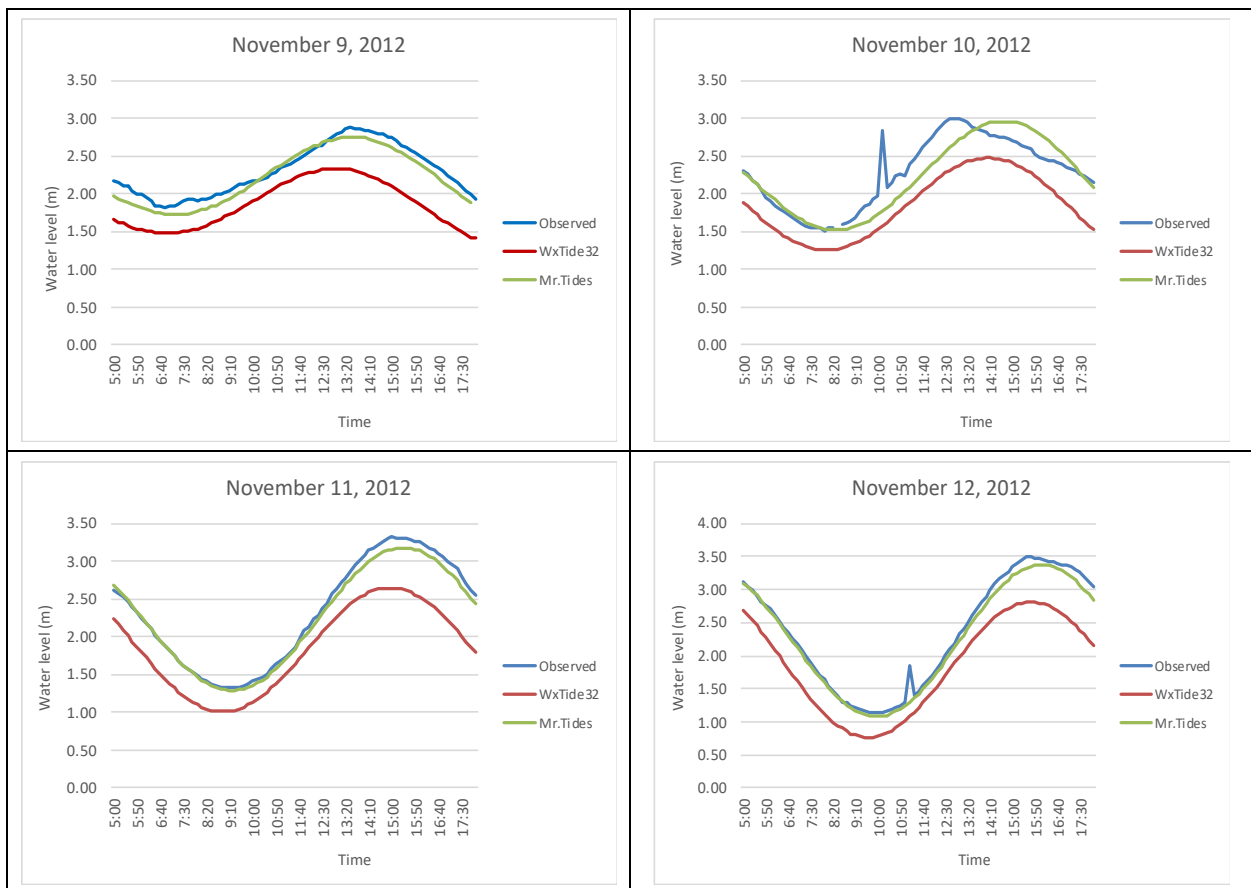


Figure 1.8. Comparison of tidal predictions for Toliara generated by WxTide32 (red line) and Mr. Tides (green line) software and observed tide levels (blue line)

Sonar data description

Raw sonar point data (n=13,563) were collected opportunistically using a consumer-grade chartplotter (Garmin GPSMap 441s) from June 2011-May 2013. The chartplotter was equipped with an integrated GPS and a dual-beam depth transducer (frequencies: 200khz/50khz, beamwidth: 10°/40°) that was mounted to a 6m-dive boat. Positional accuracy was assessed using a hand-held GPS unit (Garmin GPSMap 76Cx) that consistently indicated good signal strength from multiple satellites resulting in 2-3m positional accuracies. All GPS data were collected in UTM coordinates with the WGS84 datum. Error associated with the depths recorded by the sonar were evaluated manually, using a decameter and lead weight (RMSE 0.1m).

In order to calibrate the raw sonar data, tidal data were generated in 6-minute increments over 12-hour periods for dates and times corresponding to sonar surveys. Tidal states for each of the sonar data points was interpolated using a unique polynomial equation fitted to a 12-hour period that overlapped the actual survey dates and times (See Figure 1.9 for example). Corrected depths ($depth_{corr}$) were calculated by adding an offset to the recorded sonar depths ($depth_{sonar}$) to account for the difference between the mounted transducer location on the boat transom and the waterline ($depth_{offset} = 0.01m$), then the predicted tidal state ($depth_{pred}$) was subtracted. Once depths were corrected to the LAT tidal datum, the tidal state (1.36 m) at the time of the satellite image acquisition ($depth_{sat}$) was added back to the tidally-corrected values.

$$Depth_{corr} = depth_{sonar} + depth_{offset} - depth_{pred} + depth_{sat}$$

$Depth_{corr}$ data points corresponding to values less than 1 m were removed from the dataset, due to the inaccuracies of the sonar measurements in shallow water. Additionally, $depth_{corr}$ values greater than 12 m were removed due to insufficient data for model training at

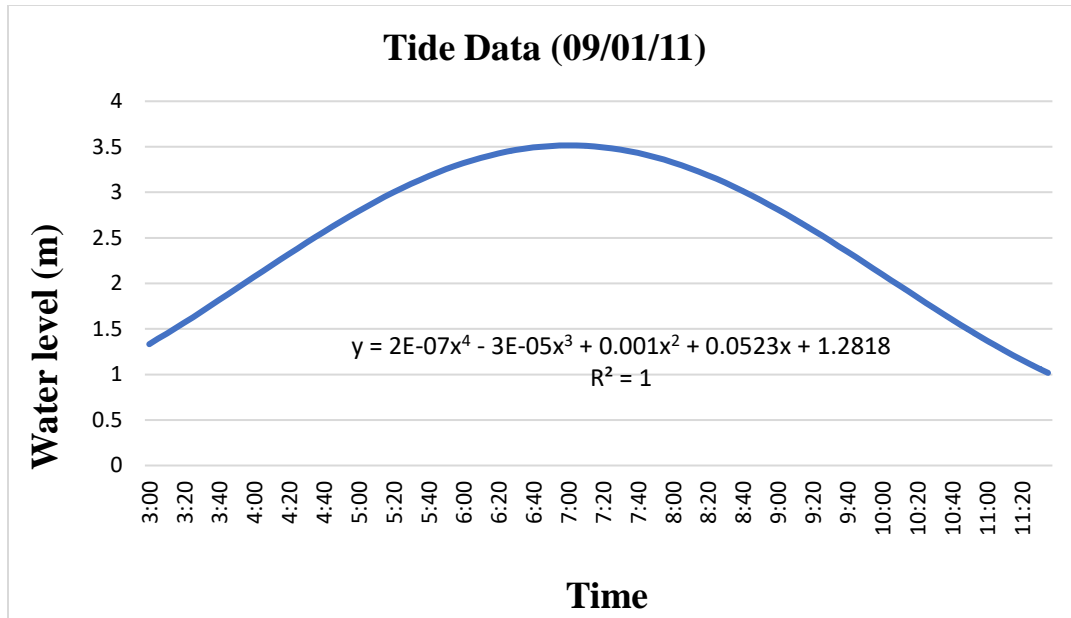


Figure 1.9. Software-generated (Mr. Tides) tidal prediction fitted with 4th-order polynomial equation used to correct sonar data to LAT

depths greater than 12 m within the lagoon, where depths greater than or equal to 12 m being found only in the reef passes. Calibrated sonar data ($depth_{adj}$) were imported into a GIS layer for further evaluation (Figure 1.10).

In conducting bathymetric surveys potential sources of error may include, but are not limited to: 1) instrument error, 2) tide stage correction error, and 3) error associated with the xyz movement and position of the survey vessel, such as heave, pitch, and roll, as related to vessel speed and/or weather conditions. Moreover, the sporadic changes in bathymetry that result from complex seafloor topography in coral reef ecosystems, due to patch reefs and coral heads, may confound bathymetric error assessment.

To assess accumulated errors in the corrected depth calculations, $depth_{corr}$, intersections in the sonar survey transects were intentionally planned to allow for a cross-track evaluation of $depth_{corr}$ values originating from identical locations, but from differing dates / times / tidal stages. For the cross-track evaluation, data points were mapped to a satellite image using ArcGIS 9.3

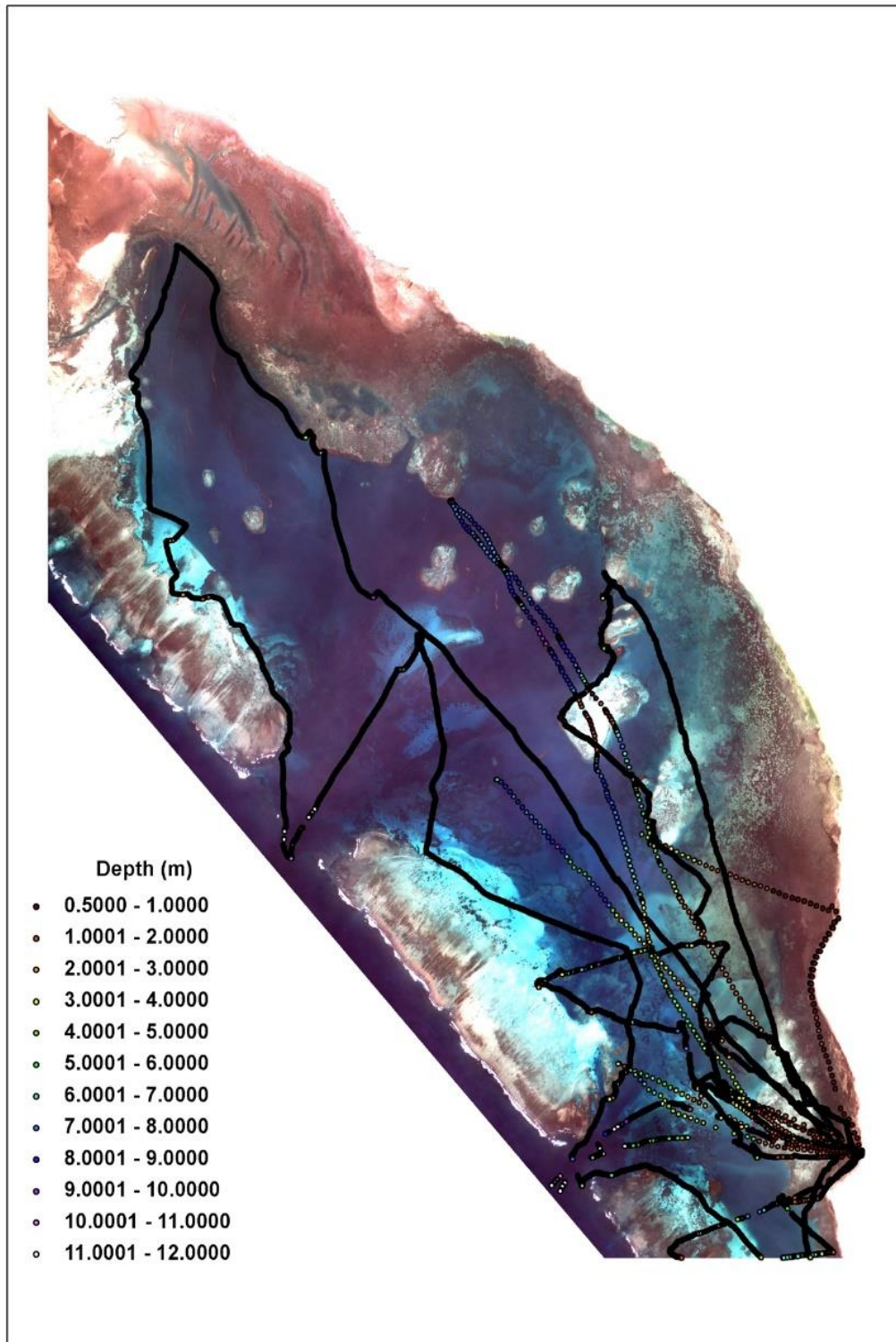


Figure 1.10. IKONOS RGB image of the Bay of Ranobe, with sonar track point file overlay

(ESRI, Redlands). Coefficients of variation were calculated for data point clusters that were spatially separated by less than 2m. In total, 46 cross-track data clusters were identified, consisting of 2-point (n=31), 3-point (n=9), 4-point (n=5), and 7-point (n=1) clusters. Additionally, comparisons were made between data point clusters originating from a single day of sampling versus two days. Comparisons of all data clusters (CV=0.47, n=46), single-day clusters (CV=0.53, n=14), and multi-day clusters (CV=0.45, n=32) suggest that much of the measurement error may be attributed to weather, sea-state, and/or boat speed, given that errors resulting from tidal prediction software would result in higher CVs in the multi-day clusters. Figure 1.11 illustrates the relationship between variation in boat speed and the variation in sonar measurements. Although there is no clear relationship, there appears to be some effect that is likely confounded with weather / sea-state. To minimize the error associated with the depth measurements, data points were locally averaged. This was achieved by converting the $depth_{adj}$ shapefile to grid format (cell resolution=5m, cell value=mean), then converting the grid back to a shapefile, resulting in 5m-localized mean point values (n=9346). In the final shapefile, the mean $depth_{corr}$ values represent the response variable used for regression model training and testing, and the point locations were used for sampling the predictor variables, the satellite data. Processing and analyses of the satellite imagery is described further in the following sections.

Satellite remote sensing data

IKONOS satellite data description

The IKONOS satellite platform collects images in 11 km swaths, following a sun-synchronous, circular, polar orbit, at 681 km above the earth. Satellite sensors record 11-bit data composed of four multispectral bands (MS; blue, green, red, and near-infrared) and one panchromatic band (PAN). An imagery grant awarded by the GeoEye Foundation provided four

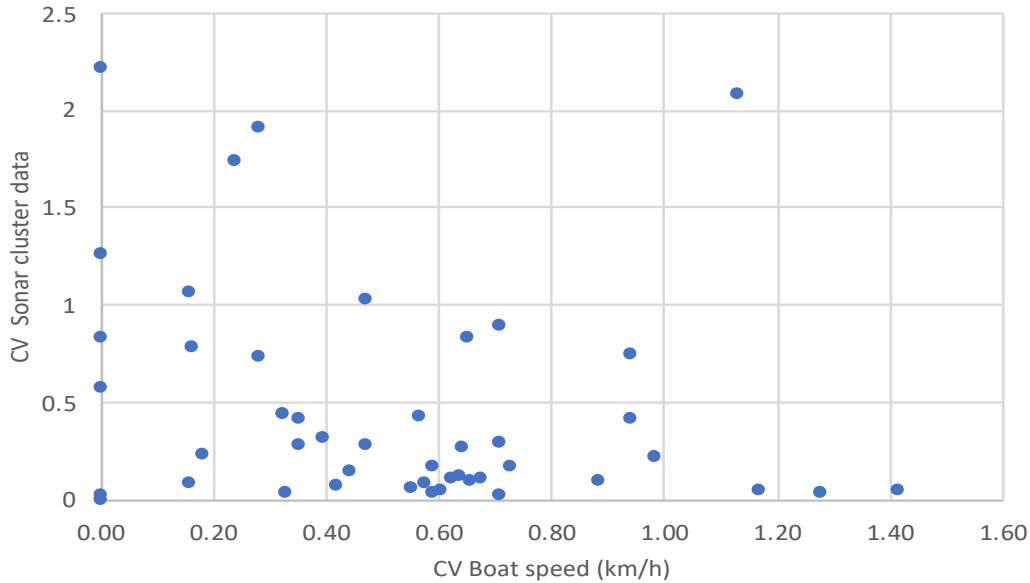


Figure 1.11. Relationship of the coefficients of variation (CV) for recorded sonar depth and boat speed, with potential confounding effects of weather / sea state

multispectral satellite images that were evaluated for the present study and described below. A single scene (Image ID #470991) representing 78% of the lagoon (Figure 1.12), collected by the IKONOS-2 sensor was selected for further analysis (See Tables 1.1-1.2 for summary). At the time of acquisition (March 16, 2007, 07:15 GMT), favorable conditions resulted in a cloud-free, glint-free image. The image was received as a standard geometrically corrected product, projected into UTM/WGS84, in an uncompressed GeoTIFF file format. Images representing the extreme north and south of the lagoon were not analyzed any further, given that these shallow, reef flat environments were less suitable for the boat-based fishing activities studied here.

Table 1.1. Details of the satellite images used in the present study

Image ID	Sensor	Date	Spatial Resolution (m)		Nb. Bands	Data
			MS	Pan		
470990	IKONOS-2	2007-03-19	3.28	0.81	4+pan	11-bit
470991	IKONOS-2	2007-03-16	3.28	0.81	4+pan	11-bit
470992	IKONOS-2	2003-10-31	3.28	0.81	4+pan	11-bit
470998	GeoEye-1	2009-07-05	1.64	0.41	4+pan	11-bit

Table 1.2. IKONOS-2 band description

Bands	Bandwidth	Spatial Resolution
Blue	445-516 nm	4m
Green	506-595 nm	4m
Red	632-698 nm	4m
Near Infrared	757-853 nm	4m
Panchromatic	526-929 nm	1m

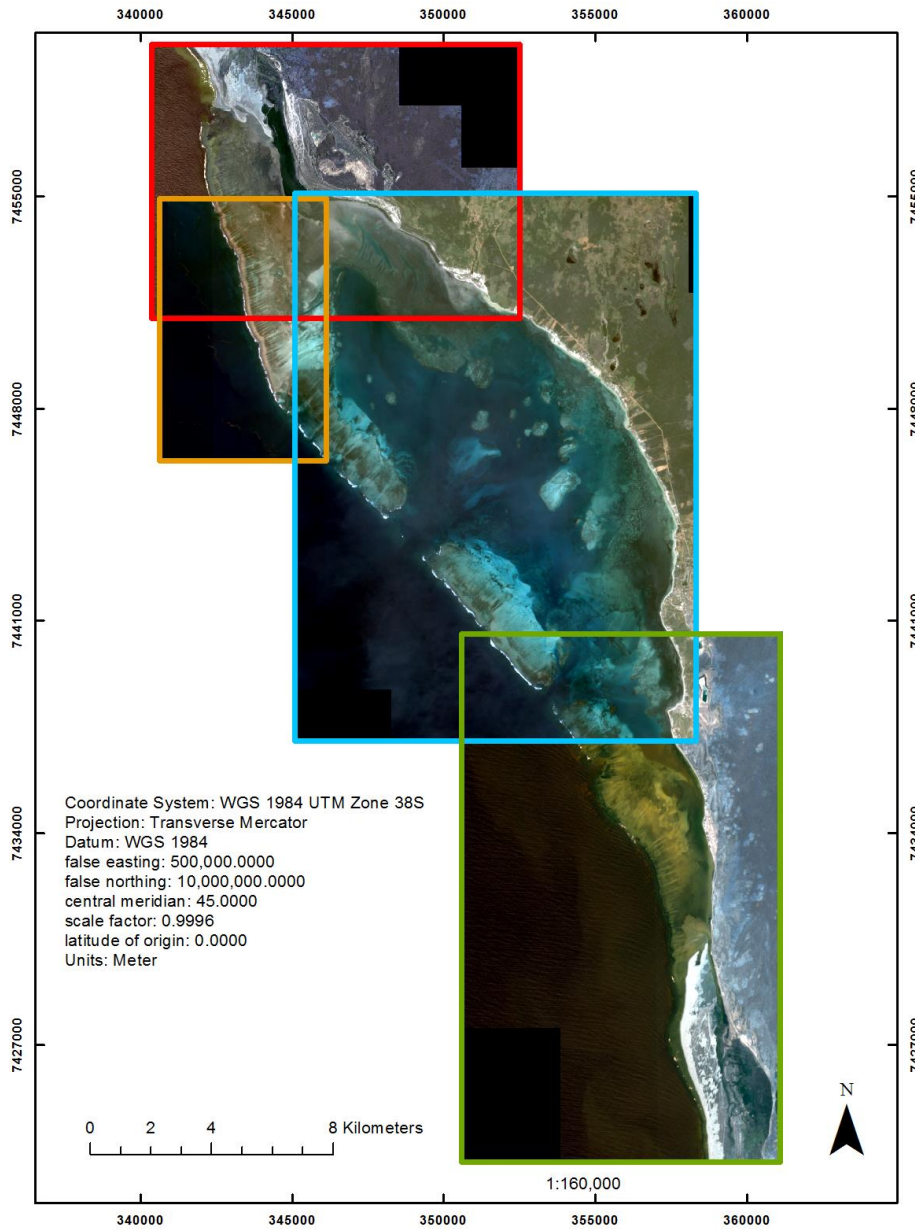


Figure 1.12. IKONOS-2 and GEOEYE-1 images awarded by the GeoEye Foundation for full coverage of the Bay of Ranobe; image outlined in blue was selected for further research

Satellite data pre-processing

Initial image pre-processing involves a series of processing steps of original satellite image data that corrects for geometric, radiometric, and atmospheric distortions present, in varying degrees, in all satellite images. Geometric distortions may arise from the position of the satellite platform as function of: pitch, roll, yaw of the platform, or the acquisition angle. Radiometric calibration allows for the data recorded by the satellite, referred to as digital numbers (DNs) or brightness values, to be converted to an actual physical property, radiance, based on the custom parameters of a specific satellite sensor. Atmospheric correction endeavors to account for the numerous ways in which the path between solar irradiance, the targeted study area, and the satellite sensor may be confounded by the scattering / absorption of atmospheric constituents. Steps followed for the image pre-processing workflow are depicted in Figure 1.13, and described further in the sections to follow.

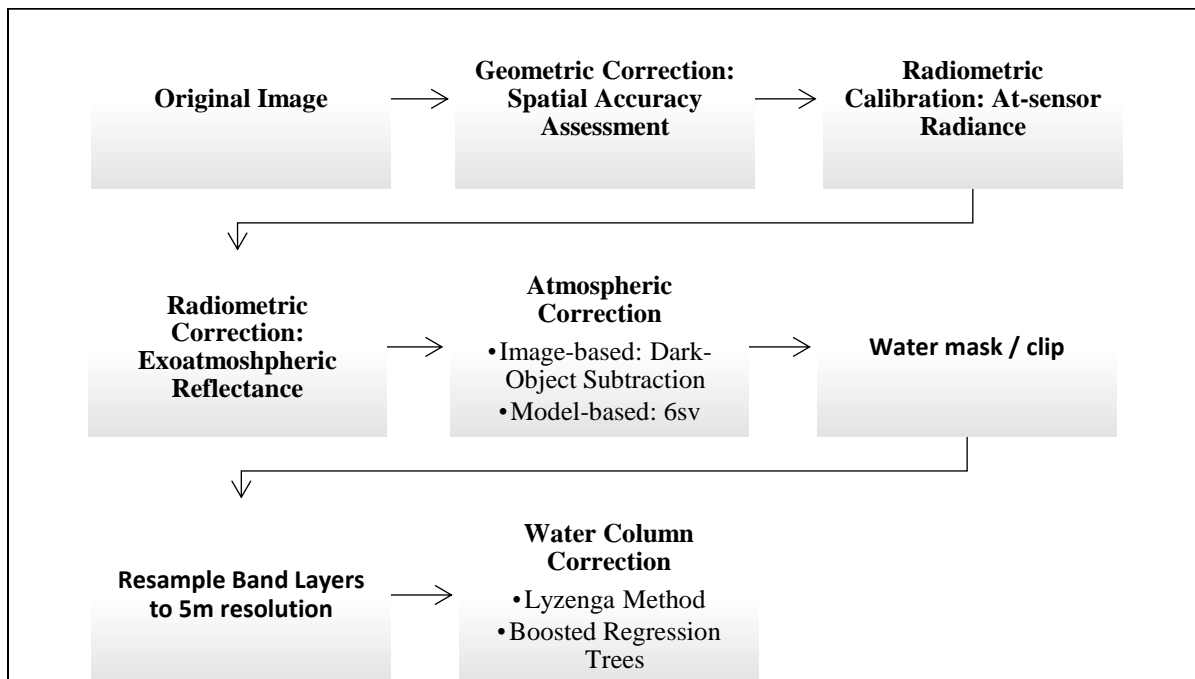


Figure 1.13. Workflow for the steps followed in the processing of the selected satellite image

Geometric correction: Spatial accuracy assessment

To assess the spatial accuracy of the IKONOS image, ground control points (GCPs) were created (n=25) by plotting points on the high-resolution PAN layer at semi-permanent locations, such as at the corners of concrete structures (See Appendix 1.2). Using a consumer-grade, hand-held GPS (Garmin GPSMap 76cx), ground-truthing was conducted to verify GCP locations. To maximize accuracy of the acquired GPS coordinates, ground-truthing was conducted at times of low cloud cover to allow for strong satellite fixes, with ample time being provided to allow for stable positioning. Spatial error was calculated for the differences between the GCPs and the manually-collected coordinates (Total RMSE = 3.59 m). Spatial accuracy indicated by the GPS, as a function of the number and strength of satellite fixes, were consistently in the 2-3 m range. Considering the spatial error associated with consumer-grade GPS units, the total calculated RMS error was deemed adequate for the purposes of the present study. Moreover, with the 5-meter spatial averaging of the sonar data, as discussed above, and the degradation of the image resolution to 5 meters, as discussed below, the calculated total RMSE falls within a single image pixel. Lastly, as a measure to preserve the integrity of the original data that would be altered by a data transformation inherent in the geometric correction process, it was considered best to not pursue further any minor improvements that may be made through a geometric correction, given that the image was delivered in the desired coordinate system format, Universal Transverse Mercator (UTM).

$$\text{Total RMSE} = \sqrt{\frac{1}{n} \sum_i^n (\Delta X_i^2 + \Delta Y_i^2)} = 3.59$$

Radiometric calibration: Top-of-atmosphere radiance

To convert raw satellite data measured in DN's to spectral radiance, L , for each of four multispectral bands of the IKONOS image, L_λ , the following equation was used:

$$L_\lambda = \frac{10^4 \cdot DN_\lambda}{CalCoef_\lambda \cdot Bandwidth_\lambda} \quad \text{Equation 1}$$

where,

$CalCoef_\lambda$ = Radiometric calibration coefficient [(DN)/(mW/cm² · sr)] (Table 1.3)

$Bandwidth_\lambda$ = Bandwidth of spectral band λ (nm) (Table 1).

Radiometric Correction: Exoatmospheric Reflectance

Radiance was converted to apparent reflectance, or planetary reflectance, ρ_p , following the equation below:

$$\rho_p = \frac{\pi \cdot L_\lambda \cdot d^2}{E_{SUN_\lambda} \cdot \cos\theta_s} \quad \text{Equation 2}$$

where,

ρ_p = Unitless planetary reflectance,

L_λ = Radiance for spectral band λ at the sensor's aperture,

d = Earth-Sun distance in astronomical units,

$E_{sun\lambda}$ = Mean solar exoatmospheric irradiances (Table 1.4),

θ_s = Solar zenith angle.

Values for coefficients from Formulas 1-2 are found in Table 1.3. For the Earth-Sun distance, d , the value was calculated by linear interpolation of bounding values provided in Table 1.4 for the Julian day (JD = 75), corresponding to the image acquisition date ($d = 0.9961$). Solar zenith angle, θ_s , is the complement of the sun angle of elevation, which is a value that is found in the image metadata file:

$$\theta_s = 90^\circ - 54.06649^\circ = 35.9331^\circ.$$

Application of the formulae to the IKONOS image was conducted in the Erdas Imagine Modeler software environment. Both coefficients and formulae were taken from Taylor (2005).

Table 1.3. IKONOS Band-dependent Parameters

IKONOS band (λ)	CalCoef _{λ} Post 02/22/01 (DN/(mW/cm ² -sr))	Bandwidth _{λ} (nm)	Esun _{λ} (W/m ² /μm)
Pan	161	403	1375.8
Blue	728	71.3	1930.9
Green	727	88.6	1854.8
Red	949	65.8	1556.5
NIR	843	95.4	1156.9

IKONOS Planetary Reflectance and Mean Solar Exoatmospheric Irradiance (Taylor, 2005)

Table 1.4. Earth-Sun distance in Astronomical Units per Julian Day

J Day	Distance								
1	0.9832	74	0.9945	152	1.0140	227	1.0128	305	0.9925
15	0.9836	91	0.9993	166	1.0158	242	1.0092	319	0.9892
32	0.9853	106	1.0033	182	1.0167	258	1.0057	335	0.9860
46	0.9878	121	1.0076	196	1.0165	274	1.0011	349	0.9843
60	0.9909	135	1.0109	213	1.0149	288	0.9972	365	0.9833

IKONOS Planetary Reflectance and Mean Solar Exoatmospheric Irradiance (Taylor, 2005)

Atmospheric correction

Images captured by satellite sensors are the result of a complex series of multiple scattering and absorption events as solar irradiance is transmitted through the atmosphere, strikes the earth, and is reflected back through the atmosphere to be recorded by the sensor. Photons, recorded as brightness values or digital numbers (DN), are not all reflected from the surface target, but are rather a composition of the target reflectance, reflectance from neighboring surfaces (adjacency effects), and atmospheric scattering events (Figure 1.14).

For scientists interested in studying the earth's surface, brightness originating from non-targeted surfaces and scattering events, known as path radiance, contribute "noise" to the data that manifests itself as a haze over the image scene. The added brightness due to path radiance is generally considered the reason for which uncorrected image histograms experience a substantial shift in pixel values to the right (Figure 1.15). Corrective measures have been developed to improve the signal-to-noise ratios introduced by these atmospheric constituents. Contributions by atmospheric constituents, *i.e.* gases, water vapor, and particulates, to the path radiance are dependent on the interaction of particle size(s) and wavelength(s) of light. On one side of the spectrum, shorter wavelengths interact more with the smaller gaseous molecules, a phenomenon known as Rayleigh scattering, while longer wavelengths interact with larger particles, such as water vapor droplets, in a process known as Mie scattering. The proper characterization of the water vapor content, aerosol optical thickness (AOT) or aerosol optical depth (AOD), is particularly important when studies are conducted on water targets (Gordon 1995, Gordon et al., 1997), such as the case in the present study.

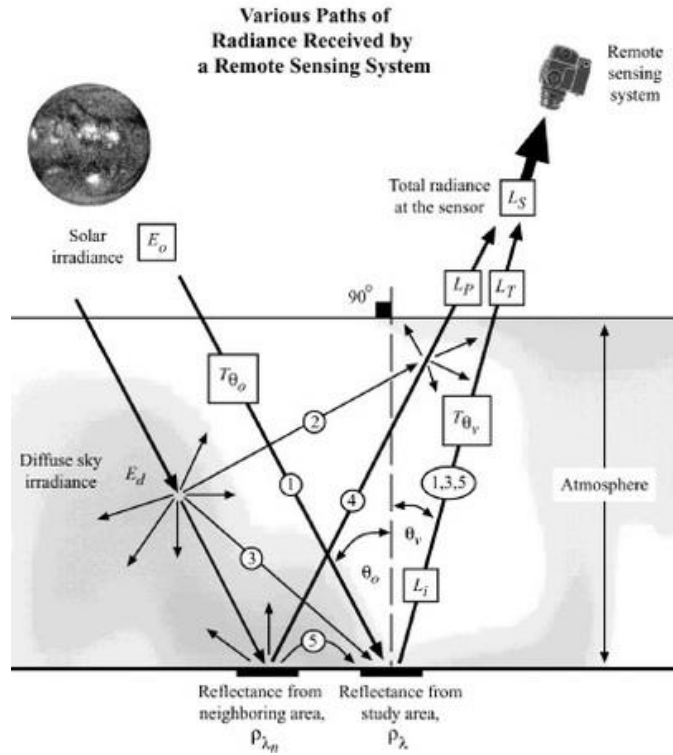


Figure 1.14. Illustration from Jensen (2007) depicting the multiple potential pathways in which scattering and non-targeted reflectance, path radiance (L_p), may corrupt the signal received by the satellite sensor.

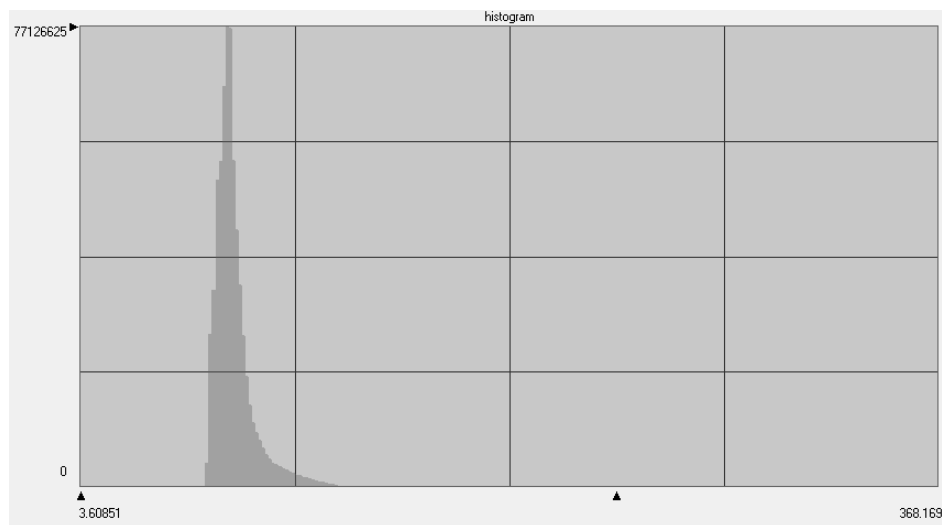


Figure 1.15. Histogram of the IKONOS blue band image file calibrated to TOA radiance; right-shifting of histogram related to path radiance

In general, the process of performing an atmospheric correction requires the subtraction of the augmented brightness values attributable to path radiance (L_p) from the recorded at-satellite radiance (L_s) values. The corrected radiance values may then be converted to reflectance in order to obtain surface reflectance ($\rho_{surface}$), as described in the simplified, 1-dimensional equation below:

$$\rho_{surface} = \frac{\pi(L_s - L_p)}{T_v(E_0 \cos(\theta_z)T_z + E_d)}. \quad \text{Equation 3}$$

Equation 3 provides some additional key parameters including the exoatmospheric solar constant, E_0 , the downwelling diffuse sky irradiance, E_d , the sun-earth transmittance constant, T_z , and the earth-satellite transmittance constant, T_v . Variants of atmospheric correction techniques employed up to present differ, essentially, in the number of simplifying assumptions made to the variables presented in Equation 3.

Over the past decades, atmospheric corrections techniques have been developed that may be categorized as: 1) image-based, requiring no *in-situ* data, 2) empirical techniques requiring some *in-situ* measurements, and 3) model-based techniques that employ a less simplified version of the Radiative Transfer Equation, requiring some *in-situ* measurements. One of the earliest and most commonly used image-based atmospheric correction techniques is dark-object subtraction, DOS (Chavez, 1989). In performing a DOS correction, a black object in the scene is selected to determine the radiance minimum for each band, $L_{(\lambda)min}$, ideally clear, deep water, *i.e.* optically deep water. For scenes lacking optically deep water, other black surfaces or shadows are commonly used to determine L_{min} . Principle assumptions of the basic DOS method are that black objects absorb all wavelengths of visible light, thus radiance values should theoretically equal zero. Any dark-object brightness values greater than zero are attributed to the path radiance and

subtracted from all pixel values, $L_s - L_p$ from Equation 3. Moreover, Equation 3 is further simplified by assuming the transmittance variables, T_v and T_z are unity and downwelling diffuse sky irradiance, E_d , is zero. As a result, the DOS correction technique accounts for only the additive and not the multiplicative components of path radiance. Some of the later modifications to the DOS method provided alternatives in the selection of the value of L_{min} , with either guidance from image histograms, or in assuming that even dark-objects would have a nominal level of reflection set at 1%, $DOS_{1\%}$ (Chavez, 1988; 1996; Moran *et al.*, 1992; Song *et al.*, 2001; Mahiny and Turner, 2007; Kim and Lee, 2005; Norjamaki and Tokola, 2007).

Another commonly used atmospheric correction technique is known as the Empirical Line Method (ELM). Use of the ELM is appropriate if *in-situ* reflectance measurements can be made at the time of the satellite overpass, which would not be possible for analyses of historical images. To implement the ELM, spectrally homogenous targets are identified for the collection of on-the-ground reflectance measurements, which are then used in a linear regression of image radiance values from those same targets. Linear relationships developed for the different bands and targets are applied to all the image pixels to correct for the atmospheric path radiance (Smith and Milton, 1999; Karpouzli and Malthus, 2003; Ariza *et al.*, 2018).

A widely-used, model-based approach to atmospheric correction that has been refined over the years is the 6S (Second Simulation of a Satellite Signal in Solar Spectrum) algorithm, formerly known as 5S, which in its current version (6SV2.1) is an open-source code that can be run through a website interface or downloaded (Vermote *et al.*, 1997; Kotchenova *et al.*, 2006; Kotchenova *et al.*, 2007; Kotchenova *et al.*, 2008). Newer versions of the code allow for improved computational accuracy in the estimation of Rayleigh and aerosol scattering through an iterative successive orders of scattering (SOS) algorithm, and the vector version (6SV) accounts

for the polarizing effects of atmospheric constituents (Zhang, 2012). The SOS algorithm divides the atmosphere into successive layers, allowing for the computation of numerical solutions of the Radiative Transfer equation to be made on a layer-by-layer basis (Kothchenova *et al.*, 2006). In addition, the integrated atmospheric profiles have been expanded to include additional atmospheric gases (e.g. CH₄, N₂O, and CO), the selection of aerosol profiles, and/or customizable, user-defined parameterization.

For the present study, two different atmospheric correction methods were applied to the IKONOS image of the study area in order to evaluate the effects of the atmospheric correction on the final bathymetry map product, the DOS_{1%} method and the 6SV approach. For the DOS_{1%} correction, an area of optically deep water was initially identified by visual assessment of image band files and histogram equalization enhancement of these files (Figure 1.16a-c). Within the area of interest, radiance values from the three raster layers were sampled at n=50 random points (Figure 1.16d-e), and a band-averaged L_{min} value was calculated.

To calculate $L_{DOS1\%}$, Equation 2 is solved for radiance and multiplied by 1%:

$$L_{\lambda_{DOS1\%}} = L_{\lambda_{min}} - 0.01[(E_0 \cos(\theta_0)) / (\pi d^2)]. \quad \text{Equation 4}$$

DOS-corrected, surface radiance images were generated by applying Equation 4, using the calculated parameter values found in Table 1.5. Atmospheric correction calculations were conducted in Erdas Imagine Modeler environment using a conditional statement to avoid negative pixel values, for example:

$$\begin{aligned} &\text{If } L_{\lambda} \geq L^*_{\lambda}, \\ &\text{Then } L_{\lambda} - L^*_{\lambda}, \\ &\text{Else } L^*_{\lambda} = 0.00001. \end{aligned}$$

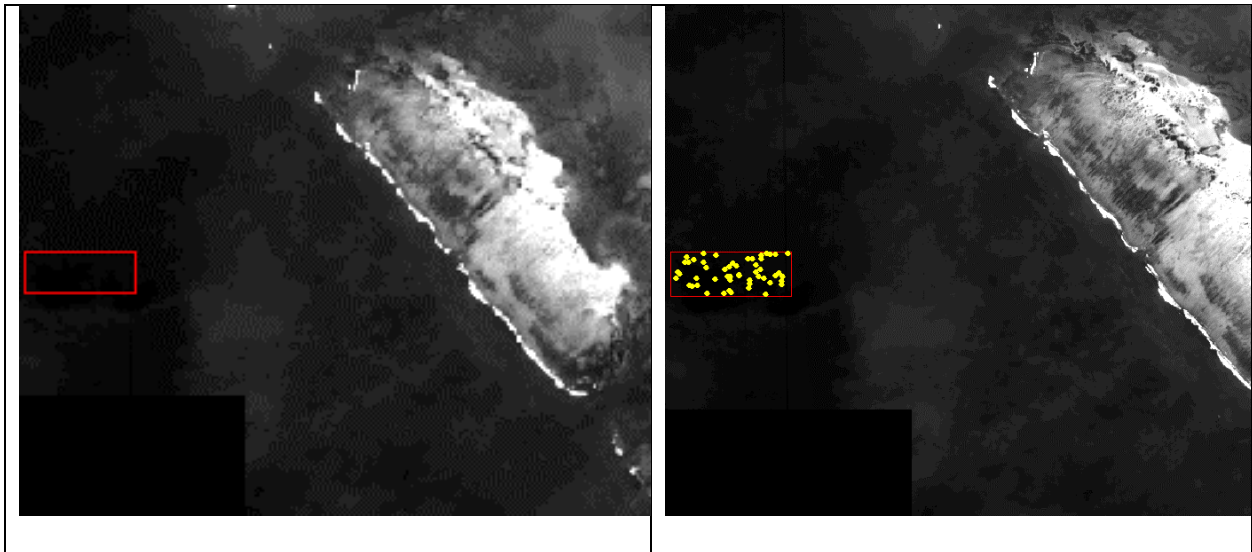


Figure 1.16. IKONOS-2 image band files: (first row) a) red band, b) green band, and c) blue band with histogram equalization enhancement, (second row) d) identification of optically-deep region, and e) random sampling of the optically-deep region applied to all bands

Table 1.5. Calculated values for the parameters of the atmospheric correction

Band	L_{min}	Cos(θ_s)	d²	E_{sun}	L1%	LDOS1%
Blue	56.062	0.810	0.992	1930.900	5.016	51.047
Green	34.310	0.810	0.992	1854.800	4.818	29.492
Red	15.854	0.810	0.992	1556.500	4.043	11.811

To evaluate two commonly used atmospheric correction techniques, the 6SV model-based correction was performed. A web-based portal is available (<http://6s.ltdri.org/pages/run6SV.html>) and was used, here, to conduct simulations. The 6SV model requires a number of inputs that allow specification of: 1) geometrical conditions, 2) atmospheric model, 3) target and sensor altitude, 4) spectral conditions, 5) ground reflectance, and 6) signal. Selection of atmospheric models are of particular importance, with options to select standard atmospheric profiles (Table 1.6) and aerosol profiles (Table 1.7). In order to determine the appropriate atmospheric profile and aerosol model, online data sources were consulted, specifically AERONET and MODIS.

AERONET (Aerosol Robotic Network; <https://aeronet.gsfc.nasa.gov/>) is a global network of ground-based sensors specifically designed for the collection of global aerosol properties. Data from the closest ground station to the study site, found on the island of Reunion, was sought for the month and year corresponding to the image acquisition (March 16, 2007; 07:15 GMT). From the available data it appeared that the ground station was not functioning on the day / time of image acquisition, consequently, data from the closest date was used, March 29 (Figure 1.17). A complete dataset for March 2008 was available, including hourly measurements (Figure 1.18) that was used to qualitatively assess water vapor content from the perspective of a monthly mean and typical hourly changes in measurement values. As water vapor content

Table 1.6. 6SV Standard Atmospheric Models

Code	Atmospheric profile	Water Vapor (g/cm²)	Ozone (cm-atm)	Solar irradiance (W/m²)
0	No gaseous absorption	0	0	934.71
1	Tropical	4.120	0.247	758.50
2	Midlatitude Summer	2.930	0.319	769.09
3	Midlatitude Winter	0.853	0.395	754.17
4	Subarctic Summer	2.100	0.480	781.54
5	Subarctic Winter	0.419	0.480	825.74
6	US standard 62	1.420	0.344	794.01

Table 1.7. 6SV Standard Aerosol Models

Code	Aerosol model	Solar irradiance (W/m²)
0	No aerosol	783.18
1	Continental model	769.09
2	Maritime model	778.94
3	Urban model	751.94
4	User's own model	739.46
5	Desert model	776.01
6	Biomass burning	772.74

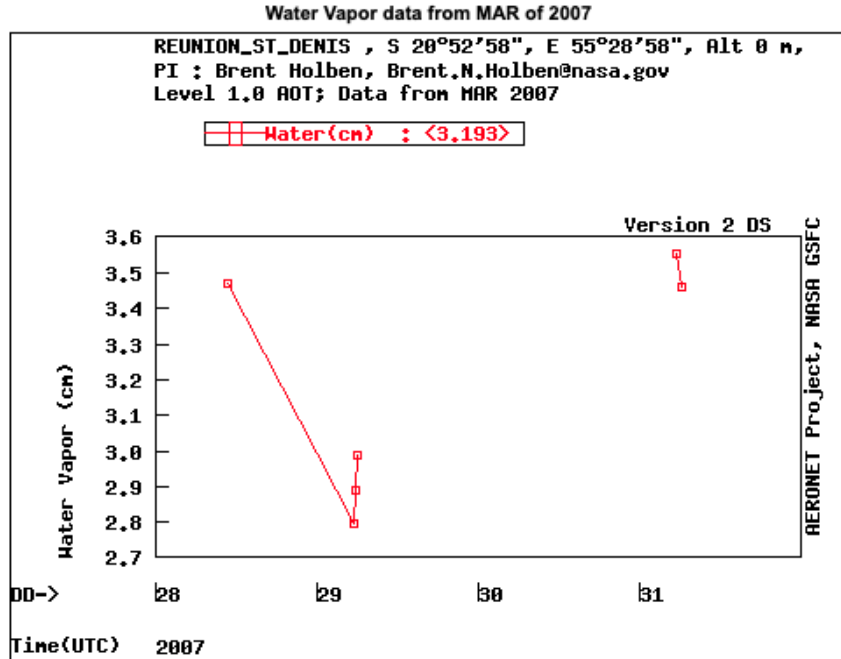


Figure 1.17. Daily water vapor density (g/cm²) measured on March 28-31, 2007 in Saint Denis, Reunion

appeared to fluctuate around 3 g/cm² for the month of March, with lower values observed in the morning hours, the Midlatitude Summer (2.930 g/cm²) profile was selected. AERONET and MODIS (Moderate Resolution Imaging Spectroradiometer) data were used to determine the aerosol optical thickness (AOT) at 550 nm value that was used as input into the 6SV simulation, AOT = 0.1 (Figures 1.19). The Maritime aerosol model was selected, given that the area of interest is the marine / sub-marine portion of the image scene. Lastly, to characterize surface reflectance, the homogenous ground reflectance type with non-directional, or Lambertian, directionality effects were chosen as options. (See Appendix 1.3-1.5 for 6SV output files)

6SV model simulations were conducted for each of the three IKONOS image bands. Results of simulations were used to determine band-specific values for: global gas transmittance, total scattering transmittance, atmospheric reflectance, and spherical albedo. Based on the

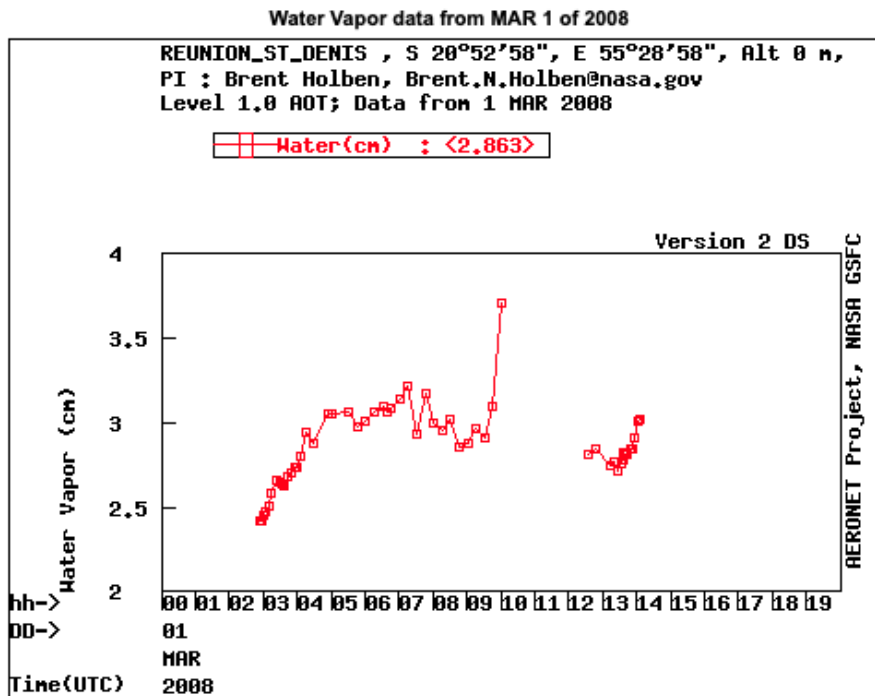
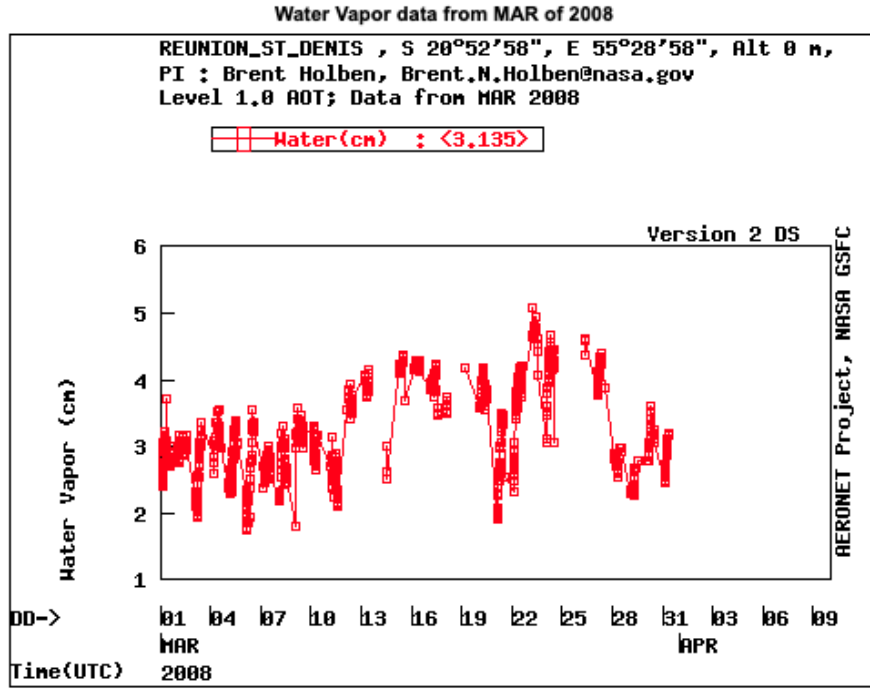


Figure 1.18. Daily (top) and hourly (bottom) water vapor density (g/cm²) measurements from March 2008 in Saint Denis, Reunion

relationship of top-of-atmosphere reflectance ($\rho_{\lambda [TOA]}$) to surface reflectance ($\rho_{\lambda [Surface]}$), presented in Equation 5 below, an algebraic solution for $\rho_{Surface}$ may be derived, as follows:

$$\rho_{\lambda [TOA]} = \text{Global gas transmittance}_{\lambda} \times (\text{Atmospheric Reflectance}_{\lambda} + (\rho_{\lambda [Surface]} \times \text{Total scattering transmittance}_{\lambda})) \quad \text{Equation 5}$$

$$A = \frac{1}{\text{Global gas transmittance} \times \text{Total scattering transmittance}}, \quad \text{Equation 6}$$

$$B = \frac{\text{Atmospheric Reflectance}}{\text{Total scattering transmittance}}, \quad \text{Equation 7}$$

$$C = (A \times \rho_{\lambda [TOA]}) - B, \quad \text{Equation 8}$$

$$\rho_{\lambda [Surface]} = \frac{C}{1 + \text{Spherical albedo} \times C}. \quad \text{Equation 9}$$

Atmospheric correction calculations were conducted in Erdas Imagine Modeler environment in a step-wise manner, using a conditional statement as a final step to remove any negative pixel values that may have resulted from the application of Equation 8, where:

If $\rho_{\lambda [Surface]} > 0$,

Then $\rho_{\lambda [Surface]} = \rho_{\lambda [Surface]}$,

Else $\rho_{\lambda [Surface]} = 0$.

Time Averaged Map of Aerosol Optical Depth 550 nm (Dark Target) daily 1 deg. [MODIS-Aqua MYD08_D3 v6.1] over 2007-03-16, Region 40.166E, 25.3125S, 43.7695E, 21.4453S

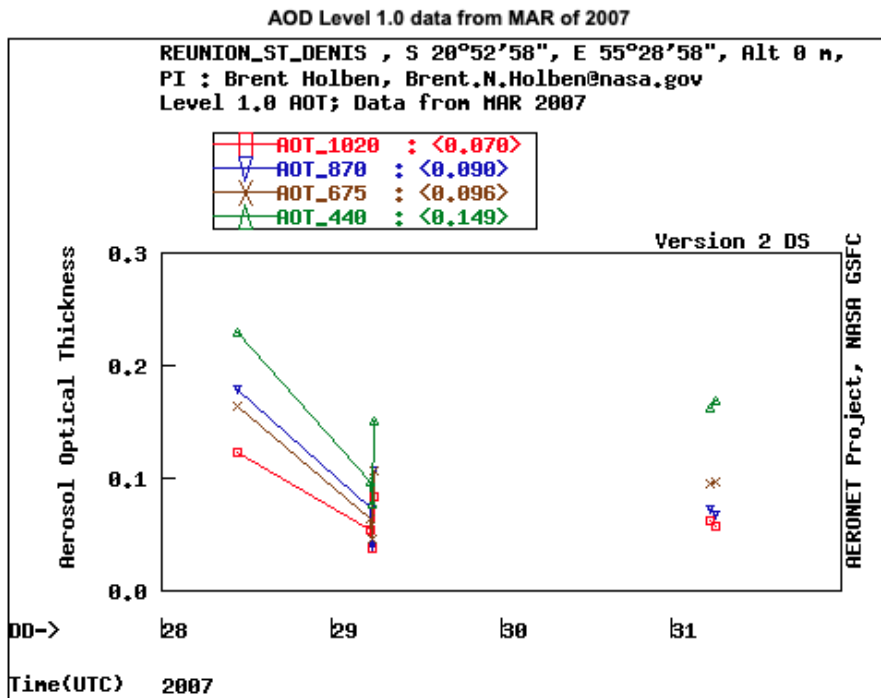
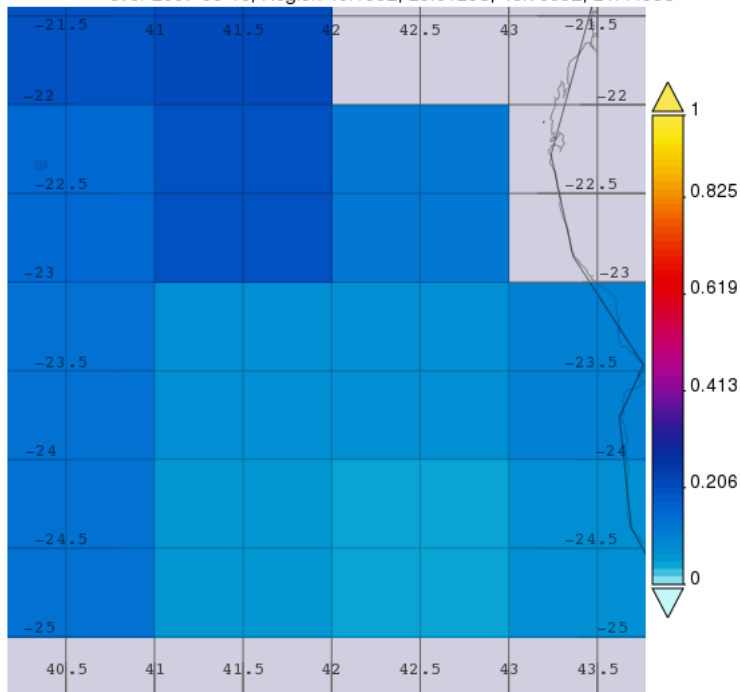


Figure 1.19. Measurements of Aerosol Optical Depth (AOD), or Aerosol Optical Thickness (AOT), collected by MODIS (March 16, 2007) on southwest coast of Madagascar (top); AERONET measurement from March 28-31, 2007, Saint Denis, Reunion (bottom)

Image Mask and Re-sampling

As a final image pre-processing step, the RGB bands representing the DOS_{1%} and 6SV atmospheric correction results were clipped using a water mask to delimit the study area. Clipped images were resampled to 5 m resolution, corresponding to the 5 meter-averaged sonar data, using the bilinear interpolation method (Figure 1.20). In addition to matching spatial resolutions of the sonar point layer and raster layers, clipping and resampling the images resulted in a reduction in file sizes to facilitate the next step in the process, statistical modeling, as described in the following section.

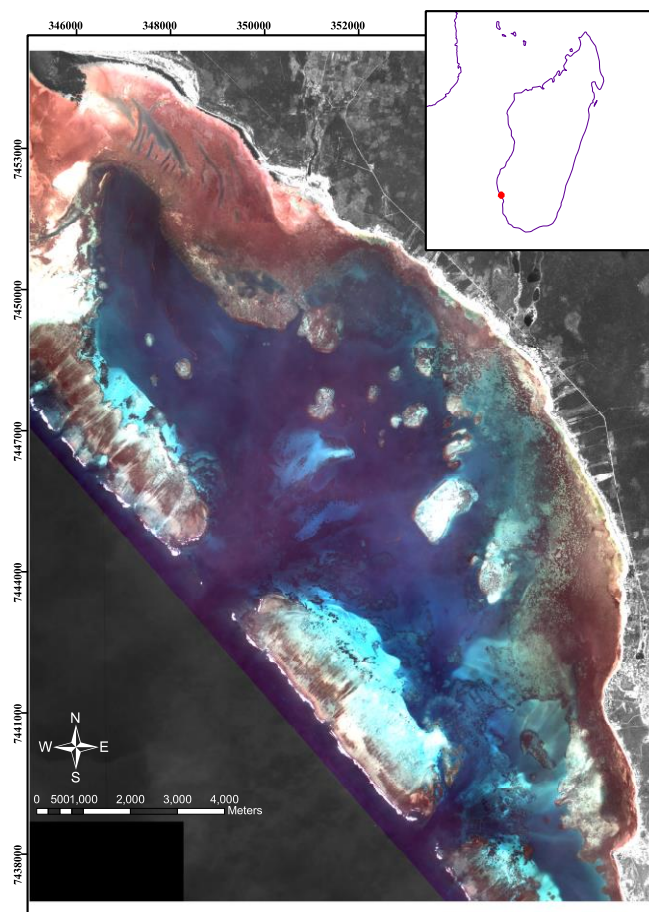


Figure 1.20. RGB image of the Bay of Ranobe after water mask, clip, and spatial resampling

Statistical models: Water depth retrieval

According to the Beer-Lambert Law of physics, the initial intensity of light, $I_0(\lambda)$, passing through a solution experiences an exponential decay, or attenuation. Attenuation of the light as it exits the solution, $I_l(\lambda)$, is related to the concentration of any solute(s), c , the absorptivity of the solute(s), α , and the pathlength traveled through the solution, l (Figure 1.21). In the realm of ocean remote sensing, the concentration of the solution is equivalent to the turbidity of sea water, a parameter referred to as the diffuse attenuation coefficient, K_d . $K_d(\lambda)$ is an apparent optical property of seawater that may be reliably estimated by the degree of absorption /scattering at 490 nm and 443 nm wavelengths, with K_d (490) being the most commonly used (Lee et al., 2005).

Based on the Beer-Lambert physical principle of the transmittance of light through a medium, Lyzenga (1985) developed a method for inverting the Beer-Lambert equation by log-transforming the at-surface radiance values, or water-leaving radiance, in order to determine the pathlength, *i.e.* depth. Water-leaving radiance values for each band are obtained through calibrating the image from digital numbers to radiance and performing an atmospheric correction, as described in the previous section. As described in Equation 10, bands are initially processed by log-transforming the atmospherically-corrected radiance values. Here, a generic dark-object subtraction atmospheric correction is described:

$$X_i = \ln [L_{TOA}(\lambda_i) - L_{\infty}(\lambda_i)], \quad \text{Equation 10}$$

where the log-transformed, corrected band, X_i , is calculated by taking the natural log of the difference of the top-of-the-atmosphere radiance values, L_{TOA} , and the optically-deep radiance

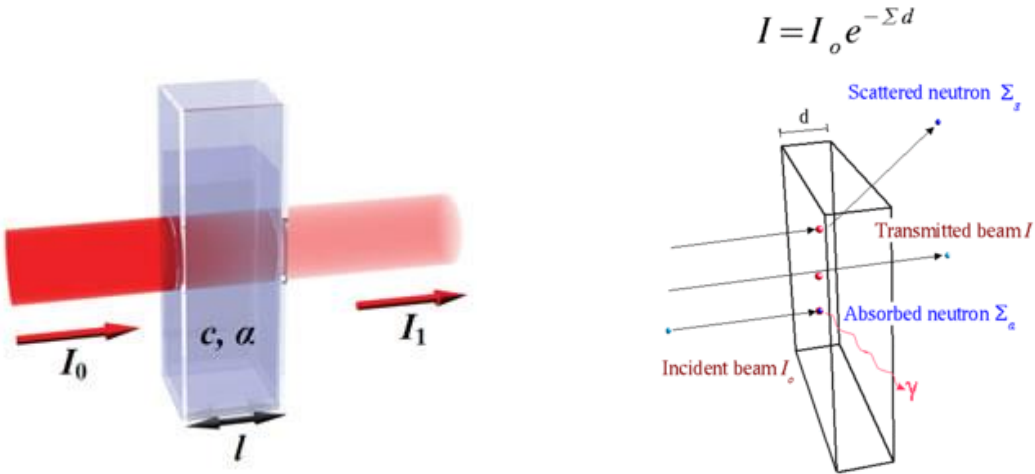


Figure 1.21. Beer-Lambert Law: Attenuation of incident light, I_0 , passing through a solution

value, L_∞ . A multiple linear regression of the corrected bands, X_i , as the dependent variables and depth, Z , as the independent variable is used to determine the $a_{0,i,j}$ parameters:

$$Z = a_0 + a_i X_i + a_j X_j + \dots \quad \text{Equation 11}$$

Since Lyzenga (1985), additional techniques have been developed for the derivation of water depth from remotely sensed imagery, employing various derivations of the Lyzenga method and/or approaches using different band combinations, band ratios, or statistical models (Philpot, 1989; Bierwirth *et al.*, 1993; Sandidge and Holyer, 1998; Lee *et al.*, 1999; Diersson *et al.*, 2003; Stumpf *et al.*, 2003; Conger *et al.*, 2006; Lyzenga *et al.*, 2006; Mishra *et al.*, 2007; Hogrefe *et al.*, 2008; Brando *et al.*, 2009; Kanno, *et al.*, 2011; Ma *et al.*, 2014; Eugenio *et al.*, 2015; Pacheco *et al.*, 2015; Shen *et al.*, 2018). Previous research, however, has indicated that the performance of these models depends greatly on the assumption of homogenous water column

properties, homogenous seafloor bottom types, and are limited to a maximum depth (Gao, 2009; Manessa *et al.*, 2018). In shallow coastal waters, where much of this research is conducted, the assumed conditions of the idealized environment are seldom the reality.

In the present research, the multiple linear regression-based method developed by Lyzenga was compared to a novel statistical approach for fitting model parameters, gradient boosting models (GBM), also known as boosted regression trees. Gradient boosting is non-parametric, machine learning regression technique with a basic regression tree-like structure. Unlike simple regression trees, boosting is an ensemble method, where the model is fit and re-fit in an iterative process that is guided by the minimization of a loss function, such as the mean squared error. Tree “branches” are added and extended in a step-wise manner until the gains in predictive ability are outweighed by the added complexity, similar to step-wise regression. Complexity of the final gradient boosting model may be controlled to avoid over-fitting the data by adjusting several model parameters: tree complexity, learning rate and bag fraction. Given that the results of the GBMs will be compared to a standard multiple linear regression model, without interactions, the GBM parameters were set to generate simplified tree structures:

Tree complexity = 1
Learning rate = 0.1
Bag fraction = 0.5.

Multiple linear regression and boosting gradient model approaches were applied using the log-transformed, atmospherically-corrected RGB bands of the IKONOS image as the independent variables (Figure 1.22), with corrected sonar data as the dependent variable. For the RGB image band files in the DOS_{1%} treatment group, raw satellite data were calibrated to TOA radiance, with the DOS correction producing at-surface radiance values. In the case of the 6SV treatment group, the atmospheric correction was performed on TOA reflectance, resulting in

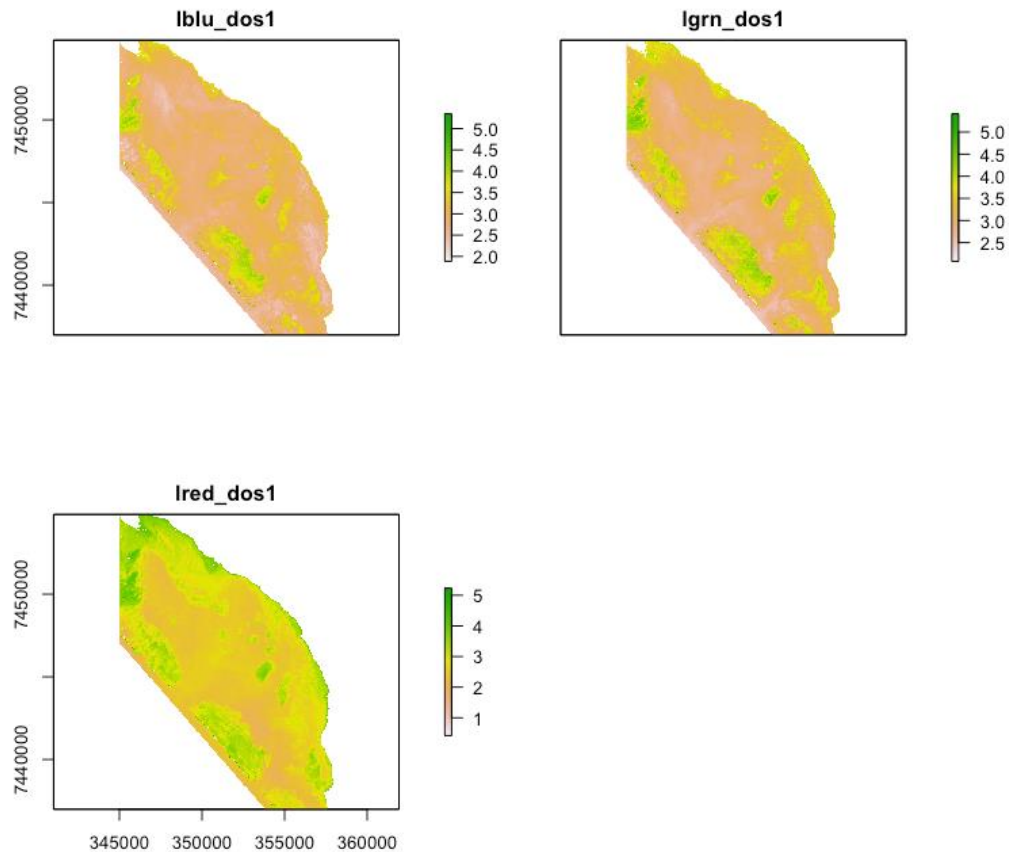


Figure 1.22. Example of the log-transformed, DOS_{1%}-corrected RGB bands used as the independent variable in the statistical models

surface reflectance values that were used in the statistical models. Sonar data (n= 9346) were randomly sampled to create 70% training and 30% testing datasets. Multiple linear regression and gradient boosting models were fitted to DOS_{1%} and 6SV corrected datasets to produce a total of four statistical model – dataset combinations. Model performance criteria, adjusted R² and predictive accuracy, were used to evaluate:

- atmospheric correction techniques – DOS_{1%} versus 6SV, and
- statistical approaches for determining depth from multispectral imagery – multiple linear regression (Lyzena method) versus gradient boosting models.

The final selected dataset and model were then used to create the bathymetric map of the Bay of Ranobe.

Benthic habitat classification

Over the last two decades, coral reef ecologists have taken advantage of the growing number, and increasing sophistication, of air- and satellite-borne spectral sensors available for the classification and mapping of benthic habitat complexity, composed of benthic habitat types and geomorphological units (Mumby *et al.*, 1997; Mumby *et al.*, 1998; Holden and LeDrew, 1998; Lubin *et al.*, 2001; Call *et al.*, 2003). At the same rate that these technologies have evolved, computing power and analytical methods have evolved at an equal pace. For example, based on principles of photogrammetry, advances in computing power have allowed for the creation of 3-dimensional images from simple RGB cameras, a technology fueled by the drone industry known as “structure from motion” (SfM). Analyses once conducted using simple linear regression and regression trees have been supplanted, in certain cases, by the development of machine learning algorithms, such as gradient boosting, as this class of analytical methods continuously progresses towards the refinement of artificial intelligence technologies. Similarly, advances in analytical approaches to image classification have been observed in recent years: object-oriented classification approaches, segmentation, artificial neural networks, and variations of regression-tree techniques, such as the random forests and gradient boosting algorithms (Bakran-Petricioli *et al.*, 2006; Hasan, *et al.*, 2012; Wahidin *et al.*, 2015). Despite the increasing sophistication of these analysis techniques, available data quantity and/or quality may affect, or limit, which approach can be used.

Although the IKONOS-2 image awarded for use in the present study, in 2011, was considered at that time a relatively ‘advanced’ technology, given its high spatial resolution, with

only three water-penetrating bands, the ability to discriminate habitat classes is limited (Mumby *et al.*, 2002; Palandro *et al.*, 2003a; Palandro *et al.*, 2003b; Collings *et al.*, 2018). In addition, as has been indicated in previous sections, the specific image scene analyzed here suffers from unusually high levels of suspended sediments for a coral reef environment, thereby reducing the signal-to-noise ratio and further diminishing discriminatory power. Consequently, a supervised / unsupervised hybrid approach was adopted, with a simple classification scheme, which allowed for the creation of a basic, yet reliable, product for use in later stages of the present research, and a foundation for future research.

The benthic habitat sampling strategy consisted, initially, in visually identifying areas of uncertainty of benthic habitat types found within the lagoon system on the satellite image. Rather than employing a random sampling approach, these areas of uncertainty were targeted for underwater visual assessments and for the collection of photo-quadrats. A total of 153 potential sites were identified for assessment, with surveys conducted in July 2013 (Figure 1.23). Of the total number of identified sites, 140 sites were sampled that were near or at the identified coordinates, depending on safety and accessibility of the site. In addition to photo-quadrats, series of aerial images for the Bay of Ranobe was obtained for reference purposes (Figure 1.24).

Image processing consisted of an unsupervised classification of the water-leaving radiances of the atmospherically-corrected RGB image bands, using the standard ISODATA algorithm (Iterative Self-Organizing Data Analysis Technique). An initial, low-cluster (3-5 clusters) ISODATA classification was conducted to isolate and extract the geomorphological unit map product. For benthic habitat classification, a “cluster-busting” approach was employed to initially partition the multivariate image data into fine clusters. ISODATA clustering parameters were set to 25-30 clusters with 95% convergence. Final convergence after 15 passes

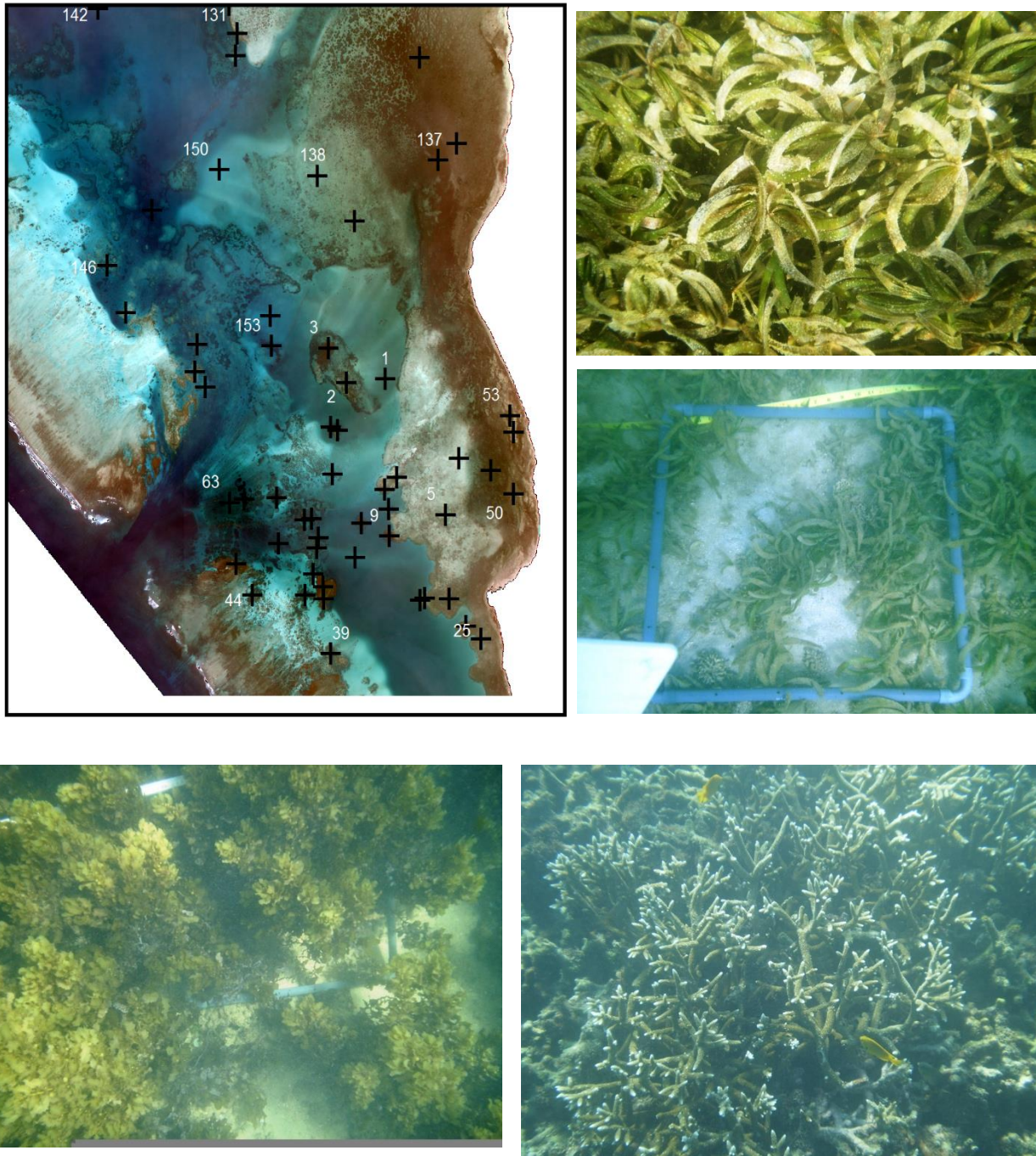


Figure 1.23. South pass in southern part of lagoon, with some of the sites targeted for benthic photo-quadrats marked with cross (+); examples of benthic habitat diversity: (clockwise) dense seagrass (*Thalassodendron ciliatum*), moderate density seagrass (*T. ciliatum*), coral thicket (*Acropora spp.*), and *Sargassum spp.*



Figure 1.24. Aerial view of the Rose Garden marine reserve (top) – a patch reef dominated by the rose-like coral of the genus, *Montipora*; located near sampling point #2 on the map in Figure 1.23

of the data produced 14 clusters with an 80% convergence rate. Data clusters were recoded manually, resulting in a re-grouping of clusters, to correspond to the best achievable benthic habitat classification scheme.

1.3 Results

Statistical models: Water depth retrieval

Multiple Linear Regression

To differentiate, in terms of performance, between the DOS_{1%} and 6SV atmospheric correction techniques, radiance values of DOS-corrected band files and reflectance values of 6SV-corrected band files were used in multiple linear regression (MLR) and gradient boosting models (GBM) to model depth. Results of the MLR-DOS indicated a significant regression equation was found ($F_{(3,6539)} = 6128$, $p < 0.001$), with an adjusted $R^2 = 0.7375$. All of the regression terms were highly significant (Table 1.8). Predictions of the final model were evaluated against test dataset, with a calculated RMSE = 1.28 m. Similarly, the results of the MLR-6SV model indicated a significant regression equation was found ($F_{(3,6539)} = 5653$, $p < 0.001$), with an adjusted $R^2 = 0.7216$. For MLR-6SV model, all of the regression terms except the intercept were found to be highly significant (Table 1.8). Predictions of the final MLR-6SV model were found to have a RMSE = 1.31 m. (See Appendices 1.6-1.7 for regression diagnostic plots)

Term plots for both of the models similarly indicate relatively strong log-linear relationships between radiance / reflectance and depth, particularly for the blue and green bands (Figure 1.25). Interestingly, based on the principles of attenuation of light, all of the bands should exhibit a negative log-linear relationship with increasing water depth. However, the blue

Table 1.8. MLR-DOS regression results

Model	Coefficient	Estimate	Std. Error	t-value	Pr(> t)
MLR-DOS	Intercept	14.72471	0.14234	103.44275	< 0.001
MLR-DOS	Lblu dos1	12.00551	0.12715	94.41750	< 0.001
MLR-DOS	Lgrn dos1	-14.96265	0.14598	-102.49185	< 0.001
MLR-DOS	Lred dos1	0.70173	0.07356	9.53842	< 0.001
MLR-6SV	Intercept	-0.08388	0.21575	-0.38877	0.69745
MLR-6SV	Lblu 6sv	13.22919	0.14615	90.51235	0.000
MLR-6SV	Lgrn 6sv	-18.69340	0.19141	-97.66052	0.000
MLR-6SV	Lred 6sv	0.91045	0.08210	11.08837	0.000

and red bands demonstrate a positive relationship, which may be indicative of high levels of suspended sediments causing increasing levels of reflected light at depth, in the case of the blue band, and interactions with benthic vegetation in the case of the red band.

The partial residual plots in Figures 1.26-1.27 illustrate how well the log-transformed image bands generally conform to a linear relationship. Results of the MLR indicate that there is partial non-linearity in the red band, as indicated by scattering of plotted residuals. Again, the low-energy, red band scatter is likely due to the influence of the reflective / absorptive properties of shallow-water bottom types, such as seagrasses and algae. Greater levels of scattering in the blue band, as compared to the green band, are the likely result of water column constituents.

Gradient Boosting Models

Results of the gradient boosting models fitted to the same DOS-corrected and 6SV-corrected datasets indicated that there was no significant difference between the datasets in predicting depth. For both the GBM-DOS1% and GBM-6SV, the optimal number of trees fitted were 1850 (Figure 1.28). Similarly, the mean total deviance (5.981), mean residual deviance

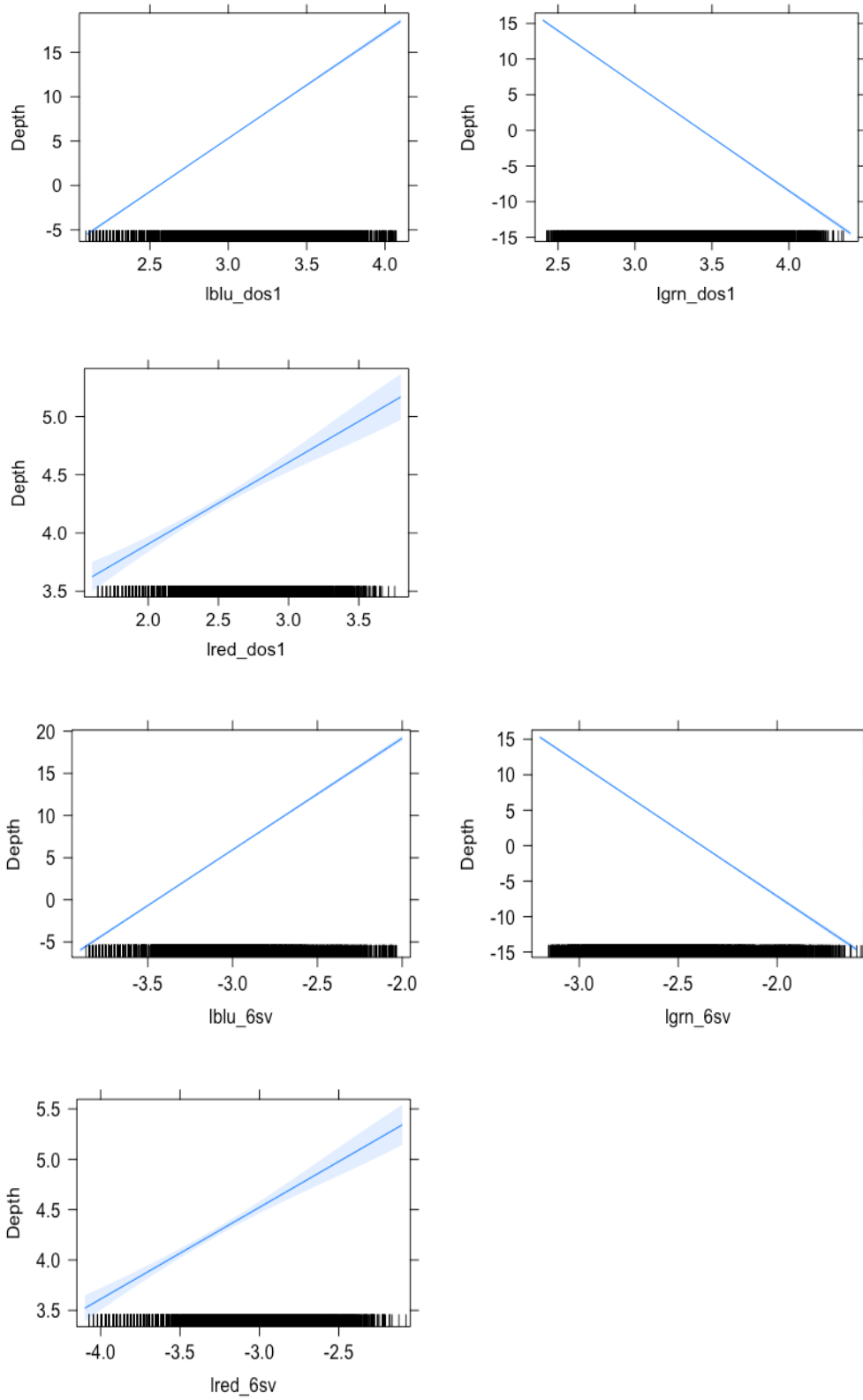


Figure 1.25. Regression term plots for the RGB DOS-corrected bands (top 3 plots) and RGB 6SV-corrected bands (bottom 3 plots)

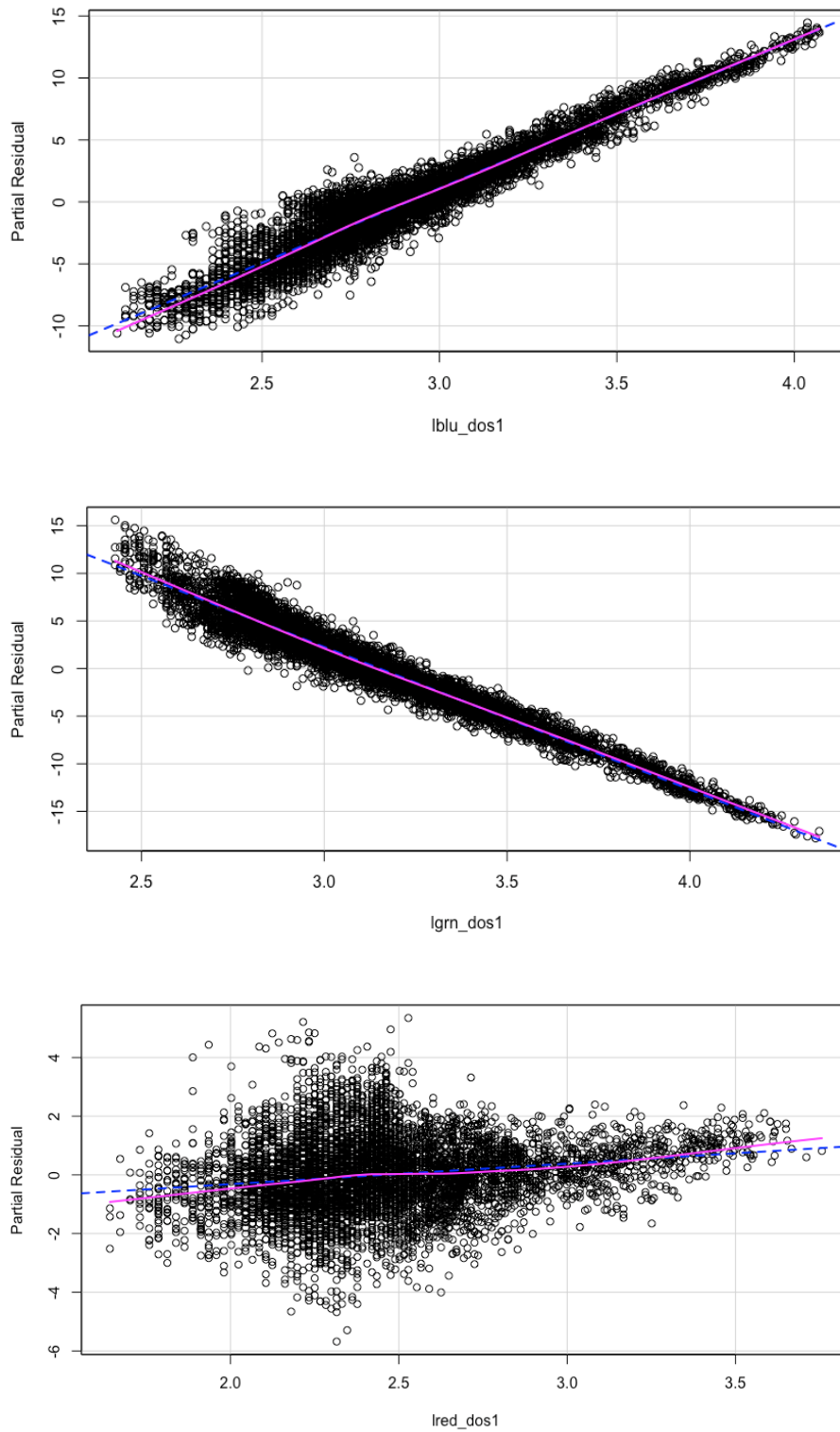


Figure 1.26. Partial residual plots of the multiple linear regression model fitted with $DOS_{1\%}$ data, with log blue band (top), log green band (middle), and log red band (bottom); loess fit (pink line) and linear fit (dashed blue line)

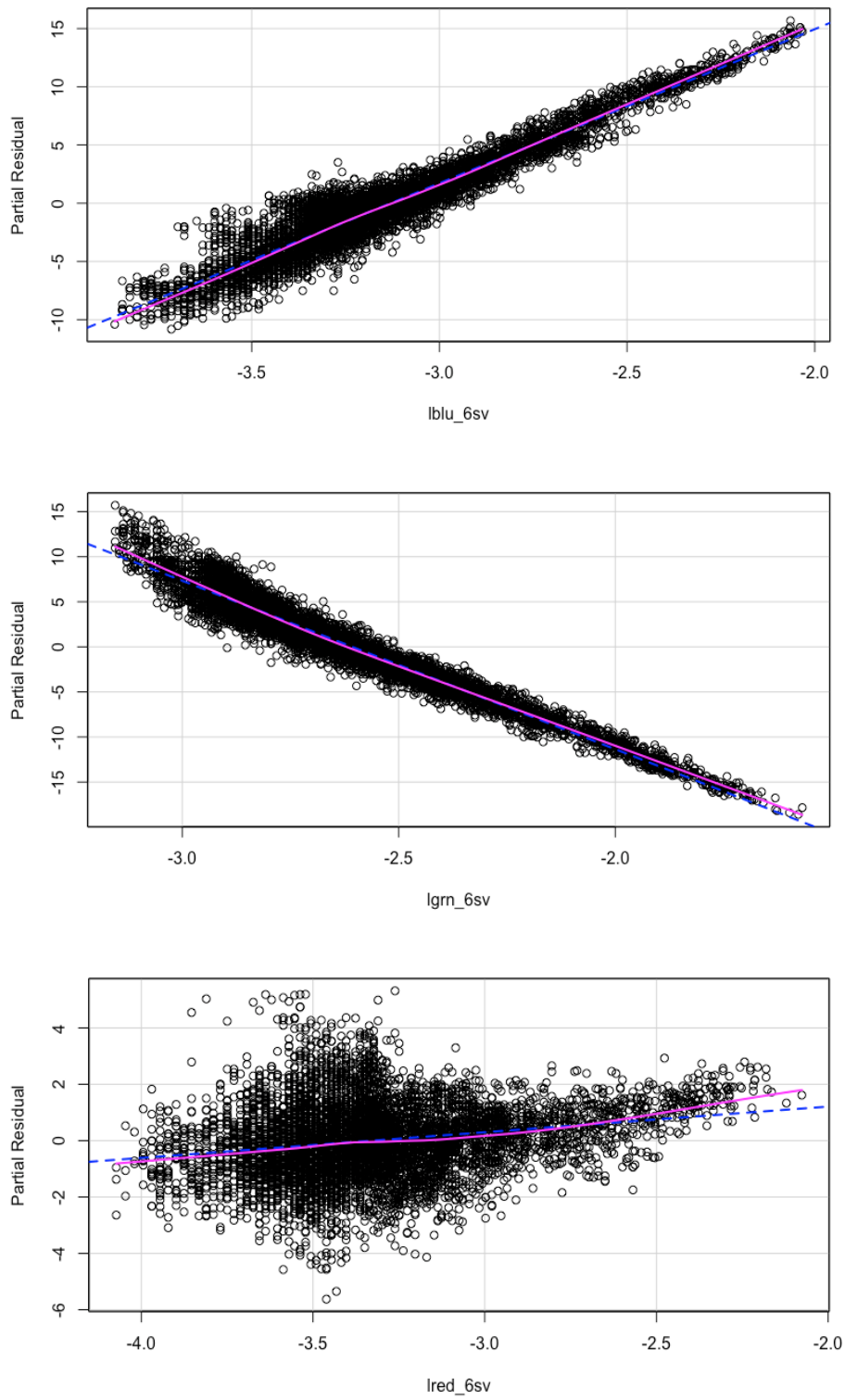


Figure 1.27. Partial residual plots of the multiple linear regression model fitted with $DOS_{1\%}$ data, with log blue band (top), log green band (middle), and log red band (bottom); loess fit (pink line) and linear fit (dashed blue line)

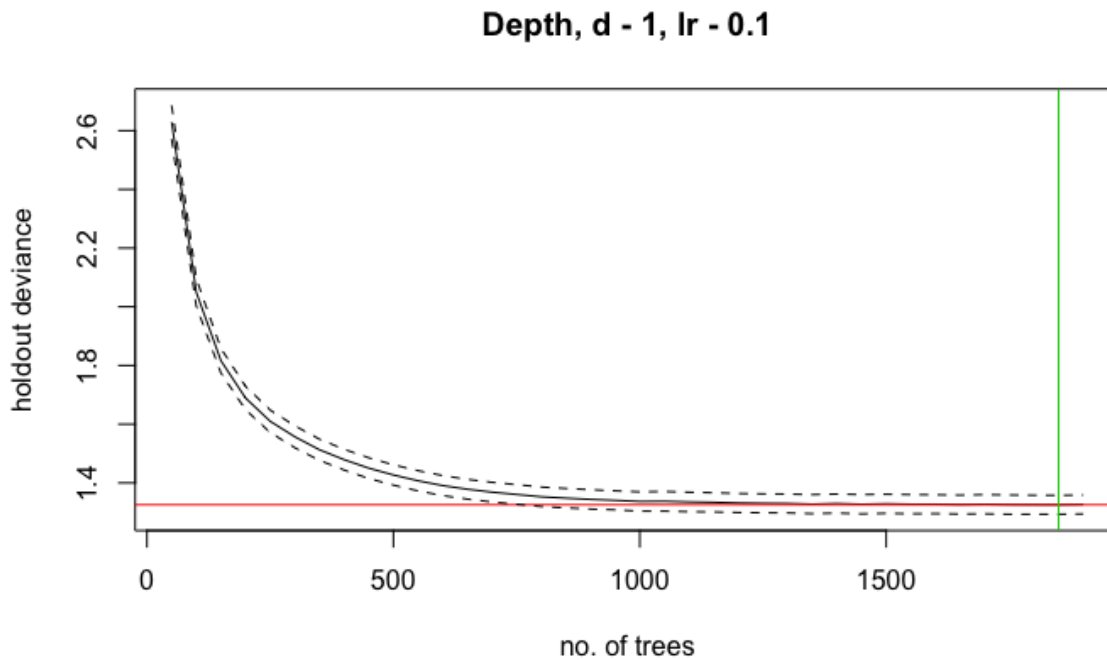


Figure 1.28. Gradient boosting algorithm model-fitting process: iterative minimization of the loss function, residual deviance, as regression trees are added to the existing model; green line indicates the final number of trees ($n = 1850$), given model parameters (tree complexity = 1, learning rate = 0.1)

(1.237), training data correlation (0.891), and predictive accuracy (RMSE = 1.175) were identical for both models. Moreover, the ranked contributions of the independent variables used in the model, a relative influence score, indicated that the partitioning of variance amongst variables was also identical (Table 1.9, Figure 1.29), resulting in identical relationships being fitted for each of the model terms (Figures 1.30-1.31).

Summary of Atmospheric Correction and Statistical Model Comparisons

Multiple linear regression and gradient boosting models were fitted to DOS1% and 6SV atmospherically corrected satellite image data to determine, firstly, which of the atmospheric correction techniques provided for the greatest predictive accuracy of modeled depths. Comparisons were based on the predictive accuracy of fitted models, as determined by the

Table 1.9. Relative influence scores for the gradient boosting models fitted to the 2 datasets

Dataset	Variable	Relative Influence Score
DOS _{1%}	Log(green) band	46.79155
DOS _{1%}	Log(red) band	31.13195
DOS _{1%}	Log(blue) band	22.07650
6SV	Log(green) band	46.79155
6SV	Log(red) band	31.13195
6SV	Log(blue) band	22.07650

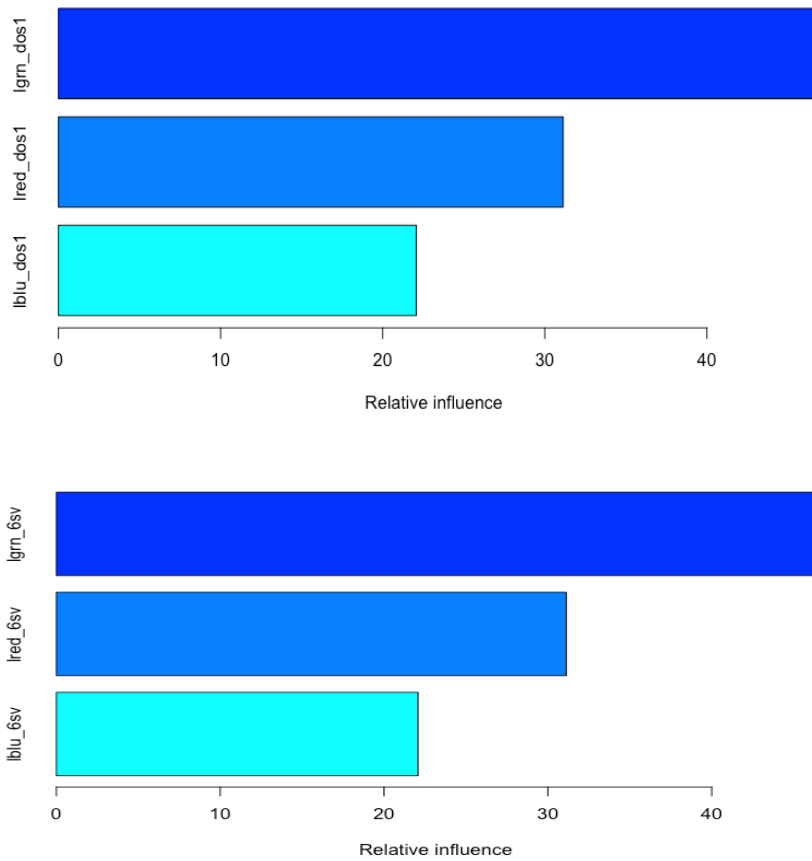


Figure 1.29. Visualization of relative influence scores for the DOS_{1%} (top) and 6sv (bottom) models

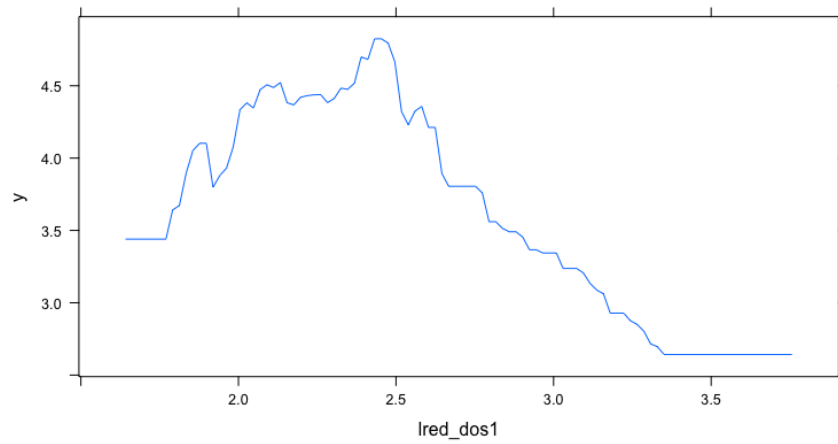
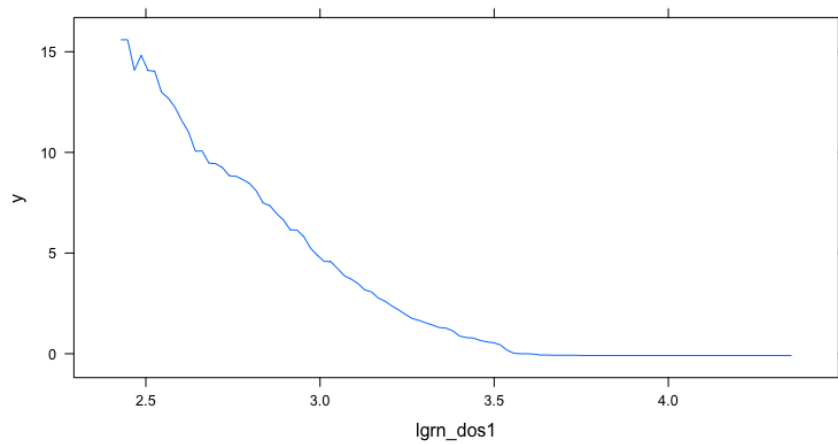
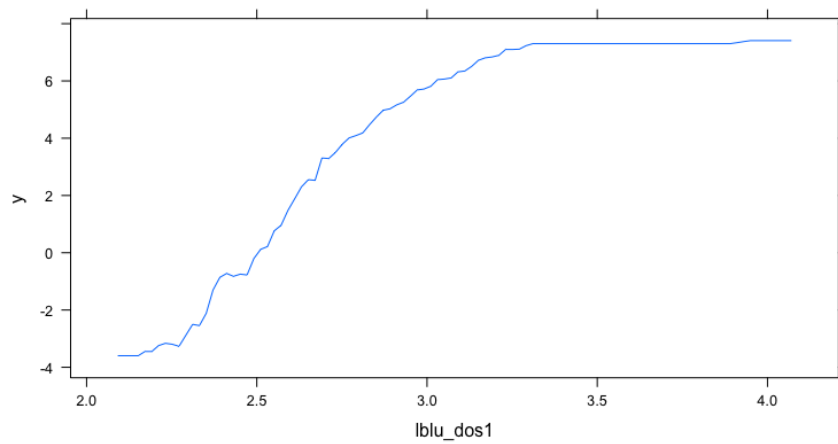


Figure 1.30. Functional relationships of the gradient boosting model fitted to log-transformed, $DOS_{1\%}$ data for each band: blue (top), green (middle) and red (bottom)

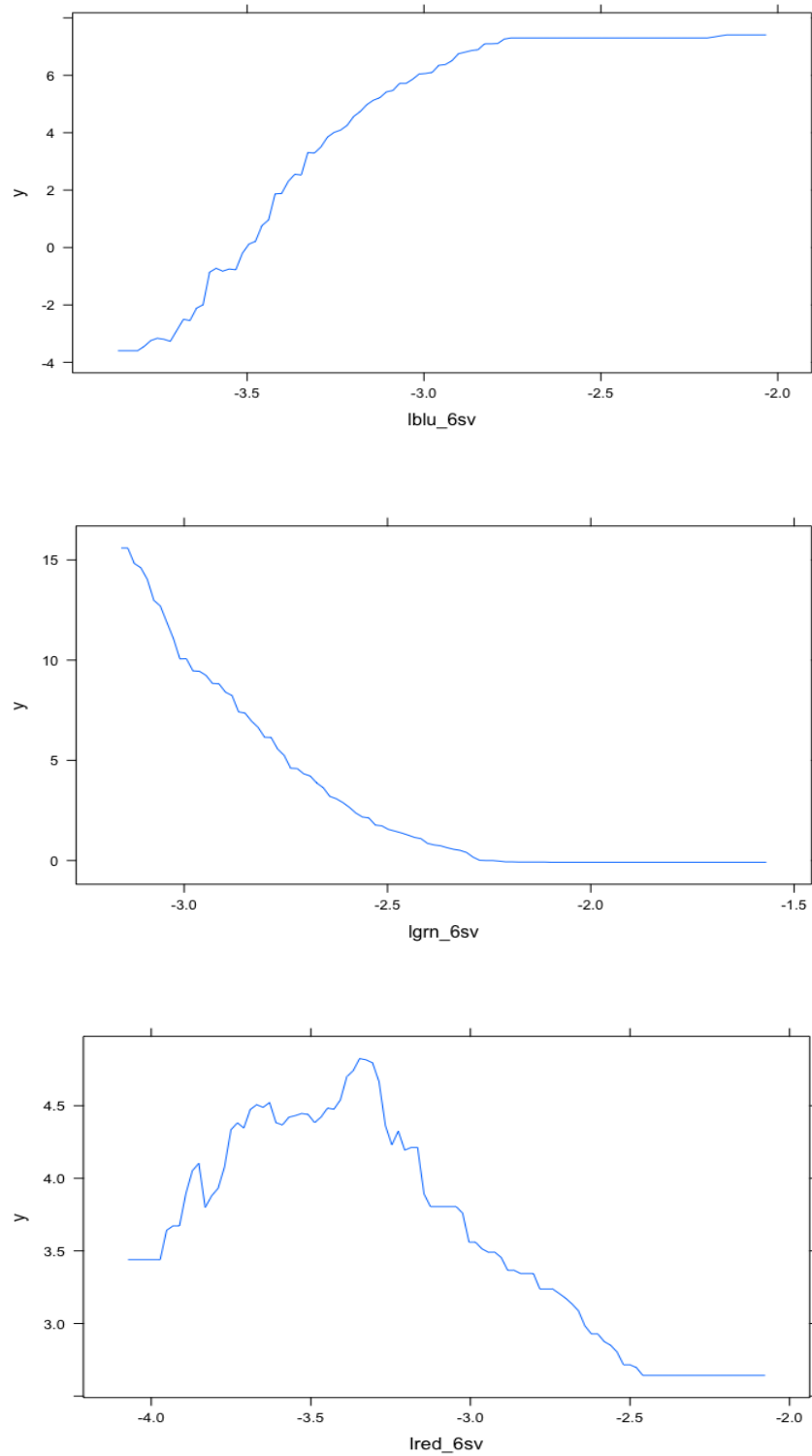


Figure 1.31. Functional relationships of the gradient boosting model fitted to log-transformed, 6SV data for each band: blue (top), green (middle) and red (bottom)

minimization of the RMSE values on a test dataset, and standard regression metrics. Metrics for the multiple linear regression models, the adjusted R^2 and RMSE values, equaling 0.7375 / 1.28 and 0.7216 / 1.31 m for the DOS_{1%} and 6SV models, respectively, indicate that DOS_{1%} technique performed marginally better. Metrics of the gradient boosting models, *i.e.* the mean total deviance (5.981), mean residual deviance (1.237), training data correlation (0.891), and predictive accuracy (RMSE = 1.175), produced identical results for the two datasets, indicating no clear advantage of either atmospheric correction method was detected using the gradient boosting model approach.

Secondly, comparisons were made between the accuracy of the multiple linear regression-based Lyzenga depth retrieval approach and that of the more modern, non-parametric, machine learning algorithm, gradient boosting. Predictive accuracy of the GBM versus MLR, 1.175 m versus 1.28-1.31 m, respectively, indicate the improved predictive abilities of even a simplified (tree complexity = 1) boosted model. Furthermore, the non-parametric nature of the GBM appears to have benefitted from the information content of the red band. In the case of the linear model, linear constraints on the functional relationship produced a weakly positive relationship for the red band (Figures 1.26 - 1.27). However, contrary to the linear model, the unconstrained GBM algorithm appears to have benefited, to some extent, from some of the unexploited information content in the blue and red bands (Figures 1.30 – 1.31). Figure 1.32 illustrate some of the biases that remain in the model residuals at the extremes of the depth range, where in the case of the GBM plot, residuals occur closer to the zero centerline.

Despite the simplicity of the approach, the statistical models trained and tested with the DOS_{1%} datasets provided marginally higher prediction accuracies, proving why the technique is still in-use today (*e.g.* Kanno and Tanaka, 2012; Figueiredo *et al.*, 2016; Manessa *et al.*, 2018).

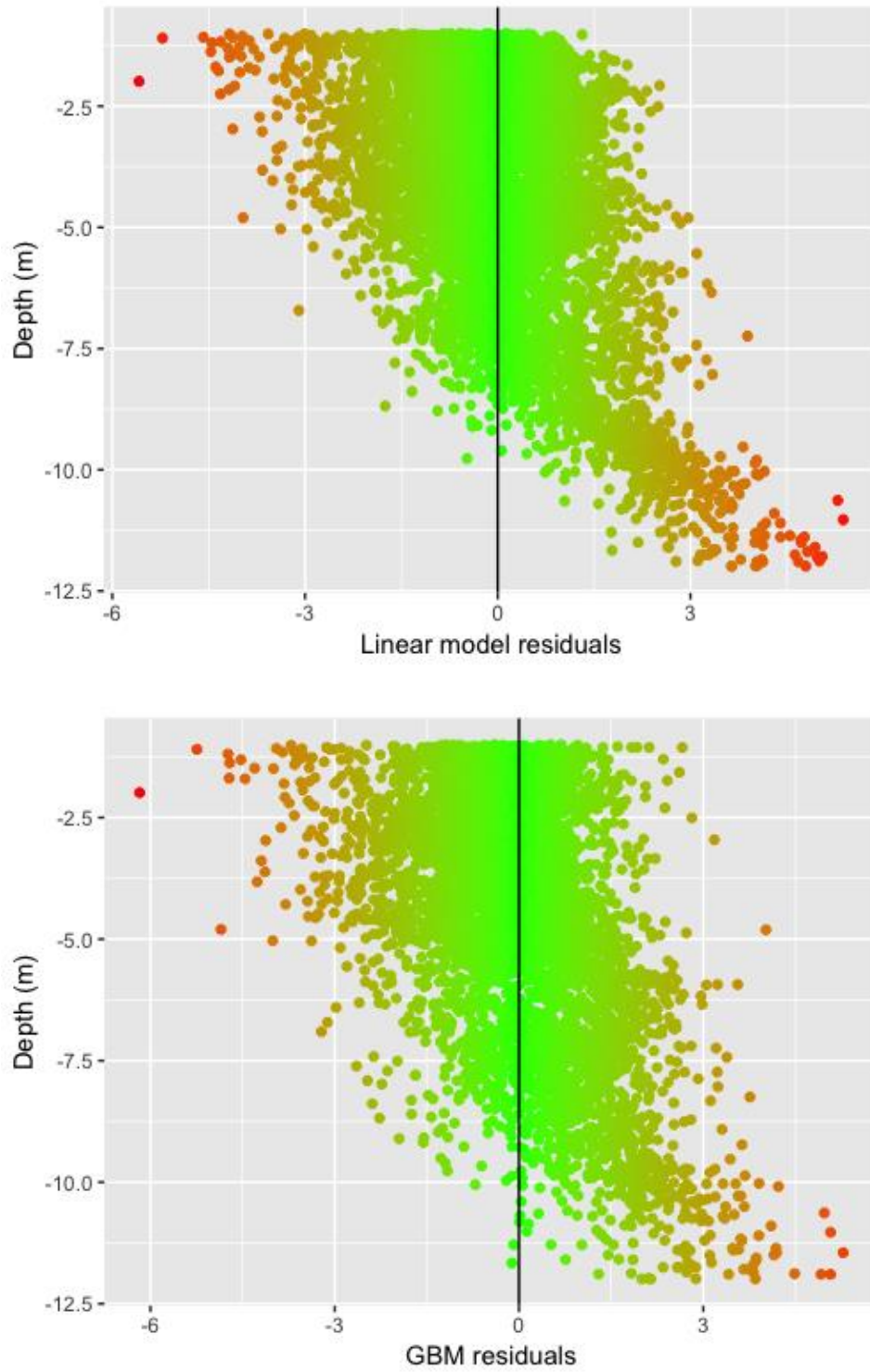


Figure 1.32. Model residuals plotted against water depth to illustrate biases resulting from each model type, MLR (top) versus GBM (bottom), particularly at depth extremes

Gradient Boosted Model Optimization

In terms of statistical models, comparisons demonstrated that the gradient boosting model not only provided marginally higher prediction accuracies, as compared to multiple linear regression, but also this technique provides the ability to fine tune the results by optimizing the model parameters, e.g. tree complexity and learning rate. Consequently, DOS1% data were modeled using gradient boosting approach to produce the final bathymetric map.

For the final model, tree complexity was increased (tree complexity = 2) to allow for some of the interaction effects that are likely occurring between RGB bands, benthic vegetation, and water depth in the shallow-water coastal zone. Output of the final gradient boosting model, comprised of 1950 trees, indicated a mean residual deviance = 0.81, a training data correlation = 0.93, and a predictive RMSE = 1.01 m. Relative influence scores suggested that, indeed, some of the explained portion of the variance shifted from the green band to the red and blue bands (Table 1.10), resulting in modifications to the functional relationships depicted in the term plots (Figure 1.33). A plot of the model residuals versus depth illustrates the reduction in model biases at extreme depths, as the residuals at the extremes move closer to the zero centerline (Figure 1.34). Prediction results of the final model were mapped to create the bathymetric map product (Figure 1.35).

Benthic Habitat and Geomorphology Products

The supervised / unsupervised hybrid classification approach of the IKONOS scene, after re-grouping and processing, produced four geomorphologic units and five basic benthic habitat types:

Geomorphological units

1. Intertidal zone

2. Reef Flat or Lagoon Floor

Table 1.10. Comparison of relative influence scores for the final GBM, tree complexity = 2, versus the scores for the GBM with tree complexity = 1

Dataset	Tree Complexity	Variable	Relative Influence Score
DOS _{1%}	2	Log(green) band	36.2054
DOS _{1%}	2	Log(red) band	35.4638
DOS _{1%}	2	Log(blue) band	28.3308
DOS _{1%}	1	Log(green) band	46.79155
DOS _{1%}	1	Log(red) band	31.13195
DOS _{1%}	1	Log(blue) band	22.07650

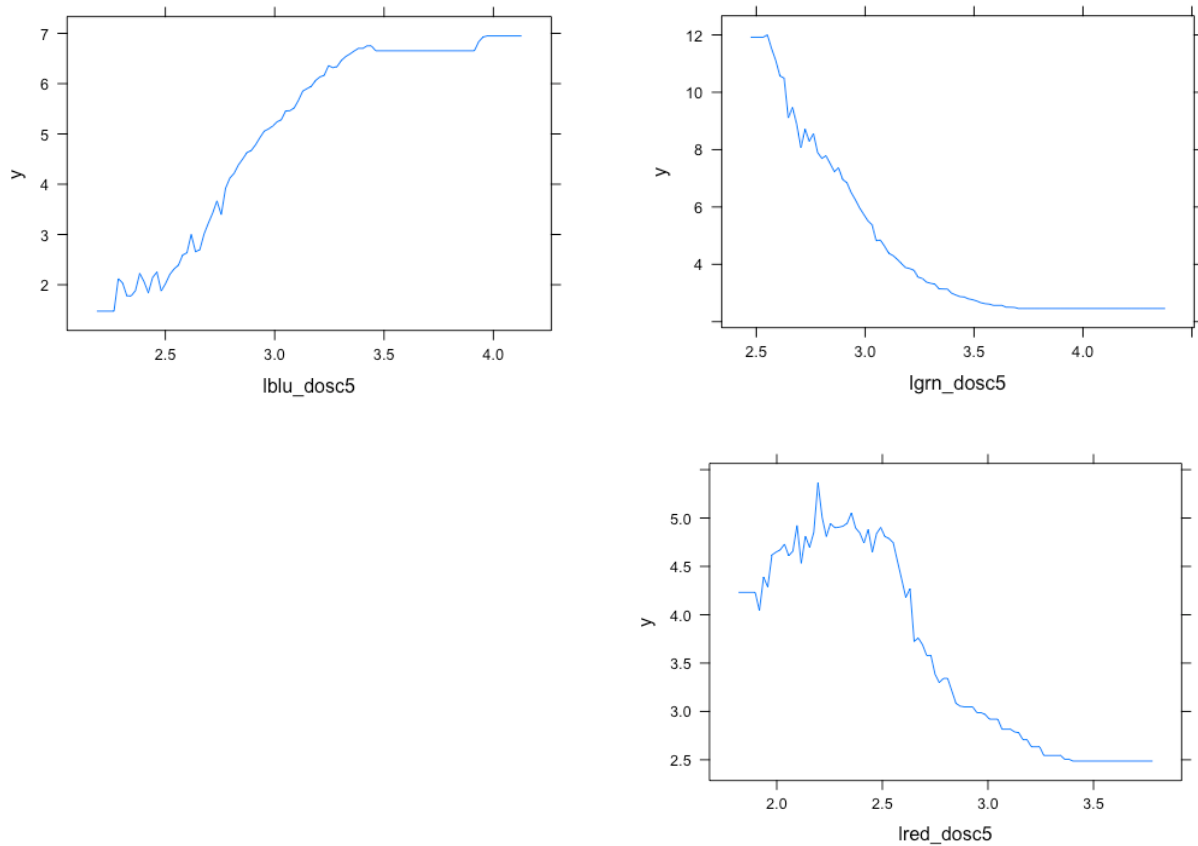


Figure 1.33. Term plots of the final gradient boosting model for each model term: log(blue), log(green), and log(red) (clockwise)

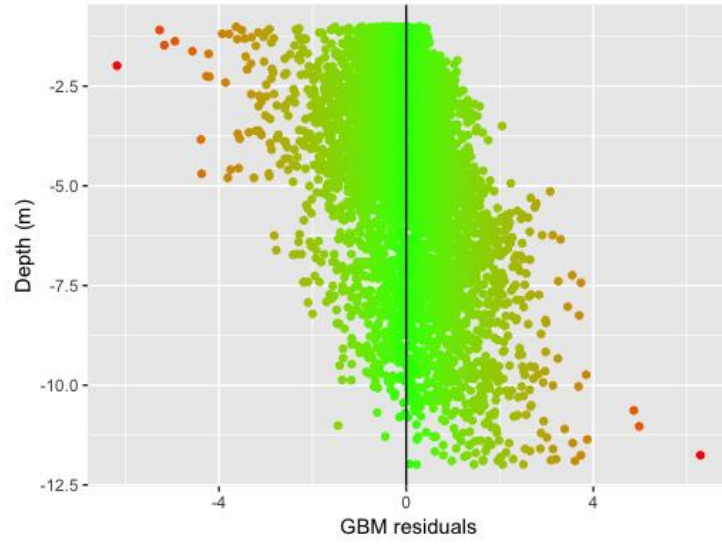


Figure 1.34. GBM final model residuals versus depth

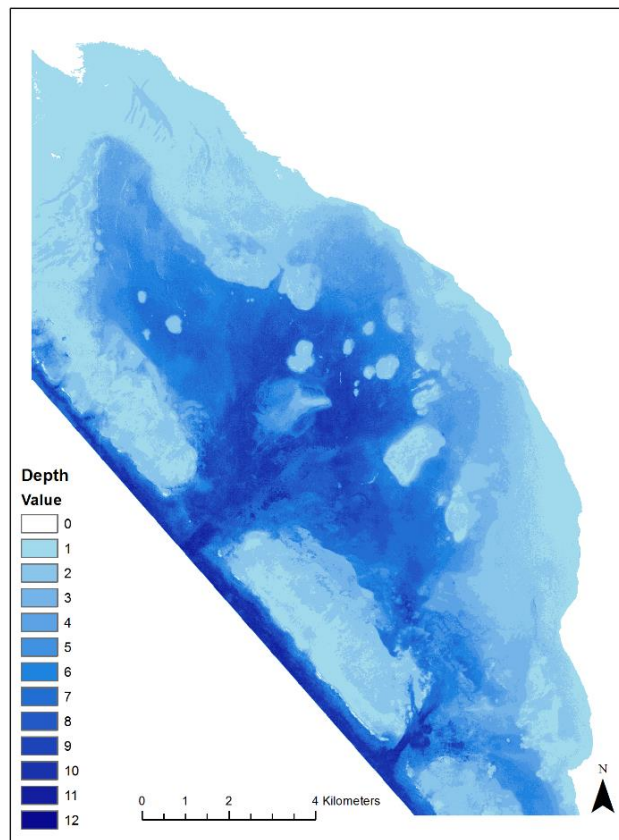


Figure 1.35. Bathymetric map product created from the prediction of the final gradient boosting model

3. Patch Reefs

4. Barrier Reef Crest

Habitat types:

1. Macroalgae

4. Sand / Silt

2. Seagrass / Macroalgae Mix

5. Sand

3. Seagrass

The inability to spectrally differentiate habitat types from multispectral image scenes, with few bands and low signal-noise, is illustrated by, amongst other things, the black patches found throughout the lagoon (Figure 1.36). The black patch at the north end of the lagoon is the result of high levels of suspended sediments originating from the river in the north, the Manombo River. Sporadic black patches and linear features are the result of seagrass windrows on the water surface. At the north pass, the optically-deep water, naturally, provides no signal of bottom reflectance, however, just inside the lagoon the water shallows and a seagrass bed is spectrally “confused” with deep water. Even at the shallow depths of the intertidal and sub-tidal zones, black patches occur where seagrass / macroalgae bottom types are spectrally indistinguishable from deep water. Given the quality of the image data, a formal accuracy assessment was not performed.

1.4 Discussion

In this chapter, the foundations were laid for future coral reef fisheries and ecological research in the Bay of Ranobe through the characterization and quantification of some of the most fundamental aspects of the marine environment: weather, water depth, and benthic habitat

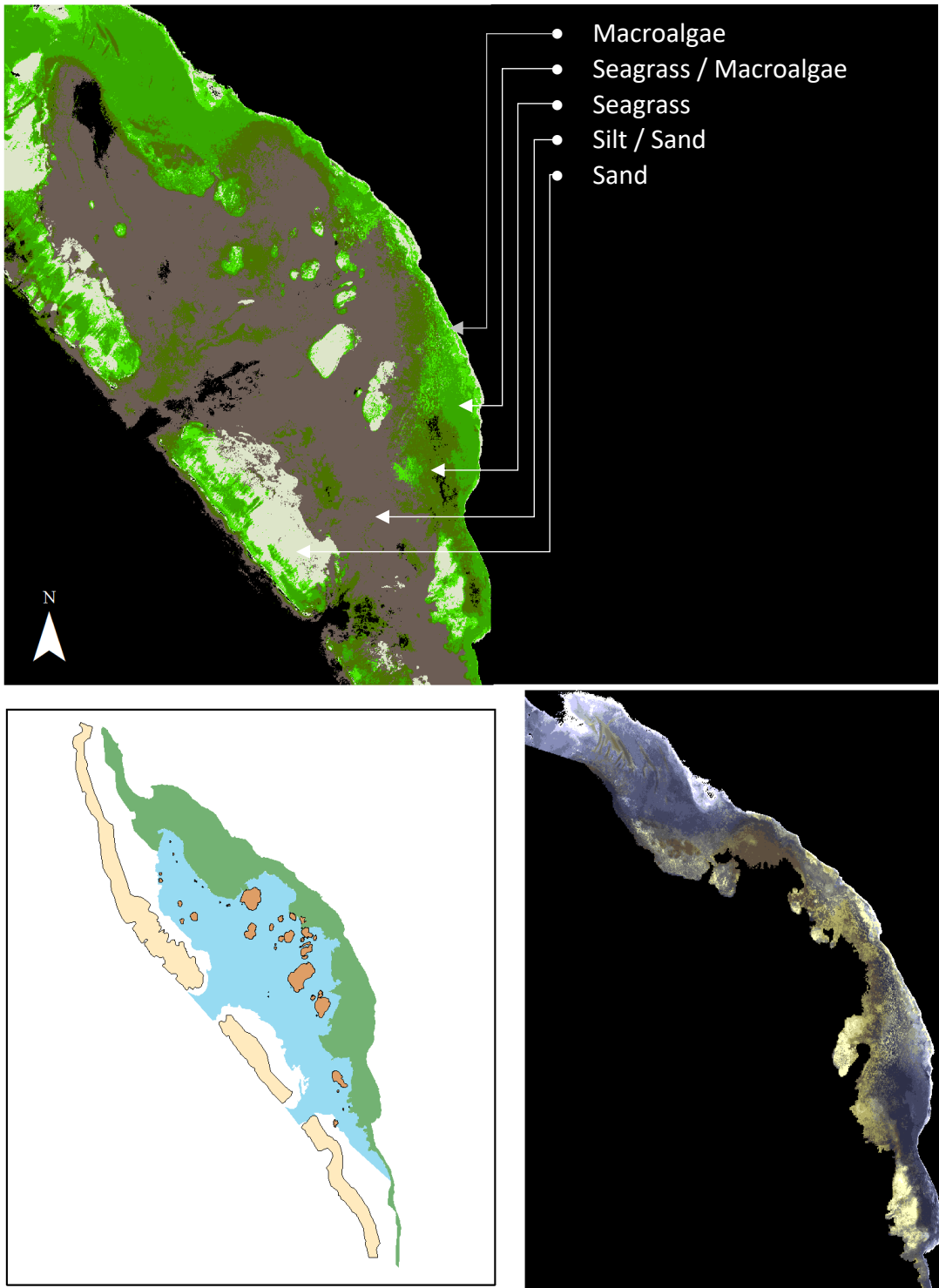


Figure 1.36. Benthic habitat classification for the Bay of Ranobe, with classes including: macroalgae, seagrass / macroalgae, seagrass, sand / silt, and sand (top); geomorphological zones of the Bay (bottom-left); example of cluster-busting classification of the intertidal zone

complexity. In the process of creating the principle products of this section, the benthic habitat and bathymetry maps, basic data collection and assessments were required, given the lack of historical research, which began with characterization of the most basic natural phenomenon, the tides.

After comparisons were made between observed and predicted tide levels, the most reliable source of tidal prediction software for the region was determined to be the open-source Mr. Tides software package. Predicted tide levels were used to correct the sonar dataset that was collected using consumer-grade equipment in an opportunistic manner. Although concerns could be raised relative to the potential inaccuracies associated with the consumer-grade sonar and/or GPS equipment used here, any inaccuracies of the sonar data, however, likely fall within the margins of error of the tidal predictions. Moreover, reducing the resolution of the analyses to 5 m may have compensated, to some extent, for any positional inaccuracies attributable to the GPS unit. Nonetheless, the opportunistic sampling of sonar data did have the potential to affect the final models, due to the spatially unbalanced distribution of sample points. As a consequence of this sampling approach, data points were, naturally, more intensively collected near the point of origin, or at the location from which the boat was launched. Sampling intensity then radiates out from the point of origin as an inverse-distance weighted function. Consequentially, the over-sampling of the shallow-water intertidal zone near the point of origin could have introduced biases into the regression models. Specifically, biases associated with the disproportionate amount of shallow-depth data that could prove influential to the determination of the regression slope, particularly for the red band where inherently the range of depths are already limited by the low-energy nature of longer wavelengths. Sources of biases implicated here are not limited to only the z-axis, but also potentially in the xy-axes, as well. Given the heterogeneity of the water

column properties across the lagoon, disproportionate sampling of the southeast corner of the lagoon could have failed to capture the variance present in the study site. The regression partial residual plots (Figures 1.26-1.27) do not appear, however, to justify these concerns. In the plots, particularly the plot of the red band model term, the mass of points on the left end of the fitted line is clearly visible. Regardless, the smooth-fit loess function does not deviate substantially from the linear model fit, indicating that the linear model was not unduly biased by the sampling strategy.

Secondly, of the comparisons made in the present chapter, the $DOS_{1\%}$ and 6SV atmospheric correction techniques were evaluated for the specific image scene used here. Within-model comparisons were made to determine which of the atmospheric correction techniques produced the best results in terms of prediction accuracies, whereas between-model comparisons were used to compare statistical approaches to modeling depth, which is discussed further in the paragraph(s) below. Results of the multiple linear regressions indicated that the model fit using the $DOS_{1\%}$ dataset provided slightly more accurate prediction results than the 6SV-corrected dataset, RMSE = 1.28 m and 1.31 m, respectively. Comparisons made using the same datasets fitted with the gradient boosting model produced identical results, RMSE = 1.175, indicating no difference between the datasets in predicting depth. Slight differences observed in the prediction accuracies of the multiple linear regression models for the two datasets could be attributed to the fact that for the $DOS_{1\%}$ correction data were calibrated to radiance values, whereas for the 6SV dataset values were calibrated to reflectance, resulting in a difference of data ranges affecting regression mechanics and not necessarily the accuracy of the datasets *per se*. Trials were conducted on centered and normalized datasets that did not produce results that significantly differed from those presented here. In general, as there were no significant

statistical differences between the atmospheric correction techniques, the simplest approach was selected for use in the principle comparison of this study, the depth retrieval models.

One of the earliest, and often cited, approaches to retrieving water depths from multispectral imagery has become to be known as the Lyzenga Method. Based on the principles of physics that describe the exponential decay, extinction, or attenuation, of wavelengths of light at depth, the Lyzenga method consists of the fitting of a log-linear regression model to the bands of multispectral imagery. Typically, only the blue and green wavelengths are used, given their abilities to penetrate water to greater depths, with blue (450 nm) reaching 200 m in depth in the clear waters of the open ocean. Depths attained by light decrease substantially in the coastal areas, where suspended sediments, phytoplankton, and other chromophores (*i.e.* collectively, the diffuse attenuation, K_d) scatter and absorb to varying degrees. Although the log-linear relationship between depth and light penetration may be robust in the presence of some suspended or dissolved chromophores, a key assumption of this approach is that chromophores are homogeneously distributed throughout the water column, vertically and laterally. In other words, it is assumed that the processes governing K_d are stationary.

Theoretically, the relatively direct application of the Beer-Lambert Law, as is done following the Lyzenga Method, is applicable at specific times and locations. However, given that coastal waters are generally characterized as hydrologically complex and dynamic environments, it may be more commonly the case that the processes governing suspended and/or dissolved species are non-stationary. As such, the relationship between depth and light may be log-linear for individual discretized “packets” of water with specific K_d properties and depth combinations, then a different log-linear relationship for a different water packet, so on and so forth. However, collectively these packets of water would exhibit a non-linear relationship.

Another conceptual model that may be appropriate, here, is to consider the water column, from an overhead perspective, as a mosaic of water column properties and depths for which a classification approach is appropriate. Regression tree modeling approaches are often used in such cases, where the classification or modeling of discontinuous phenomena is required. A tree-based regression approach, known as a gradient boosting model (GBM) was used to predict depths and produce a bathymetric map of the study area. Prediction accuracy of the GBM was compared to that of the standard Lyzenga Method. Rather than just the blue and green bands, the RGB bands were used for both models, with the parameters regulating complexity of the GBM set low for initial comparison purposes (tree complexity =1). Using a testing dataset, predictive accuracies of the models were determined to be 1.28 m and 1.175 m for the linear regression and GBM approaches, respectively. Increased tree complexity (tree complexity = 2) provided improvements on prediction results, RMSE = 1.01 m. In increasing tree complexity even further, submeter accuracies are attainable, however, risk of overfitting the model also increases. To fully optimize the GBM, ideally, an independent testing dataset would be available, rather than just a subset of the data used for training purposes. For the final GBM, tree complexity = 2 and the DOS1%-corrected image files were used as input to create the bathymetry map shown in Figure 1.35.

Differences in the predictive accuracies between the non-parametric GBM and the linear regression models indicates the presence of non-linearities, potentially non-linear interactions that are not captured by the regression model. In addition, the positive slope of the blue and red band terms in the fitted linear regression model, as compared to the form of the functional relationships achieved by the GBM approach are likely the result of the high suspended sediments predominantly affecting the blue band, and interference from bottom type(s) affecting

the red band. Nonetheless, considering the quality of the satellite image, accuracies of the Lyzenga Methods are consistent with published literature, with reported accuracies ranging from RMSE= 0.49 m – 1.27 m (Lyons et al., 2011; Bramante et al., 2013; Manessa et al., 2016). At the time that these analyses were first conceived, there were no published studies, known to the author, where the gradient boosting approach was used to model remote sensing data to retrieve water depth. Since, some studies have been conducted using statistical approaches that are similar, such as random forest regression and least square boosting, where accuracies attained were in the range of 0.50m - 0.85 m (Mannessa et al., 2016; Mohamed et al., 2016).

Results of these analyses were presented at the Western Indian Ocean Marine Science Association (WIOMSA) Symposium held in Maputo, Mozambique in 2013. (See Appendix 1.8 for presented poster)

Works Cited

- Andrefouet, Serge, Philip Kramer, Damaris Torres-Pulliza, Karen E. Joyce, Eric J. Hochberg, Rodrigo Garza-Perez, Peter J. Mumby, Bernard Riegl, Hiroya Yamano, William H. White, Mayalen Zubia, John C. Brock, Stuart R. Phinn, Abdulla Naseer, Bruce G. Hatcher and Frank E. Muller-Karger. 2003. Multi-site evaluation of IKONOS data for classification of tropical coral reef environments. *Remote Sensing of Environment*, 88: 128-143.
- Ariza, Alexander, Marina Robredo Irizar, and Steven Bayer. 2018. Empirical line model for the atmospheric correction of Sentinel-2A MSI images in the Caribbean islands. *European Journal of Remote Sensing*, 51: 765-776.
- Bakran-Petricioli, Tatjana, Oleg Antonic, Dragan Bukovec, Donat Petricioli, Ivica Janekovic, Josip Krizan, Vladimir Kusan, Sandro Dujmovic. 2006. Modelling spatial distribution of the Croatian marine benthic habitats. *Ecological Modelling*, 191: 96-105.
- Beger, Maria and Hugh P. Possingham. 2008. Environmental factors that influence the distribution of coral reef fishes: modeling occurrence data for broad-scale conservation and management. *Marine Ecology Progress Series*, 361: 1-13.
- Behrenfeld, Michael J. James T. Randerson, Charles R. McClain, Gene C. Feldman, Sietse O. Los, Compton J. Tucker, Paul G. Falkowski, Christopher B. Field, Robert Frouin, Wayne E. Esaias, Dorota D. Kolber and Nathan H. Pollack. 2001. Biospheric primary production during an ENSO transition. *Science*, 291: 2594-2597.
- Beman, J. Michael, Kevin R. Arrigo and Pamela A. Matson. 2005. Agricultural runoff fuels large phytoplankton blooms in vulnerable areas of the ocean. *Nature*, 434: 211-214.
- Bierworth, P.N., T.J. Lee, and R.V. Burne. 1993. Shallow sea-floor reflectance and water depth derived by unmixing multispectral imagery. *Photogrammetric Engineering and Remote Sensing*, 59: 331-338.
- Bigelow, Keith A., Christofer H. Boggs, Xi He. 1999. Environmental effects on swordfish and blue shark catch rates in the US North Pacific longline fishery. *Fisheries Oceanography*, 8: 178-198.
- Brando, Vittorio E., Janet M. Anstree, Magnus Wettle, Arnold G. Dekker, Stuart R. Phinn, and Chris Roelfsma. 2009. A physics based retrieval and quality assessment of bathymetry from suboptimal hyperspectral data. *Remote Sensing of Environment*, 113: 755-770.
- Bramante, James F., Durairaju Kumaran Raju, and Tsai Min Sin. 2013. Multispectral derivation of bathymetry in Singapore's shallow, turbid waters. *International Journal of Remote Sensing*, 34: 2070-2088.

- Call, Katherine A., John T. Hardy, and David O. Wallin. 2003. Coral reef habitat discrimination using multivariate spectral analysis and satellite remote sensing. *International Journal of Remote Sensing*, 24: 2627-2639.
- Chassot, Emmanuel, Sylvain Bonhommeau, Gabriel Reygondeau, Karen Nieto, Jeffrey J. Polovina, Martin Huret, Nicholas K. Dulvy, and Herve Demarcq. 2011. Satellite remote sensing for an ecosystem approach to fisheries management. *ICES Journal of Marine Science*, 68: 651-666.
- Chavez, Pat S. Jr. 1988. An Improved dark-object subtraction technique for atmospheric scattering correction of multispectral data. *Remote Sensing of the Environment*, 24: 459-479.
- Chavez, Pat S. Jr. 1996. Image-based atmospheric corrections – revisited and improved. *Photogrammetric Engineering and Remote Sensing*, 62: 1025-1036.
- Collin, A., Etienne, S. and E. Feunteun. 2017. VHR coastal bathymetry using WorldView-3: colour versus learner. *Remote Sensing Letters*, 8: 1072-1081.
- Collings, Simon, Norm A. Campbell, and John K. Keesing. 2018. Quantifying the discriminatory power of remote sensing technologies for benthic habitat mapping. *International Journal of Remote Sensing*, DOI: 10.1080/01431161.2018.1531316.
- Conger, Christopher L., Eric J. Hochberg, Charles H. Fletch, III, and Martin J. Atkinson. 2006. Decorrelating remote sensing color bands from bathymetry in optically shallow waters. *IEEE Transactions on Geoscience and Remote Sensing*, 44: 1655-1660.
- Costello, Christopher, Andrew Rassweiler, David Siegel, Giulio de Leo, Fiorenza Micheli and Andrew Rosenberg. 2010. The value of spatial information in MPA network design. *Proceedings of the National Academy of Science*, 107: 18294-18299.
- Diersson, Heidi and Richard C. Zimmerman. 2003. Ocean color remote sensing of seagrass and bathymetry in the Bahamas Banks by high-resolution airborne imagery. *Limnology and Oceanography*, 48: 444-455.
- Eugenio, Francisco. 2015. High-resolution maps of bathymetry and benthic habitats in shallow-water environments using multispectral remote sensing imagery. *IEEE Transactions on Geoscience and Remote Sensing*, 53: 3539-3549.
- Eugenio, Francisco, Javier Marcello, Javier Martin, and Dionisio Rodriguez-Esparragon. 2017. Benthic habitat mapping using multispectral high-resolution imagery: Evaluation of shallow water atmospheric correction techniques. *Sensors*, 17: 2-23.
- Figueirido, Isabel N., Luis Pinto, and Gill Goncalves. 2016. A modified Lyzenga's model for multispectral bathymetry using Tikhonov regularization. *IEEE Geoscience and Remote Sensing Letters*, 13: 53-57.

- Gao, Jay. 2009. Bathymetric mapping by means of remote sensing: methods, accuracy and limitations. *Progress in Physical Geography*, 33: 103-116.
- Gordon, H.R. 1995. Remote sensing of ocean color: A methodology for dealing with broad spectral bands and significant out-of-band response. *Applied Optics*, 34: 8363-8374.
- Gordon, H.R. 1997. Atmospheric correction of ocean color imagery in the Earth Observing System era. *Journal of Geophysical Research*, 102: 17081-17106.
- Halls, J. and K. Costin. 2016. Submerged and emergent land cover and bathymetric mapping of estuarine habitats using 660rldview-2 and LiDAR imagery. *Remote Sensing*, 8: 1-21.
- Hasan, Rozaimi Che, Daniel Ierodiaconou, and Jacquomo Monk. 2012. Evaluation of four supervised learning methods for benthic habitat mapping using backscatter from multi-beam sonar. *Remote Sensing*, 4: 3427-3443.
- Hedley, J., Roelfsema, C., Koetz, B. and S. Phinn. 2012. Capability of the Sentinel 2 mission for tropical coral reef mapping and coral bleaching detection. *Remote Sensing of Environment*, 120: 145-155.
- Hogrefe, Kyler, Dawn J. Wright, and Eric J. Hochberg. 2008. Derivation and integration of shallow-water bathymetry: Implications for coastal terrain modeling and subsequent analyses. *Marine Geodesy*, 31: 299-317.
- Holden, H. and E. LeDrew. 1998. Spectral discrimination of healthy and non-healthy corals based on cluster analysis, principal components analysis, and derivative spectroscopy. *Remote Sensing of Environment*, 65: 217-224.
- IHO, 2016. Resolutions of the International Hydrographic Organization, Publication M-3 2nd Edition – 2010 Updated to December 2016. SECTION 2.2 – TIDES AND WATER LEVELS para 2 note (i)
- Jensen, J. R. 2007. Remote sensing of the environment: An earth resource perspective (2nd ed.). Upper Saddle River, NJ: Pearson Education, Inc
- Kanno, Ariyo and Yoji Tanaka. 2012. Modified Lyzenga's method for estimating generalized coefficients for satellite-based predictor of shallow water depth. *IEEE Geoscience and Remote Sensing Letters*, 9: 715-719.
- Karpouzli, E. and T. Malthus. 2003. The empirical line method for the atmospheric correction of IKONOS imagery. *International Journal of Remote Sensing*, 24: 1143-1150.
- Kim, Yongseung and Kwangjae Lee. 2005. An experimental study on the image-based atmospheric correction methods for high resolution multispectral data. *IEEE International Geoscience and Remote Sensing Symposium*.

- Klemas, Victor V. 2009. Remote sensing of coastal resources and environment. *Environmental Research, Engineering and Management*, 2: 11-18.
- Kotchenova, Svetlana Y., Eric F. Vermote, Raffaella Matarrese, and Frank J. Klemm Jr. 2006. Validation of a vector version of the 6S radiative transfer code for atmospheric correction of satellite data. Part I: Path radiance. *Applied Optics*, 45: 6762-6774.
- Kotchenova, Svetlana Y. and Eric F. Vermote. 2007. Validation of a vector version of the 6S radiative transfer code for atmospheric correction of satellite data. Part II. Homogenous Lambertian and anisotropic surfaces. *Applied Optics*, 46: 4455-4464.
- Kotchenova, Svetlana Y. Eric F. Vermote, R. Levy, and A Lyapustin. 2008. Radiative transfer codes for atmospheric correction and aerosol retrieval: intercomparison study. *Applied Optics*, 47: 2215-2226.
- Knudby, Anders, Ellsworth LeDrew, and Alexander Brenning. 2010. Predictive mapping of reef fish species richness, diversity and biomass in Zanzibar using IKONOS imagery and machine-learning techniques. *Remote Sensing of Environment*, 114: 1230-1241.
- Lee, Zhong-Ping, Kendall L. Carder, Curtis D. Mobley, Robert G. Steward, and Jennifer S. Patch. 1999. Hyperspectral remote sensing for shallow waters: 2. Deriving bottom depths and water properties by optimization. *Applied Optics*, 38: 3831-3843.
- Lee, Zhong-Ping, Mirosław Darecki, Kendall L. Carder, Curtiss O. Davis, Dariusz Stramski, and W. Joseph Rhea. 2005. Diffuse attenuation coefficient of downwelling irradiance: An evaluation of remote sensing methods. *Journal of Geophysical Research*, 110: 1-9.
- Lorenzen, Kai, Robert S. Steneck, Robert R. Warner, Ana M. Parma, Felicia C. Coleman and Kenneth M. Leber. 2010. The spatial dimensions of fisheries: putting it all in place. *Bulletin of Marine Science*, 86: 169-177.
- Lubin, Dan, Wei Li, Phillip Dustan, Charles H. Mazel, and Knut Stamnes. 2001. Spectral signatures of coral reefs: Features from space. *Remote Sensing of Environment*, 75: 127-137.
- Lyons, Mitchell, Stuart Phinn, and Chris Roelfsema. 2011. Integrating Quickbird multi-spectral satellite and field data: mapping bathymetry, seagrass cover, seagrass species and change in Moreton Bay, Australia in 2004 and 2007. *Remote Sensing*, 3: 42-64.
- Lyzenga, D.R. 1978. Passive remote sensing techniques for mapping water depth and bottom features. *Applied Optics*, 17: 379-383.
- Lyzenga, D.R. 1981. Remote sensing of bottom reflectance and water attenuation parameters in shallow water using aircraft and Landsat data. *International Journal of Remote Sensing*, 2: 71-82.

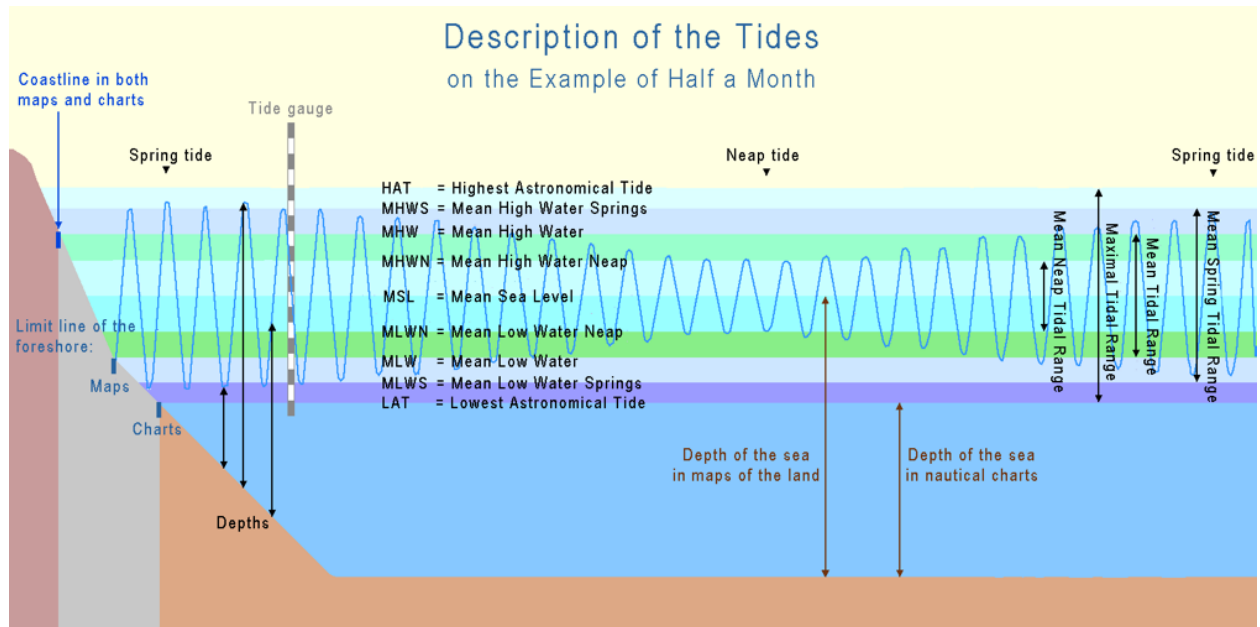
- Lyzenga, David R. 1985. Shallow-water bathymetry using combined lidar and passive multispectral scanner data. *International Journal of Remote Sensing*, 6: 115-125.
- Lyzenga, David R. Norman P. Malinas, and Fred J. Tanis. 2006. Multispectral bathymetry using a simple physically based algorithm. *IEEE Transactions on Geoscience and Remote Sensing*, 44: 2251-2259.
- Ma, S., Tao, Z., Yang, X., Yu, Y., Zhou, X. and Z. Li. 2014. Bathymetry retrieval from hyperspectral remote sensing data in optical-shallow water. *IEEE Transactions on Geoscience and Remote Sensing*, 52(2), pp.1205-1212.
- Mahiny, Abdolrassoul and Brian J. Turner. 2007. A comparison of four common atmospheric correction methods. *Photogrammetric Engineering and Remote Sensing*, 73: 361-368.
- Manessa, M.D.M., A. Kanno, M. Sekine, M. Haider, K. Yamamoto, T. Imai, and T. Higuchi. 2016. Satellite-derived bathymetry using random forest algorithm and Worldview-2 imagery. *Geoplanning*, 2: 117-126.
- Manessa, Masita Dwi Mandini, Ariyo Kanno, Tatsuyuki Sagawa, Masahiko Sekine, and Nurjannah Nurdin. 2018. Simulation-based investigation of the generality of Lyzenga's multispectral bathymetry formula in Case-1 coral reef water. *Estuarine, Coastal and Shelf Science*. 200: 81-90.
- Mishra, Deepak, Sunil Nuarumalani, Merlin Lawson, and Donald Rundquist. 2004. Bathymetric mapping using IKONOS multispectral data. *GIS Science and Remote Sensing*, 41: 301-321.
- Mishra, D.R., Narumalani, S., Rundquist, D., Lawson, M. and R. Perk. 2007. Enhancing the detection and classification of coral reef and associated benthic habitats: A hyperspectral remote sensing approach. *Journal of Geophysical Research: Oceans*, 112: 1-18.
- Mohamed, Hassan, Abdelazim Negm, Kazuo Nadoaka, Tark Abdelaziz, and Mohamed Elshabi. 2016. Comparative study of approaches to bathymetry detection in Nasser/Nubia Lake using multispectral SPOT-6 satellite imagery. *Hydrological Research Letters*, 10: 45-50.
- Moran, Susan M., Ray D. Jackson, Philip N. Slater, Phillippe M. Teillet. 1992. Evaluation of simplified procedures for retrieval of land surface reflectance factors from satellite sensor output. *Remote Sensing of Environment*, 41: 169-184.
- Mumby, P.J., E.P. Green, A.J. Edwards, and C.D. Clark. 1997. Coral reef habitat mapping: how much detail can remote sensing provide? *Marine Biology*, 130: 193-202.
- Mumby, P.J., E.P. Green, C.D. Clark, and A.J. Edwards. 1998. Digital analysis of multispectral airborne imagery of coral reefs. *Coral reefs*, 17: 59-69.

- Mumby, Peter J. and Alasdair J. Edwards. 2002. Mapping marine environments with IKONOS imagery: enhanced spatial resolution can deliver greater thematic accuracy. *Remote Sensing of Environment*, 82: 248-257.
- Mumby, Peter J., William Skirving, Alan E. Strong, John T. Hardy, Ellsworth F. LeDrew, Eric J. Hochberg, Rick P. Strumpf and Laura T. David. 2004. Remote sensing of coral reefs and their physical environment. *Marine Pollution Bulletin*, 48: 219-228.
- Norjamaki, I. and T. Tokola. 2007. Comparison of atmospheric correction methods in mapping timber volume with multitemporal Landsat images in Kainuu, Finland. *Photogrammetric Engineering and Remote Sensing*, 73: 155-163.
- Pacheco, A., Horta, J., Loureiro, C. and O. Ferreira. 2015. Retrieval of nearshore bathymetry from Landsat 8 images: A tool for coastal monitoring in shallow waters. *Remote Sensing of Environment*, 159, pp.102-116.
- Palandro, D., S. Andrefouet, P. Dustan, and F.E. Muller-Karger. 2003a. Change detection in coral reef communities using Ikonos satellite sensor imagery and historic aerial photographs. *International Journal of Remote Sensing*, 24: 873-878.
- Palandro, David, Serge Andrefouet, Frank E. Muller-Karger, Phillip Dustan, Chuanmin Hu, and Pamela Hallock. 2003b. Detection of changes in coral reef communities using Landsat-5 TM and Landsat-7 ETM+ data. *Canadian Journal of Remote Sensing*, 29: 201-209.
- Philpot, William D. 1989. Bathymetric mapping with passive multispectral imagery. *Applied Optics*, 28: 1569-1578.
- Pittman, S.J., J.D. Christensen, C. Caldow, C. Menza and M.E. Monaco. 2007. Predictive mapping of fish species richness across shallow-water seascapes in the Caribbean. *Ecological Modelling*, 204: 9-21.
- Pittman, Simon J., Bryan M. Costa, and Tim A. Battista. 2009. Lidar bathymetry and boosted regression trees to predict diversity and abundance of fish and corals. *Journal of Coastal Research*, 53: 27-38.
- Rees, M.J., Knott, N.A., Neilson, J., Linklater, M., Osterloh, I., Jordan, A. and A.R. Davis. 2018. Accounting for habitat structural complexity improves the assessment of performance in no-take marine reserves. *Biological Conservation*, 224: 100-110.
- Renema, Willem. 2017. Terrestrial influence as a key driver of spatial variability in large benthic foraminiferal assemblage composition in the Central Indo-Pacific. *Earth-Science Reviews*, 177: 514-544.
- Richards, Benjamin L., Ivor D. Williams, Oliver J. Vetter, and Gareth J. Williams. 2012. Environmental factors affecting large-bodied coral reef fish assemblages in the Mariana archipelago. *PloS One*, 7: 1-25.

- Roelfsema, C., Kovacs, E., Ortiz, J.C., Wolff, N.H., Callaghan, D., Wettle, M., Ronan, M., Hamylton, S.M., Mumby, P.J. and S. Phinn. 2018. Coral reef habitat mapping: A combination of object-based image analysis and ecological modelling. *Remote sensing of environment*, 208: 27-41.
- Sandidge, Juanita C. and Ronald J. Holyer. 1998. Coastal bathymetry from hyperspectral observations of water radiance. *Remote Sensing of Environment*, 65: 341-352.
- Santos, A. Miguel P. 2000. Fisheries oceanography using satellite and airborne remote sensing methods: a review. *Fisheries Research*, 49: 1-20.
- Shen, Xiang, Liming Jiang, and Quingquan Li. 2018. Retrieval of near-shore bathymetry from multispectral satellite images using generalized additive models. *IEEE Geoscience and Remote Sensing Letters*.
- Smith, G.M. and E.J. Milton. 1999. The use of the empirical line method to calibrate remotely sensed data to reflectance. *International Journal of Remote Sensing*, 20: 2653-2662.
- Song, Conghe, Curtis E. Woodcock, Karen C. Seto, Mary Pax Lenney, and Scott A. Macomber. 2001. Classification and change detection using Landsat TM data: when and how to correct atmospheric effects? *Remote Sensing of Environment*, 75: 230-244.
- Stumpf, Richard P., Kristine Holdried, and Mark Sinclair. 2003. Determination of water depth with high-resolution satellite imagery over variable bottom types. *Limnology and Oceanography*, 48: 547-556.
- Taylor, Martin. 2005. Ikonos Planetary Reflectance and Mean Solar Exoatmospheric Irradiance. Space Imaging Inc., Thornton, Colorado.
- Traganos, D. and P. Reinartz. 2018. Mapping Mediterranean seagrasses with Sentinel-2 imagery. *Marine pollution bulletin*, 134: 197-209.
- Traganos, D., Poursanidis, D., Aggarwal, B., Chrysoulakis, N. and P. Reinartz. 2018. Estimating satellite-derived bathymetry (SDB) with the google earth engine and sentinel-2. *Remote Sensing*, 10: 859.
- Vermote, Eric F., Didier Tanre, Jean Luc Deuze, Maurice Herman, and Jean-Jacques Morcrette. 1997. Second simulation of the satellite signal in the solar spectrum, 6S: An overview. *IEEE Transactions on Geoscience and Remote Sensing*, 35: 675-686.
- Wahidin, Nurhalis, Vincentius P. Siregar, Bisman Nababan, Indra Jaya, Sam Wouthuyzen. 2015. Object-based image analysis for coral reef benthic habitat mapping with several classification algorithms. *Procedia Environmental Sciences*, 24: 222-227.

- Walker, B.K. 2008. A model framework for predicting reef fish distributions across the seascape using GIS topographic metrics and benthic habitat associations. Proceedings of the 11th International Coral Reef Symposium, Ft. Lauderdale, Florida, 7-11 July 2008.
- Wentz, Frank J., Chelle Gentemann, Deborah Smith and Dudley Chelton. 2000. Satellite measurements of sea surface temperature through clouds. *Science*, 288: 847-850.
- Yates, K.L., Mellin, C., Caley, M.J., Radford, B.T. and J.J. Meeuwig. 2016. Models of marine fish biodiversity: assessing predictors from three habitat classification schemes. *PloS ONE*, 11: 1-16.
- Zhang, Yin, Xiaoqin Wang, and Yunzhi Chen. 2012. An improved 6S code for atmospheric correction based on water vapor content. *Advances in Remote Sensing*, 1: 14-18.

Appendix



Appendix 1.1. Tidal datum commonly used in maritime navigation and bathymetry charts; Mean Lower Low Water (MLLW) conventionally used in U.S. charts; Lowest Astronomical Time (LAT) conventionally used in the U.K. and Australia (https://en.wikipedia.org/wiki/Chart_datum#/media/File:Tide_legal_use.gif)



Appendix 1.2. IKONOS PAN image used for the identification of ground-truthing targets

```

***** 6SV version 1.1 *****
*
*          geometrical conditions identity
*          -----
*          user defined conditions
*
* month: 3 day : 16
* solar zenith angle: 35.93 deg solar azimuthal angle: 58.29 deg
* view zenith angle: 24.40 deg view azimuthal angle: 93.52 deg
* scattering angle: 159.30 deg azimuthal angle difference: 35.23 deg
*
*          atmospheric model description
*          -----
*          atmospheric model identity :
*          midlatitude summer (uh2o=2.93g/cm2,uo3=.319cm-atm)
*          aerosols type identity :
*          Maritime aerosol model
*          optical condition identity :
*          visibility : 63.66 km opt. thick. 550 nm : 0.1000
*
*          spectral condition
*          -----
*          constant
*          value of filter function :
*          wl inf= 0.450 mic wl sup= 0.530 mic
*
*          Surface polarization parameters
*          -----
*
* Surface Polarization Q,U,Rop,Chi 0.00000 0.00000 0.00000 0.00
*
*          target type
*          -----
*          homogeneous ground
*          spectral clear water reflectance 0.042
*
*          target elevation description
*          -----
*          ground pressure [mb] 1013.00
*          ground altitude [km] 0.000
*
*****

```

Appendix 1.3. 6SV model output: blue band (450-530 nm)

```

*****
*
*          integrated values of :
*          -----
*
*    apparent reflectance 0.1198726  appar. rad.(w/m2/sr/mic)  60.879
*    total gaseous transmittance 0.983
*
*****
*
*          coupling aerosol -wv :
*          -----
*
*    wv above aerosol :   0.120      wv mixed with aerosol :   0.120
*    wv under aerosol :   0.120
*
*****
*
*          integrated values of :
*          -----
*
*    app. polarized refl. 0.0056   app. pol. rad. (w/m2/sr/mic)  0.229
*    direction of the plane of polarization-12.93
*    total polarization ratio 0.047
*
*****
*
*          int. normalized values of :
*          -----
*
*          % of irradiance at ground level
*    % of direct irr.   % of diffuse irr.   % of enviro. irr
*    0.800             0.194             0.006
*
*          reflectance at satellite level
*    atm. intrin. ref.  background ref.  pixel reflectance
*    0.086             0.006             0.028
*
*          int. absolute values of
*          -----
*
*          irr. at ground level (w/m2/mic)
*    direct solar irr.  atm. diffuse irr.  environment irr
*    1139.534          276.698          8.643
*
*          rad at satel. level (w/m2/sr/mic)
*    atm. intrin. rad.  background rad.  pixel radiance
*    43.718            3.013            14.149
*
*
*    int. funct filter (in mic)          int. sol. spect (in w/m2)
*    0.0800000                          157.638
*
*****

```

Appendix 1.3 cont. 6SV model output: blue band (450-530 nm)

```

*****
*
*               integrated values of :
*               -----
*
*               downward      upward      total
* global gas. trans. :    0.99070    0.99173    0.98255
* water " " :          1.00000    1.00000    1.00000
* ozone " " :          0.99070    0.99173    0.98255
* co2 " " :            1.00000    1.00000    1.00000
* oxyg " " :            1.00000    1.00000    1.00000
* no2 " " :            1.00000    1.00000    1.00000
* ch4 " " :            1.00000    1.00000    1.00000
* co " " :              1.00000    1.00000    1.00000
*
* rayl. sca. trans. :    0.90922    0.91841    0.83504
* aeros. sca. " :       0.98624    0.98903    0.97542
* total sca. " :        0.89607    0.90750    0.81319
*
*
*               rayleigh      aerosols      total
* spherical albedo :    0.12534    0.03141    0.14511
* optical depth total:  0.16151    0.10390    0.26541
* optical depth plane:  0.16151    0.10390    0.26541
* reflectance I :       0.07803    0.01003    0.08744
* reflectance Q :       0.00459    0.00078    0.00516
* reflectance U :      -0.00207    0.00000   -0.00250
* polarized reflect. :  0.00504    0.00078    0.00573
* degree of polar. :    6.45         7.82         6.56
* dir. plane polar. :  -12.15        0.00        -12.91
* phase function I :    1.38950    0.27916    0.95482
* phase function Q :   -0.08987   -0.02825   -0.06575
* phase function U :   -1.34522    0.02587   -0.80847
* primary deg. of pol: -0.06468   -0.10120   -0.06886
* sing. scat. albedo :  1.00000    0.98950    0.99589
*
*
*****

```

Appendix 1.3 cont. 6SV model output: blue band (450-530 nm)

```

***** 6SV version 1.1 *****
*
*      geometrical conditions identity
*      -----
*      user defined conditions
*
*      month: 3 day : 16
*      solar zenith angle: 35.93 deg solar azimuthal angle: 58.29 deg
*      view zenith angle: 24.40 deg view azimuthal angle: 93.52 deg
*      scattering angle: 159.30 deg azimuthal angle difference: 35.23 deg
*
*      atmospheric model description
*      -----
*      atmospheric model identity :
*      midlatitude summer (uh2o=2.93g/cm2,uo3=.319cm-atm)
*      aerosols type identity :
*      Maritime aerosol model
*      optical condition identity :
*      visibility : 63.66 km opt. thick. 550 nm : 0.1000
*
*      spectral condition
*      -----
*      constant
*      value of filter function :
*      wl inf= 0.520 mic wl sup= 0.610 mic
*
*      Surface polarization parameters
*      -----
*
*      Surface Polarization Q,U,Rop,Chi 0.00000 0.00000 0.00000 0.00
*
*      target type
*      -----
*      homogeneous ground
*      spectral clear water reflectance 0.054
*
*      target elevation description
*      -----
*      ground pressure [mb] 1013.00
*      ground altitude [km] 0.000
*
*****

```

Appendix 1.4. 6SV model output: green band (520-610 nm)

```

*****
*
*          integrated values of :
*          -----
*
*   apparent reflectance  0.0929562  appar. rad.(w/m2/sr/mic)  44.510
*   total gaseous transmittance  0.919
*
*****
*
*          coupling aerosol -wv :
*          -----
*
*   wv above aerosol :    0.093      wv mixed with aerosol :    0.093
*   wv under aerosol :    0.093
*
*****
*
*          integrated values of :
*          -----
*
*   app. polarized refl.  0.0034      app. pol. rad. (w/m2/sr/mic)  0.148
*   direction of the plane of polarization-14.47
*   total polarization ratio  0.037
*
*****
*
*          int. normalized values of :
*          -----
*
*          % of irradiance at ground level
*   % of direct irr.      % of diffuse irr.      % of enviro. irr
*   0.843                 0.152                 0.005
*
*          reflectance at satellite level
*   atm. intrin. ref.    background ref.    pixel reflectance
*   0.049                 0.006                 0.038
*
*          int. absolute values of
*          -----
*
*          irr. at ground level (w/m2/mic)
*   direct solar irr.    atm. diffuse irr.    environment irr
*   1137.065            205.229                7.105
*
*          rad at satel. level (w/m2/sr/mic)
*   atm. intrin. rad.    background rad.    pixel radiance
*   23.543                2.882                 18.085
*
*
*   int. funct filter (in mic)                int. sol. spect (in w/m2)
*   0.0900000                                167.203
*
*****

```

Appendix 1.4 cont. 6SV model output: green band (520-610 nm)

```

*****
*
*               integrated values of :
*               -----
*
*               downward      upward      total
*
* global gas. trans. :    0.95517    0.95993    0.91855
* water " " :          0.99195    0.99274    0.98637
* ozone " " :          0.96287    0.96691    0.93108
* co2 " " :            1.00000    1.00000    1.00000
* oxyg " " :            1.00000    1.00000    1.00000
* no2 " " :            1.00000    1.00000    1.00000
* ch4 " " :            1.00000    1.00000    1.00000
* co " " :              1.00000    1.00000    1.00000
*
*
* rayl. sca. trans. :    0.94718    0.95274    0.90242
* aeros. sca. " :      0.98696    0.98960    0.97669
* total sca. " :       0.93436    0.94225    0.88040
*
*
*               rayleigh      aerosols      total
*
* spherical albedo :    0.07624    0.03001    0.09823
* optical depth total:  0.08989    0.09948    0.18937
* optical depth plane:  0.08989    0.09948    0.18937
* reflectance I :       0.04356    0.00940    0.05279
* reflectance Q :       0.00251    0.00085    0.00323
* reflectance U :      -0.00128    0.00000   -0.00179
* polarized reflect. :  0.00282    0.00085    0.00369
* degree of polar. :    6.47      9.06      7.00
* dir. plane polar. :  -13.55     0.00     -14.48
* phase function I :    1.38950    0.27575    0.80441
* phase function Q :   -0.08987   -0.03372   -0.06037
* phase function U :   -1.34522    0.02710   -0.62429
* primary deg. of pol: -0.06468   -0.12229   -0.07505
* sing. scat. albedo :  1.00000    0.98943    0.99445
*
*
*****

```

Appendix 1.4 cont. 6SV model output: green band (520-610 nm)

```

***** 6SV version 1.1 *****
*
*          geometrical conditions identity
*          -----
*          user defined conditions
*
* month: 3 day : 16
* solar zenith angle: 35.93 deg  solar azimuthal angle: 58.29 deg
* view zenith angle: 24.40 deg  view azimuthal angle: 93.52 deg
* scattering angle: 159.30 deg  azimuthal angle difference: 35.23 deg
*
*          atmospheric model description
*          -----
*          atmospheric model identity :
*          midlatitude summer (uh2o=2.93g/cm2,uo3=.319cm-atm)
*          aerosols type identity :
*          Maritime aerosol model
*          optical condition identity :
*          visibility : 63.66 km  opt. thick. 550 nm : 0.1000
*
*          spectral condition
*          -----
*          constant
*          value of filter function :
*          wl inf= 0.640 mic  wl sup= 0.720 mic
*
*          Surface polarization parameters
*          -----
*
* Surface Polarization Q,U,Rop,Chi  0.00000  0.00000  0.00000  0.00
*
*          target type
*          -----
*          homogeneous ground
*          spectral clear water reflectance 0.035 |
*
*          target elevation description
*          -----
*          ground pressure [mb] 1013.00
*          ground altitude [km] 0.000
*
*****

```

Appendix 1.5. 6SV model output: red band (640-720 nm)

```

*****
*
*          integrated values of :
*          -----
*
*    apparent reflectance 0.0570227  appar. rad.(w/m2/sr/mic)  22.114
*          total gaseous transmittance 0.912
*
*****
*
*          coupling aerosol -wv :
*          -----
*
*    wv above aerosol : 0.057      wv mixed with aerosol : 0.057
*          wv under aerosol : 0.057
*
*****
*
*          integrated values of :
*          -----
*
*    app. polarized refl. 0.0024  app. pol. rad. (w/m2/sr/mic)  0.074
*          direction of the plane of polarization-15.89
*          total polarization ratio 0.042
*
*****
*
*          int. normalized values of :
*          -----
*
*          % of irradiance at ground level
*    % of direct irr.   % of diffuse irr.   % of enviro. irr
*          0.876         0.122         0.002
*          reflectance at satellite level
*    atm. intrin. ref.  background ref.  pixel reflectance
*          0.028         0.003         0.026
*
*          int. absolute values of
*          -----
*
*          irr. at ground level (w/m2/mic)
*    direct solar irr.  atm. diffuse irr.  environment irr
*          971.780      135.495      2.437
*          rad at satel. level (w/m2/sr/mic)
*    atm. intrin. rad.  background rad.  pixel radiance
*          10.666       1.272       10.176
*
*          int. funct filter (in mic)          int. sol. spect (in w/m2)
*          0.0800000                          120.375
*
*****

```

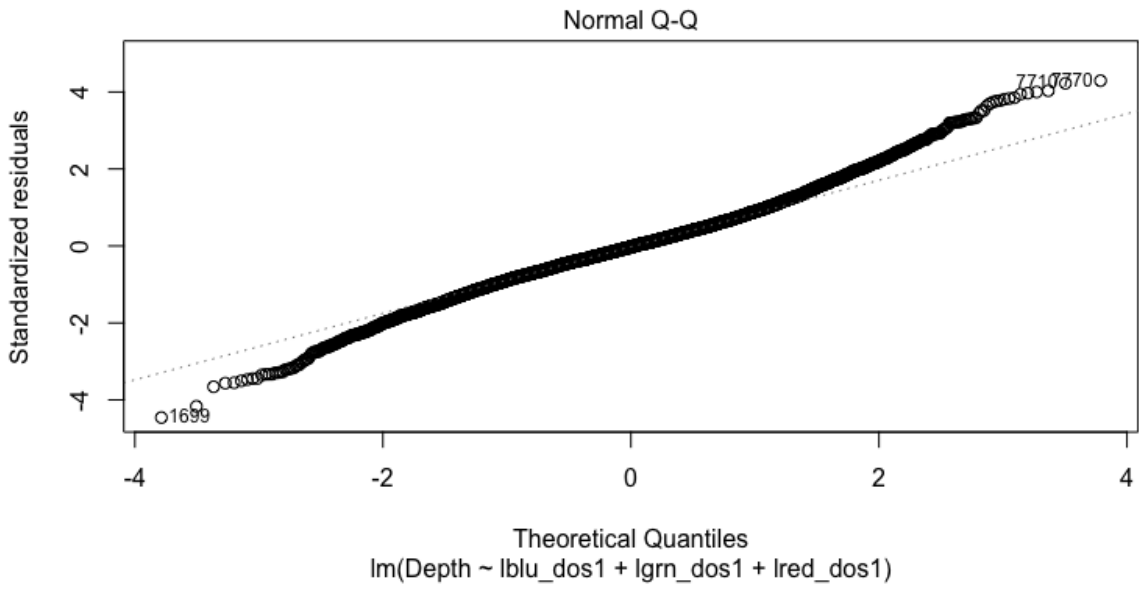
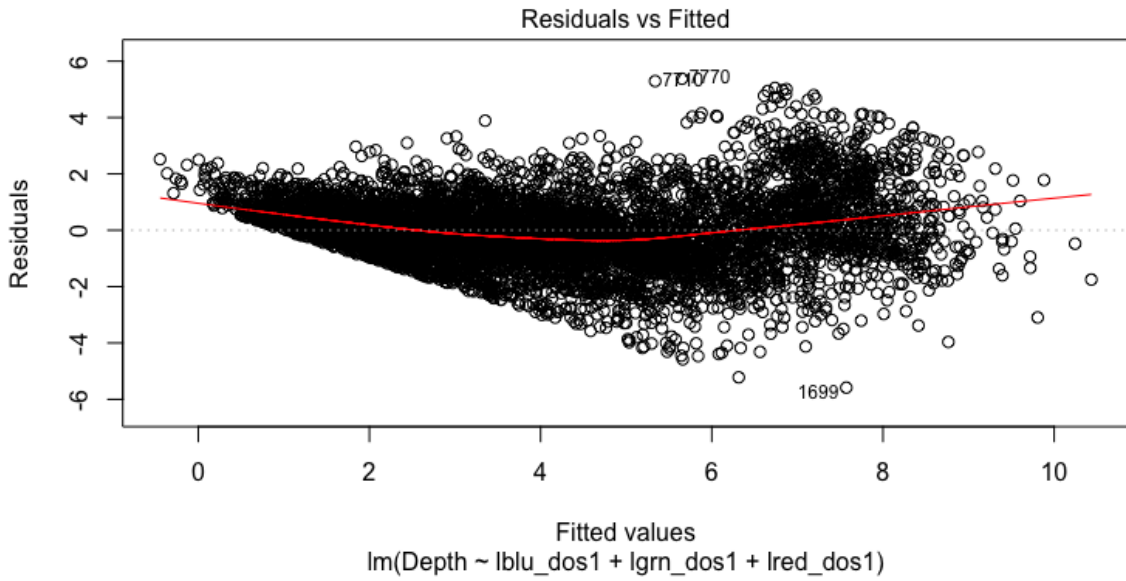
Appendix 1.5 cont. 6SV model output: red band (640-720 nm)

```

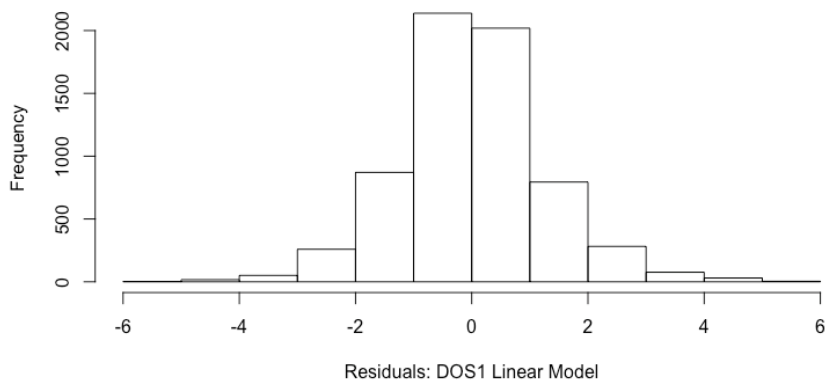
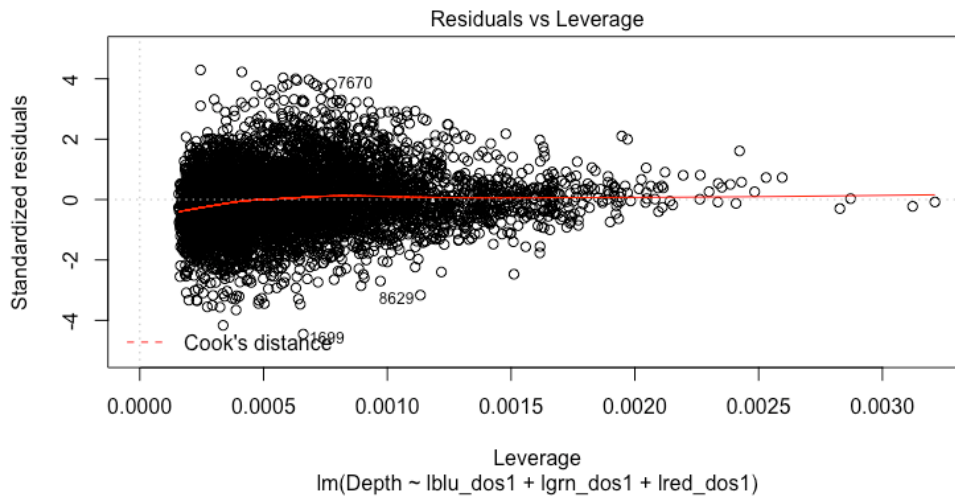
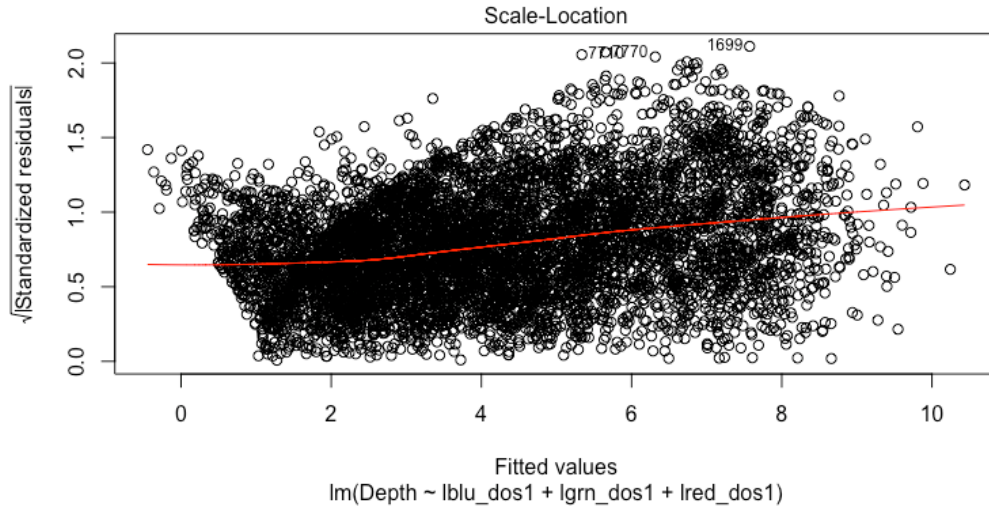
*****
*
*               integrated values of :
*               -----
*
*           downward           upward           total
* global gas. trans. :    0.94451    0.94917    0.91171
* water " " :    0.97054    0.97293    0.95451
* ozone " " :    0.98444    0.98615    0.97086
* co2 " " :    1.00000    1.00000    1.00000
* oxyg " " :    0.98908    0.98972    0.98507
* no2 " " :    1.00000    1.00000    1.00000
* ch4 " " :    1.00000    1.00000    1.00000
* co " " :    1.00000    1.00000    1.00000
*
* rayl. sca. trans. :    0.97456    0.97731    0.95245
* aeros. sca. " :    0.98774    0.99020    0.97806
* total sca. " :    0.96231    0.96739    0.93092
*
*
*           rayleigh           aerosols           total
* spherical albedo :    0.03843    0.02852    0.06240
* optical depth total:    0.04208    0.09465    0.13674
* optical depth plane:    0.04208    0.09465    0.13674
* reflectance I :    0.02024    0.00894    0.02920
* reflectance Q :    0.00114    0.00110    0.00216
* reflectance U :    -0.00066    0.00000    -0.00134
* polarized reflect. :    0.00131    0.00110    0.00254
* degree of polar. :    6.49    12.27    8.71
* dir. plane polar. :    -14.97    0.00    -15.91
* phase function I :    1.38950    0.27649    0.61904
* phase function Q :    -0.08987    -0.04348    -0.05776
* phase function U :    -1.34522    0.03433    -0.39025
* primary deg. of pol:    -0.06468    -0.15725    -0.09330
* sing. scat. albedo :    1.00000    0.98960    0.99280
*
*
*****

```

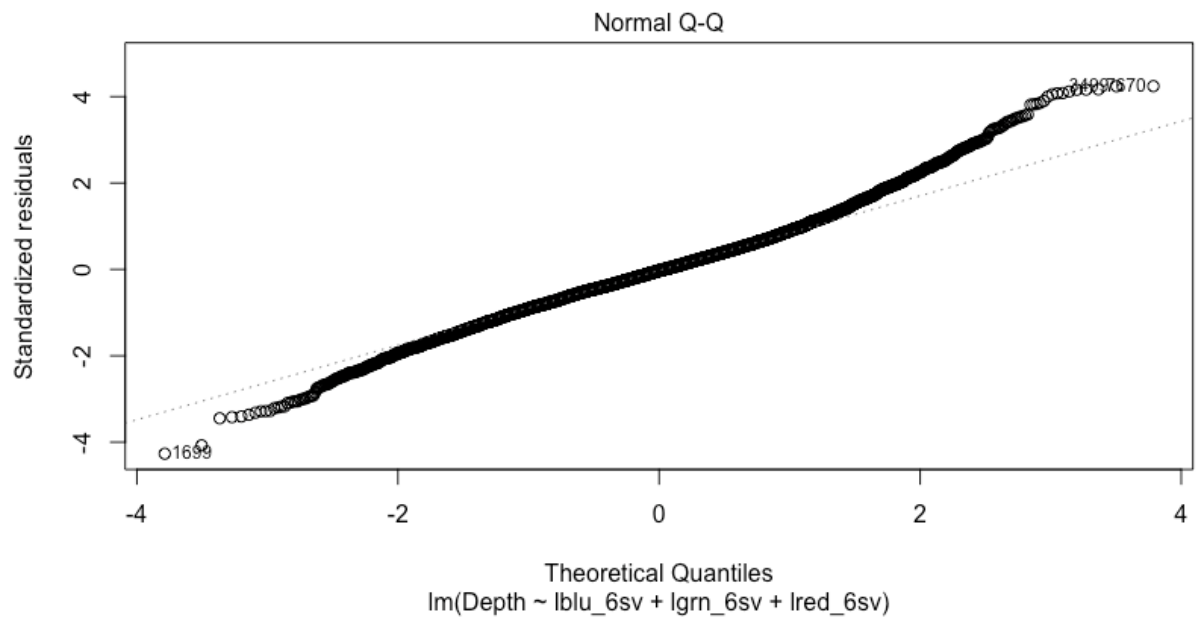
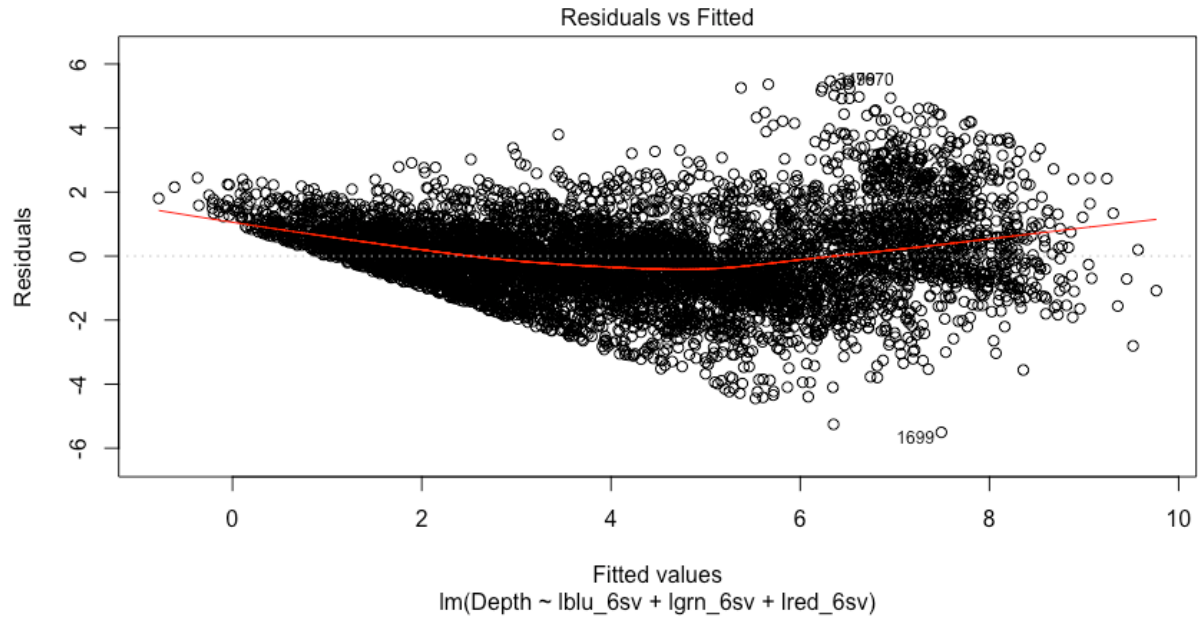
Appendix 1.5 cont. 6SV model output: red band (640-720 nm)



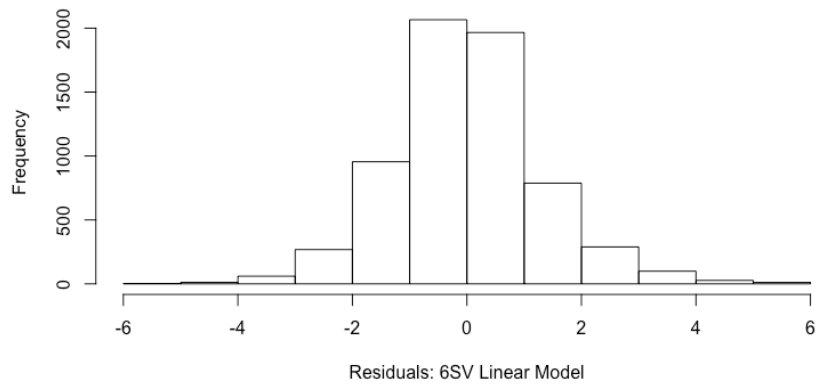
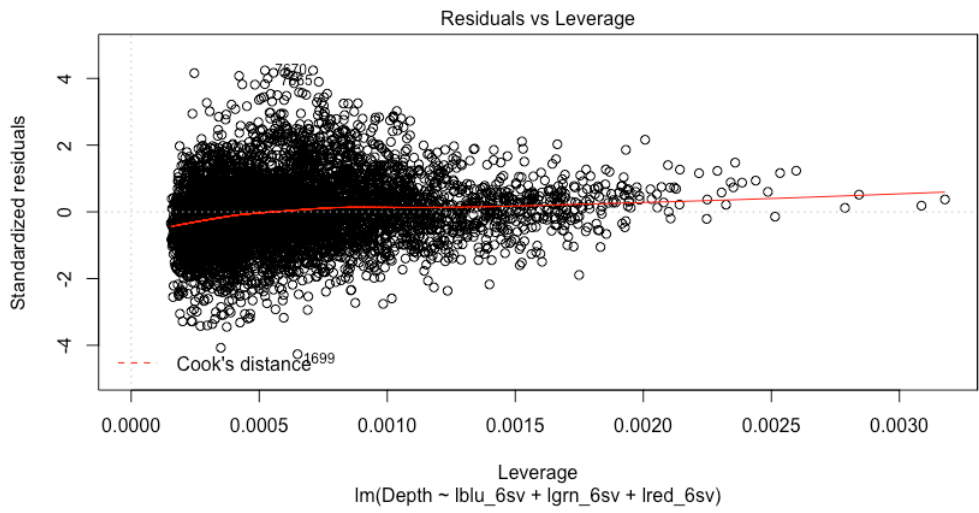
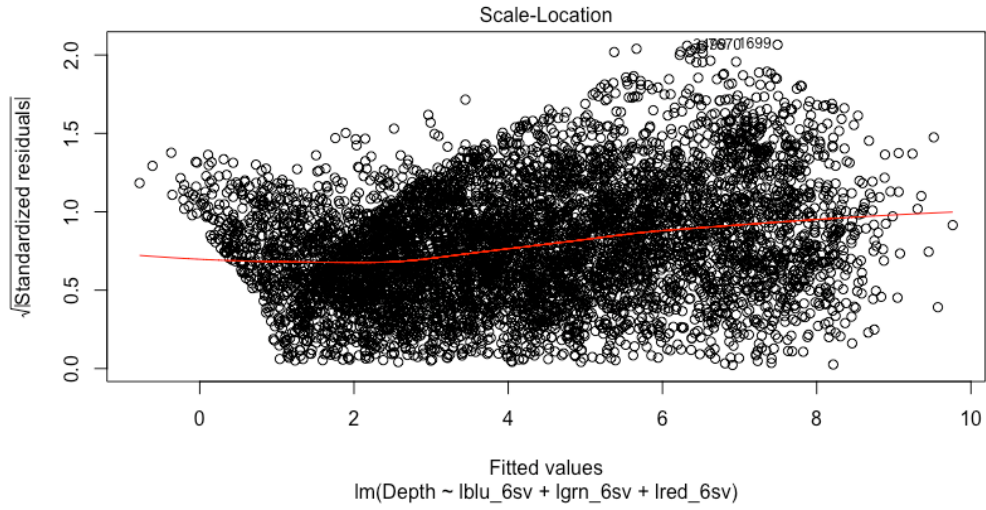
Appendix 1.6. Regression diagnostic plots for the multiple linear regression of DOS_{1%} data



Appendix 1.6 cont. Regression diagnostic plots for the multiple linear regression of DOS_{1%} data



Appendix 1.7. Regression diagnostic plots for the multiple linear regression of 6SV data



Appendix 1.7 cont. Regression diagnostic plots for the multiple linear regression of 6SV data

Optimization of bathymetric retrievals from multispectral imagery of complex coastal environments



Shane M. Abeare, *MSc, MSc, PhD* candidate, University of New Orleans, New Orleans, USA; !
Director, ReefDoctor, Toliara, Madagascar!



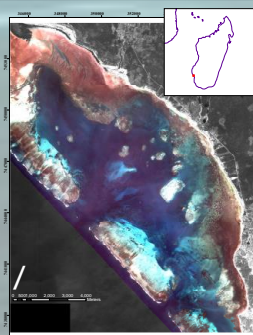
Introduction!

Given the close species-habitat associations that exist in coral reef ecosystems, a prerequisite to any research, or management action, is a firm understanding of local bathymetry¹ and the state / extent of local benthic habitats^{2,4,5}. In recent years, much research attention has focused on applications of multi-spectral satellite imagery in deriving water depth and habitat types of coral reef environments^{6,7,8}. One of the oldest and, still, the most commonly used method for multi-spectral bathymetric / benthic habitat inversions is the Lyzenga Method (LM)^{9,10}. The LM is based on the physical law, known as the Beer-Lambert Law, which describes the exponential extinction of light in water. However, water column properties of coastal environments are spatially and temporally complex, consequently, the log-linear constraints imposed by the LM are often violated (e.g. Exploratory Data Analysis, right). Errors in the derivation of depth are propagated to the benthic habitat product!

Objective!

The aim of the present study is to evaluate the performance of a more sophisticated statistical modeling approach, whose functional response is effectively unconstrained, boosted regression trees. !

Study area!



Location and extent of IKONOS-2 image used in the present study (black-and-white); extent of study area, Bay of Ranobe, Madagascar (RGB true color image) !

WIOMSA Symposium 2013!

Methods!

Sonar Data!

10,219 sonar data points were collected opportunistically between 2011-2013 using a commercial-grade, dual-beam sonar/GPS unit. Sonar data were standardized to LAT tidal datum and ! resampled to a 5m grid using mean values. Given that depths exceed 12m only in the reef passes, ! data points at depths 0.5m-12m (n=9,974) were selected for model fitting routines. Data points ! were split 70/30 for model training and validation, respectively.!

Image Pre-processing!

Image acquisition / properties: 16 March, 2007 at 07:15 GMT / Bands: 4 MS+pan; 11-bit data!
Radiometric correction: Raw digital counts were converted to exoatmospheric reflectance (R_{rs}) following published methods: !

$$L_i = \frac{10^4 \cdot DN_i}{CalCoef \cdot Bandwidth_i} \quad \rho_r = \frac{\rho \cdot L_i \cdot d^2}{E_{sun} \cdot \cos \theta_s} = R_{rs}$$

Atmospheric correction: A variant of the dark-object subtraction (DOS-1) was used, where image histograms were used for the determination of cut-off points.!

Geometric correction: Images were resampled to 5m resolution to correspond with the sonar data layer and to minimize GPS positional error.!

Statistical Models.

Lyzenga Method (OLS regression)

$$\log(\text{depth}) = \beta_0 + \beta_1(X_1) + \beta_2(X_2) + \beta_3(X_3) + c.$$

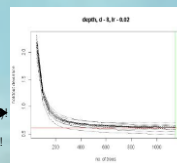
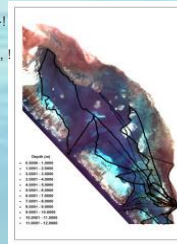
Predictors = $X_{ijk} = \ln(R_{rs,red,green,blue}) * 1000$!

Boosted regression tree model!

$$\text{aggregation: } \hat{f}_A(\cdot) = \sum_{m=1}^{mstop} a_m \hat{g}^{(m)}(\cdot)$$

! mstop → 0-fold cross validation (see plot →)

*Analyses conducted using R Statistical Computing software, package (dismo); ArcGIS 9.3 and Erdas Imagine!
**BRT "tuning parameters" used in the final model: tree.complexity=8, learning rate=0.02, bag.fraction=0.5, ! tolerance.method="auto", tolerance=0.01!



Exploratory data analysis!

IKONOS RGB image bands after histogram equalization for visual enhancement of suspended sediment plume (red ellipse, top-right); sediment plume signal appears strongest at red/blue wavelengths. !

Due to these highly-variable, complex water column properties, extinction of the log-transformed wavelengths at depth is non-linear; see generalized additive model terplot, below. !

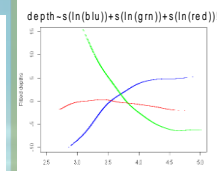
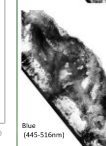
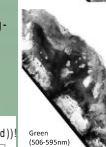
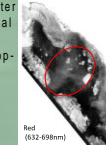
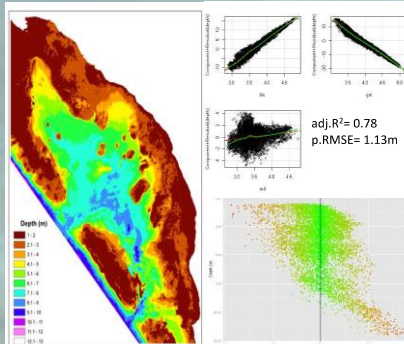


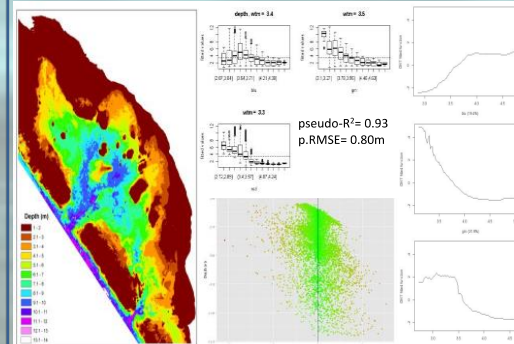
Figure. 3D image: IKONOS RGB draped over BRT model results

! Results!

Lyzenga Method !



Boosted Regression Tree!



Discussion!

Coral reef ecosystems are often found in the data-poor regions of the world in which little research is conducted. In such situations, satellite images represent a valuable source of historic and current data. Given the complexity of partitioning the satellite signal into its constituent air / sea / land components, optimization of this valuable data (re)source presents many challenges. Nonetheless, advances in statistical modeling and signal processing technologies offer promising tools for improvements in accuracy, such was the case for the present study. Results presented here demonstrate the improved predictive accuracy and performance afforded by the more-advanced, model-fitting algorithm – boosting.

1. Dreyer and Russingham, 2009. Mar. Sci. Prog. Ser. 361: 1-13!
2. Pittman et al. 2007. Ecological Modelling, 204: 9-21!
3. Walker, 2009. Proc. 11th Inter. Coral Reef Symp., 7-11 July 2008!
4. Pittman et al. 2009. J. of Coastal Research, 53: 27-38!
5. Knudby et al. 2010. Remote Sensing of Env., 114: 1230-1241!
6. Andrefouet et al. 2003. Remote Sensing of Env., 88: 128-143!
7. Mumby and Edwards, 2002. Remote Sensing of Env., 82: 248-257!
8. Mumby et al. 2004. Marine Pollution Bulletin, 48: 219-228!
9. Lyzenga, 1978. Applied Optics, 17: 379-383!
10. Lyzenga, 1981. Int. J. Remote Sensing, 2: 71-82!



Vevo Fishing Communities: Small-area population estimates, demographics, and socioeconomics

2.1 Introduction

As one of the only countries in the world where per capita GDP has continuously declined over the last 30 years (Figure 2.1), Madagascar is considered one of the poorest countries by many measures. In 2015, the World Bank adjusted the international poverty level, which was previously based on economic data from 1996, from \$1 per day to the current definition of \$1.90 per day. Nonetheless, with $\approx 90\%$ of the population of Madagascar living on less than \$2 per day, while 77% live on less than \$1.25 per day, the country's poverty crisis is clearly widespread and severe (Akire *et al.*, 2011; World Bank, 2014; Pamen and Kuepie, 2017).

Over the past decade the definition of poverty has been expanded from a simple monetary index to more inclusive multidimensional approaches. For example, the Oxford Multidimensional Poverty Index (MPI) is comprised of measures of education, health, and standards of living. The Human Development Index (HDI), developed by the United Nations Development Program, is a composite index comprised of the basic dimensions of human development: 1) the ability to lead a long and healthy life, measured by the life expectancy at birth, 2) the ability to acquire knowledge, measured by the mean years of schooling, and 3) the ability to achieve a decent standard of living, measured by gross national income (GNI) per capita (UNDP, 2018). In terms of health and education, as compared to other sub-Saharan African countries, Madagascar scores on the higher end of the scale, given the comparatively

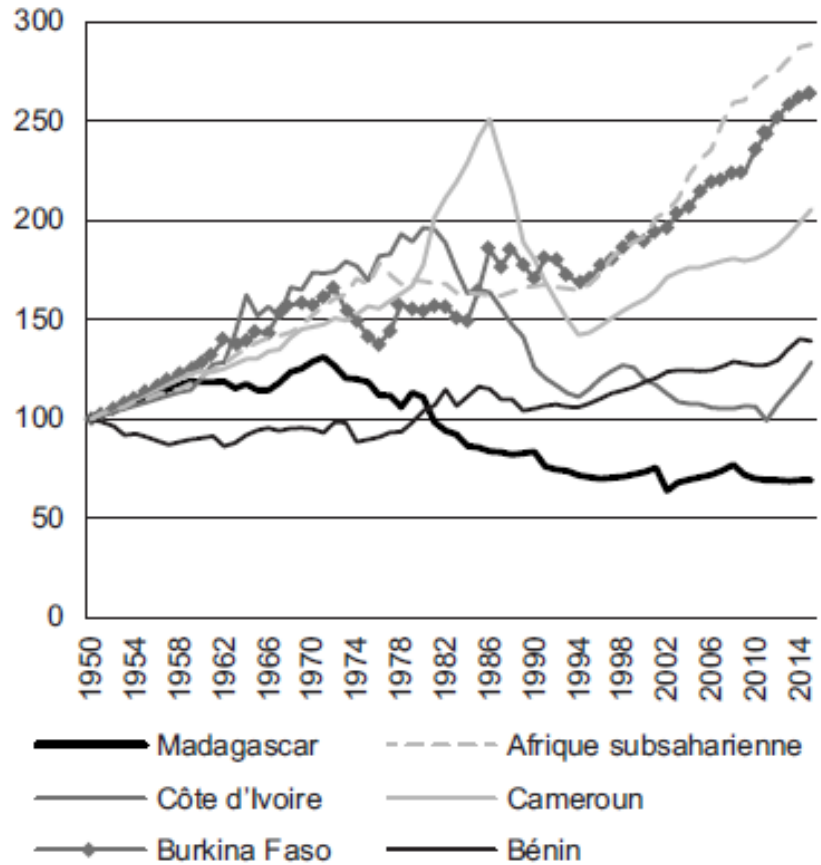


Figure 2.1. GDP per capita: Madagascar compared to other African countries: Ivory Coast (*Cote d'Ivoire*), Burkina Faso, Cameroon (*Cameroun*), Benin, and Sub-Saharan Africa (*Afrique subsaharienne*) as a whole (Source: Razafindrakoto *et al.*, 2017)

high life expectancy at birth (66.3 years) and expected years of schooling (10.6 years). In addition, the prevalence of HIV in Madagascar is quite low, as compared to other sub-Saharan countries. On the other hand, the country continuously struggles to control outbreaks of bubonic plague, as a result of poor waste management and rat infestations in the larger cities and prisons (Boisier *et al.*, 1997; Andrianaivoarimanana *et al.*, 2013). Similarly, although Madagascar performs comparatively well in a sub-Saharan context for the mean number of years of schooling, only 15% of Malagasy teachers have received any formal training (World Bank, 2014). In terms of ‘the ability to achieve a decent standard of living’ criteria of the HDI, the

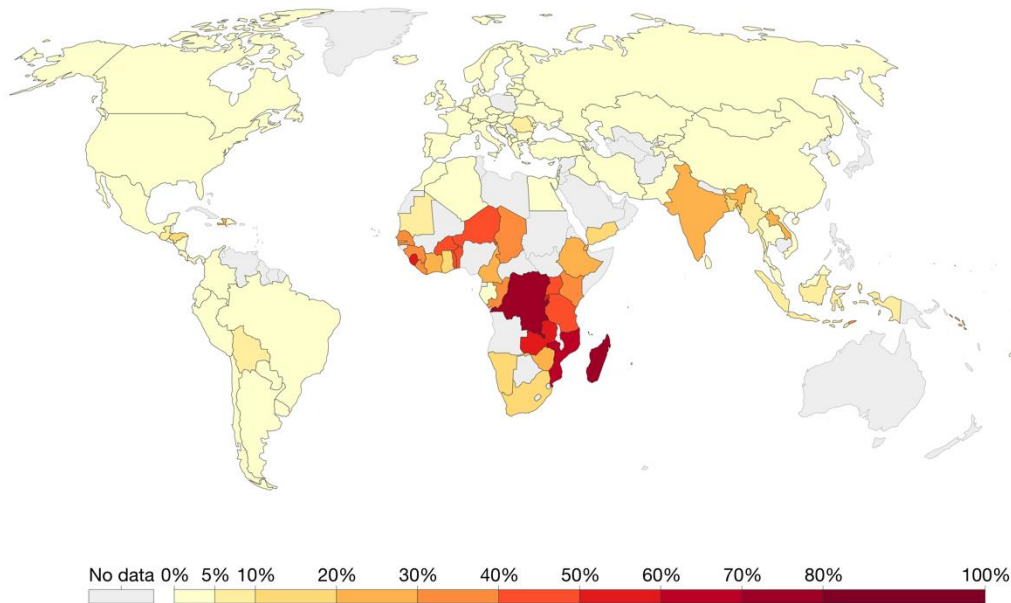
GNI per capita score for Madagascar of \$1358 per year is low even amongst other sub-Saharan countries (Figure 2.2), resulting in an overall HDI score (HDI=0.519) and ranking of 161 out of 189 countries (UNDP, 2018).

While sources of demographic and economic indicators exist at the national level, information and disaggregated data sources at finer scales, such as sub-national, provincial or local level, are limited or non-existent. The lack of fine-scale demographic and socioeconomic data greatly complicates the task of identifying and targeting local communities in need of conservation, natural resource management, medical, and other humanitarian interventions. This problem has been recognized by the wider community of international development and conservation organizations, and over the past decade, efforts have been made to collect and disseminate finer-scale information. However, the accuracy of many of these efforts, in the case of Madagascar, is questionable, given that the source of data is often from the outdated census information collected in 1993 by the national census bureau of Madagascar, *Institut National de la Statistique* (INSTAT).

Given the clear linkages between human population density to epidemiology, and poverty to public health, many medically-related studies have attempted to disaggregate census data to obtain information at a meaningful scale (Baker *et al.*, 2013). For example, epidemiological studies of Malaria (Clouston *et al.*, 2015; Kang *et al.*, 2018) and Typhoid Fever (Marks *et al.*, 2016) applied a spatially-explicit regression model to determine spatial patterns and relationships between disease prevalence and the accessibility of healthcare facilities based on the prevalence of poverty at the provincial and commune level. However, even at this level of detail, the level of aggregation of the data limits the datasets usefulness (see Figure 2.3, Administrative boundaries).

Share of the population living in extreme poverty, 2017

Extreme poverty is defined as living with per capita household consumption below 1.90 international dollars per day (in 2011 PPP prices). International dollars are adjusted for inflation and for price differences across countries.



Source: World Bank

OurWorldInData.org/extreme-poverty/ • CC BY

Figure 2.2. Percentage of population living in extreme poverty by country (Source: <https://ourworldindata.org/extreme-poverty>)

A clear need exists for high-resolution, reliable estimates of global human population distributions, demographics, and dynamics, whether for poverty relief, epidemiology, disaster response, national security, sustainable development, or natural resource management. Over the years, the problem of spatially disaggregating census data to a more exploitable resolution has come to be known as the “small-area estimate” problem. In the past decade, a number of institutions and governments have risen to the challenge, forming large, international collaborations. For example, the Center for International Earth Science Information Network of the Earth Institute, Columbia University (www.ciesin.columbia.edu) has worked in collaboration

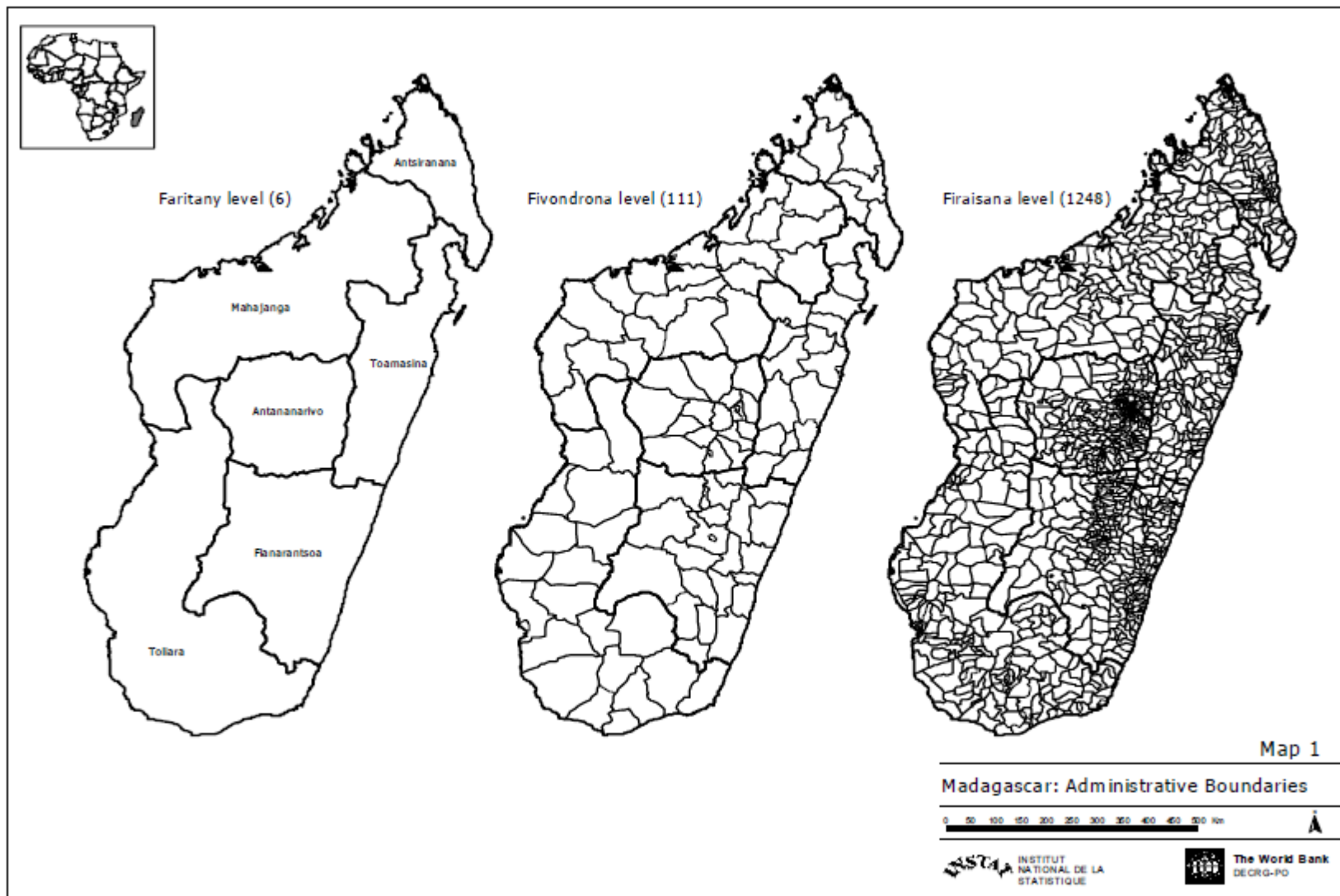


Figure 2.3. Madagascar administrative boundaries used for the aggregation of census data: province (*Faritany*), district (*Fivondronas*), and commune (*Firaisanas*) (Mistiaen *et al.*, 2002)

with the NASA Socioeconomic Data and Applications Center (SEDAC, www.sedac.ciesin.columbia.edu), and a number of other international organizations and collaborative groups, such as the organization, WorldPop (www.worldpop.org), and University of Southampton (www.southampton.ac.uk). As a result, more sophisticated methods are being developed and employed, with advances in modern computing power, to estimate small-area human population distributions around the world (Wardrop et al., 2018).

Since the 1970's, a growing body of research has focused on the applications of remotely sensed images and various statistical modeling approaches to study land-use / land- change and urban expansion as a proxy for human population growth (e.g. Clayton and Estes, 1980; Iisaka and Hegedus, 1982; Hasse and Lathrop, 2003; Allen and Lu, 2003; Sudhira *et al.*, 2004, Wu *et al.*, 2005), and the consequences thereof, in terms of declining biodiversity and the impacts on global climate change (Houghton, 1999; Kalnay *et al.*, 2003; Jetz *et al.*, 2007). Small-area human population estimation methods often employ a dasymetric approach, where the geographic units, or administrative boundaries, of course-scale population census datasets are further sub-divided into smaller areal estimates based on ancillary information and statistical models. Within the course-scale geographic unit, population counts are attributed to areas that are more suitable for human settlement, such as land versus water, or slope characteristics, resulting in the spatial disaggregation of the census data. Statistical models used in the spatial disaggregation of census data commonly use covariates derived from remotely-sensed data sources, including: land cover, slope, primary productivity, observed lights at night, visible infrared, and climatic data, such as rainfall and mean annual temperature (Stevens *et al.*, 2015). Improvements in the spatial resolution of satellite imagery in recent years have allowed, in

certain cases, the enumeration of houses, or dwellings, as an additional covariate (Li and Weng, 2005; Hillson *et al.*, 2015).

Today, access to high-quality satellite imagery captured at much higher spatial and spectral resolutions than ever before, combined with significant improvements in computing power and statistical machine learning algorithms, has resulted in the production of the highest resolution human population datasets to date (Tatem *et al.*, 2007; Anderson *et al.*, 2014; Stevens *et al.*, 2015; Grippa *et al.*, 2019). For Madagascar, the 100 m resolution map produced by the WorldPop (www.worldpop.org) program, following the methodology of Stevens *et al.* (2015), represents the best estimates of population distributions at present (Figure 2.4). The accuracy of even the most sophisticated, state-of-art approaches to producing small-area human population estimates, however, are challenged by the conditions encountered in developing countries. In the case of Madagascar, where between 2010 -2013, 66% of the population lived in rural areas and <10% of the rural population had access to electricity (Data: World Bank <https://data.worldbank.org>, accessed May 23, 2019), the commonly used covariate of lights-at-night would clearly be of limited value. The relationship between human population density and that of the most commonly used covariate, land-use / land-change (LULC), varies widely between developed and undeveloped countries, between urban and rural populations, and even within the rural sector of the population. Clearly, the terrestrial footprint of a village of farmers substantially differs from that of a village of herders, while the terrestrial footprint of fishing communities would pose even greater challenges to detection, such is the case in the present study (Figure 2.5). Ideally, statistical models used to interpolate population densities would have the ability to accommodate the nonstationary nature of this functional response. Furthermore, even with modern day computing power, current global human population mapping initiatives are required to limit their

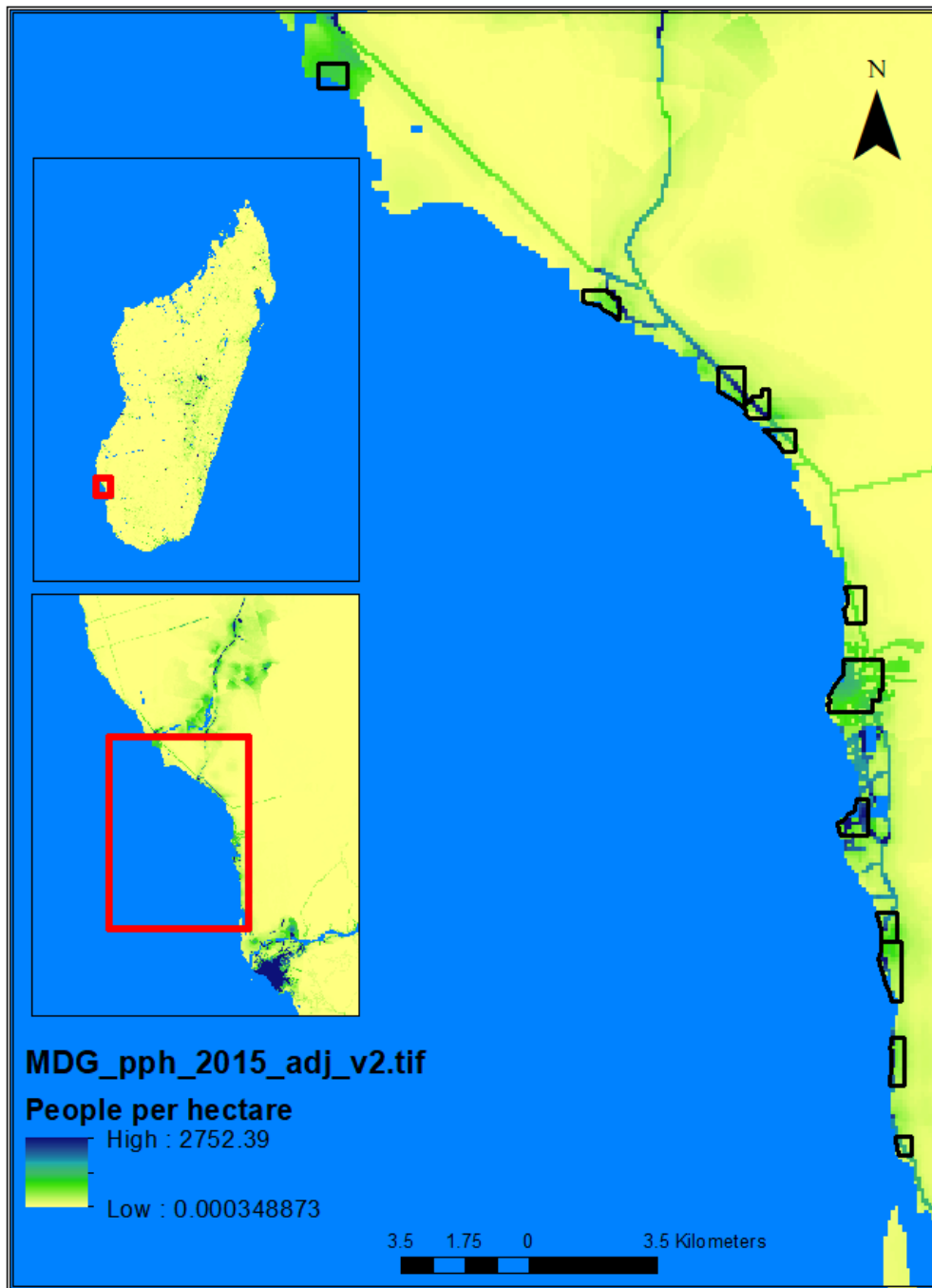


Figure 2.4. Madagascar human population distribution map at 100 m grid resolution, with map legend colors corresponding to the number people per hectare along the coast of the Bay of Ranobe, and locations of the 12 villages of Bay (black polygons); (inset, left-top) view of study location within country (red polygon); (inset, bottom-left) regional view of study location relative to the city of Toliara (dark blue) (Source: WorldPop, 2017; version 2.0 estimates adjusted to United Nations Population Division estimates)



Figure 2.5. IKONOS panchromatic image illustrates the fishing village of Ifaty (yellow polygon) separated by an area of salt flats from the herding village of Tsivinoe (red circle), with the outlying areas of land-use / deforestation

processing demands to some extent. Often, this is achieved through the use of images of mid-range spatial and spectral resolutions, namely Landsat products (30 m resolution) (Frye *et al.*, 2018). In a village setting, where many houses measure 4-5 m wide by 6-7 m long, mid-range resolution imagery prohibits the identification of individual dwellings, and thus, the use of one of the more powerful and direct measures of human population, the enumeration of households (Figure 2.6). Moreover, given that the majority of dwellings are constructed of dry vegetation, their spectral signatures would be nearly indistinguishable from the surrounding vegetation with only a limited number of image bands (pers.obs.), making an automated object-based recognition routine infeasible (Figure 2.7).



Figure 2.6. IKONOS high-resolution panchromatic image used to illustrate resolution required to conduct dwelling unit enumeration; inset demonstrates the typical resolution of Landsat products (30 m) and the loss of discernibility of dwelling units at reduced resolution



Figure 2.7. Photo illustrates roofing material and sized of typical village-style houses

Over a backdrop of extreme poverty, natural resource depletion, and political instability, since the 1990's, the government of Madagascar has pursued an agenda of decentralization, a movement that became popular and swept across the African continent starting in the mid-1980's (Brosio, 2000). In 1996, the government of Madagascar adopted a law, known as GELOSE (*Gestion Locale Sécurisé*), that allows for the limited transfer of the rights and responsibilities associated with natural resource management to local communities. Although decentralization, in an idealized world, could potentially enhance democratic processes and allow for increased involvement and input from communities in regards to local issues, a lack of infrastructure and source of revenue (*i.e.* tax base) for local governments leads to less than ideal outcomes (Kull, 2002; Sarrasin, 2009; Pollini and Lassoie, 2011; Burnod *et al.*, 2013; Cullman, 2015). In fact, it has the potential to make things much worse in adding additional layers of government susceptible to corruption and bribery (Fan *et al.*, 2009; Burnod *et al.*, 2013).

At the village level, the national GELOSE law provided recognition of a traditional system that had been in-use for generations of setting community standards, rules, or guidelines, known locally as a *dina*. Later, the GELOSE framework was supported further with additional laws (Law number 2001-004 of October 25, 2001, *Portant réglementation générale des Dina en matière de sécurité publique*) that provided a path to legitimize *dinas* through the local court system, *homologation*, which at the same time, allowed for some scrutiny and oversight of the village laws being created. Over the decades that followed the formalization of the *dina*, as an instrument for natural resource management and conservation, international organizations seized upon the opportunity to promote community-based approaches through the creation of *dinas* (Rakotoson and Tanner, 2006; Andriamalala and Gardner, 2010; Harris, 2011).

Historically, natural resource management and conservation research has focused on the ecological needs, distributions, and abundances of plants / wildlife species of concern. Nonetheless, a growing body of research has focused on ‘bridging the gap’ between the needs of local communities and the needs of wildlife, an approach that has come to be known as Social and Ecological Systems research (SES) (*e.g.* Cinner and Pollnac, 2004; Cinner *et al.*, 2009). Given that marine fisheries resources are a key source of income and nutrition in the developing world, an understanding of the demographic, socioeconomic, and cultural factors that affect fishing effort intensity and distribution are of critical importance. Demographic processes, such as population growth and immigration / emigration resulting from environmental degradation and/or political instability, may lead to the erosion of traditional values, customs, and taboos, thereby undermining the role(s) of traditional village leaders, usually village elders and the chief (Jones *et al.*, 2008; Wahab *et al.*, 2012; Merkle *et al.*, 2017). Erosion of culture and of the role of traditional leaders may then lead to the erosion of customary forms of resource management, such as adherence to local *dinas* (Cinner *et al.*, 2007). In addition, socioeconomic factors, *e.g.* wealth, age, education, distance to market, play a significant role in determining the intensity, distribution, and selectivity of the fishing pressure, having clear implications on the choice, use, and acceptability of fisheries management measures, such as the placement of marine reserves (Cinner and Pollnac, 2004; Cinner, 2007; Klein *et al.*, 2008; Ban and Klein 2009; Cinner *et al.*, 2009; Brewer *et al.*, 2012). Naturally, the imposition of management-related restrictions of resource-use on communities living in extreme poverty requires substantial community acceptance, or else will suffer serious compliance issues (Westerman and Gardner, 2013). Even in the face of severe depletion of fisheries resources, research has shown that it is those living in

extreme poverty that are the least likely to exit the fishery and seek alternatives (Cinner *et al.*, 2008).

The aim of the present chapter is to address existing knowledge gaps through a descriptive approach, allowing for the characterization and quantification some of the basic socioeconomic information relevant and useful to fisheries management and conservation. Specifically, the research presented here will provide:

1. Estimates of human populations inhabiting the coastal villages of the Bay of Ranobe, as an indicator of fishing effort;
2. Patterns of infrastructure development, as an indicator of demographic processes and recent shifts in human population density;
3. Estimates of income of fishermen and the economic value of fisheries products, as an economic indicator of poverty level and for use as the baseline, or threshold, to be exceeded by international development organizations considering alternative livelihood projects.

2.2 Methodology

Study site

The greater Bay of Ranobe community, as defined here, is composed of the villages bounded by the escarpment of the Mahafaly Plateau in the east, the coastline to the west, and the Manombo River and Fiherenana River to the north and south, respectively. The 21 villages within the region are comprised, predominantly, of 3 of the 18 known ethnicities of Madagascar: Mahafaly, Sakalava, and Antandroy (Grenier, 2013) (Figure 2.8a). Although, technically, not considered one of the official ethnic groups, the semi-nomadic, fishing communities that inhabit

the southwest coast of Madagascar are known as the Vezo, meaning “those that struggle with the sea” (Astutti, 1995). The cultural identity of the Vezo people appears to be linked more to their lifestyle than to their ancestral lineage (Grenier, 2013). Similarly, the people that live on the “interior” of the island that farm and raise livestock are known as the Masikoro. Of the 21 villages within the greater Bay of Ranobe community, there are 9 inland Masikoro villages and 12 Vezo villages located along the coast, whose location and distribution are largely determined by proximity to the only transport route. Access to goods, services, and movements of people within the region are regulated by a single road, namely the National Road- 9, or *Route Nationale-9*. The 12 Vezo villages, representing the Vezo fishing community of the Bay of Ranobe, are the subject of the research presented here, and include, from south to north (Figure 2.8b):

- | | |
|-------------------|-------------------|
| 1. Ambotsibotsike | 7. Amboaboaka |
| 2. Tsongeritelo | 8. Madorano |
| 3. Beravy | 9. Betsibaroka |
| 4. Ambalaboy | 10. Ambolomailaka |
| 5. Ifaty | 11. Andrevo |
| 6. Mangily | 12. Fitsitke. |

In general, the 12 Vezo villages of the Bay of Ranobe are quite similar in terms of the livelihoods of the inhabitants, which are inextricably linked to the sea and marine resources. On average, 70% of the inhabitants directly engage in fishing activities as their primary source of income, while approximately 20% cite fishing as a secondary revenue-generating activity. Indirectly, sales and distribution of fisheries products accounts for the primary activity of 2.5%

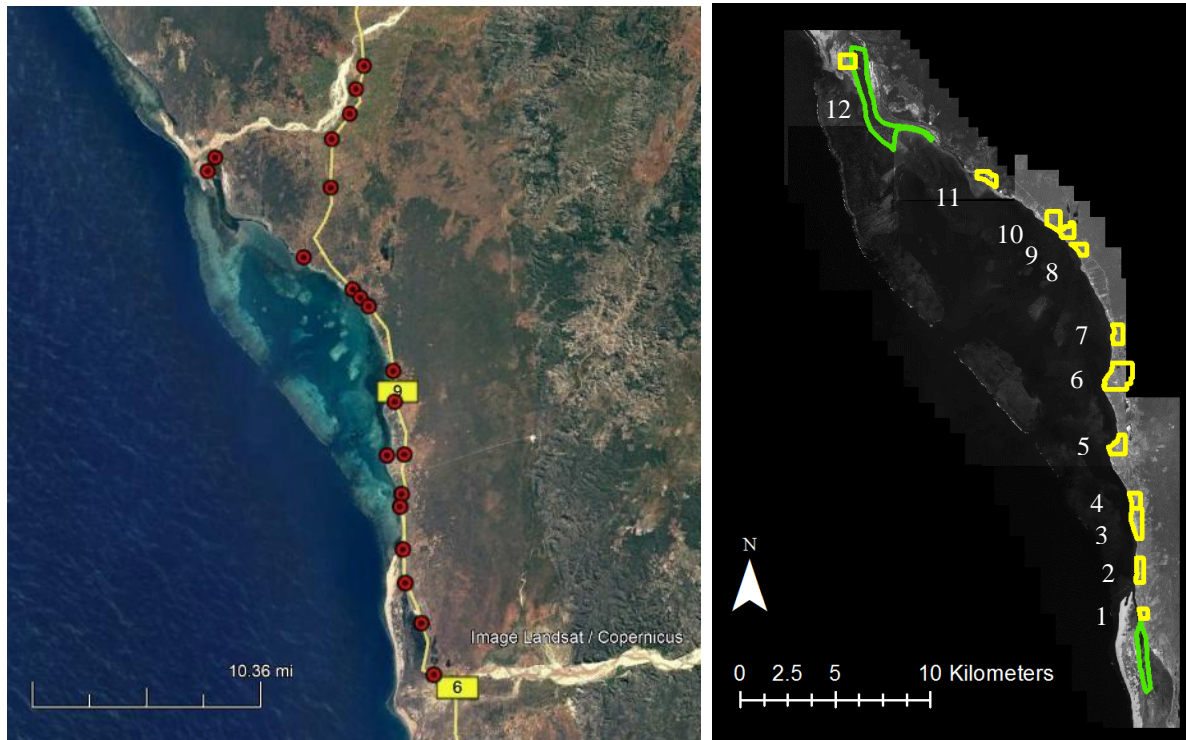


Figure 2.8. a) The 21 villages of the Bay of Ranobe community (red circles, left); b) the 12 coastal Vezo villages (yellow polygons, right) and mangroves at the north-south extremes fo the Bay (green polygon)

of the population, with 34% participating as a secondary occupation (Davies et al., 2009). It is worth noting, however, that the study conducted by Davies et al. (2009) was fairly limited in scope, with surveys conducted over only several months in the 3 southern villages of Beravy, Ifaty, and Mangily. Some spatial variation in occupation percentages likely exists as a function of distance from the principle markets in the provincial capital, Tulear. Additionally, the inclusion of the biggest tourism destination in the study area, Mangily, may have influenced the calculated percentages. Nonetheless, documented percentages of participation in the fishery may be generally applicable and are indicative of the heavy reliance of the Vezo community on fisheries resources.

Population Estimates and Demographics – Enumeration of Dwelling Units

Population estimates, and decadal change thereof, for the 12 Vezo villages of Bay of Ranobe were determined following a bottom-up approach, in which dwelling units were enumerated and correlated to the Bay-wide average number of persons-per-dwelling calculated from micro-census surveys (Wu *et al.*, 2005; Cardenas-Silvan *et al.*, 2010; Udjo, 2015; Wardrop *et al.*, 2018). Population estimates for each village were determined to provide a contemporaneous index of fishing effort corresponding to the fisheries data collection campaign that occurred from 2013-2015. Additionally, population demographic information was examined to provide insights into the spatially changing fishing pressures exerted on local fisheries resources in the decade leading up to the fisheries research presented in chapters 3-4.

To enumerate dwelling units, four IKONOS panchromatic images (Table 2.1) were used to, initially, create a sampling grid in ArcGIS to aid in the systematic enumeration of dwelling units. From the high-resolution panchromatic images, a coastline shapefile was created to which a 1-km buffer was added to encompass the entirety of the coastal fishing villages. Given that all fishermen must leave their boats on the beach, their houses are never far away from the shore, with the majority being within hundreds of meters from the beach (pers. obs.). The 1-km buffer polygon of the shoreline was bisected to obtain the landward side (42.77 km²) (Figure 2.9a). Within the buffer polygon, a 100 m grid was created and divided into 4 arbitrary zones to facilitate the workflow (Figure 2.9b). Each grid cell was labeled with a unique ID (n= 5173) and the 4 grid sections were exported as kml files for importation into Google Earth (Figure 2.10).

Enumeration of dwelling units was conducted using the high-resolution imagery of Google Earth (Yang *et al.*, 2012), with the Google Earth time-lapse feature allowing for the determination of changes in the number of dwelling units over a 12-year period. A dual monitor

Table 2.1. Details of the panchromatic images (Pan) used in the present study

Image ID	Sensor	Date	Spatial Resolution (m)		Nb. Bands	Data
			MS	Pan		
470990	IKONOS-2	2007-03-19	3.28	0.81	4+pan	11-bit
470991	IKONOS-2	2007-03-16	3.28	0.81	4+pan	11-bit
470992	IKONOS-2	2003-10-31	3.28	0.81	4+pan	11-bit
470998	GeoEye-1	2009-07-05	1.64	0.41	4+pan	11-bit

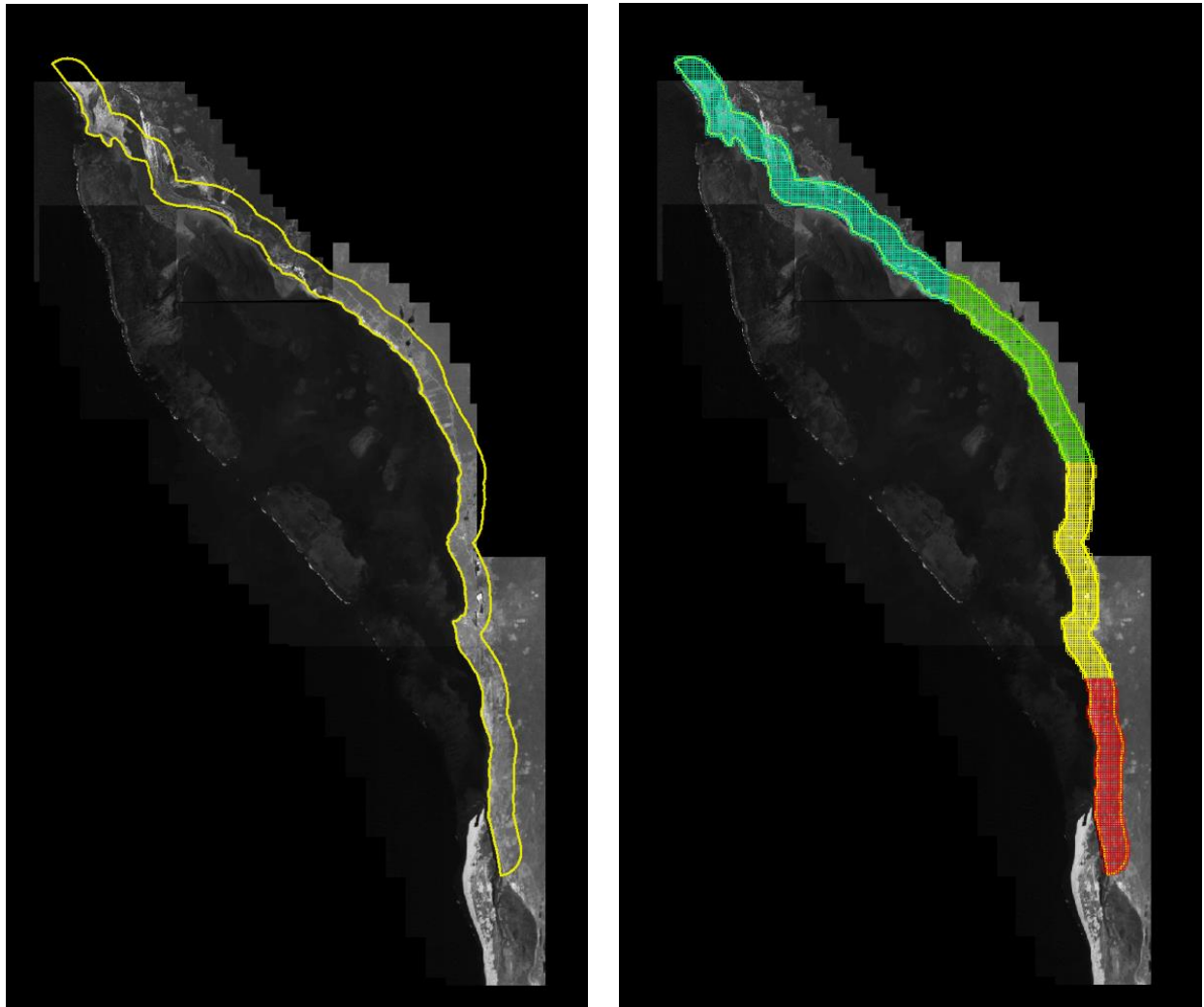


Figure 2.9. a) 1-km buffer region created as boundary on landward side of the shore; b) 100 m grid divided into sections for export to Google Earth



Figure 2.10. 100-m grid shapefile imported into Google Earth, labeled with unique numbering system for individual grid cells, corresponding to dwelling-unit count (top); close-up view demonstrates clarity of image and resolution; note, individual boats, *pirogues*, visible on beach (bottom)

system was used in which visual counts of dwelling units, corresponding to a uniquely identified grid cell, were recorded into the attribute table of the original 100 m grid shapefile in ArcGIS. Dwelling units falling within the established grid system were systematically counted at four points in time, covering a period of 12 years. Specific dates within a given year were selected to achieve the best overall consistency between the different villages. However, given that the availability and quality of image tiles varied, whenever specific image-dates were unavailable the next closest date was used. For example, the top row of Table 2.2 illustrates a case-in-point, where the most closely aligned image-dates for the villages of Ambotsibotsike, Ifaty, and Betsibaroka are 7-Mar-16, 7-Mar-16, and 29-Feb-16, respectively. Additionally, the time steps, Δt , for a given period and village were selected based on image availability and quality: Δt_1 (2004-2009), Δt_2 (2009-2012), and Δt_3 (2012-2016). (Table 2.2)

Percent change in the number of dwelling units was calculated for each village and time step (Δt_{1-3}). Percentages were then annualized for standardization purposes by determining the number of days between time steps, then dividing by 365 days. Annualized percent change was calculated by dividing the change in dwelling unit, DU , by fractional years, Y (Table 2.3).

$$\text{Annualized \% Change} = ((DU_t - DU_{t+1}) / DU_{t+1}) / Y$$

Population Estimates and Demographics – Residential Headcount / Micro-census

In order to generate population estimates based on the enumeration of dwelling units, a micro-census survey was conducted March-May 2015 to determine the average number of people per household and per building. Villages were first delimited in GIS based on actual and/or effective village limit, when the actual boundaries were unknown. Effective village limit

Table 2.2. Selected image dates for each of the 12 Vezo villages

Village	Date	Village	Date	Village	Date
Ambotsibotsike	7-Mar-16	Ifaty	7-Mar-16	Betsibaroaka	29-Feb-16
	12-Sep-12		12-Sep-12		15-Mar-12
	9-Jun-09		9-Jun-09		4-Apr-09
	24-Apr-04		29-Apr-04		24-Apr-04
Tsongeritelo	7-Mar-16	Mangily	16-Feb-16	Ambolomailaka	29-Feb-16
	12-Sep-12		12-Sep-12		5-Mar-13
	20-Jun-09		9-Jun-09		4-Apr-09
	24-Apr-04		29-Apr-04		24-Apr-04
Beravy	7-Mar-16	Amboaboaka	16-Feb-16	Andrevo	29-Feb-16
	12-Sep-12		12-Sep-12		15-Mar-12
	9-Jun-09		9-Jun-09		4-Jul-09
	24-Apr-04		29-Apr-04		24-Apr-04
Ambalaboy	7-Mar-16	Madiorano	29-Feb-16	Fitsitke	23-Feb-16
	12-Sep-12		15-Mar-12		15-Mar-12
	9-Jun-09		4-Apr-09		4-Jul-09
	29-Apr-04		24-Apr-04		15-Jun-03

Table 2.3. Fractional year, Y , per time-step and village

Village	Y	Village	Y	Village	Y
Ambotsibotsike	3.48	Ifaty	3.48	Betsibaroaka	3.96
	3.26		3.26		2.95
	5.13		5.12		4.95
Tsongeritelo	3.48	Mangily	3.43	Ambolomailaka	2.99
	3.23		3.26		3.92
	5.16		5.12		4.95
Beravy	3.48	Amboaboaka	3.43	Andrevo	3.96
	3.26		3.26		2.70
	5.13		5.12		5.20
Ambalaboy	3.48	Madiorano	3.96	Fitsitke	3.95
	3.26		2.95		2.70
	5.12		4.95		6.06

was defined as a polygon of the area encompassing >90% of the residential structures. Target villages were selected for the micro-census to maximize the spatial variation along the coastline of the Bay of Ranobe, and included the villages of: Ifaty, Mangily, Betsibaroka, Ambolomailaka, and Fitsitke. Within each of the village polygons random points were generated, representing sample locations. Households located at or near the random points were surveyed, if the head(s) of the household were present (Figure 2.11). In addition to headcounts, data were collected on the number of buildings associated with the family, considering that many families may have separate building structures for sleeping and cooking that would be included in dwelling unit count. Census data allowed for the calculation of the average number of people per structure multiplier used in conjunction with the dwelling unit count, allowing for the estimation of village populations.

Fisheries Socioeconomic Surveys

During the first year of the fisheries surveys (2013 – 2015), socioeconomic surveys were conducted from May-October 2013 on fishermen originating from the same villages targeted by the fisheries surveys: Beravy, Ifaty, Ambolomailaka, and Andrevo. It is worth noting that, culturally, all boat-based fishing activities, which is the subject of the present dissertation, are conducted by men, hence the use of the term “fishermen” and not the gender-neutral term “fisherfolk”. In Vezo culture, women and children actively participate in intertidal gleaning activities, but are not usually involved in boat-based activities. Thus, all fisheries-related survey information was provided by the fishermen of the targeted villages, and is discussed further in Chapter 3.

Survey questions were designed to obtain sociological, demographic, and economic data on those directly involved in the Bay of Ranobe, day-time, boat-based fisheries. Questions

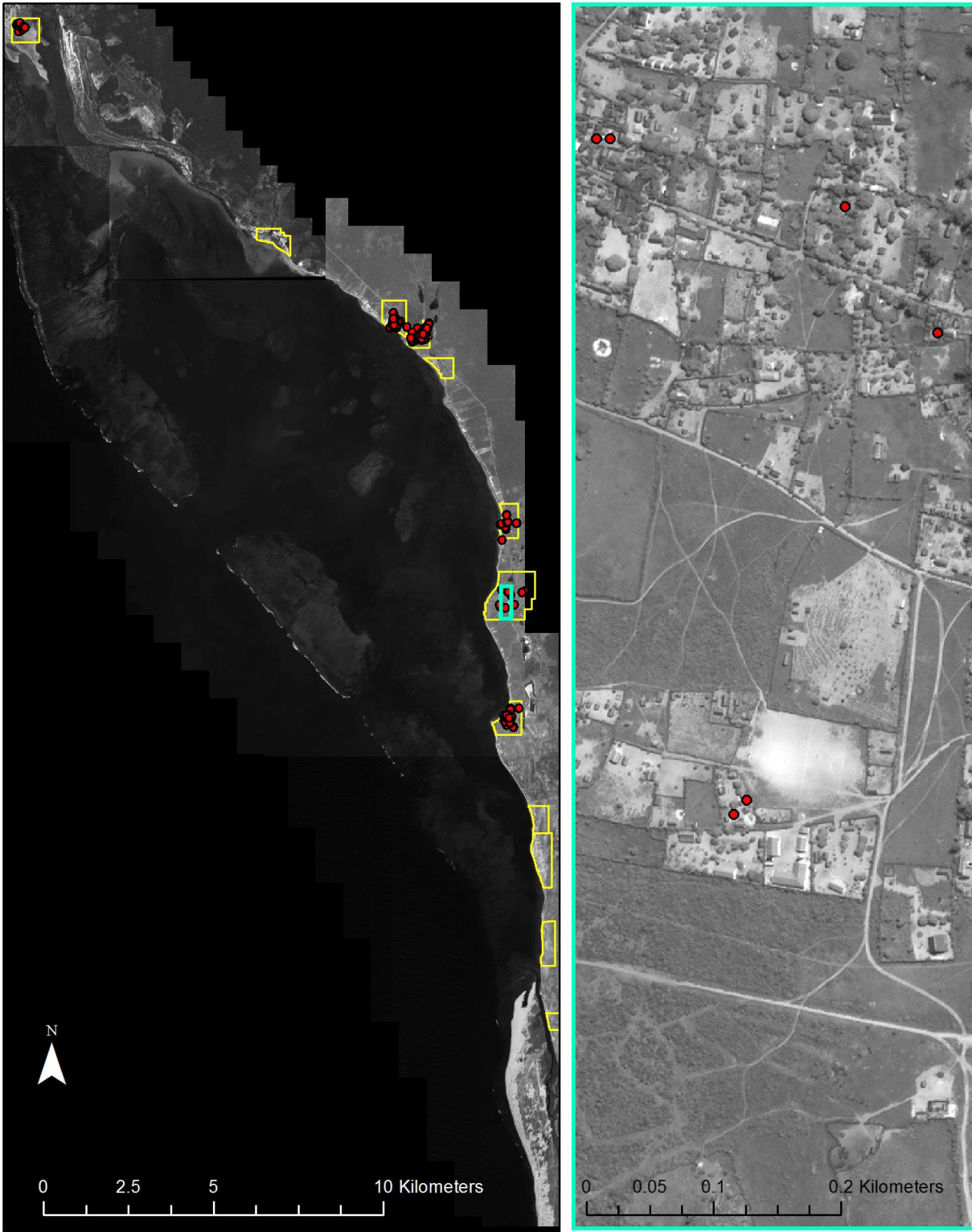


Figure 2.11. Spatial distribution of household surveys conducted (red circles) in the villages of Ifaty, Mangily, Amboaboaka, Betsibaroka, Ambolomailaka, and Fitsitke, south to north

addressed each individual member of a given boat-based group from the “head fishermen”, or boat owner, to all others assisting. Sociological and demographic questions assessed the fishermen’s village of origin, village of birth, year in which they moved (if applicable), age, and number of children. The economic portion of the survey strived to understand the financial benefits obtained by the fishermen, specifically addressing the number, weight, and species of catch kept by the fishermen for personal consumption versus the portion of the catch that was destined to be sold. Additionally, information was collected on the anticipated price that would be obtained for the various species and quantities to be sold, as an indicator of revenue. (See Appendix 2.1 for datasheet)

Surveys were conducted following a spatially stratified design in which the designated landing zones of targeted villages were divided into 3 sub-zones, whose assigned length of shoreline was inversely proportional to the number of boats on the beach in order to maintain consistency in the total number of boats within a specific zone. Additionally, the use of sub-zones ensured that the entire shoreline within the targeted village were covered by the sampling effort. Landing zone lengths varied from approximately 500 m to 1025 m (Figure 2.12). A trained team of 3-4 people recruited from the local population collectively formed the fisheries data collection team, with one member of the team tasked with the socioeconomic survey as the others surveyed the catch. A ticketing system was used in which, at sunrise, tickets were distributed following a roving survey approach, as the survey team systematically patrolled the zone encountering fishermen as they depart (Ma *et al.*, 2018). Fishermen that received a ticket in the morning were intercepted as they returned for surveying purposes. Given that the boats used in the Bay of Ranobe fisheries are unregistered / unmarked, hand-made canoes, a fully randomized approach based on registration numbers was not feasible for the purposes of this

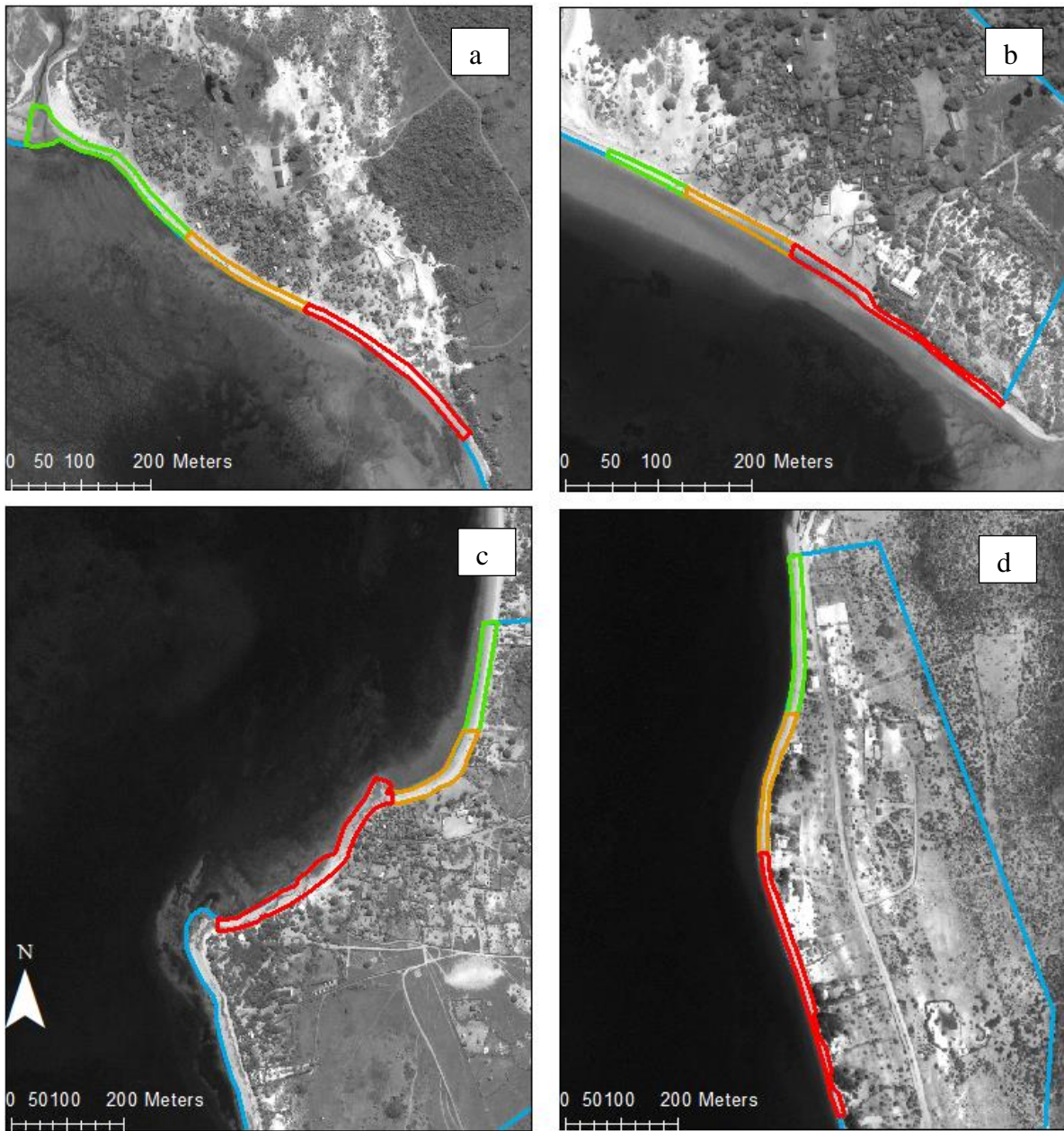


Figure 2.12. Village landing zones (LZ) divided into sub-zones (green, orange, and red) for surveying purposes: a) Andrevo (LZ = 785m), b) Ambolomailaka (LZ= 500m), c) Ifaty (LZ= 620m), and d) Beravy (LZ= 1025m)

study. An early attempt was made, by the author, to register all of the boats participating in local fisheries: a numbering system was devised and hundreds of boats had registration numbers painted on the hulls. However, strong winds and blowing sands, removed nearly all of the registration numbers from most of the boats within 3-5 months.

2.3 Results & Discussion

Population Estimates

To determine human population distributions and densities contemporaneous to the fisheries data collection campaign, dwelling unit counts were conducted on residential structures within a distance of 1 km of the shoreline along the entire coast of the Bay of Ranobe, using Google Earth images from 2016 that covered an area of 42.77 km² at a 100 m grid resolution. Household micro-census surveys conducted at random points (n= 124) were used to determine the average number of people per building (mean = 3.27, SD= 0.99) in 6 of the 12 coastal villages of the Bay: Ifaty (n= 31), Mangily (n= 10), Amboaboaka (n= 8), Betsibaroka (n= 54), Ambolomailaka (n= 18), and Fitsitke (n= 3). Previous household survey studies have found similar results, with the mean number of persons per sleeping room ranging from 3.0 – 3.4, while 70% of households have only 1 sleeping room (<https://www.statcompiler.com>)(See Table Appendix 2.2). Expansion of dwelling unit counts to population numbers produced a total population for households living within 1 km of the shore in the year 2016 equaling 31,850 people, with 28,046 persons living within the boundaries of the coastal villages studied, here (Figure 2.13).

Since the last national population census, in 1993, the government of Madagascar has been projecting national population numbers based on estimated global rates of population

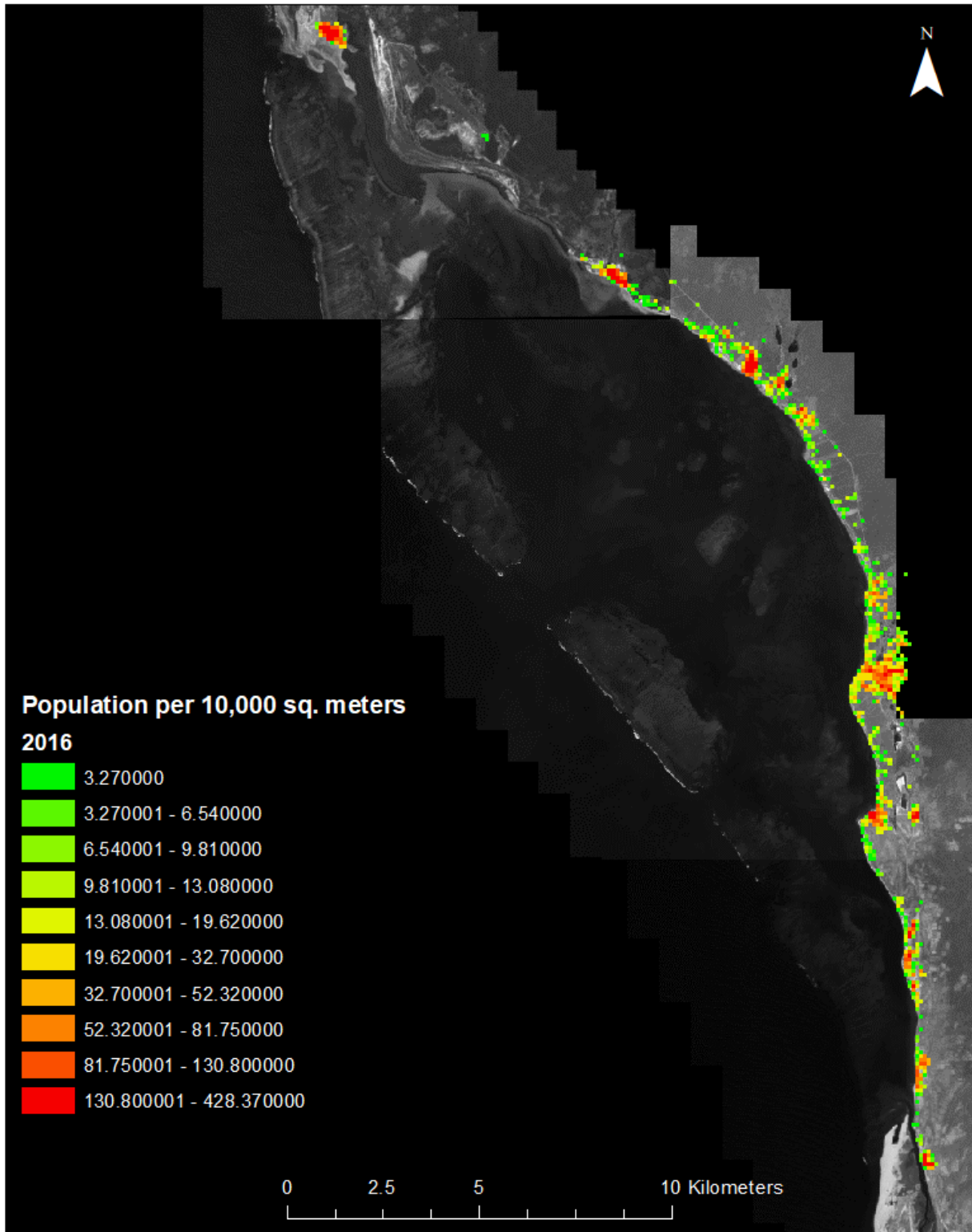


Figure 2.13. Population distribution within 1 km of shore per 100 m grid cell; map legend symbology based on deciles of population count per grid cell

growth that have fluctuated annually, with gradual declines observed during the period 2007-2016 from 2.888% to 2.689%, respectively (<https://data.worldbank.com>). For comparison purposes, population estimates made in 2007 for the villages of the Bay of Ranobe were obtained from a governmental online source and projected for 2016 based on the average rate of growth of 2.78%. Population projections, based on 2.78% growth, are compared to the population estimates calculated from the dwelling unit census and sociological surveys (Table 2.5).

Results of the comparison demonstrate that the population estimates and growth rates calculated following the methods of the present study differ substantially from the official estimates and rates. On a village-by-village basis, growth rates varied from 2.96% to 6.83%, with an average growth rate of 4.63%, as compared to the national average of 2.78%. Although the growth rates calculated for the Bay of Ranobe coastal villages are substantially higher than the national average, previous research has found that growth rates in the poorest regions of the country are considerably greater than the national average, ranging from 3% - 4% in many areas of Madagascar and even +4% in others (Harrison *et al.*, 2000; Bruggemann *et al.*, 2012).

Elevated population growth rates in the Bay of Ranobe are likely attributable to multiple factors:

- 1) increased birth rates that are commonly observed amongst the poorest households as a response to create more “helping hands” around the house (Delaunay, 2013);
- 2) waves of immigration in response to catastrophic events, such as drought, locust outbreaks, and general food insecurity that periodically occurs in southern Madagascar (FAO, 2016; IOM, 2017);
- 3) urban exodus associated with violence resulting from periods of political instability (See “2009 Malagasy political crisis”, Wikipedia);
- 4) a general attraction to the area for the exploitation of marine resources, and/or employment opportunities in the local eco-tourism sector (pers. obs.).

Table 2.4. Population estimates per village based on projections of a global average population growth rate of 2.78% (2007 and 2016), values used by the government of Madagascar, and population estimates based on dwelling unit counts for 2004 and 2016

Village	<u>Population Projection @2.78%</u>		<u>Population Estimates</u>		Growth rate
	2007*	2016	2004	2016	
AMBOTSIBOTSIKE	864	1106	889	1262	2.96%
TSONGERITLO	1,049	1343	824	1442	4.77%
BERAVY	853	1092	988	1691	4.58%
AMBALABOY	762	975	471	870	5.25%
IFATY	2,130	2726	1628	2338	3.06%
MANGILY	1,818	2327	3231	6363	5.81%
AMBOABOAKA	946	1211	713	1203	4.45%
MADIORANO	383	490	664	1125	4.49%
BETSIBAROKA	472	604	464	1027	6.83%
AMBOLOMAILAKA	964	1234	1861	3734	5.97%
ANDREVO	900	1152	1887	3044	4.06%
FITSITIKE	1,683	2154	2678	3947	3.28%
Total	12,824	16,413	16,298	28,046	

*https://www.madacamp.com/images/madagascar/Effectif_Population_par_Fokontany_Madagascar.xls

As a final note on population growth rate estimates for Madagascar, one month prior to submitting the present dissertation (August 2019), the government of Madagascar published provisional results of the most recent population census, conducted from May-June 2018 (INSTAT-CCER, 2019). Unsurprisingly, growth rates were significantly higher than the 2.78% average that has been used by the government since 1993. According to the latest figures, growth in the population between the years 1993 – 2018 reached 3.01% as a national average, resulting in a total population of 25,680,342 people. Regional growth rates varied considerably from 2.29% - 4.81%, with the region of the present study, *Atsimo-Andrefana*, exhibiting a 3.60% growth rate.

A comparison of the population map product from the present study (Figure 2.13) to the map produced by the WorldPop algorithm (Figure 2.4) demonstrates some of key shortcomings

of this method, as identified in the Introduction. Specifically, in regions of the world where access to electricity is limited or non-existent, the lights-at-night covariate used in the statistical model is ineffective. More importantly, the relationship between patterns of land-use and population density may be highly irregular in certain regions of the world, such is the case for the Bay of Ranobe. The WorldPop map (Figure 2.4) correctly identifies a center of population density to the south of the Bay of Ranobe, which represents the urban population of the provincial capital city, Toliara. Following the WorldPop map north from Toliara, there is some indication of coastal populations, particularly for the biggest village in the area, Mangily. High population densities are then erroneously detected in the village of Fitsitke, which is constructed on a sand spit naturally lacking vegetation. However, the WorldPop algorithm appears to interpret this as human-caused land transformation. Moreover, at the point where the principle route turns away from the coast (see Figure 2.8a), it can be seen that the population identified in the WorldPop map corresponds to the 5 villages along the *route nationale* south of the Manombo River. The footprint of these 5 agricultural villages is disproportionately large, with respect to their actual populations, due to the fact that this area represents the site of a previous irrigation project. Diversions of water from the Manombo River to this area have allowed for a greater expanse and intensity of cultivation than is normally observed in this arid region. A disproportionately high land-use / land change rate relative to local human population numbers and proximity to the route national, covariates used in the model, likely resulted in the prediction biases observed in the WorldPop population distribution predictions for the Bay of Ranobe communities. Although some degree of prediction error is understandable, with a significant proportion of the world's population living near the coast, systematic biases resulting in the underestimation of coastal populations could have serious consequences.

Demographics

Dwelling units counts conducted for years 2004, 2009, 2012, and 2016 allow for the quantification of the shifts in population density that occurred leading up to, and throughout, the study period: ΔT_1 (2004-2009), ΔT_2 (2009-2012), and ΔT_3 (2012-2016). Given that the majority of village houses are impermanent structures, with walls and roofing materials built of dry grasses and wood, they can be easily erected, disassembled, and moved, thereby acting as a reliable proxy of human population movements. Figure 2.14 illustrates the overall pattern of development of the coastline during the period 2004 – 2016, with the open spaces between the villages that existed in 2004 becoming developed.

To evaluate incremental changes in population distribution for time periods T_1 - T_3 , the percent change that occurred within each time period was calculated and mapped (Figure 2.15; Table 2.5). In the earliest time period, T_1 , the general economy of Madagascar was on the rise and the tourism sector was growing. The highest growth rate during this period was observed for the village of Mangily (12.5%), known primarily as an international tourist destination, and secondarily, as a vacation destination for residents. As such, within the village of Mangily, there are a number of internationally-recognized hotels and restaurants. The northern cluster of villages, including the villages of Betsibaroka (10.10%), Ambolomailaka (9.2%), and Madiorano (7.9%), also exhibited high percentages of growth during this period. Again, tourism is likely the most significant factor here, as well, with the village of Ambolomailaka hosting 2-3 large hotels that target international tourists, while the village of Madiorano is the preferred vacation destination in the Bay-area for residents. On the other hand, in the case of Betsibaroka, no tourist infrastructure exists, thus the relatively high growth observed here is likely due to the

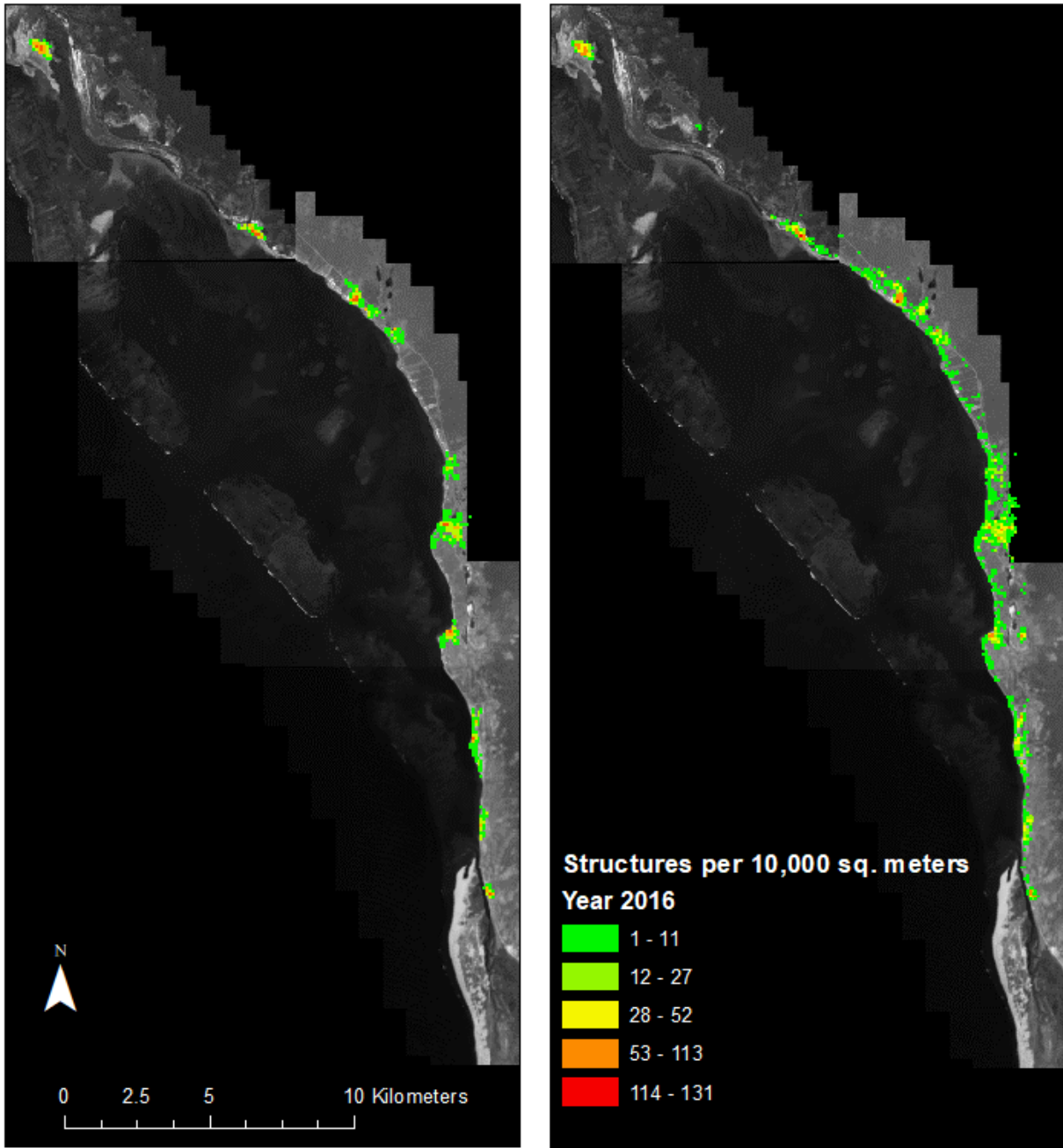


Figure 2.14. Number of dwelling units per 100 m grid cell (10,000 m²) within 1 km of the coast for years 2004 (left) and 2016 (right)

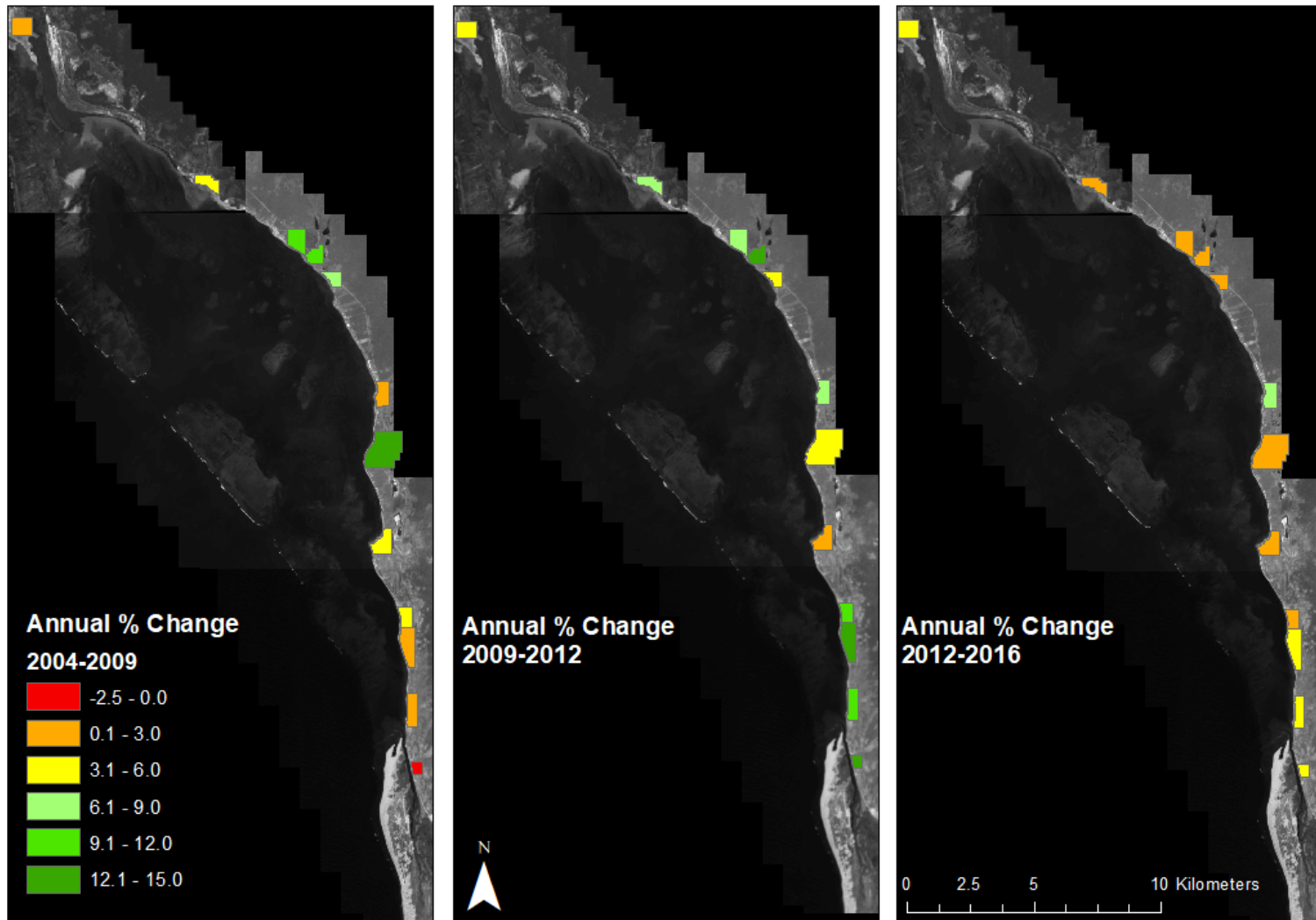


Figure 2.15. Spatial representation of percent change in dwelling unit counts for the 3 time periods, T_1 - T_3 , studied here: 2004-2009, 2009-2012, 2012-2016

Table 2.5. Percent change in dwelling unit count for 3 time periods, T₁-T₃, spanning years 2004 – 2016

Village	<u>Annual % Change</u>		
	2004-2009	2009-2012	2012-2016
	<i>T₁</i>	<i>T₂</i>	<i>T₃</i>
Ambotsibotsike	-2.50%	13.6%	3.7%
Tsongeritelo	1.50%	10.8%	5.8%
Beravy	0.80%	12.5%	4.9%
Ambalaboy	5.30%	11.1%	2.0%
Ifaty	4.20%	2.7%	2.4%
Mangily	12.50%	4.1%	1.7%
Amboaboaka	1.30%	7.2%	8.1%
Madorano	7.90%	4.9%	1.6%
Betsibaroka	10.10%	12.9%	1.7%
Ambolomailaka	9.20%	6.8%	3.0%
Andrevo	3.50%	8.9%	2.6%
Fitsitke	2.60%	4.6%	3.3%

proximity of the village to these former tourist destinations. Residents of Betsibaroka were likely benefitting from the growing need of resources driven by the tourist industry, acting as suppliers of fish, charcoal, and/or wood for construction, which fueled comparatively high growth in the village.

In contrast to the comparatively high growth associated with villages involved directly / indirectly with the tourism sector, the southern villages that are closest to the regional capital, Toliara, exhibited the lowest, and even negative, growth rates during the T₁ period: Ambostkebotske (-2.50%), Tsongeritelo (1.5%), Beravy (0.80%), and Amabalaboy (5.30%). Low growth in the southern villages of the lagoon may be a reflection of the depletion of fisheries resources that had already occurred by the early 2000's, as a result of the demand of the nearby urban population of Toliara. The negative correlation between distance to markets and abundance of fisheries resources is a well-documented phenomenon (*e.g.* Brewer *et al.*, 2009;

Brewer *et al.*, 2012; Brewer *et al.*, 2013; Cinner *et al.*, 2013).

During the T₂ period (2009-2012), a near complete reversal occurred, where the southern villages with the lowest growth rates became the fastest growing villages, and the growth in the villages associated with tourism declined dramatically. Reversal in growth trends observed during this period, particularly the double-digit growth in southern villages of Ambostkebotske (13.50%), Tsongeritelo (10.8%), Beravy (12.5%), and Amabalaboy (11.1%) and the substantial reductions in tourism-related growth, are likely the direct result of the 2009 political crisis. In 2009, a *coup d'état* abruptly ended a brief period of economic growth, with the eruption of violence in some cities, tourism suddenly and dramatically declined and local residents fled the violence and looting of the urban centers. Unfortunately, this phenomenon has occurred on multiple occasions in Madagascar's history and is considered the principle contributing factor to the country's overall sub-standard level of development and economic well-being (Figure 2.16). During the T₃ period (2012-2016), growth in all the villages stabilized, with growth rates ranging from 1.6% - 8.1%.

Fisheries Socioeconomics

Fisheries socioeconomic surveys were conducted from May – October 2013 that specifically targeted fisherman participating in boat-based fishing activities from the villages where surveys of catch were conducted. Survey questions were designed to elicit sociological information from each fisherman, such as family and origin information, and the economic data necessary to obtain estimates of revenue, such as percent of catch kept vs. sold and selling prices. In total, n= 968 fishermen participated in the survey from the four targeted villages: Beravy (n= 190), Ifaty (n= 240), Ambolomailaka (n= 225), and Andrevo (n= 313). Responses to questions concerning age resulted in an overall average age of 28.1 years, with a range of 6 – 80 years old.

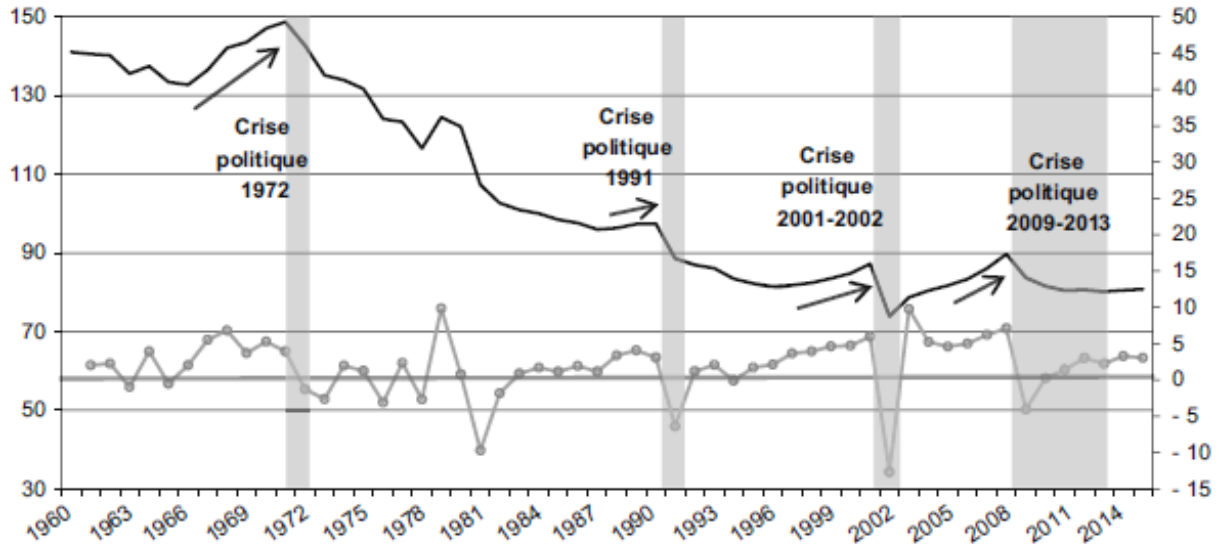


Figure 2.16. Short-lived periods of economic growth in Madagascar, GDP per capita (black line, primary y-axis), interrupted by political crises (*crise politique*), including the political crisis that occurred during the present study, 2009 – 2013; GDP growth rate (gray line, secondary y-axis (%)) (Source: Razafindrakoto *et al.*, 2017)

In response to number of children, survey results produced an average of 2.4 children, with a range of 0 – 21 (See Table 2.7 for summary per village). Given that polygamy is commonly practiced in villages across Africa, and specifically amongst the Vezo, it is indeed feasible that an older man (60-80 y.o.), with 3 – 4 wives, fathered 20+ children. In addition to age and family size, fishermen were asked their village of residence and village of birth to evaluate the percentage of fishermen that were native to the village in which they are currently living, and the general level of immigration experienced within the village. Results of fishermen surveyed at landing points within each of the targeted villages indicated that the percentage of native fishermen for Beravy, Ifaty, Ambolomailaka, and Andrevo, were 70.5%, 76.2%, 44.9%, and 55.9%, respectively. The percentage of native vs non-native fishermen in a village may serve as an indicator of cultural values and respect for village authorities, which in turn, would have implications on the level of compliance to community-based fisheries regulations. As discussed

Table 2.6. Average ages and family size of fishermen per village

Village	n	Mean	Age			Number of Children		
			SD	Min	Max	Mean	Min	Max
Beravy	190	27.69	11.76	12	70	2.27	0	12
Ifaty	240	26.86	12.41	7	80	2.02	0	21
Ambolomailaka	225	27.74	12.24	6	77	2.27	0	11
Andrevo	313	30.09	13.98	12	80	2.94	0	20

in the Introduction section, locally-based rules or laws, known as *dinas*, are a commonly-used instrument for the management of natural resources in Madagascar. Enforcement of *dinas* relies on community compliance and the committee of village elders, *hazomanga*, of which the village chief is a member. In rare cases, dina-related infractions could be, and have been, pursued in the criminal court system. However, the legal framework required to bridge village law and the justice system has not been adequately detailed to produce efficient and satisfactory results.

For the economic portion of the survey questions, data were collected on the weights of fish kept by the fishermen for personal consumption, the weight and identity of species sold, and the price received by the fishermen for their catch from a single-day trip. Data on weights of catch kept and/or sold were, initially, analyzed to determine the percentage / frequency / probability of the four potential outcomes of a fishing-trip event: 1) frequency of events of zero catch, thus zero fish kept for consumption and zero fish sold (0/0), the frequency of trips resulting in zero fish kept and positive sales (0/+), the frequency of trips in which all catch was kept for consumption and zero sold (+/0), and the frequency of trips resulting in enough catch for both personal consumption and sales (+/+). Of the total number of responses (n= 2696), 6.2 % of the fishing days resulted in zero catch for the period surveyed. For successful fishing days, 69.2% fishermen sold all of their catch and kept none for personal consumption, while 12.9%

kept all of their catch for personal consumption, and 11.7% caught enough to keep a portion and sell the rest. (See Table 2.8 for a summary of results per village)

Analyses of weights and economic value of surveyed catches indicated that the overall average quantity of fisheries products kept for daily consumption of \bar{x} = 0.23 kg versus the weight of products sold, \bar{x} = 3.70 kg. On average, 6.3% of the catch was kept for personal consumption, while the portion destined for sale generated a revenue of \$3.11 per trip, selling at a price of \$0.86 / kg (See Table 2.9 for a summary of results per village). Table 2.10 provides a listing of fisheries species identified in the catch, including finfish and economically important invertebrate species, ranked by average price per kilogram. Economic value of landings is discussed further in Chapter 4.

Table 2.7. Counts and percentages of fishing daytrip outcomes, kept versus sold, per village

Village	Counts					Percentages			
	<i>0 Kept</i>	<i>0 Kept</i>	<i>(+) Kept</i>	<i>(+) Kept</i>	<i>Total</i>	<i>0 Kept</i>	<i>0 Kept</i>	<i>(+) Kept</i>	<i>(+) Kept</i>
	<i>0 Sales</i>	<i>(+) Sales</i>	<i>0 Sales</i>	<i>(+) Sales</i>		<i>0 Sales</i>	<i>(+) Sales</i>	<i>0 Sales</i>	<i>(+) Sales</i>
Ambolomailaka	33	417	43	55	548	6.0%	76.1%	7.8%	10.0%
Andrevo	48	532	106	76	762	6.3%	69.8%	13.9%	10.0%
Beravy	10	276	69	37	392	2.6%	70.4%	17.6%	9.4%
Ifaty	69	429	88	123	709	9.7%	60.5%	12.4%	17.3%

Table 2.8. CPUE, total and average weights, and average sales prices of catch per village

Village	<i>Trip Ct¹</i>	Total Wt		Average Wt		<i>% Kept (Wt)</i>	Average Sale Price		
		<i>Kept (kg)</i>	<i>Sold (kg)</i>	<i>Kept (kg)</i>	<i>Sold (kg)</i>		<i>MGA</i>	<i>USD³</i>	<i>USD/kg</i>
Ambolomailaka	654	89.66	2853.62	0.16	5.26	3%	8189.30	3.69	0.70
Andrevo	858	134.01	2341.24	0.18	3.08	5%	5665.74	2.55	0.83
Beravy	415	153.01	1248.85	0.39	3.19	11%	7570.57	3.41	1.07
Ifaty	769	147.24	2335.93	0.21	3.29	6%	6237.41	2.81	0.85

1. Trip Count equals the number of fishermen interviewed per day per village
2. Conversion of Malagasy Ariary (MGA) to USD based on conversion from Oct 15, 2013 (1 USD: 0.00045 MGA)

Table 2.9. Species identified in the catch ranked by economic value in local currency, Malagasy Ariary (MGA)

Species	Freq occurrence in catch	Total Wt. Sold (kg)	Avg Wt. Sold (kg)	Avg. Price / kg (MGA)	SD Price (MGA)
<i>Scoberomorus commerson</i>	2	11.50	5.75	7082	2649
<i>Parupeneus barberinus</i>	1	3.60	3.60	5833	-
Lobster (unidentified spp)	23	88.52	3.85	5535	2731
<i>Kyphosus vaigiensis</i>	2	6.10	3.05	4586	357
Squid (unidentified spp)	94	199.24	2.12	3729	1014
<i>Lutjanus kasmira</i>	2	11.18	5.59	3647	644
<i>Hemiramphus far</i>	3	8.82	2.94	3603	1898
<i>Scarus psittacus</i>	3	9.87	3.29	3532	572
<i>Chlorurus cynaescens</i>	1	2.02	2.02	3465	-
<i>Lutjanus quinquelineatus</i>	3	7.34	2.45	3359	2396
<i>Terapon jarbua</i>	1	3.06	3.06	3268	-
<i>Lutjanus fulviflamma</i>	2	2.06	1.03	3242	568
<i>Caesio xanthonota</i>	1	3.40	3.40	3235	-
<i>Myripristis adusta</i>	1	25.70	25.70	3113	-
<i>Strongylura incisa</i>	10	32.65	3.27	3003	606
<i>Siganus spinus</i>	5	17.05	3.41	2995	1479
<i>Siganus sutor</i>	113	441.65	3.91	2893	1557
<i>Caesio caerulea</i>	6	22.51	3.75	2765	1656
<i>Rhynchobatus djiddensis</i>	2	5.06	2.53	2749	1924
<i>Gymnothorax undulatus</i>	1	4.80	4.80	2708	-
<i>Mulloidichthys flavolineatus</i>	21	81.42	3.88	2641	1133
<i>Mulloidichthys vanicolensis</i>	2	12.04	6.02	2611	820
<i>Herklotsichthys quadrimaculatus</i>	24	232.05	9.67	2610	2603
<i>Plectorhincus gibbosus</i>	4	10.51	2.63	2604	916
<i>Leptoscarus vaigiensis</i>	31	97.00	3.13	2591	1206
<i>Scarus ghobban</i>	12	53.12	4.43	2569	1079
<i>Lethrinus nebulosus</i>	4	32.41	8.10	2566	483
<i>Naso brevirostris</i>	1	0.90	0.90	2556	-
<i>Abudefduf sexfasciatus</i>	1	4.70	4.70	2553	-
<i>Gerres filamentosus</i>	38	150.51	3.96	2540	773
<i>Tripterodon orbis</i>	1	3.18	3.18	2516	-
<i>Taeniura lymna</i>	1	1.60	1.60	2500	-
<i>Cetoscarus bicolor</i>	1	0.80	0.80	2500	-
<i>Acanthurus xanthopterus</i>	1	5.20	5.20	2500	-
<i>Lethrinus harak</i>	51	126.76	2.49	2489	2443
<i>Naso unicornis</i>	6	34.66	5.78	2488	661

Table 2.9 cont. Species identified in the catch ranked by economic value in local currency, Malagasy Ariary (MGA)

<i>Chelinus trilobatus</i>	17	59.07	3.47	2457	719
<i>Lethrinus borbonicus</i>	20	28.22	1.41	2417	847
<i>Priacanthus hamrur</i>	2	6.56	3.28	2412	44
<i>Hyporhamphus affinis</i>	5	8.35	1.67	2373	1007
<i>Naso annulatus</i>	1	8.47	8.47	2361	-
<i>Calotomus spinidens</i>	1	8.95	8.95	2346	-
<i>Plectorhincus gaterinus</i>	2	13.58	6.79	2317	259
<i>Platycephalus indicus</i>	2	4.53	2.27	2260	715
<i>Pempheris mangula</i>	8	108.52	13.57	2252	1165
<i>Cheilio inermis</i>	1	4.90	4.90	2245	-
<i>Plectorhincus flavomaculatus</i>	7	12.54	1.79	2237	515
<i>Leptomelanosoma indicum</i>	2	21.40	10.70	2235	880
<i>Sargocentron diadema</i>	5	34.95	6.99	2186	665
<i>Plectorhincus paulayi</i>	1	6.95	6.95	2158	-
<i>Thalassoma hebracium</i>	1	3.30	3.30	2121	-
<i>Spratelloides delicatulus</i>	14	200.33	14.31	2116	660
<i>Octopus cyanea</i>	322	1036.23	3.22	2100	1862
<i>Papilloculiceps longiceps</i>	22	89.12	4.05	2083	597
<i>Lethrinus rubrioperculatus</i>	4	13.51	3.38	2052	774
<i>Acanthurus triostegus</i>	2	10.17	5.09	1986	1031
<i>Sphryaena barracuda</i>	1	2.52	2.52	1984	-
<i>Lethrinus olivaceus</i>	2	9.03	4.52	1980	28
<i>Scomberoides commersonianus</i>	13	58.53	4.50	1967	821
<i>Abudefduf vaigiensis</i>	10	27.52	2.75	1937	792
<i>Lethrinus lentjan</i>	2	3.72	1.86	1916	476
<i>Monotaxis grandoculis</i>	1	2.88	2.88	1910	-
Shrimp (unidentified spp)	2	7.00	3.50	1795	181
<i>Chirocentrus dorab</i>	15	65.91	4.39	1783	463
<i>Naso fageni</i>	1	3.40	3.40	1765	-
<i>Conger cinerus</i>	10	42.44	4.24	1748	869
<i>Torpedo sinuspersici</i>	2	3.70	1.85	1632	893
<i>Gymnothorax javanicus</i>	2	6.22	3.11	1563	91
<i>Plotosus lineatus</i>	48	328.16	6.84	1563	1000
<i>Sphyrna lewini</i>	1	16.20	16.20	1543	-
<i>Fistularia commersonii</i>	1	8.64	8.64	1389	-
<i>Taeniamia fucata</i>	3	18.60	6.20	904	103
<i>Heteropriacanthus cruentatus</i>	1	1.30	1.30	769	-

Works Cited

- Akire, S., J. Foster, and M.E. Santos. 2011. Where did identification go? *Journal of Economic Inequality*, 9: 501-505.
- Allen, J. and K. Lu. 2003. Modeling and prediction of future urban growth in the Charleston region of South Carolina: a GIS-based integrated approach. *Conservation Ecology*, 8: 2.
- Anderson, Weston, Seth Guikema, Ben Zaitchik, William Pan. 2014. Methods for estimating population density in data-limited areas: evaluating regression and tree-based models in Peru. *PLOS ONE*, 9: 1-15.
- Andriamalala, G. and C.J. Gardner. 2010. L'utilisation du dina comme outil de gouvernance des ressources naturelles: leçons tirés de Velondriake, sud-ouest de Madagascar. *Tropical Conservation Science*, 3 : 447-472.
- Andrianaivoarimanana, V., Kreppel, K., Elissa, N., Duplantier, J.M., Carniel, E., Rajerison, M. and R. Jambou. 2013. Understanding the persistence of plague foci in Madagascar. *PLoS Neglected Tropical Diseases*, 7: 1-8.
- Astuti, R. 1995. People of the sea: Identity and descent among the Vezo of Madagascar. Cambridge: Cambridge University Press.
- Baker, Jack D., Adelamar Alcantara, Xiamin Ruan, Srini Vasan, and Crouse Nathan. 2013. An evaluation of the accuracy of small-area demographic estimates of population at risk and its effect on prevalence statistics. *Population Health Metrics*, 11: 1-11.
- Ban, Nathalie Corinna and Carissa Joy Klein. 2009. Spatial socioeconomic data as a cost in systematic marine conservation planning. *Conservation Letters*, 2: 206-215.
- Bosier, P., M. Rasolomaharo, G. Ranaivoson, B. Rasoamanana, L. Rakoto, Z. Andrianirina, B. Andriamahefazafy, and S. Chanteau. 1997. Urban epidemic of bubonic plague in Majunga, Madagascar: epidemiological aspects. *Tropical Medicine and International Health*, 2: 422-427.
- Brewer, T.D., Cinner, J.E., Green, A. and J.M. Pandolfi. 2009. Thresholds and multiple scale interaction of environment, resource use, and market proximity on reef fishery resources in the Solomon Islands. *Biological Conservation*, 142: 1797-1807.
- Brewer, Tom D., Joshua E. Cinner, Rebecca Fisher, Alison Green, Shaun K. Wilson. 2012. Market access, population density, and socioeconomic development explain diversity and functional group biomass of coral reef fish assemblages. *Global Environmental Change*, 22: 399-406.

- Brewer, T.D., Cinner, J.E., Green, A. and R.L. Pressey. 2013. Effects of human population density and proximity to markets on coral reef fishes vulnerable to extinction by fishing. *Conservation Biology*, 27: 443-452.
- Brosio, G. 2000. Decentralization in Africa. International Monetary Fund. Washington, DC. Processed, 40.
- Bruggemann, J. Henrich, Martine Rodier, Mireille M.M. Guillaume, Serge Andrefouet, Robert Arfi, Joshua E. Cinner, Michel Pichon, Frederic Ramahatratra, Faravavy Rasoamanendrika, Jens Zinke, and Tim R. McClannahan. 2012. Wicked social-ecological problems forcing unprecedented change on latitudinal margins of coral reefs: the case of southwest Madagascar. *Ecology and Society*, 17: 47.
- Burnod, P., Gingembre, M. and R.A. Ratsialonana. 2013. Competition over authority and access: International land deals in Madagascar. *Development and change*, 44: 357-379.
- Cardenas-Silvan, Jose L., Le Wang, Peter Rogerson, Changshan Wu, Tiantian Feng, and Benjamin D. Kamphaus. 2010. Assessing fine-spatial-resolution remote sensing for small-area population estimation. *International Journal of Remote Sensing*, 31: 5605-5634.
- Cinner, J.E. and R.B. Pollnac. 2004. Poverty, perceptionis and planning: why socioeconomics matter in the management of Mexican reefs. *Ocean & Coastal Management*, 47: 479-493.
- Cinner, Joshua E., Stephen G. Sutton, and Trevor G. Bond. 2007. Socioeconomic thresholds that affect use of customary fisheries management tools. *Conservation Biology*, 21: 1603-1611.
- Cinner, J.E. 2007. Designing marine reserves to reflect local socioeconomic conditions: lessons from long-enduring customary management systems. *Coral Reefs*, 26: 1035-1045.
- Cinner, J.E., T. Daw, and T.R. McClanahan. 2008. Socioeconomic factors that affect artisanal fishers' readiness to exit a declining fishery. *Conservation Biology*, 23: 124-130.
- Cinner, Joshua E., Timothy R. McClanahan, Tim M. Daw, Nicholas A.J. Graham, Joseph Maina, Shaun K. Wilson, and Terrence P. Hughes. 2009. Linking social and ecological systems to sustain coral reef fisheries. *Current Biology*, 19: 206-212.
- Cinner, J.E., Graham, N.A., Huchery, C. and M.A. MacNeil. 2013. Global effects of local human population density and distance to markets on the condition of coral reef fisheries. *Conservation Biology*, 27: 453-458.
- Clayton, C. and J. Estes. 1980. Image analysis as a check on census enumeration accuracy. *Photogrammetric Engineering and Remote Sensing*, 46: 757-764.

- Clouston, Sean A.P., Josh Yukich, and Phil Anglewicz. 2015. Social inequalities in malaria knowledge, prevention and prevalence among children under 5 years old and women aged 15-49 in Madagascar. *Malaria Journal*, 14: 1:10.
- Cullman, G. 2015. Community forest management as virtualism in northeastern Madagascar. *Human Ecology*, 4: 29-41.
- Davies, T.E., N. Beanjara, and T. Tregenza. 2009. A socio-economic perspective on gear-based management in an artisanal fishery in south-west Madagascar. *Fisheries Management and Ecology*, 16: 279-289.
- Delaunay, Valerie. 2013. L'exploitation économique des enfants à Madagascar à partir de l'enquête démographique et de sante 2008. *Population*, 68: 331-348.
- Fan, C.S., Lin, C. and D. Treisman. 2009. Political decentralization and corruption: Evidence from around the world. *Journal of Public Economics*, 93: 14-34.
- FAO, Food and Agriculture Organization. 2016. Réponse à l'invasion acridienne à Madagascar, Campagne 2015/16, Rapport Final.
- Frye, Charlie, Earl Nordstrand, Dawn J. Wright, Carmelle Terborgh, Jeanne Foust. 2018. Using classified and unclassified land cover data to estimate the footprint of human settlement. *Data Science Journal*, 17: 1-12.
- Grenier, Christophe. 2013. Genre de vie Vezo, pêche traditionnelle et mondialisation sur le littoral sud-ouest de Madagascar. *Annales de Géographie*, 693: 549-571.
- Grippa, T., Linard, C., Lennert, M., Georganos, S., Mboga, N., Vanhuyse, S., Gadiaga, A. and E. Wolff. 2019. Improving Urban Population Distribution Models with Very-High Resolution Satellite Information. *Data*, 4: 13.
- Harris, A.R. 2011. Out of sight but no longer out of mind: a climate of change for marine conservation in Madagascar. *Madagascar Conservation & Development*, 6: 7-14.
- Harrison, Paul, Fred Pearce, and Peter H. Raven. 2000. AAAS Atlas of Population & Environment. University of California Press, 186-187.
- Hasse, J.E. and R.G. Lathrop. 2003. Land resource impact indicators of urban sprawl. *Applied Geography*, 23: 159-175.
- Hillson, R., Alejandro, J.D., Jacobsen, K.H., Ansumana, R., Bockarie, A.S., Bangura, U., Lamin, J.M. and D.A. Stenger. 2015. Stratified sampling of neighborhood sections for population estimation: A case study of Bo City, Sierra Leone. *PloS one*, 10: p.e0132850.
- Houghton, R.A. 1999. The annual net flux of carbon to the atmosphere from changes in land use 1850–1990. *Tellus B*, 51: 298-313.

- INSTAT-CCER. 2019. Troisième recensement général de la population et de l'habitation (RGPH-3). Institut National de la Statistique, Cellule Centrale d'Exécution du Recensement. Février 2019.
- Iisaka, J. and E. Hegedus. 1982. Population estimation from Landsat imagery. *Remote Sensing of the Environment*, 12: 259-272.
- International Organization for Migration (IOM), UN Migration Agency. 2017. Evidencing the impacts of the humanitarian crisis in Southern Madagascar on migration, and the multisectorial linkages drought-induced migration has on other sectors of concern. Assessment Report, January 2017.
- Jetz, W., Wilcove, D.S. and A.P. Dobson. 2007. Projected impacts of climate and land-use change on the global diversity of birds. *PLoS Biology*, 5: 157.
- Jones, J.P., Andriamarivololona, M.M. and N. Hockley. 2008. The importance of taboos and social norms to conservation in Madagascar. *Conservation Biology*, 22: 976-986.
- Kalnay, E. and M. Cai. 2003. Impact of urbanization and land-use change on climate. *Nature*, 423: 528.
- Kang, Su Yun, Katherine E. Battle, Harry S. Gibson, Arsene Ratsimbaoa, Milijoana Randrianariveolosia, Stephanie Ramboarina, Peter A. Zimmerman, Daniel J. Weiss, Ewan Cameron, Peter W. Gething, and Rosalind E. Howes. 2018. Spatio-temporal mapping of Madagascar's malaria indicator survey results to assess *Plasmodium falciparum* endemicity trends between 2011 and 2016. *BMC Medicine*, 16: 1-15.
- Klein, C.J., A. Chan, L. Kircher, A.J. Cundiff, N. Gardner, Y. Hrovat, A. Scholz, B.E. Kendall, and S. Airame. 2008. Striking a balance between biodiversity conservation and socioeconomic viability in the design of marine protected areas. *Conservation Biology*, 22: 691-700.
- Kull, C.A. 2002. Empowering pyromaniacs in Madagascar: ideology and legitimacy in community-based natural resource management. *Development and Change*, 33: 57-78.
- Li, G. and Q. Weng. 2005. Using Landsat ETM+ imagery to measure population density in Indianapolis, Indiana, USA. *Photogrammetric Engineering & Remote Sensing*, 71: 947-958.
- Ma, Hongguang, Tom K. Ogawa, Thomas R. Sminkey, F. Jay Breidt, Virginia M. Lesser, Jean D. Opsomer, John R. Foster, David A. Van Voorhees. 2018. Pilot surveys to improve monitoring of marine recreational fisheries in Hawaii. *Fisheries Research*, 204: 197-208.
- Marks, Florian, Natahlie Rabehanta, Stephen Baker, Ursula Pazner, Se Eun Park, Julius N. Fobil, Christian G. Meyer, and Raphael Rakotozandrindrainy. 2016. A way forward for healthcare in Madagascar? *Clinical Infectious Diseases*, 62: S76-S79.

- Merkle, Ortrun, Julia Reinold, and Melissa Siegel. 2017. A study on the link between corruption and the causes of migration and forced displacement. Maastricht: GIZ Anti-Corruption and Integrity Programme.
- Mistiaen, Johan, Berk Ozler, Tiaray Razafimanantena, Jean Razafindravonona. 2002. Putting welfare on the map in Madagascar. Africa Region Working Paper Series No. 34 Oxford Poverty and Human Development Initiative (OPHI). Global MPI Country Briefing 2018: Madagascar (Sub-Saharan Africa). Country Briefing December 2018.
- Pamen, Feubi and M. Keupie. 2017. An application of the Akire-Foster's multidimensional poverty index to data from Madagascar: Taking into account the dimensions of employment and gender inequality. *AFD Research Paper Series*, No. 2017-43.
- Pollini, J. and J.P. Lassoie. 2011. Trapping farmer communities within global environmental regimes: the case of the GELOSE legislation in Madagascar. *Society & Natural Resources*, 24: 814-830.
- Rakotoson, L.R. and K. Tanner. 2006. Community-based governance of coastal zone and marine resources in Madagascar. *Ocean & Coastal Management*, 49: 855-872.
- Razafindrakoto M., Roubaud F., J.M. Wachsberger. 2017. L'énigme et le paradoxe: économie politique de Madagascar, IRD/AFD Éditions, Paris & Marseille, 283 p.
- Sarrasin, B., 2009. La Gestion Locale Sécurisée (GELOSE): L'expérience malgache de gestion décentralisée des ressources naturelles. *Etudes Caribéennes*, (12).
- Stevens, F.R., Gaughan, A.E., Linard, C. and A.J. Tatem. 2015. Disaggregating census data for population mapping using random forests with remotely-sensed and ancillary data. *PloS one*, 10: 0107042.
- Sudhira, H.S., Ramachandra, T.V. and K.S. Jagadish. 2004. Urban sprawl: metrics, dynamics and modelling using GIS. *International Journal of Applied Earth Observation and Geoinformation*, 5: 29-39.
- Tatem, A.J., Noor, A.M., Von Hagen, C., Di Gregorio, A. and S.I. Hay. 2007. High resolution population maps for low income nations: combining land cover and census in East Africa. *PloS one*, 2: 1298.
- Udjo, Eric O. 2015. Projecting population, numbers of households and dwelling units in South Africa 2011-2021. *African Population Studies*, 29: 1510-1525.
- United Nations Development Programme (UNDP). 2018. Human development indices and indicator: 2018 Statistical update. 2018. Retrieved from http://hdr.undp.org/sites/default/files/2018_human_development_statistical_update.pdf

- Wardrop, N.A., W.C. Jochem, T.J. Bird, H.R. Chamberlain, D. Clarke, D. Kerr, L. Bengtsson, S. Juran, V. Seaman, and A.J. Tatem. 2018. Spatially disaggregated population estimates in the absence of national population and housing census data. *Proceedings of the National Academy of Science*, 115: 3529-3537.
- Wahab, E.O., S.O. Odunsi, and O.E. Ajibouye. 2012. Causes and consequences of rapid erosion of cultural values in a traditional African society. *Journal of Anthropology*, 2012: 1-7.
- Westerman, Kame and Charlie J. Gardner. 2013. Adoption of socio-cultural norms to increase community compliance in permanent marine reserves in southwest Madagascar. *Conservation Evidence*, 10: 4-9.
- World Bank. 2014. Face of poverty in Madagascar – poverty, gender and inequality assessment. Poverty Reduction and Economic Management, Africa Region. Report No. 78131-MG.
- WorldPop. 2017. Madagascar 100m Population, Version 2. University of Southampton. DOI: 10.5258/SOTON/WP00535.
- Wu, Shuo-sheng, Xiaomin Qiu, and Le Wang. 2005. Population estimation methods in GIS and remote sensing: A review. *GIScience and Remote Sensing*, 42: 58-74.
- Yang, Xiaoying, Geng-Ming Jiang, Xingzhang Luo, Zheng Zheng. 2012. Preliminary mapping of high-resolution rural population distribution based on imagery from Google Earth: A case study in the Lake Tai basin, eastern China. *Applied Geography*, 32: 221-227.

Appendix

Date:	Ticket #:	Pirogue #:	Village:		
<hr/>					
<i>Nb. Pêcheurs:</i>					
	1	2	3	4	5
<i>Vill. Résid:</i>					
<i>Vill Naiss:</i>					
<i>Année Demang:</i>					
<i>Age:</i>					
<i>Nb. Enfants:</i>					
Poids Espèces Consomme: _____					
Poids Espèces Vendu: _____ Prix de vente: _____					
Détails de vente					
Espèces	Nb	Poids (g)	Prix/unité	Unité	

Appendix 2.1. Fisheries socioeconomic survey datasheet

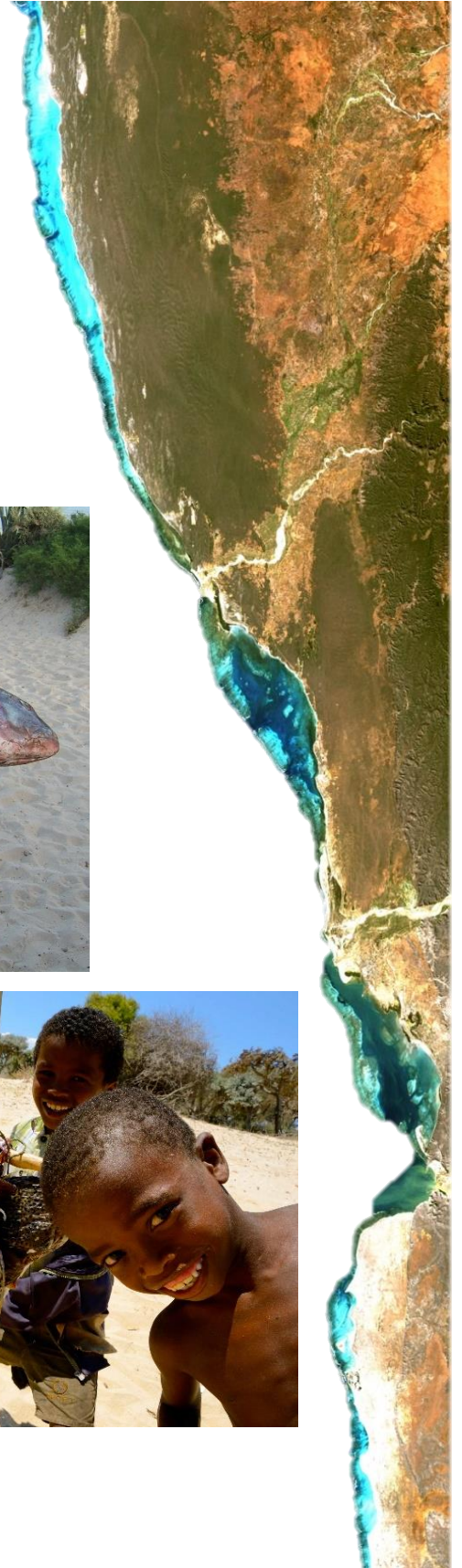
Country	Survey	% Households with one room for sleeping	% Households with two rooms for sleeping	% Households with three or more rooms for sleeping	Mean number of persons per sleeping room	Mean number of household members
Madagascar	2016 MIS	70.1	23	6.9	3	4.2
Madagascar	2013 MIS	69	24.1	6.8	3.2	4.6
Madagascar	2011 MIS	66.1	24.8	9	3.4	4.9
Madagascar	2008-09 DHS	68.9	24.1	6.6	3.4	4.7
Madagascar	2003-04 DHS					4.6
Madagascar	1997 DHS	71.7	21.5	6.7	3.6	4.9
Madagascar	1992 DHS	66.3	25.1	8.4	3.4	5.2

<https://www.statcompiler.com/en/>

Appendix 2.2. Results of database query: The STATcompiler, Demographic and Health Surveys (DHS) of U.S. Agency for International Development (USAID); accessed September 2019

PART II

Artisanal fisheries of the Vezo communities of the Bay of Ranobe: Effort and catch dynamics



Vevo Artisanal Fisheries: Fishing capacity, nominal effort, and spatio-temporal dynamics

3.1 Introduction

Global Fisheries

Since the 1970's, global fishing capacity and effort have steadily increased, with growth stabilizing as recently as 2010, attaining levels 6-10 times of those observed in the 1950's (Watson *et al.*, 2013; Bell *et al.*, 2016). Throughout much of this period, the European fleets dominated global fisheries (Anticamara *et al.*, 2010), however at some point between the years 2000 and 2010, the Asian fleets began to dominate (Bell *et al.*, 2016), increasing their effective fishing effort 25-fold since 1950 (Watson *et al.*, 2013). According to the Food and Agriculture Organization (FAO), by 2007, 52% of global fish stocks were considered fully exploited, 28% were overexploited, and 20% were moderately exploited (Anticamara *et al.*, 2010). After 40 years of increasing industrialization and continuous growth in global fishing effort, catches peaked at 90 – 130 million tons sometime between the late 1980's and 1990's, and began declining at a rate of approximately half million ton per year, more than a decade prior to the eventual stabilization of effort in 2010 (Swartz *et al.*, 2010; Watson *et al.*, 2013; Bell *et al.*, 2016; Pauly and Zeller, 2016).

The growth of fisheries effort and landings of the 1970's to the 1990's was fueled largely by geographic expansion, as fishing fleets of the industrialized countries abandoned the over-fished waters of the northern hemisphere and began fishing the seas of the southern hemisphere (Swartz *et al.*, 2010), initiating a cycle of global serial depletion of fisheries resources

(Armstrong *et al.*, 1998; Karpov *et al.*, 2000; Ainley and Blight, 2009; Anderson *et al.*, 2011; Cardinale *et al.*, 2011; Srinivasan, *et al.*, 2012). Consequently, geographic expansion and seemingly untapped resources of the southern hemisphere fueled the growth of global fisheries from the 1980's to 1990's. By the mid-1990's, the average distance traveled by fleets had doubled, catch per unit area declined by 22% (Tickler *et al.*, 2018), and one-third of the ocean and two-thirds of the continental shelves were exploited at levels that surpassed the primary productivity of these regions by 10% according some estimates (Swartz *et al.*, 2010), while others have found fisheries yields exceeding primary production by as much as 17 – 112% (Chassot *et al.*, 2010).

The global decline of fisheries landings, in the 1990's, marks the tipping point where further geographic expansion was no longer viable, as fleets gradually over-exploited the fisheries resources of all the large marine ecosystems (LMEs) of the globe, covering more than 90% of the world's oceans (Tickler *et al.*, 2018) at levels exceeding their average primary productivity (Watson *et al.*, 2014). Unsurprisingly, at the time of globally-declining fisheries resources, illegal, unreported, and unregulated (IUU) fishing activities reached historic levels (Agnew *et al.*, 2009). Ultimately, the excess capacity of the global industrialized fishing fleets that lead to the legal overfishing of LMEs, combined with the pervasive IUU fishing activities that infringe upon the exclusive economic zones (EEZs) and territorial waters of developing countries, jeopardize livelihoods and food security of the world's poorest people (Pauly *et al.*, 2005; Pauly, 2006; Flothmann *et al.*, 2010; Watson *et al.*, 2013). Case in-point, in West Africa alone, estimated IUU catches are equivalent to 65% of the legal reported catch, representing an economic loss of 2.3 billion USD annually (Doubouya *et al.*, 2017). Likewise, in the Western Indian Ocean region, estimates of the percentage of unreported catch are at 50-60% of the

reported catch, however, reported catch statistics vary wildly from year-to-year, casting doubt on any estimates of catch (Van der Elst *et al.*, 2005).

To fully appreciate and understand the impacts and reach of global fisheries, spatial information is critical. It has been recognized for over two decades the importance of spatialized catch per unit effort (CPUE) information to fisheries management (Swartzmann *et al.*, 1992; Booth, 2000; Walters, 2000; Walters, 2003; Wilen, 2004; Babcock *et al.*, 2005; Bordalo-Machado, 2006), and the risks of ignoring spatial structure (Tian *et al.*, 2009; Ying *et al.*, 2011; Guan *et al.*, 2013). However, limited progress was made in the early years, likely due to technological limitations that would have permitted only visual representations at scales too coarse to provide any insights. More recently, researchers have begun employing novel techniques to acquire spatialized fishing effort and catch data at finer resolutions through the use of: aerial surveys (Tinsman and Whitmore, 2006; Smallwood *et al.*, 2012), vessel-based sightings (Breen *et al.*, 2014; Turner *et al.*, 2015), participatory approaches (Pascual *et al.*, 2013; Selgrath *et al.*, 2017; Thiault *et al.*, 2017), the Automatic Identification System (AIS) (Natale *et al.*, 2015), the Vessel Monitoring System (VMS) in combination with logbook data (Wit and Godley, 2007; Bastardie *et al.*, 2010; Gerritsen and Lordan, 2011; Joo *et al.*, 2015), and satellite data (Al-Abdulrazzak and Pauly, 2014). From these sources of data, mapping products of increasing resolution and sophistication are being created from the spatially less-detailed FAO landings statistics to the more detailed AIS / VMS datasets of commercial fisheries (Watson and Kitchingman, 2004; Dunn *et al.*, 2010; Stewart *et al.*, 2010; Watson and Pauly, 2013; Kroodsmas *et al.*, 2018). Technological advances, as with the vast majority of previous works in fisheries science, have largely focused on and benefitted the commercial fisheries sector, neglecting small-scale fisheries that are, arguably, of equal or even greater importance economically and

ecologically (Batista *et al.*, 2014; Kolding *et al.*, 2014; Junior, *et al.*, 2016; Selgrath *et al.*, 2018). Some progress is being made, however, as research attention begins to turn towards coastal fisheries issues, a critical piece of the puzzle that has been historically absent (Stewart *et al.*, 2010; Johnson *et al.*, 2017; Selgrath *et al.*, 2018).

Of the 120 million people that are directly dependent on capture fisheries, 90% work in the small-scale fisheries (SSF) sector, whose catch represents more than 50% of the global total (World Bank/FAO/WorldFish, 2010; Mills *et al.*, 2011). Most SSF may be classified as IUU fisheries, as there is little to no data being systematically collected on, ostensibly, the largest sub-sector of fisheries. Unlike commercial fisheries, research into SSF has substantially lagged, gaining some attention over the past decade (Purcell and Pomeroy, 2015). In part, the lack of research in the SSF sector may be explained by the difficult situational, socio-political, and/or environmental contexts in which SSFs are embedded, and the unique nature of the unorganized and spatially dispersed landings along potentially hundreds of kilometers of shoreline (Salas *et al.*, 2007). Moreover, the multi-species catches taken with multiple gears, which are often modified, complicates data analyses once surveys are completed. The very definition of small-scale fishery is rather ill-defined, and is sometimes used interchangeably with the term artisanal fisheries (Halim *et al.*, 2019; Smith and Basurto, 2019). Many adopt the FAO definition of artisanal fishery:

Traditional fisheries involving fishing households (as opposed to commercial companies), using relatively small amount of capital and energy, relatively small fishing vessels (if any), making short fishing trips, close to shore, mainly for local consumption (FAO Fisheries and Aquaculture Department, FAO, 2014).

Although the definition remains vague and has been applied to fisheries ranging from a one-man canoe to a 20m trawler, for the present study emphasis is placed on the low-tech / high-artisanality end of the spectrum, as described by Batista *et al.* (2014), in characterizing the fisheries of the Vezo communities of southwest Madagascar.

Commercial and artisanal fisheries of Madagascar

In Madagascar, the legal commercial fisheries sector is limited to shrimp trawling operations that have occurred mainly along the west coast since the 1960's (Van der Elst *et al.*, 2009; Le Manach *et al.*, 2012), and through a series of fishing agreements with the European Union dating back to 1986 (Le Manach *et al.*, 2013), fishing rights to the country's tuna resources are permitted for the seining and longlining fleets of Spain, Portugal, Italy, and France. Commercial harvests are almost entirely exported along with most of their economic and nutritional value. At a smaller scale, an artisanal fishery exists for sea cucumbers that are exported both legally and illegally (McVean *et al.*, 2005; Purcell *et al.*, 2013) to supply the demands of Chinese markets, as well as other targeted invertebrates (Barnes and Rawlinson, 2009). Similarly, the legal artisanal shark fishery has been commandeered to support the illegal international trade in shark fins (McVean *et al.*, 2006; Robinson and Sauer, 2013). At a national level, a ban was placed on the marine turtle fishery through presidential decree in 2006, however the fishery still persists largely unencumbered (Rakotonirina and Cooke, 1994; Walker and Roberts, 2005; Humber *et al.*, 2011). Artisanal finfish fisheries are likely the single most important fishery in terms of biomass productivity and economic benefits provided to the Malagasy people, yet comparatively have received little research attention (Van der Elst *et al.*, 2005). In a comparison of marine fisheries publications originating from nine Western Indian Ocean countries, only 1.4% of the research publications addressed the marine fisheries of

Madagascar (Van der Elst *et al.*, 2005), *e.g.* Laroche and Ramananarivo (1995) and Laroche *et al.* (1997). Since, a few studies have been published, documenting the artisanal finfish fisheries catch and effort, either through direct observation (Doukakis *et al.*, 2008; Davies *et al.*, 2009; Brenier *et al.*, 2011) or fishermen interviews (Barnes-Mauthe *et al.*, 2013), with study sites located in the southwest (Davies *et al.*, 2009; Brenier *et al.*, 2011; Barnes-Mauthe *et al.*, 2013) and in the north of the country (Doukakis *et al.*, 2008). One of the published studies from southwest Madagascar (Davies *et al.*, 2009) was conducted in the Bay of Ranobe, which is the location of the present study.

Artisanal fisheries of the Vezo

Origins of the people of Madagascar, the Malagasy, may be traced back, at least in part, to the arrival of Austronesians in *ca.* 500 ACE (Chambers, 2001) (Figure 3.1). Seafaring technologies used by the modern-day Vezo fishermen remain largely unchanged from that of its founders, where the more ancestral vessel design is characterized by a single-outrigger style, dug-out canoe equipped with a diagonally-mounted mast and triangular mainsail, generally known as the proa. The variant of this design used in Madagascar often consists of a square sail mounted to a double mast, or double sprit, arranged in a v-shape, indicating the likely influence of Indian and/or Sri Lankan cultures (Mahdi, 1999) (Figure 3.2). Known locally by the Vezo as a *lakana* (Malagasy), elsewhere in Madagascar as *lakagna*, (Malagasy), the vessel will hereinafter be referred to by the more generally-used term, *pirogue* (French).

Pirogues are constructed from a locally-harvested tree, *Givotia madagascariensis* (family Euphorbiaceae), known locally as *farafatse*, whose soft, low-density wood is similar to that of the balsa, *Ochroma lagopus*, originating from Central and South America. Historically, pirogues were likely constructed from a single trunk, however, as trunks decrease in diameter due to

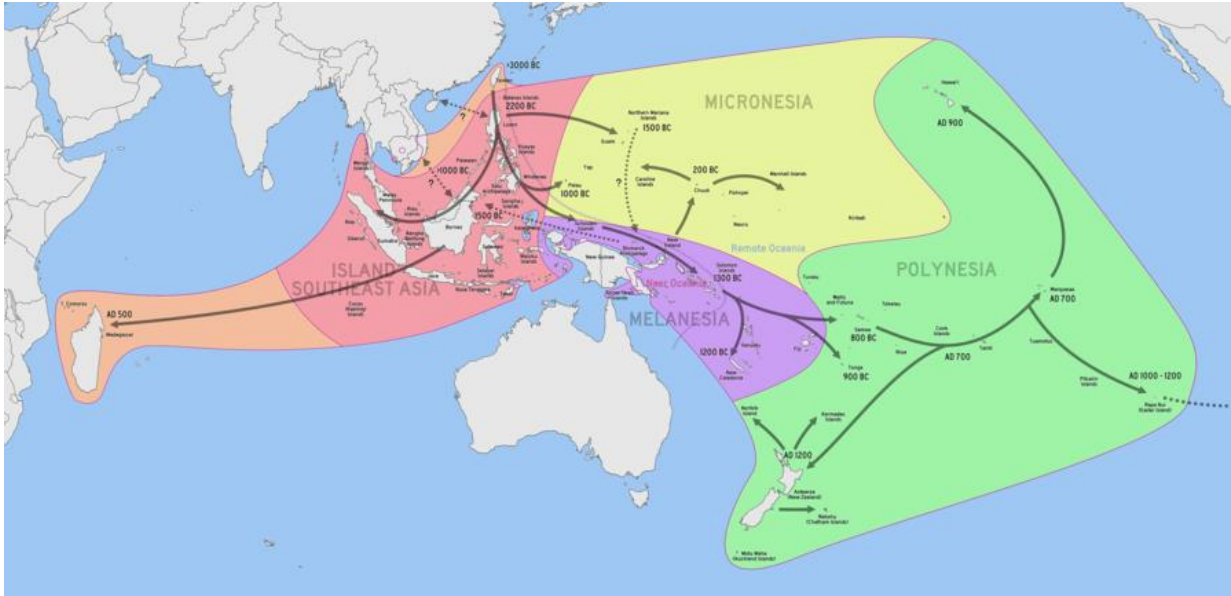


Figure 3.1. Early movement of peoples from the Austronesian region to Madagascar (image reproduced from Chambers, 2001)

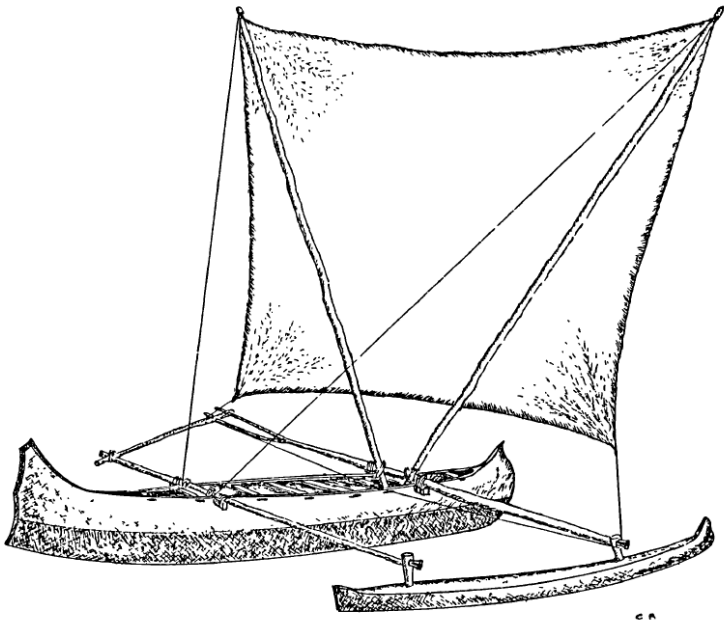


Figure 3.2. Drawing of the Vezo pirogue (image reproduced from Astuti, 1991)

overharvesting of this species, a single trunk may be carved to form the floor and partial side-walls of the hull. Side-walls may be extended with planks and gunwale attached, without the use of metal, using a specific drilling technique and wooden dowels. Tar is applied below the waterline to provide additional water-proofing. Cross-bracing and masts are constructed from a select number of hardwood species.

In Vezo society, the pirogue is an object of central importance to their cultural identity (Astuti, 1991). Boys from an early age learn to construct small toy pirogues, and shortly thereafter, are sharpening their skills using the full-size version (Figure 3.3). As in many traditional fishing cultures, boat-based fishing activities are considered the work of males, whereas females and small children, mainly but not exclusively, spend parts of their day fishing on-foot, gleaning in the intertidal zone, collecting shell fish, urchins, octopus, sea cucumbers, and maybe some fish trapped in intertidal pools (Barnes and Rawlinson, 2009) (Figure 3.4). Once fishermen return mid-day, women play the principle role in the commercialization of the fisheries products (Figure 4.5). Catches may be sold directly by the family within the village of residence or in neighboring villages, sold to a local collector that ensures the transport and sale of fisheries products in the city, Toliara, or an attempt may be made by the families to get better prices for their products by personally rushing them via local transport, bush-taxi, to the scattered fisheries markets throughout the city.

Here, in Chapter 3, data collection and analyses focused on the characterization of fishing effort associated with the day-time, pirogue-based, finfish fisheries of the Bay of Ranobe, Madagascar. In-depth analyses of gears, spatial and temporal components of fishing effort, and considerations of factors influential in determining the realized fishing effort allow for the distinction of latent effort versus actual effort.



a



b



d



c



e

Figure 3.3. Stages of construction of the Vezo pirogue (a-b); the apprenticeship of young Vezo boys, acquiring boating and navigation skills (c-e)



Figure 3.4. Women (n=13) collecting marine resources, intertidal gleaning



Figure 3.5. Fishermen returning with the day's catch, with collection and marketing activities commencing immediately upon landing

3.2 Methodology

Study Site

The Bay of Ranobe (23°05'S, 43°33'E) is a coastal lagoon situated along the southwestern coast of Madagascar, approximately 20 km northwest of the provincial capital city, Toliara. The Bay of Ranobe (BoR) region may be geographically defined by the Manombo River and Fiherenana River that form the northern and southern borders, respectively. The lagoon system extends *ca.* 32 km along its southeast-northwest axis, measures *ca.* 8 km at the widest point, covering *ca.* 163 km² with maximum depths approaching 12 m within the lagoon. The lagoon experiences a semi-diurnal tidal regime with a spring tidal range of ± 2.3 m. The system is characterized by an inner reef flat composed of: patch reefs, sand, seagrass, macroalgae, and mangrove habitats, with a barrier reef forming the seaward boundary. The 32 km section of barrier reef that delimits the lagoon from the Mozambique Channel forms part of the greater Toliara Barrier Reef complex. Two passes naturally divide the lagoon into three zones (see Chapter 1 for further description of the environment).

Lifestyles of the inhabitants of the 12 villages of the Bay of Ranobe are quite similar in that they are inextricably linked to the sea and marine resources. However, some differences do exist between the villages, relative to fishing activities, that are likely attributable to the location of the village along the shore of the Bay and access to fishing grounds. Villages located near the mangroves in the north and south of the Bay tend to fish with seine nets to capture smaller fish and invertebrates, such as mangrove crabs. Moving along the coast from the northern and southern extremes, the villages closest to the two principle passes in the reef tend to fish the passes and will venture not far outside the pass to fish deeper waters. Villages located more centrally along the coast have the farthest to travel to the barrier reef, thus tend to fish the patch

reefs of the lagoon, but will travel to the backreef slope of the barrier reef. Although these tendencies are gross generalizations, and in reality, fishermen travel widely with ranges overlapping substantially, accessibility to fishing grounds affects the size of fish and species caught, which in turn, has ecological and economic repercussions.

Datasets

To address the objectives of the study and characterize the fishing effort of the BoR, six independent datasets were collected and analyzed: 1) Annual Pirogue Count, 2) Pirogue Registration, 3) Weather Data, 4) Fishing Effort, 5) Daily Pirogue Count, and 6) Spatialized Effort. Datasets and methodologies are described below.

Annual Pirogue Count

As a first step in characterizing the fishing effort of the BoR, the fisheries team, consisting of 3-4 people, surveyed the beaches of the 12 coastal villages to establish the number of pirogues per village. Pirogue counts were conducted opportunistically at times when weather deterred fishermen from going to sea, and the number of beached pirogues was maximized, which usually occurs during the summer months. Counts were conducted at the outset of the fisheries data collection campaign in 2013, and again at the end of the study in 2015.

Pirogue Registration

After acquiring pirogue counts from all the villages in 2013, and the selection was made of the four villages targeted for fisheries surveys, a Pirogue Registration campaign was initiated (March-April 2013). For the Pirogue Registration, the fisheries team circulated between the villages selected for the fisheries landings survey, namely Andrevo, Amobolimailaka, Ifaty, and Beravy, collecting data on pirogue lengths. Measured pirogues were marked with registration numbers using spray paint and stencil in an opportunistic manner. Although having unique

identifiers marked on all of the pirogues from the participating villages would have facilitated fisheries data collection and management, unfortunately, during the following cyclone season, all of the registration numbers were removed by rain and blowing sand. Nonetheless, pirogue-length data was collected on 70% of the pirogues, providing a representative sample that is analyzed and discussed further in the Results section.

Weather Data

A solar-powered Davis Vantage Pro weather station was used to collect windspeed and direction data at 30-minute intervals throughout the study period. The weather station was mounted atop a water tower, approximately 15m above sea-level, at the base of operations for the project located in the village of Ifaty. Directionality of the wind vane was calibrated using a Suunto Kb-14 Precision Global Compass. A datalogger installed in the weather station allowed for periodic downloading of data.

Fisheries Landing Survey – Fishing Effort Dataset

Fisheries landing surveys were conducted from April 3, 2013 – December 18, 2015 in the villages of Andrevo, Ambolomailaka, Ifaty, and Beravy. Selection of villages participating in the fisheries study were based on three criteria: 1) villages with the largest pirogue-based fisheries, as identified from the 2013 Annual Pirogue Count dataset, 2) adequate geographic representativity to characterize the fisheries of the entire BoR, and 3) and accessibility of the villages to the fisheries survey team. Surveys were conducted on a monthly basis, with 5 days of fisheries data collection per village per month, totaling 20 days of surveys per month throughout the study period. Scheduling of monthly surveys were based on lunar cycles, ensuring surveys were conducted over full-moon and new moon phases, with villages alternating monthly. For example, in April 2014, Beravy was surveyed for 5 days centered on the date of the full moon

and Ambolomailaka for 5 days of the new moon, while the other villages were surveyed in the intervening weeks. In the following month, Andrevo and Ifaty were surveyed during the full moon and new moon, respectively, while Ambolomailaka and Beravy were surveyed during intervening weeks. Alternating village and lunar phases ensured balanced sampling relative to lunar phases and tidal stages, and constituted the first-stage sampling frame of the fisheries survey design. (See Appendix 3.1 for extract of survey schedule)

From a spatial perspective, villages often have a focal point, where the frequency of landings and density of beached pirogues are greatest. The landing zone, as designated for the present study, extended out from the focal point of landings in both directions along the shore far enough to include >90% of pirogues owned by the fishermen of the targeted villages. Another important point worth noting, in a village setting such as this, fishermen and their landing sites are not randomly distributed along the coast (pers. obs.). Often, the more senior members of the village, and their family groups, occupy the more favorable areas of the beach, *e.g.* more sheltered, easier access to markets, etc., which are usually at, or near, the focal point of landing sites for the village. Implications of the structured organization of landing sites extends beyond simple family affiliations, given that the more senior families of fishermen may be more experienced / skilled fishermen, and potentially, favor specific fishing gears. Moving further-and-further out from the focal point of landings, families that have arrived more recently to the village, and likely have less fishing experience, find a place along the shore to land their pirogue. Consequently, a gradient exists of fishing gears and experience that radiates out from the focal point to the margins of the village, where less experienced fishermen have established themselves. In this region, the less experienced fishermen are known to use gears that require less skill and that are less discriminating, such as beach seines and mosquito nets. In order to

obtain an unbiased and representative sample across the spectrum of gear-use and skill-level, village landing zones were divided into three sub-zones to ensure a balanced distribution of survey effort (Figure 3.6). Sub-zones represent a subsample of the primary sampling units, the four targeted villages, which are fully sampled on a monthly basis.

On a given day, the fisheries survey team travelled to the assigned village, according to the monthly survey schedule, and conducted fisheries surveys within a specific sub-zone. Survey effort would then focus on the next sub-zone the following day, cycling through the sub-zones of all the targeted villages every month. Before fishermen began returning to the beach around mid-day, timing of which was highly-dependent on tides, the first data collection task involved a count of the number of pirogues on the beach that had not participated in day-time fishing activities, within the specific sub-zone being surveyed (Figure 3.7). After the fishermen have landed and the fisheries data collection portion of the survey had been completed, the survey team re-initiated the count of pirogues to determine the total number of pirogues present within the designated landing sub-zone. The Daily Pirogue Count dataset provided estimates of the percentage of pirogue-use across the surveyed zones and villages, allowing for a more accurate assessment of latent fishing capacity, thereby providing more accurate estimates of actual fishing effort (see Appendix 3.2 for example datasheet).

Following an access-point creel survey approach (Pollock, 1997) fishing effort and catch surveys were conducted within the designated villages and landing sub-zones, according to the pre-determined monthly sampling schedule, following a sampling in space and time approach (Stamatopoulos, 2002). As daytime fishermen returned, which occurred over a relatively small window of time, the fisheries survey team initiated contact with fishermen, as they landed in a haphazard manner (Figure 3.8). While one member of the survey team conducted the effort

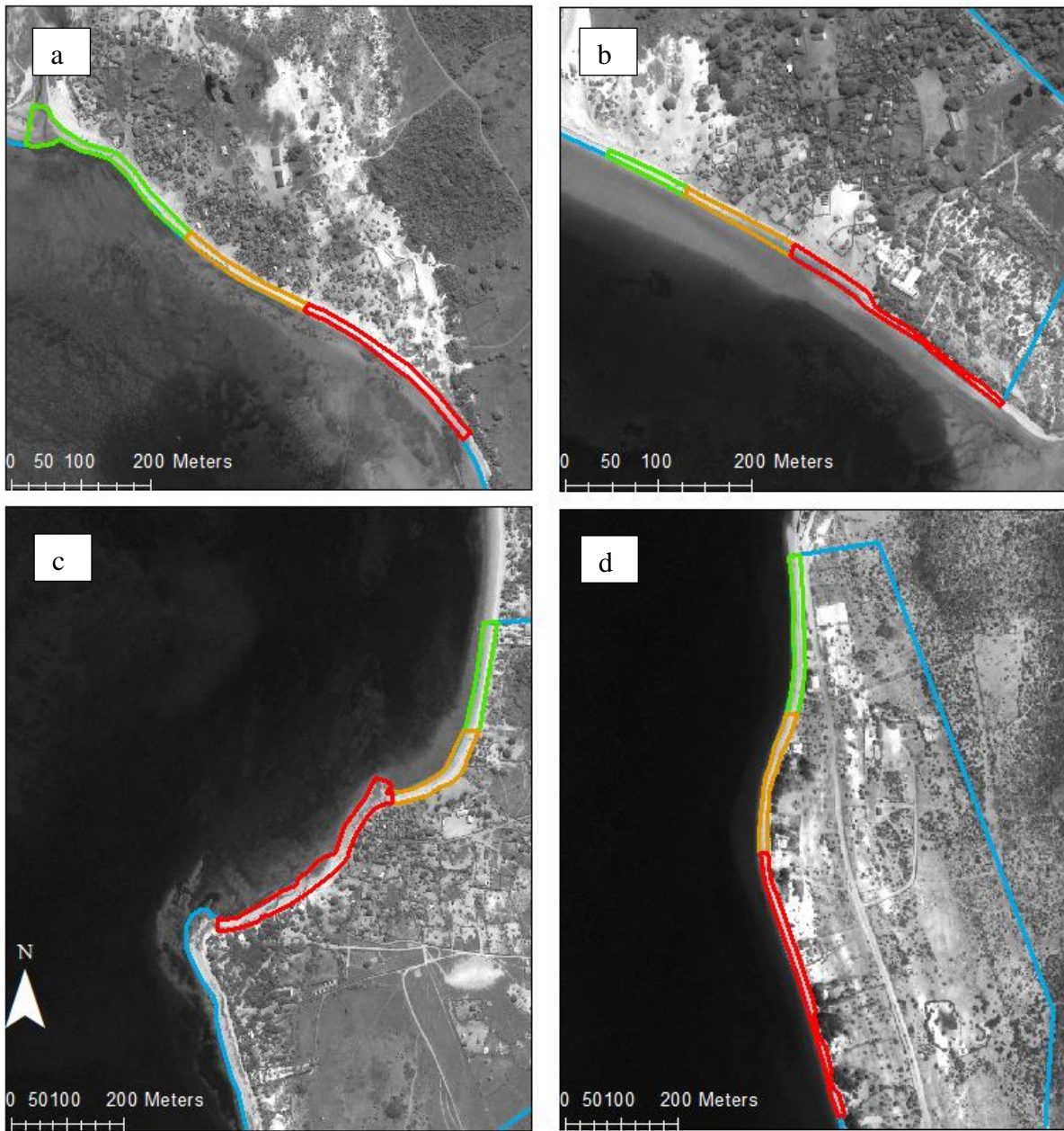


Figure 3.6. Village landing zones (LZ) divided into sub-zones (green, orange, and red) for surveying purposes: a) Andrevo (LZ = 785m), b) Ambolomailaka (LZ= 500m), c) Ifaty (LZ= 620m), and d) Beravy (LZ= 1025m)



Figure 3.7. Inactive pirogues on the beach mid-morning, latent capacity



Figure 3.8. A view of fishermen returning to shore in a loosely coordinated manner

survey, the other members of the team characterized the catch, collecting species-specific length and weight data, which is described further in Chapter 4. To maintain good-will and continued participation in the fisheries survey, incentives were provided to fishermen, in the form of coffee, snacks, and tobacco products, to offset the inconvenience of the data collection process, and to compensate for any delays that may have been caused in getting their products to the market.

The standard objective of the fishing-effort portion of the landings survey was to collect data that would allow for the characterization of the spatiotemporal and gear-related components of daytime fishing trips. Specific data collected included: departure / return time, number of people per pirogue, length of pirogue, fishing grounds, frequency of fishing for $t_{(-1)}$, $t_{(-2)}$, and $t_{(-3)}$ days, type of gear(s) used, gear characteristics (*e.g.* length, width, mesh size, number lines / hooks), number of gear sets, and depth of gear (*i.e.* bottom, mid-water, or surface) (see datasheet Appendix 3.3). Typical gears used by modern Vezo fishermen include: gillnets, harpoons, spearguns, and hook-and-line (Figure 3.9 a-d). In more recent years, the use of modified mosquito bed-nets has grown in popularity, as a stand-alone seining gear (Figure 3.9 e-f) and as a modification of existing gears, for example gill nets and beach seines with mosquito-net panel additions (Figure 3.10). Use of mosquito netting in fisheries has been increasing over the past decade across the developing world (Bush *et al.*, 2017; Short *et al.*, 2018), which is likely the result of declining catches and the free-distribution of mosquito bed-netting by humanitarian organizations as part of their efforts to control malaria. Similarly, another widely-distributed product whose intended use is meant to control the spread of sexually-transmitted diseases and reduce unwanted pregnancies has proven to be useful to Vezo fishermen. For night-time speargun fishing activities, Vezo fishermen are commonly known to use condoms to water-proof



Figure 3.9. Commonly-used fishing gears by the Vezo of the Bay of Ranobe: gillnets (a-b), harpoons (c), spearguns (d), small mesh nets / mosquito netting (e-f)



Figure 3.10. Aerial view of typical beach seine hauling operation in the BoR; mosquito net paneling often inserted into wings and/or cod-end

inexpensive, plastic flashlights. Interestingly, despite these innovative applications of cheap and abundant materials, the fish trapping technology / techniques that are common in northern Madagascar (*e.g.* Narozanski, *et al.*, 2011) and along the East African coast (*e.g.* d la Torre-Castro and Ronnback, 2004) have not been adopted by the Vezo. Nonetheless, as the focus of the present study is the daytime, pirogue-based fisheries of the BoR, only the fishing effort associated with the following gears are considered in future analyses:

- 1) Boat seine,
- 2) Hook-and-line,
- 3) Gillnet,
- 4) Mosquito Net,
- 5) Gillnet modified with mosquito netting,
- 6) Speargun.
- 7) Harpoon.

Although pirogues may be used to initially set a beach seine net 50 m – 100 m from shore, which is then hauled in by a team of 4-6 people, beach seines are excluded from any further analysis. Furthermore, given that beach seining activities are, spatially, highly-dispersed and highly-variable along the coast and often occur during the night, the sampling design employed in the present study prohibits an accurate characterization of this specific gear-type.

Spatiotemporal Dynamics of Fishing Effort

Spatialized indicators of fishing effort are essential in evaluating changes in catch rates (CPUE), in assessing the potential impacts of fishing activities on benthic habitats, and in moving fisheries management towards an ecosystem-based approach (Swartzmann *et al.*, 1992; Booth, 2000; Walters, 2000; Walters, 2003; Wilen, 2004; Babcock *et al.*, 2005). In the present study, fishing effort is mapped using satellite imagery, following a grid-based approach similar to the one used in Chapter 2 to enumerate dwelling units. Using ArcGIS, a 500 m grid system was created and overlaid on the IKONOS-2 used in previous chapters, which was acquired on March 16, 2007 at 07:15 GMT. Given that the spatial resolution of the multispectral bands associated with the image file is insufficient for the visual identification of the pirogues at-sea, only the Pan image was used (acquired nominal ground sampling distance - cross scan: 0.9851 m and along scan: 0.8977 m). Standard deviation contrast enhancements, and minimal adjustment of the gamma levels, were applied to the Pan image to optimize identification of pirogues. Pirogues were enumerated in each grid cell, which was visually scanned in a systematic manner at a 1:3000 scale. The 500 m sampling grid was converted to a .kml file and imported into Google Earth. Similarly, the grid-based process of enumeration of pirogues at-sea was repeated on more recent Google Earth images (Figure 3.11). Cloud-free and speckle-free Google Earth image tiles were identified that allowed for the reliable enumeration of pirogues at-sea. Multiple

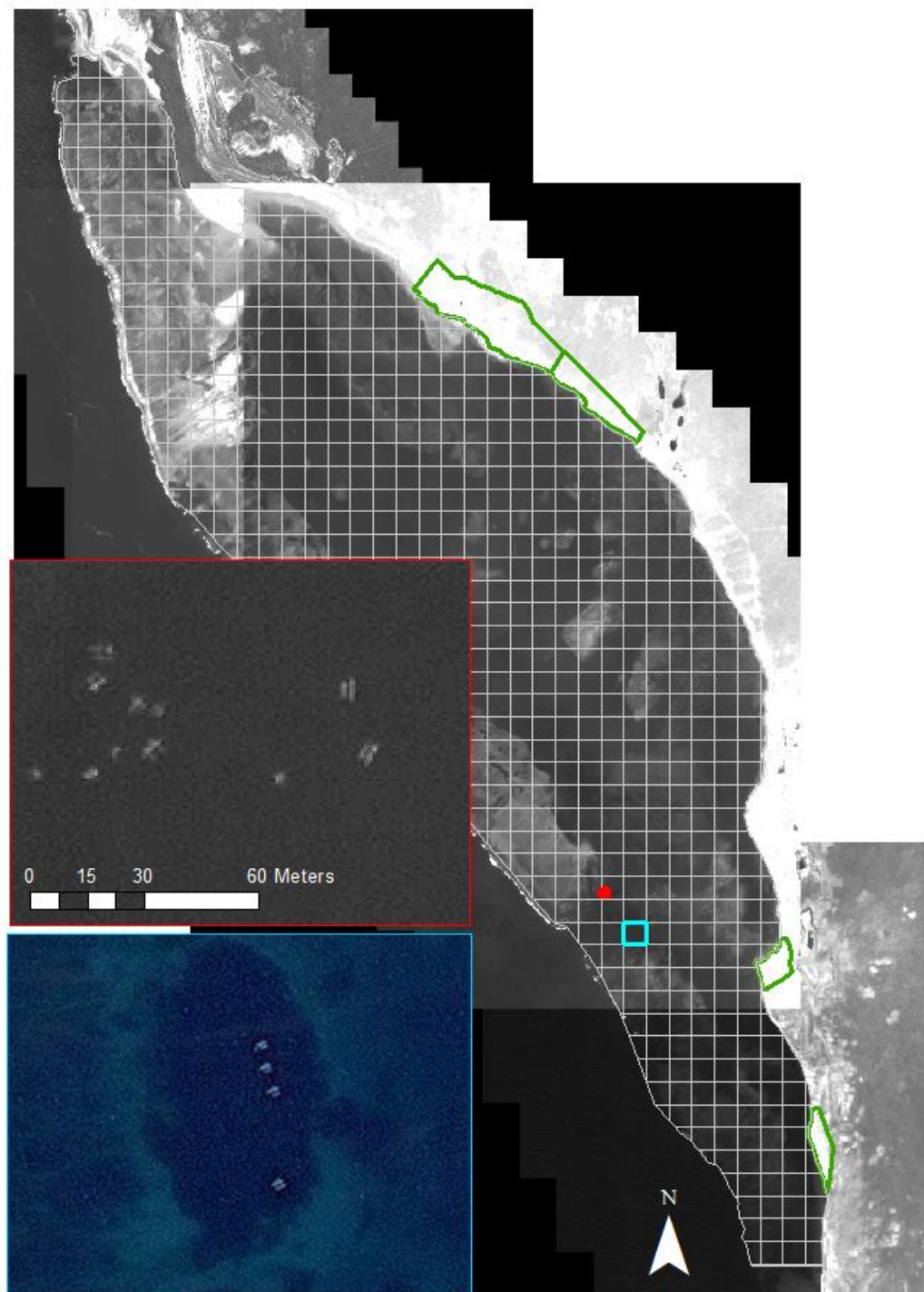


Figure 3.11. IKONOS image mosaic (black / white) with 500 m sampling grid overlay and the location of villages targeted for fisheries surveys (green polygon); insets illustrate the resolution of the IKONOS image (red border) and location (red square) and that for the Google Earth image (blue border) and the location within the BoR (blue square); note, image resolution allows for distinction of pirogue hull and smaller outrigger float

image tiles were required to achieve complete coverage of the BoR. Dates of image tiles used include: February 17, 2016, March 8, 2016, and June 3, 2018.

Grid-based pirogues counts obtained from the four images, the IKONOS Pan image and three Google Earth image tiles, were converted to a commonly-used measure of spatial effort, boat*meters per square kilometer (pirogue*meters / km) (Stewart *et al.*, 2010). For the conversion, counts were multiplied by the mean pirogue length, as determined from the Pirogue Registration dataset, and divided by the grid cell area (0.25 km²). A composite image was created by combining all image dates into single image, with the averaging of values only in areas of overlap. In the final composite image, the shallow north-south extremes of the BoR were covered by single-date layers, whereas the values of the central part of the lagoon that is more important to the fisheries was comprised of averages based on 2-3 date-layers of data, depending on degree of overlap.

A final presentation of the spatial distribution of fisheries effort was produced from the grid-based spatiotemporal composite image by converting the grid polygons to points and applying an interpolation function. The natural neighbor interpolation method was selected and used to produce the final BoR fisheries effort distribution map at a 100-m resolution.

3.3 Results

Fishing Capacity – Pirogue Characteristics

Length data collected during the course of the Pirogue Registration campaign (March-April 2013), were used to develop length-density profiles, and to evaluate differences that may exist in “fleet” characteristics amongst the villages targeted for fisheries data collection. Length data were collected on pirogues from the four targeted villages: Andrevo n= (250),

Ambolomailaka (n=215), Ifaty (n= 221), and Beravy (n= 115), totaling 801 pirogue measurements (overall \bar{x} = 5.32 m, sd = 1.38 m, range = 3.0 – 9.0 m). From the fleet profiles, informal inferences may be made on the distances traveled by fishermen from the respective villages to preferred fishing grounds (Figure 3.12). For example, in general, shorter pirogues are likely used for fishing within lagoon on patch reefs not far from shore, while longer pirogues would allow fishermen to fish in the reef passes and on the exterior of barrier reef. The length distribution profiles for the Andrevo (\bar{x} = 4.9, sd = 1.1) and Ifaty (\bar{x} = 5.0, sd = 1.2) fleets present similar right-skewed characteristics, except in the case for Andrevo a secondary peak exists in the profile at 6 m, indicative of a greater need / capacity to travel further. Similarly, the length distributions for Beravy and Amobolomailaka are indicative of the distances traveled to fishing grounds, with Beravy (\bar{x} = 4.8 m, sd =1.0 m) being the closest to the barrier reef and having the smallest pirogues and Amoblomailaka (\bar{x} = 6.4 m, sd = 1.5 m) being the furthest from the barrier reef and having the longest pirogues. Results of Levene's Test ($F_{(3)} = 11.893$, $p < 0.001$) indicated the existence of significant difference(s) in variances amongst village groups, violating the homogeneity of variance assumption of ANOVA. Consequently, pair-wise comparisons were conducted amongst the four villages to determine differences in pirogue lengths, with p-values adjusted following the Bonferroni correction method. Results indicated that the mean pirogue length for the village of Ambolomailaka was significantly different from all the other villages ($p < 0.001$). Pair-wise comparisons amongst the other villages found no significant differences in mean pirogue lengths (Figure 3.13).

In 2013 and 2015, a bay-wide Pirogue Census was conducted to determine the total number of pirogues in all of the villages as a means of establishing the sampling universe, or population, of the fisheries surveys (Table 3.1). Pirogue counts from the 2013 Pirogue Census

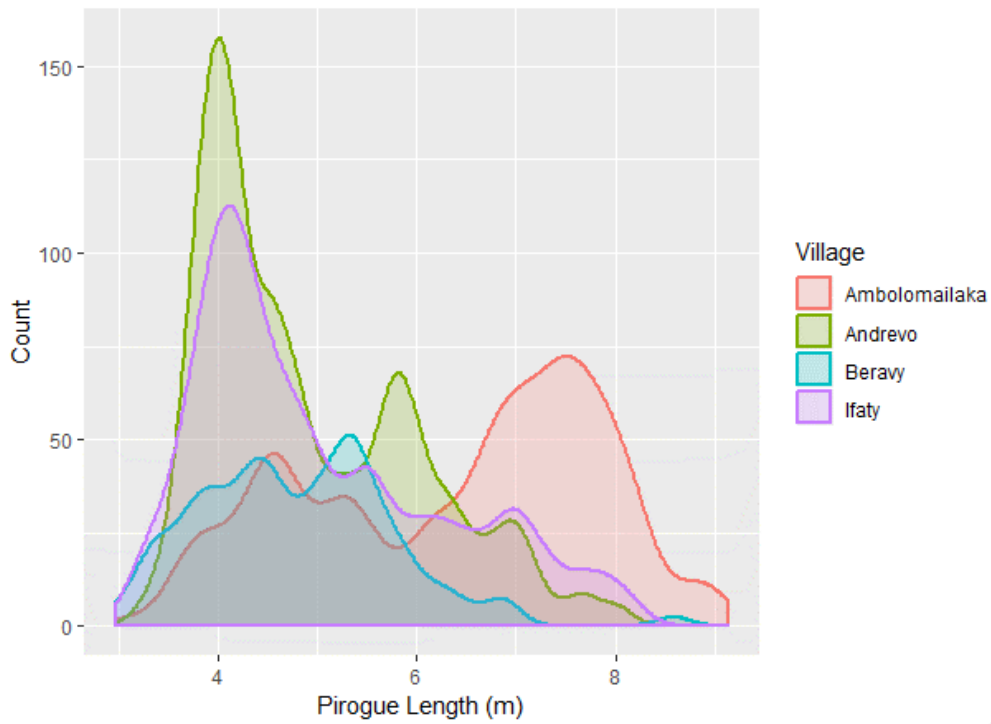


Figure 3.12. Smoothed histograms, or density profiles, of pirogue length data collected from the four targeted villages during Pirogue Registration campaign

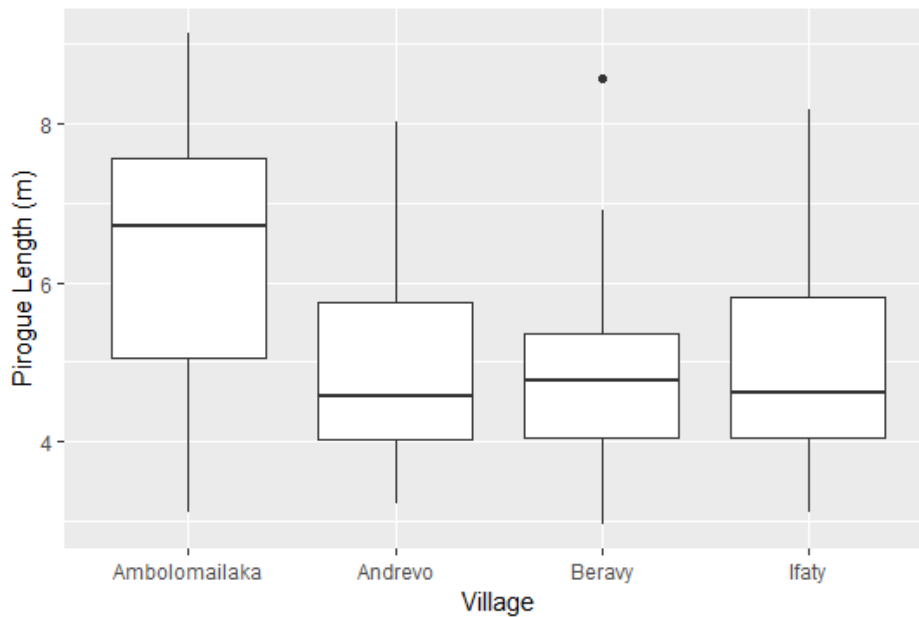


Figure 3.13. Boxplots of the of pirogue length data collected from the four targeted villages during Pirogue Registration campaign; mean pirogue length for the village of Ambolomailaka is significantly different from the other villages

Table 3.1. Total number of pirogues per the 12 villages of the Bay of Ranobe collected during the Annual Pirogue Count in 2013 and 2015, with targeted villages shaded

Village	Year	
	2013	2015
Fitsitke	363	388
Andrevo	364	338
Ambolomailaka	263	284
Betsibaroka	76	78
Madiorano	92	91
Amboaboaka	141	134
Mangily	161	180
Ifaty	290	244
Ambalaboy	50	32
Beravy	164	139
Tsongeritelo	133	88
Ambotsibotsike	122	97
Total	2,219	2,093

compared to the number of pirogues registered and measured in 2013 indicate that on average 74.1% of the pirogues were accounted for from the 4 targeted villages (see Table 3.2 for summaries per village), while the number of registered pirogues (n= 801) represents 36.1% of the bay-wide pirogue count (n= 2219), according to the 2013 Pirogue Census data. Village-specific length frequency data from the 4 villages that participated in the Pirogue Registration campaign in 2013 were used to determine total pirogue length in meters per village, as a component of fishing effort indices. For the other 8 villages in which the Pirogue Registration campaign did not occur, thus detailed length frequencies were not available, length frequencies from the 4 surveyed villages were pooled and used to create a generalized histogram with 0.5-m bins (Figure 3.14). Length frequencies from the generalized histogram were then used to calculate the number of pirogues in each length size class, from 2.5 m – 10 m in 0.5 m increments and scaled using the 2013 Pirogue Census data (Appendix 3.4). Pirogue counts binned into size classes were multiplied by the size class to determine total length per bin, then

Table 3.2. Summary of pirogue lengths and counts per targeted village: counts of pirogues registered, and pirogue counts from census, Annual Pirogue Count 2013, and percent coverage of registration

Village	Length (m)		Total	Ct. Pirogues		% Registered
	Avg	SD		Registered (2013)	Census (2013)	
Ambolomailaka	6.4*	1.5	1373.8	215	263	81.7%
Andrevo	4.9	1.1	1228.7	250	364	68.7%
Beravy	4.8	1.0	550.5	115	164	70.1%
Ifaty	5.0	1.2	1107.8	221	290	76.2%

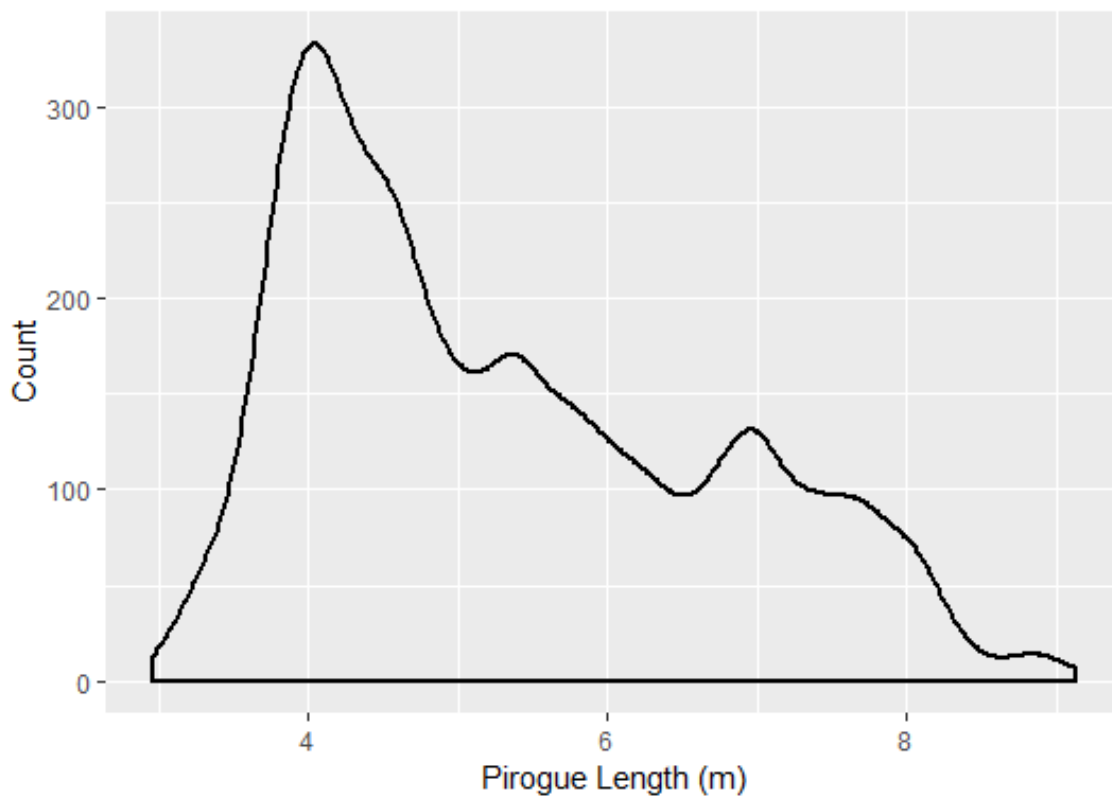


Figure 3.14. Generalized density profile for pirogue lengths of all pirogues recorded in the Pirogue Registration from the villages of Andrevo, Ambolomailaka, Ifaty, and Beravy

summed to obtain total length per village (Appendix 3.5). Pirogue counts and total pirogue lengths per village are presented in Table 3.3, and represent a key component of the total *potential* fishing effort, or fishing capacity, that exists in the Bay of Ranobe.

A simple linear regression was calculated to predict the number of fishermen based on pirogue length. A significant regression equation was found ($F_{(1,12397)} = 1.213 \times 10^4$, $p < 0.001$), with an R^2 value of 0.4944 (Table 3.4). The predicted number of fishermen is equal to $-1.236 + 0.6143 \times$ (pirogue length), with pirogue length measurements in meters. The number of fishermen per pirogue increased 0.6143 for each meter increase in pirogue length. The fitted linear regression is presented in Figure 3.15.

Table 3.3. Pirogue counts for the 12 villages of the Bay of Ranobe, with total length in meters

Village	Count (2013)	Total Length (m)
Fitsitke	363	2021
Andrevo	364	1880
Ambolomailaka	263	1747
Betsibaroka	76	423
Madiorano	92	512
Amboaboaka	141	785
Mangily	161	896
Ifaty	290	1524
Ambalaboy	50	278
Beravy	164	826
Tsongeritelo	133	740
Ambotsibotsike	122	679
Total	2,219	12,311

Table 3.4. Results of simple linear regression of number of fishermen and pirogue length

Model	Coefficients		t-value	Pr(> t)	95% Confidence Interval	
	Estimate	Std. Error			Lower	Upper
Intercept	-1.236	0.0304	-40.7	<0.001	-1.2954	-1.1764
Pir. Length	0.6143	0.0056	110.1	<0.001	0.6034	0.6252

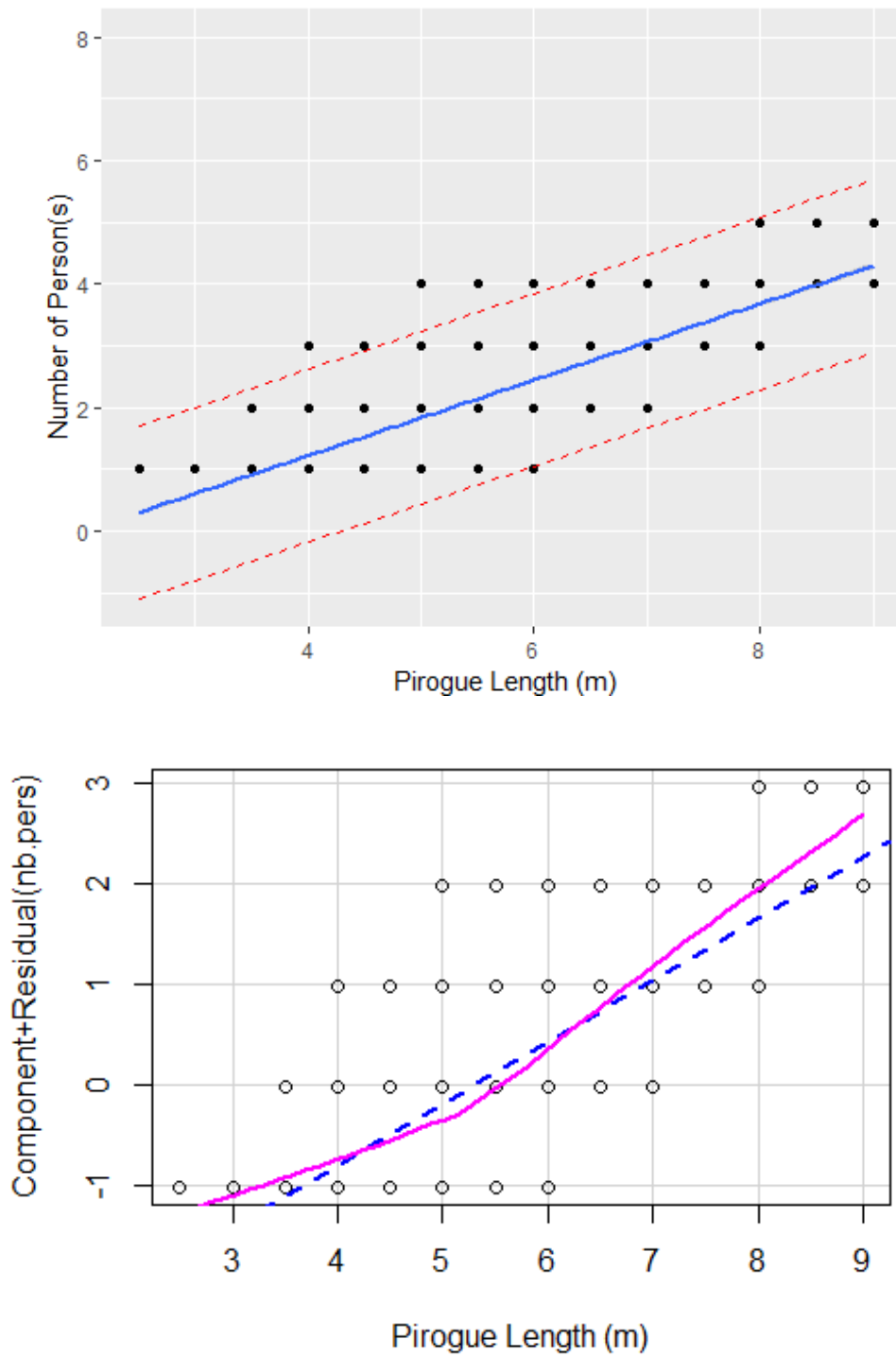


Figure 3.15. Regression plot of observed number of people versus pirogue length with fitted regression line, confidence interval (blue) and prediction interval (red dash) (top); Component plus residual plot with linear fit (dashed blue) and smooth fit (magenta)

Based on the pirogue-length profiles for each of the 12 villages, where pirogue counts are distributed amongst 0.5 m length classes (described above and presented in Appendix 3.4), the total number of pirogue-based fishermen per village, $\hat{y}_{village}$, was predicted using the linear regression coefficients, as follows:

$$\hat{y}_{village} = \sum_i^j n_{i..j} (\beta_1 * LC_{i..j} - \beta_0) ,$$

where $LC_{i..j}$ represents length classes from 2.50 m – 10.0 m in 0.50 m increments and $n_{i..j}$ represents pirogue counts per length class. Regression estimates for the total number of pirogue-based fishermen per village were compared to the village-specific population estimates calculated for the year 2013, using the annual growth rate determined for the period from 2004-2015 (Chapter 2). To determine the potential human capacity per village, as a percentage of the village population, the predicted number of fishermen corresponding to the fishing fleets from each village, assuming all the pirogues counted in the census were used simultaneously, was divided by the population estimates. Results indicate that the overall average percentage of the Bay of Ranobe community that could potentially participate in pirogue-based fishing activities equals 19.7%, with specific village estimates ranging from 6.6% in the village of Mangily to 29.2% in Amboaboaka (Table 3.5).

Fishing Capacity – Gear Characteristics

The principle source of data for the analyses included in the present chapter is the Fishing Effort dataset that includes 13,830 records of effort / gear characteristics, corresponding to the catches analyzed in the following chapter (see datasheet in Appendix 3.3). In terms of fishing gear, the Vezo fishermen of the Bay of Ranobe use 4 principle gear types, listed in order of

Table 3.5. Pirogue counts, population estimates from 2013, and regression predictions of number of fishermen based on pirogue-length profiles, as percentage of total population per village

Village	Pirogue Count (2013)	Population Est. (2013)	Predicted Nb fishermen	% Pop
Fitsitke	363	3581	793	22.1%
Andrevo	364	2700	705	26.1%
Ambolomailaka	263	3136	748	23.9%
Betsibaroka	76	841	166	19.7%
Madiorano	92	986	201	20.4%
Amboaboaka	141	1055	308	29.2%
Mangily	161	5371	352	6.6%
Ifaty	290	2135	578	27.1%
Ambalaboy	50	746	109	14.6%
Beravy	164	1493	305	20.4%
Tsongeritelo	133	1253	290	23.1%
Ambotsibotsike	122	1156	266	23.0%
Total	2,219	24,453	4,821	

importance: 1) gillnets, 2) hook-and-line, 3) harpoons, and 4) spear guns. These 4 gear types collectively account for 91.7% of the reported gear usage, with gillnet, hook-and-line, harpoon, and spear gun usage accounting for 31.8%, 24.3%, 22.5%, and 13.1%, respectively. Other gears, gear modifications, and methods recorded in the Fishing Effort dataset, include: boat seining (4.9%), mosquito net (2.4%), and gillnets modified with mosquito netting (0.67%) (Figure 3.16 a). Similar to the distinct pirogue-length profiles generated for each of the 4 surveyed villages in the previous section, each of the villages exhibits a distinct gear-usage profile (Figure 3.16 b-e). As was the case with the pirogue-length profiles, again, the villages of Andrevo and Ifaty exhibit strong similarities in terms of gear-usage. However, in the case of Ifaty, the use of spearguns is more pronounced. The composition, and relatively even distribution, of gear-usage by fishermen of Amobolomailaka, suggests a less specialized approach, while fishermen of Beravy are heavily reliant on the use of gillnets.

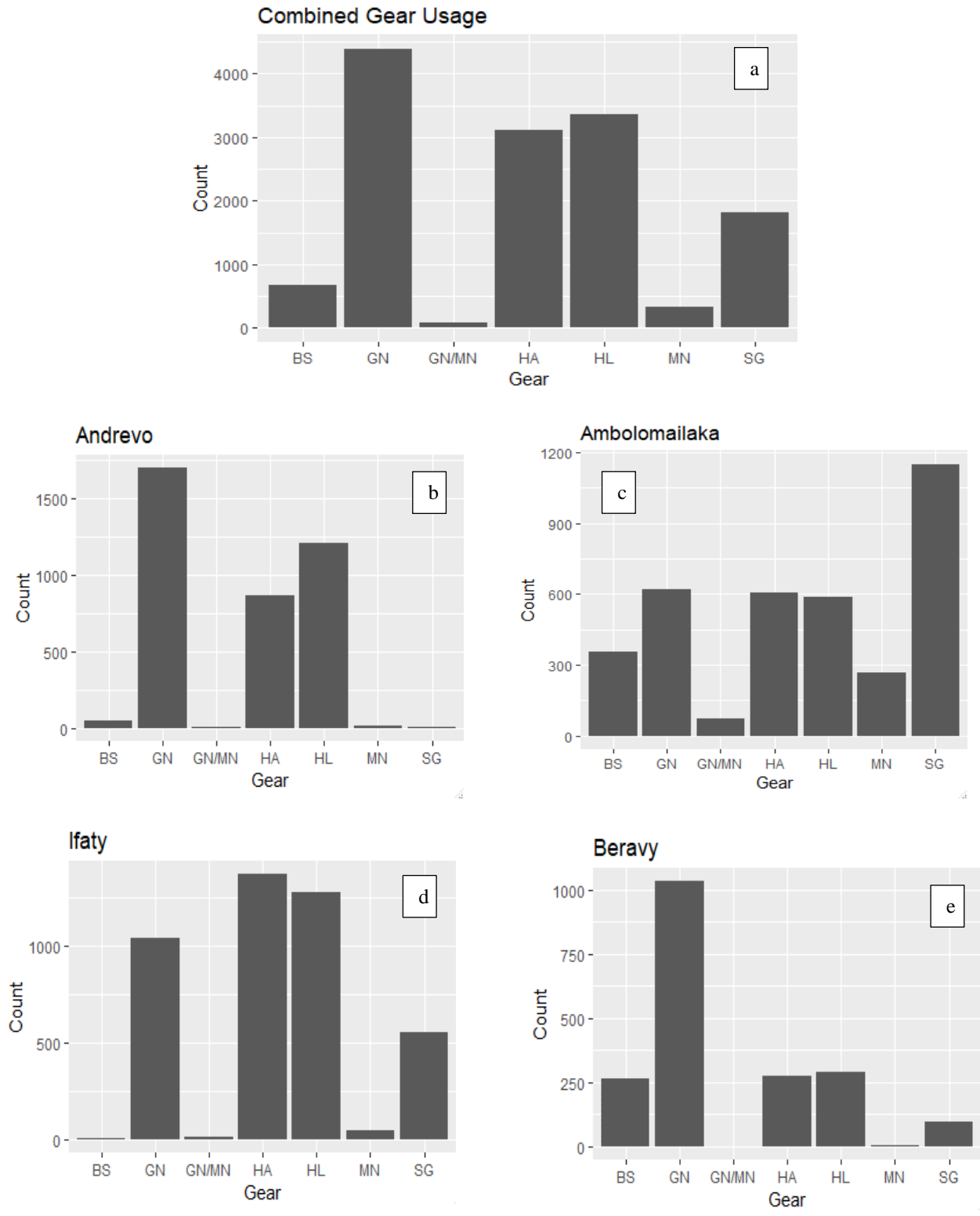


Figure 3.16. Gear usage profiles: a) for all villages combined, b) Andrevo, c) Ambolomailaka, d) Ifaty, and e) Beravy (BS= boat seine, GN= gillnet, GN/MN= gillnet modified w/ mosquito net, HA= harpoon, HL= hook-line, MN= mosquito net, and SG= speargun)

A GLM model was used to determine the relationship between gear type and length of pirogues used by fishermen. A significant relationship was determined ($\chi^2(6) = 5939.90$, $p < 0.001$), indicating that all gear type factor levels were highly significant (see Table 3.6), however, due to the high variability in pirogue length (Figure 3.17), the pseudo- R^2 values varied from 0.11-0.31, depending on method used for the calculation. Nonetheless, coefficient estimates indicated the ranges of pirogue lengths commonly used by fishermen per gear type, where the longest pirogues were associated with gillnet, mosquito net, spear gun, gillnet modified, harpoon, and hook-and-line, in descending order (Figure 3.18).

Temporal Dynamics and Realized Fishing Effort

Fishing frequency and time spent at-sea are key components to the calculation of fishing effort. For the traditional Vezo fishermen, whose vessel technology consists of unmotorized wooden *pirogues*, equipped with sails made from rice sacks or cotton, the sea state and weather conditions play a much greater role than in industrialized fisheries in determining day-to-day fishing activities, and ultimately the total annual effort exerted. In this section, multiple datasets are analyzed to differentiate latent fishing capacity from active annual fishing effort. Datasets include: 1) wind speed and direction data collected from 2013 – 2016, with a gap in data due to weather station malfunction; 2) the Fishing Effort dataset that covered the period from 04/03/2013 – 12/18/15; and 3) the Daily Pirogue Activity dataset that covered the period from 05/02/2013 – 03/24/2015.

Wind speeds in southern Madagascar are highly variable, as cold fronts emanating from the sub-Antarctic push north to Madagascar, colliding with the high day-time heat (Figure 3.19). Weather station data indicated an overall average wind speed of 7.43 kph for all years of data

Table 3.6. Summary of GLM results for model pirogue length ~ gear type

Model	Coefficients		t-value	Pr(> t)	95% Confidence Interval	
	Estimate	Std. Error			Lower	Upper
Intercept	6.39	0.04	162.94	< 0.001	6.32	6.47
Gillnet	-0.21	0.04	-5.07	< 0.001	-0.30	-0.13
Gillnet (MN)	-1.23	0.11	-10.82	< 0.001	-1.45	-1.01
Harpoon	-1.50	0.04	-34.61	< 0.001	-1.58	-1.41
Hook/Line	-1.74	0.04	-40.42	< 0.001	-1.82	-1.65
Mosq. Net	-0.92	0.07	-13.33	< 0.001	-1.05	-0.78
Spear Gun	-0.97	0.05	-21.09	< 0.001	-1.06	-0.88

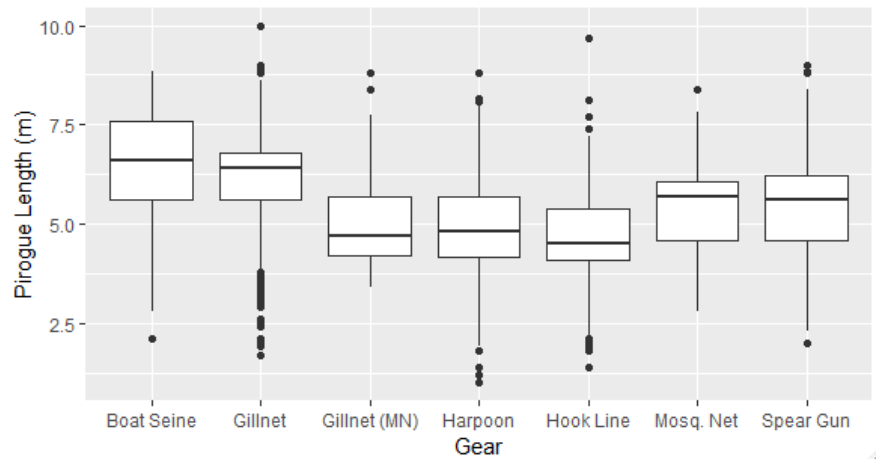


Figure 3.17. Boxplot of pirogue length by gear type

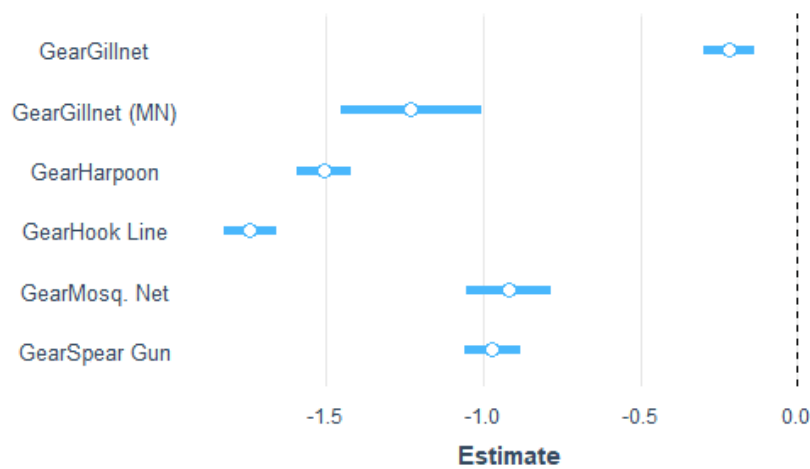


Figure 3.18. Plot of scaled regression coefficients with 95% confidence intervals, indicating relative pirogue lengths associated with gear usage from shorter to longer pirogues (left to right)

availability, with speeds ranging from 0 - 62.8 kph. During the morning hours winds are more stable, however, by mid-day the temperature increases and the winds become significantly stronger ($F_{(1,41345)} = 2223$, $p < 0.001$) (Figure 3.20). Predominant winds approach from the southwest and to a lesser extent from the southeast, and only rarely from northern directions, which is usually considered a sign of regional cyclonic activity (Figure 3.21).

To determine the effect of wind on the temporal aspects of fishing effort, as part of the fisheries survey campaign, data were collected pertaining to two types of indicators of daily fishing activity, namely time spent fishing and daily pirogue counts. Time spent fishing, or time at-sea, is a standard measure of fishing effort, where the time difference is calculated between the departure time and return time. Secondly, pirogue counts were conducted within the specific village and fishing zone being surveyed on a given day, with the initial count being conducted mid-morning (median time= 11:00, range= 9:00 -13:00) after the daytime fishermen have departed, usually around sunrise, 5:00 – 7:00 (Figure 3.22), to determine the number pirogues remaining on the beach, or the unused capacity. A second count was conducted after the fishermen have returned, 10:00 – 13:00 (Figure 3.22) and the fisheries data have been collected (median time= 13:00, range= 10:00-17:00) in order to obtain the maximum count, or total capacity for the specific village and fishing zone. The percentage of active pirogues was calculated as $1 - (\text{pirogue count (am)} / \text{pirogue count (pm)})$ and used as an indicator of *active* effort.

From the Fishing Effort dataset, time spent fishing was analyzed and compared to wind speed to determine whether wind affected the number of hours spent at-sea fishing by the fishermen of the targeted villages of Andrevo, Amobolomailaka, Ifaty, and Beravy. Overall, for

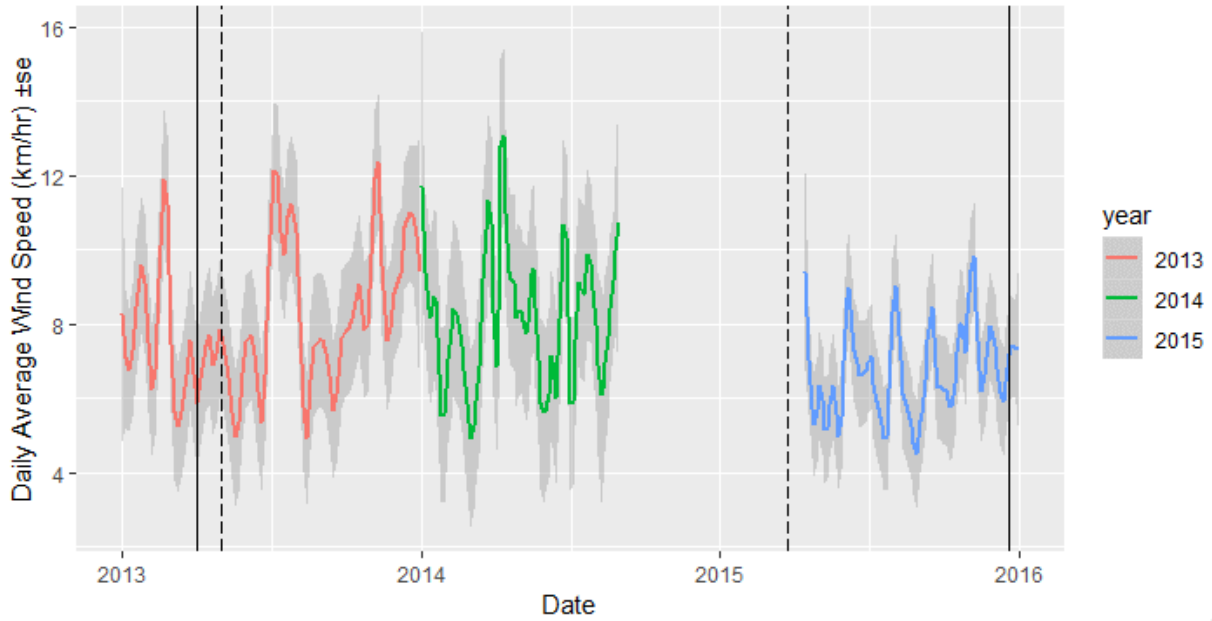


Figure 3.19. Daily average wind speeds color coded by year (\pm standard error in gray), with vertical lines representing the period covered by the fisheries catch and effort surveys (solid black) and the daily pirogue count survey (dashed black)

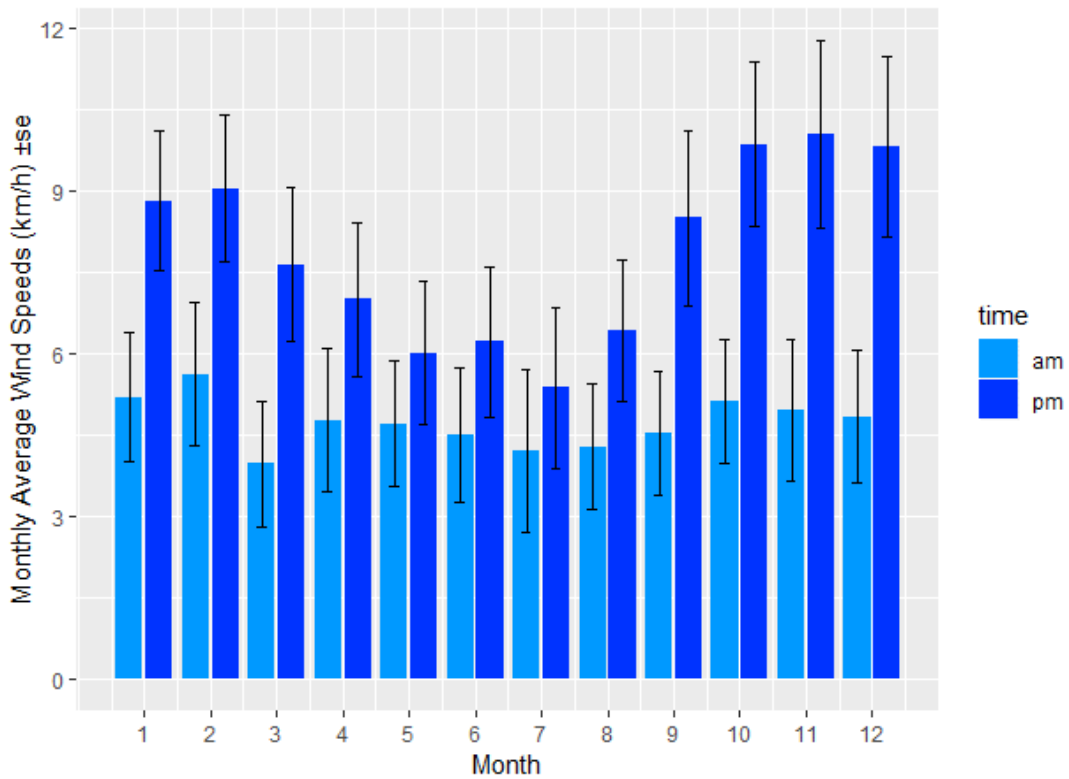


Figure 3.20. Monthly averaged wind speeds (kph \pm se) for the morning and afternoon hours

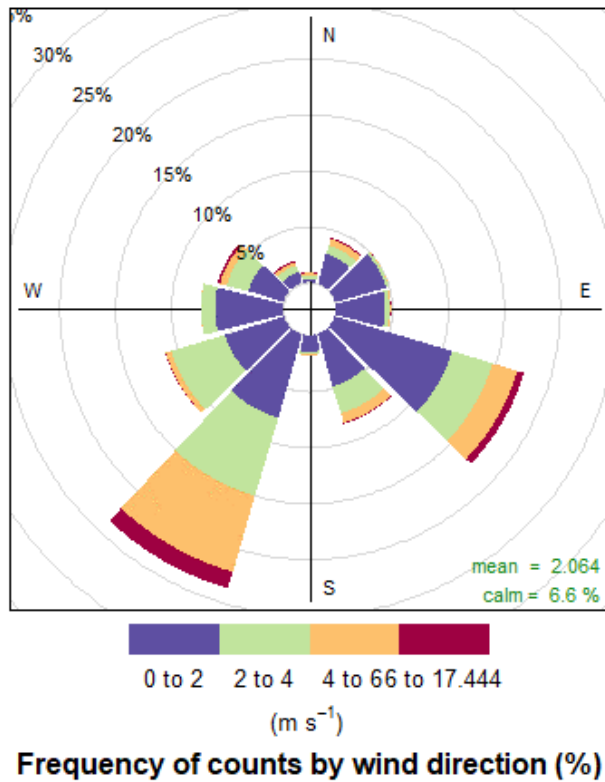


Figure 3.21. Circular histogram of wind speed (m s⁻¹) according to wind direction counts

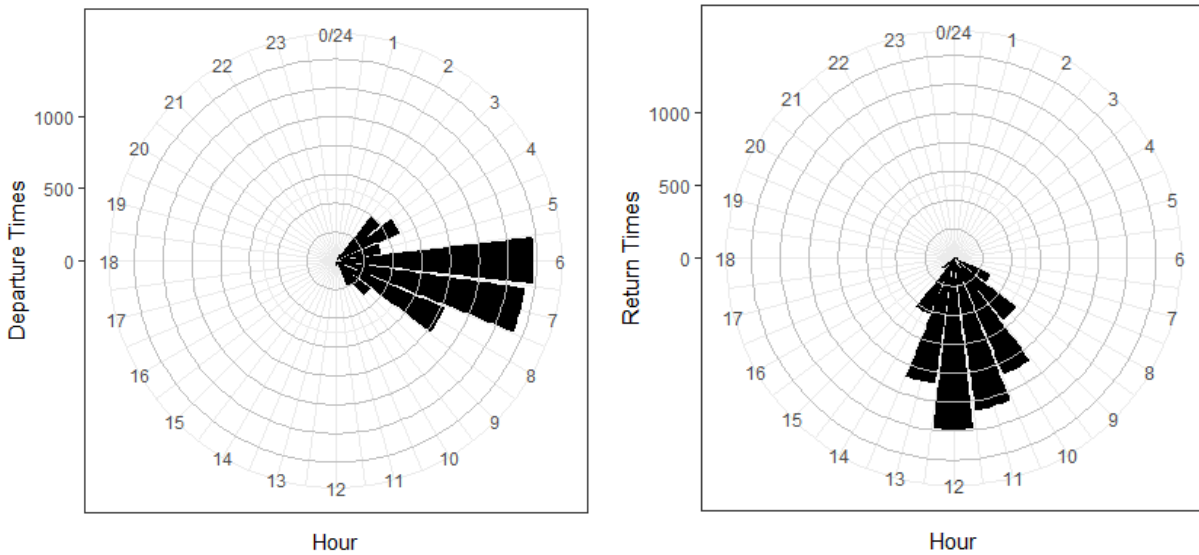


Figure 3.22. Circular histogram for the departure (left) and return (right) times of fishermen recorded in the Fishing Effort dataset

Table 3.7. Average daily time spent fishing per targeted village

Village	Avg. Time Fishing	SD	n
Andrevo	5.43	1.52	3862
Ambolomailaka	5.36	1.92	3678
Ifaty	4.75	1.99	4339
Beravy	4.79	1.73	2017
<i>All Data</i>	<i>5.11</i>	<i>1.84</i>	<i>13,896</i>

all years of the dataset (2013-2015), an analysis of variance (ANOVA) found that significant differences exist between the four villages in terms of time spent fishing ($F_{(3,13822)} = 140.1$, $p < 0.001$). A post-hoc comparison, using Tukey's HSD, indicated that the average number of hours spent fishing by the two northern villages of Andrevo ($\bar{x} = 5.43$) and Ambolomailaka ($\bar{x} = 5.46$) both differed significantly ($p < 0.001$) from the southern villages of Ifaty ($\bar{x} = 4.75$) and Beravy ($\bar{x} = 4.79$) (Table 4.5). Monthly averages of time spent fishing varied from 4.34 to 5.54 hours per day, where less time was spent fishing during the austral spring / summer, ostensibly the result of increasing air temperatures and wind speeds (Table 3.8, Figure 3.23).

To determine the relationship between average daily time spent fishing and daily average wind speed, initially, a GAM was fitted to the dataset. Results of the GAM indicated a strong linear relationship, thus a simple linear regression was calculated. Alternative simple linear regression models were evaluated to determine the optimal window of time for windspeed to be included in the final model, as a means to explore the decision-making process of the fishermen. For example, a morning-hour (00:00 – 12:00) windspeed model was tested to determine if windspeeds in the hours before departure influenced time spent at-sea. Secondly, a daytime (06:00 – 18:00) windspeed model to determine if windspeeds throughout day influenced time

Table 3.8. Average monthly time spent fishing for the four targeted villages combined

Month	Avg. Time Fishing	SD	n
1	4.92	1.86	24
2	5.34	1.79	28
3	5.10	1.70	18
4	5.32	1.65	21
5	5.54	2.01	16
6	5.31	1.74	19
7	5.31	1.56	17
8	5.54	1.73	20
9	5.22	1.98	18
10	4.63	1.97	21
11	4.66	1.94	21
12	4.34	1.55	18

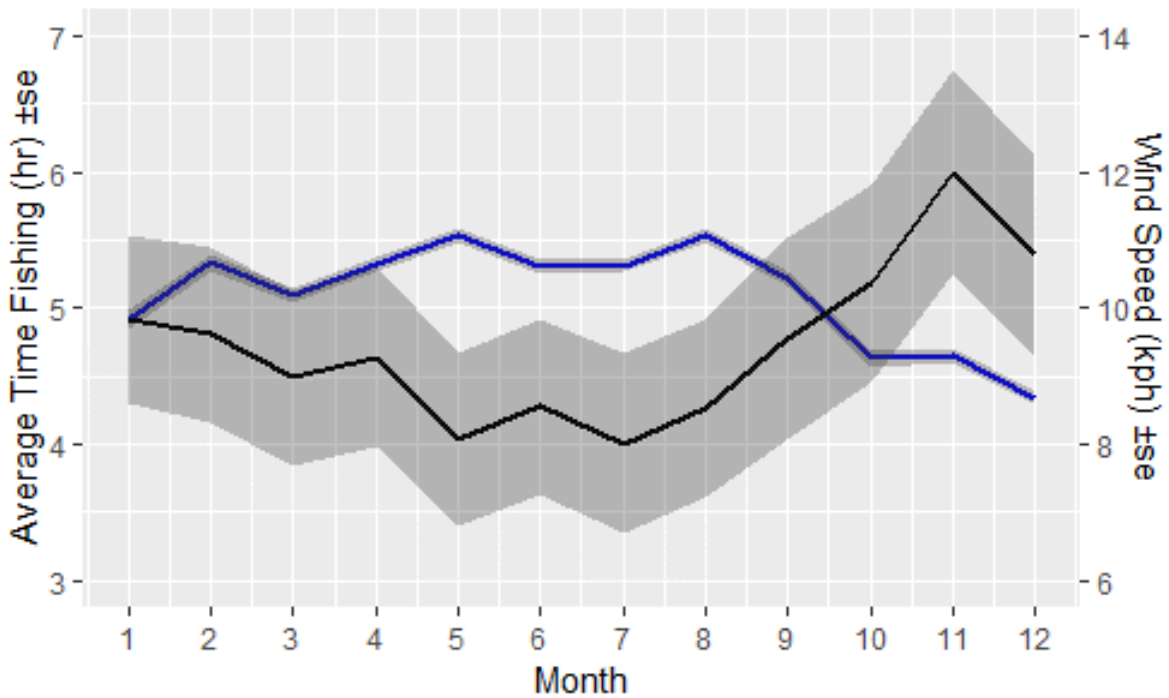


Figure 3.23. Average monthly time (hours) spent fishing (blue line) \pm standard error (gray) as compared to monthly average wind speeds (kph; black line) \pm standard error (gray)

spent at-sea. Lastly, a time-lagged model where daytime wind (06:00 – 18:00) from the previous day was used to determine if the knowledge of windspeed of the previous day influenced time spent at-sea. The morning-hour winds model produced the poorest results and was eliminated. A comparison of the same-day versus the time-lagged daytime-wind model indicated that the windspeeds of the previous day influenced more greatly the time spent at-sea, where adjusted R^2 values equaled 0.0652 versus 0.1034, respectively. For the final model, a significant regression equation was found ($F_{(1,445)} = 52.45$, $p < 0.001$), with an adjusted R^2 value of 0.1034 (Table 3.9) after the removal of extreme outliers ($n=6$). The predicted amount time spent fishing, in hours, is equal to $5.700 - 0.069 * (\text{wind speed})$, with wind speed measurements in kilometers per hour. The fitted linear regression is presented in Figure 3.24 (see Appendix 3.6 for regression diagnostic plots).

Analyses similar to those conducted for windspeed, above, were also conducted on the Daily Pirogue Count dataset, an independent dataset of pirogue-use frequency. A global average of the percentage of pirogue-use, using all data pooled ($n = 351$), indicated that 62.8% of pirogues counted within the fishing zones of the four targeted fishing villages were used on a daily basis. An ANOVA was conducted to investigate differences in pirogue activity rates between villages, using an arcsine-square root transformation of percentages to approximate normality. Results indicated that no significant difference exists in the average activity rates between villages ($F_{(3, 347)} = 1.385$, $p = 0.247$), where average percentages of pirogue-use per village equaled: Andrevo (61.5%), Ambolomailaka (63.9%), Ifaty (60.2%), and Beravy (65.1%) (Table 3.10). For visual comparison purposes, a GAM smooth line was fitted to the individual villages, which suggested that there may be some village-specific responses to windspeed, particularly at windspeeds >10 kph (Figure 3.25).

Table 3.9. Summary of GLM results for the model: fishing time (hr) ~ wind speed (kph), with the same-day wind speeds (Date model) and wind speeds from the previous day (Date-1 model)

Model		Coefficients		t-value	Pr(> t)	95% Confidence Interval	
		Estimate	Std. Error			Lower	Upper
Date	Intercept	5.572	0.0978	56.986	< 0.001	5.3795	5.7638
	Wind Speed	-0.055	0.0097	-5.659	< 0.001	-0.0741	-0.0359
Date (-1)	Intercept	5.700	0.0947	60.210	< 0.001	5.5142	5.8863
	Wind Speed	-0.069	0.0095	-7.242	< 0.001	-0.0873	-0.0500

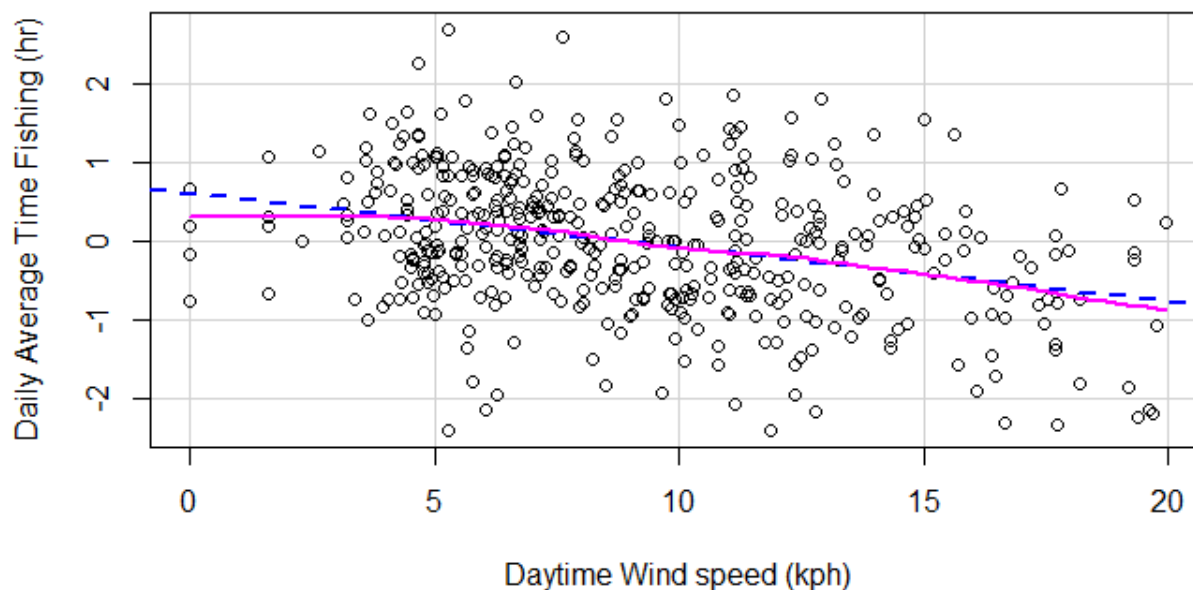


Figure 3.24. Component plus residual plot for the fitted GLM fishing time ~ wind speed) with linear fit (blue dash line) and smooth fit (magenta line) for comparison purposes

Table 3.10. Average activity, measured as percentage of pirogue-use, per targeted village

Village	Avg. Activity (%)	SD	Zone Counts			Count
			1	2	3	
Andrevo	61.5	16.8	35	30	18	83
Ambolomailaka	63.9	15.5	39	37	23	99
Ifaty	60.2	19.8	33	27	19	79
Beravy	65.1	16.4	40	32	18	90
<i>All Data</i>	<i>62.8</i>	<i>17.1</i>				<i>351</i>

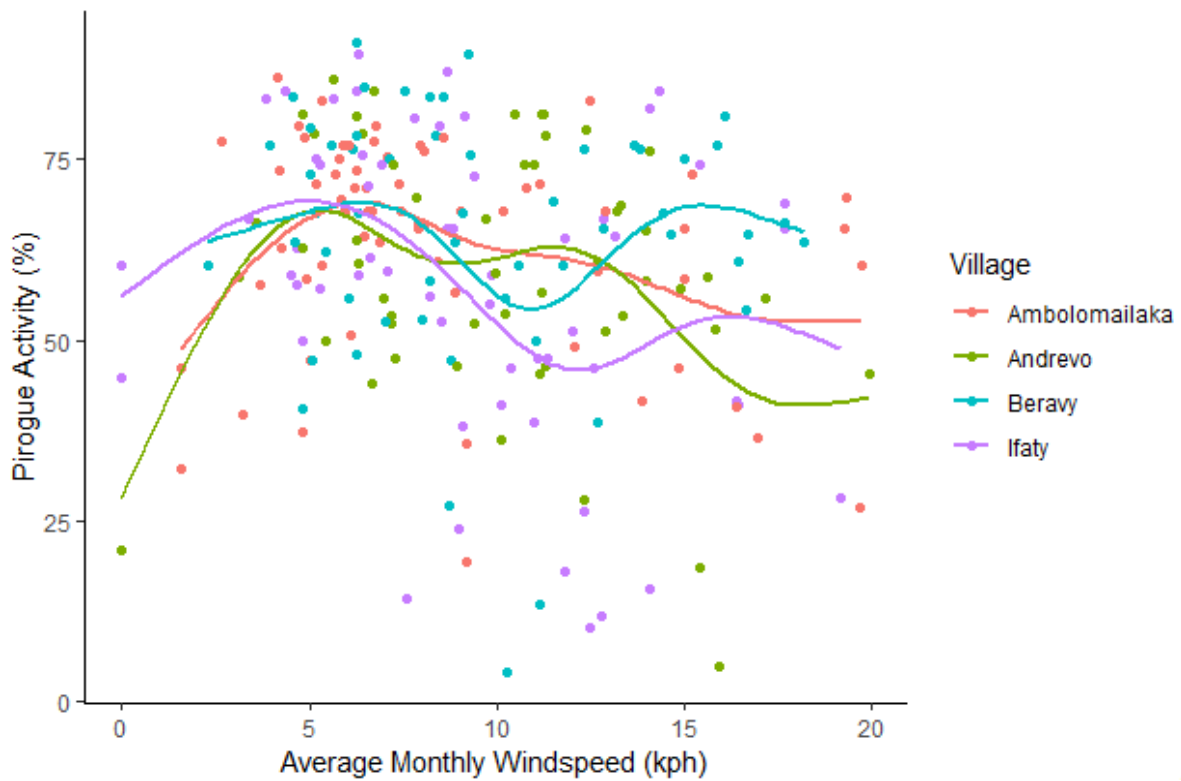


Figure 3.25. Changes in pirogue activity, percentage-use, relative to wind speed per targeted village

Monthly averages of the percentage of pirogue-use indicated fluctuations in activity over the year, with percentages varying from 54.6 % in May to 69.9% in August (Table 3.11), and a general correspondence to fluctuations in monthly average windspeeds (Figure 3.26). GAM models were fitted to the daily pirogue activity and daily-averaged wind speed data (n = 229), with same-day and lagged windspeed models evaluated to determine the best fit. Models were fit using the “mgcv::gam” library in R statistical software, with the standard GAM smoothing function and restricted maximum likelihood optimization (method=REML):

$$\% \text{ Pirogue Activity} \sim s(\text{Daily Average Windspeed}).$$

Results of the time-lagged GAM indicated that daily average windspeed was a significant predictor ($F_{(2.072, 2.646)} = 3.576$, $p = 0.0239$), however the overall fit is quite poor (adjusted $R^2 = 0.0365$, deviance explained = 4.53%) (Figure 3.27). Results of the same-day GAM indicated that windspeed was a highly significant predictor ($F_{(4.582, 5.643)} = 5.124$, $p < 0.001$) and an improved fit (adjusted $R^2 = 0.109$, deviance explained = 12.7%) (Figure 3.28). Given the relatively poor fit, the usefulness of either model for prediction purposes is questionable.

Fishing Effort Spatiotemporal Dynamics

For the Annual Pirogue Count dataset, the total number of pirogues were counted in the 12 villages in years 2013 and 2015 at moments of inclement weather (January – April) in order reasonably ensure that counts were accurate. During this time period, a -5.7% change in the total number of pirogues was observed, with n = 2219 pirogues in 2013 and n = 2093 in 2015. After calculating the percent change per village, a general trend emerged indicating an overall reduction in fishing effort and a potential shifting of effort from the southern villages to the northern villages (Table 4.10).

Table 3.11. Monthly average activity, or pirogue-use, with data from all four targeted villages combined

Month	Avg. Activity (%)	SD	n
1	68.4	10.7	30
2	61.2	13.8	31
3	58.7	19.9	29
4	54.6	15.5	21
5	62.5	17.9	35
6	64.5	22.0	26
7	57.0	16.7	33
8	69.9	14.4	30
9	68.3	12.0	30
10	63.8	20.4	30
11	60.9	20.5	26
12	61.8	14.5	30

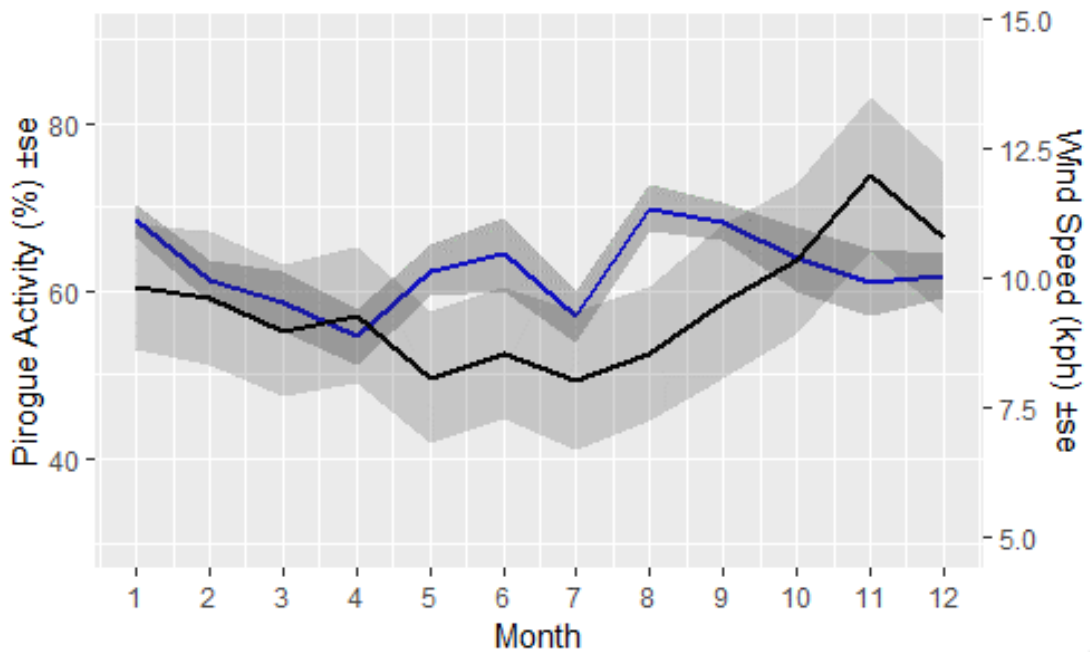


Figure 3.26. Monthly variations in pirogue activity, percentage of pirogues in-use, relative to the monthly changes in wind speed

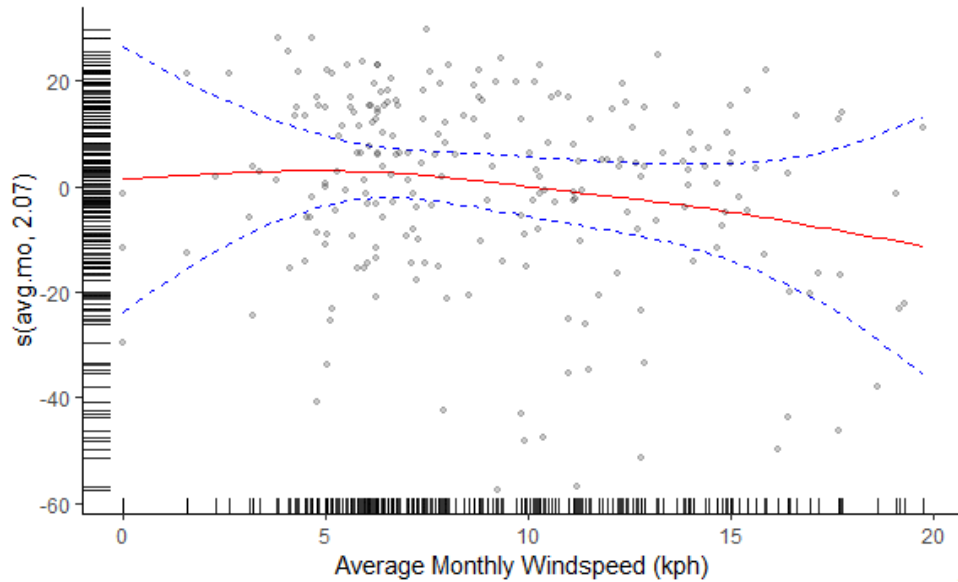


Figure 3.27. Time-lagged model: GAM fit (red line) with 95% confidence intervals (blue dash) and model residuals (adjusted $R^2 = 0.0365$, deviance explained = 4.53%); rug plot – marks on axes indicate observed data values

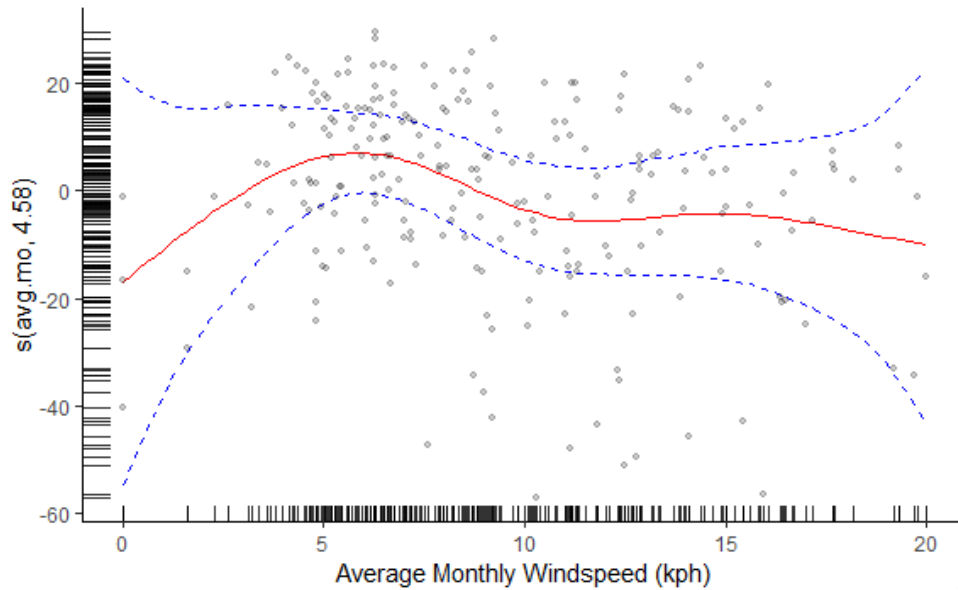


Figure 3.28. Same-day model: GAM fit (red line) with 95% confidence intervals (blue dash) and model residuals (adjusted $R^2 = 0.109$, deviance explained = 12.7%); rug plot – marks on axes indicate observed data values

Spatiotemporal Dynamics of Fishing Effort

Responses of fishermen to the Fishing Effort survey question regarding fishing location provided the first glimpse of the potential spatial diversity and wide distribution of effort throughout the BoR. From the Fishing Effort dataset, representing 13,897 man*days of fishing effort, responses of fishermen indicated the existence of 100+ uniquely-named fishing sites. Although, at the time, we were unable to establish the spatial coordinates that correspond to these traditional fishing sites, the potential exists to produce a fishing effort distribution map of low resolution based solely on the geo-localization of the traditional fishing sites. For example, the 500 m grid system developed for the present study was comprised of $n = 735$ grid cells, whereas 100+ locations are identified following the traditional naming system. However, although sites names may be unique, actual locations, shapes, and sizes of the site may not be distinct nor unique across all named sites, complicating the usefulness of the information for survey work.

The Annual Pirogue Count dataset, where counts were conducted in all 12 villages of the BoR in 2013 and 2015, provided the first evidence that a shift, or a re-distribution, of fishing effort had occurred during the study period. Pirogue counts indicated that overall a 5.68% reduction in effort occurred across the Bay from 2013-2015. For each village, the total percent change and annual percent change were calculated. Results indicated a general decline in the number of pirogues present in the southern villages of the Bay, and evidence of a re-distribution of fishing effort to the villages in the north (Table 3.12).

Localization and enumeration of pirogues at-sea, based on IKONOS and Google Earth satellite imagery, allowed for a time-averaged characterization of the spatial distribution of fishing effort. Using an IKONOS Pan image and Google Earth image tiles, initial spatial images

Table 3.12. Percent change in village fleets from 2013-2015 from Annual Pirogue Count dataset, with villages ordered from north to south

Village	Year		Total % Change	Annual Change	
	2013	2015			
Fitsitke	363	388	6.9%	3.4%	
Andrevo	364	338	-7.1%	-3.6%	
Ambolomailaka	263	284	8.0%	4.0%	
Betsibaroka	76	78	2.6%	1.3%	
Madiorano	92	91	-1.1%	-0.5%	
Amboaboaka	141	134	-5.0%	-2.5%	
Mangily	161	180	11.8%	5.9%	
Ifaty	290	244	-15.9%	-7.9%	
Ambalaboy	50	32	-36.0%	-18.0%	
Beravy	164	139	-15.2%	-7.6%	
Tsongeritelo	133	88	-33.8%	-16.9%	
Ambotsibotsike	122	97	-20.5%	-10.2%	
<i>Total</i>	<i>2219</i>	<i>2093</i>	<i>-5.68%</i>	<i>-2.84%</i>	

of pirogue density were created for each of the four image dates: 16 March 2007, 17 February 2016, 8 March 2016, and 3 June 2018, with 625, 329, 114, and 205 pirogues counted in each image, respectively (Figure 3.29). A composite image was created by averaging pirogue count data from the multi-date imagery that was converted to pirogue*meters per square kilometer. Results of the grid-based spatial averaging of fishing effort indicated that approximately 60.0% of the grid cells experienced positive levels of fishing effort, while the fishing effort in the other 40% of grid cells equaled zero. In grid cells where fishing effort was greater than zero, the average level of fishing effort equaled 33.3 pirogue*meters / km² per day, with an overall average fishing intensity for the entire lagoon equal to 17.9 pirogue*meters / km² per day. The composite image grid was converted to points, with points then being interpolated to create the final map image at 100 m resolution, using the natural neighbor interpolation method. The final

image illustrates the locations of high fishing effort that occurs around the margins of the lagoon in areas of greatest depth change, where the shallow waters of the reef flat and beach shelf drop to floor of the lagoon, changes in depth associated with patch reefs, and in the north / south reef passes (Figure 3.30).

3.4 Discussion

In the present study, fishing effort data collected from 2013 – 2015 describing the Vezo artisanal fisheries of four villages of the Bay of Ranobe was characterized and analyzed to allow for a deeper understanding of the fisheries of the Bay, and to provide adequate representativity, in time and space, for the generalization of results. Initially, the bay-wide pirogue census, Annual Pirogue Count, allowed for the establishment of the sampling frame, and the subsequent determination of four villages targeted for fisheries surveys (*i.e.* Andrevo, Ambolomailaka, Ifaty, and Beravy) that collectively represent 48.7% of the pirogue-based fishing effort. From data collected in the targeted villages, village-specific pirogue length and gear profiles allowed for an appreciation of the distinct fleet characteristics that exist at the village-level, whereas, in averaging the data across villages, the generic profiles permit for the extrapolation of results across the Bay. Regression analysis demonstrated the relationship that exists between pirogue length and gear-use, where intuitively, larger gears (*e.g.* gillnets) require larger pirogues. Larger pirogues, and the use of larger fishing gears, require the involvement of more people to manage the pirogue / gear. A regression equation was determined to allow for the prediction of the number of fishermen according to pirogue length, which was used to predict the number of fishermen bay-wide based on the 4 custom and 8 generic pirogue-length profiles established for the 12 villages of the Bay. Prediction results indicate that approximately 21.4% of the

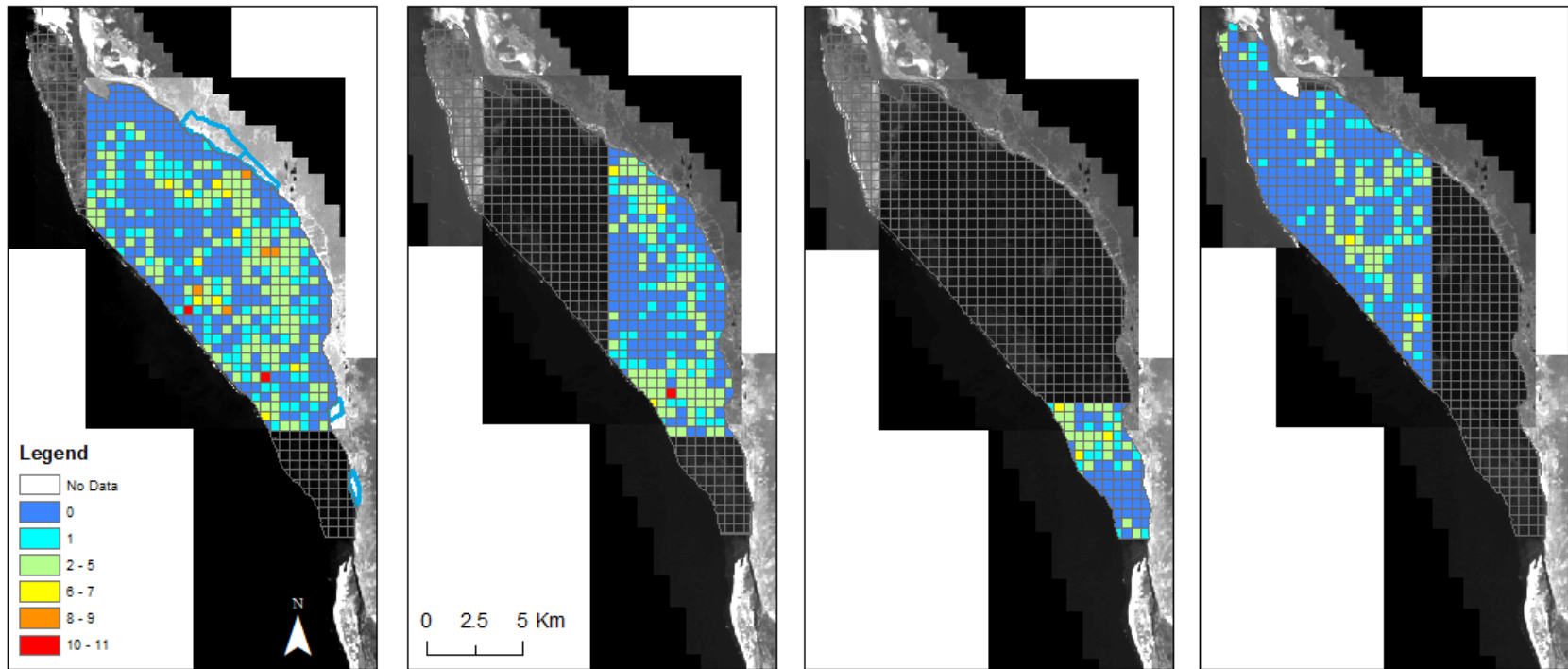


Figure 3.29. Spatial distribution of fishing effort based on the enumeration of pirogues at 500 m grid sampling resolution; colored grid cells indicate extent of image and intensity of effort for images from multiple dates and platforms: (left to right) IKONOS Pan image captured 16 March 2007 and Google Earth images from 17 February 2016, 8 March 2016, and 3 June 2018

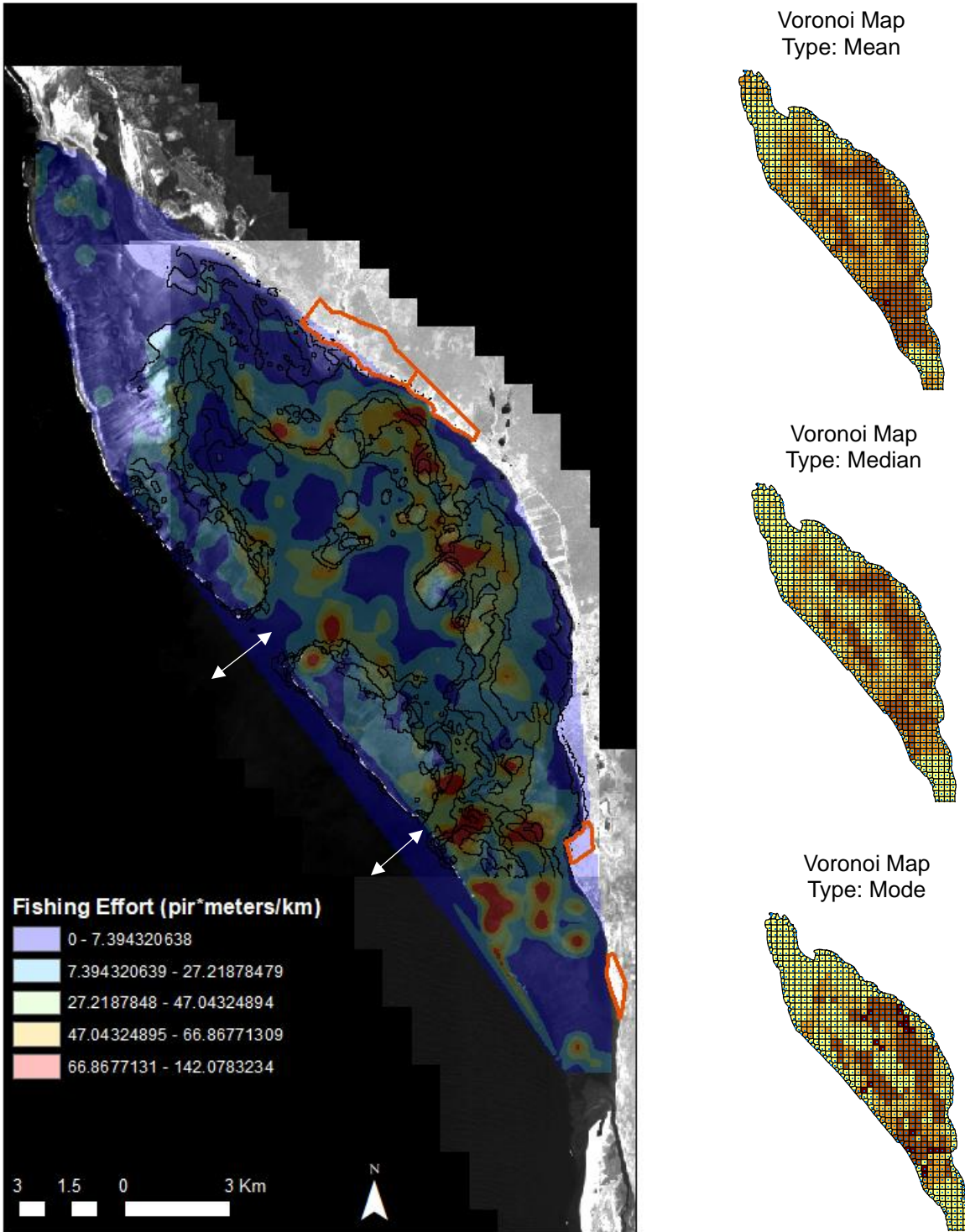


Figure 3.30. Spatial distribution of fishing effort (pirogue-meters km^{-2}) within the Bay of Ranobe interpolated using the natural neighbor at 100m resolution, with villages indicated by orange-red polygons and arrows indicating the north-south passes (left); Voronoi map representations of data: mean, median, and mode (right)

population of the Bay, as determined by human population estimates from Chapter 2, are involved in the pirogue-based fisheries. The results, and associated analyses, discussed above represent the characterization and quantification of the total fishing capacity, latent plus active fishing capacity, that exists in Bay of Ranobe in terms of fishermen, vessels, and gear.

To determine the active fraction of the total fishing capacity, temporal data relevant to fishing effort were analyzed, namely time spent fishing and daily pirogue activity, and the potential effects of wind in mitigating these measures of fishing activity. Early in the design phase of the fisheries survey, it was noted that, at times, periodic strong winds prohibited fishermen from fishing. Given that all of the boats in the fishery are unmotorized, the effect of the wind on total annual effort could, theoretically, be quite substantial. However, analyses of wind speed data revealed that the greatest variation and strongest winds occurred in the afternoon hours after most / all of the daytime fishermen had returned. Wind is likely more influential in determining fishing effort in the nighttime fisheries than it is for daytime fisheries, however, that was not the focus of the present study. Regression analyses of windspeed on daily averages of time spent fishing and the percentage of active pirogues were statistically significant, however, r-squared values were quite low, 0.1034 and 0.109, respectively. Interestingly, the best fit for the “time spent fishing” model was for wind speeds lagged by one day, whereas for the “pirogue activity” model the best fit was achieved using the same-day wind speeds. Logically it seems that the actual time spent fishing in a given day is based upon prior knowledge of wind patterns from the day(s) previous, as implied by the regression of time spent fishing, and that significant deviations from the fishermen’s prediction of the day’s weather could lead to the canceling of fishing activities, as implied by the same-day pirogue-activity regression results. Clearly, weather / wind is an important factor in seasonally shaping the amount of total fishing effort (*i.e.*

time spent fishing and pirogue activity) exerted in this fishery comprised of small, sail-powered vessels, as illustrated in figures 3.23 and 3.26. Results of the Daily Pirogue Counts indicated that the overall daytime pirogue activity was 62.8%, varying from 54.6% - 69.9% on a monthly basis. It is worth noting that the “inactive” fraction of pirogues may not be truly inactive, with the majority likely used in nighttime fishing activities and a small proportion reserved for special uses, such as guided trips for tourism. Moreover, as part of the fishing effort survey, fishermen were asked the number of days they had fished over the previous 3 days and, if applicable, the reasons for which they had missed a day of fishing. Of 115 responses, 71.3% indicated that they had missed a day due to wind, with most of these responses occurring in the months of November, December, and February. Nonetheless, the regression analyses conducted here do not appear to have appreciably captured the full effect of the wind on fishing effort, likely the result of issues of scale, and to a lesser extent, nonlinearities. In the present study, same-day and previous-day models were evaluated, however, weather effects are quite likely operating at multiple time-scales, necessitating a hierarchical analysis approach. Although the fitted regression models were linear and quasi-linear, sailing requires some wind, thus increasing wind speeds are likely preferred by fishermen up to a certain extent, then wind speed becomes a deterrent.

Another factor commonly known to affect departure and return times are the tides. Along much of the coastline of the Bay, the intertidal zone extends several hundred meters from shore, effectively blocking poorly-timed boat movements. Tides synchronize, to some extent, fishermen returning, which can be an advantage when conducting landing surveys. Other reasons provided for missed fishing days, from the fishing effort survey, include: funerals (10.4%), fatigue (7.8%), sickness (3.5%), and church (3.5%). As Kroodsmas *et al.* (2018) noted

the observance of holidays in the global commercial fishing fleets, for the Vezo, there are several holidays that are generally observed: Christmas, New Year's, and Independence Day (June 26). It is interesting to note that although fishing effort may approach zero in observance of holidays, it intensifies in the weeks prior as a means to generate additional income and insure sufficient funds for food, drink, and festivities (pers. obs.).

A critical component in assessing fisheries, and in evaluating the environmental impacts thereof, is an understanding of the spatial distribution of fishing effort. Research over the past decade has begun assessing the spatialized fishing effort for global commercial fisheries, however, only in more recent years has the focus turned to the substantial amount of fishing pressure occurring in nearshore waters exerted by the small-scale fisheries sector. Stewart et al. (2010) quantified and mapped fishing pressures in coastal waters around the globe, however, the clear lack of data that exists for many parts of the globe, particularly Madagascar, raises questions about the accuracy of such efforts. The Stewart et al. (2010) study found that fishing pressure along the coasts of Madagascar was relatively low (0.01 – 0.05 boat-meters km⁻²). The present study provides the first estimates of spatial fishing effort for Madagascar that are based on actual satellite-based pirogue counts, with estimates of fishing pressure for the Bay of Ranobe (33.3 pirogue-meters km⁻²) greatly exceeding previous estimates.

Within the Bay of Ranobe, the 2013/2015 Annual Pirogue Counts indicate a re-distribution of fishing effort from the south to the north, with a 16% change occurring from the village of Mangily northward. Comparatively high fishing pressures in the lagoon south of Mangily, as indicated by the spatial distribution of fishing effort map product (see Figure 3.30), may be the underlying cause. In Chapter 4, evaluations of catch-per-unit-effort will be conducted to determine whether the catch rates in the villages of the southern part of the Bay are

indeed declining as a result of localized fishing pressures, and whether declining catch rates are the potential cause of the northward migration.

Works Cited

- Agnew, D.J., Pearce, J., Pramod, G., Peatman, T., Watson, R., Beddington, J.R. and T.J. Pitcher. 2009. Estimating the worldwide extent of illegal fishing. *PloS one*, 4: p.e4570.
- Ainley, D.G. and L.K. Blight. 2009. Ecological repercussions of historical fish extraction from the Southern Ocean. *Fish and Fisheries*, 10: 13-38.
- Al-Abdulrazzak, Dalal and Daniel Pauly. 2014. Managing fisheries from space: Google Earth improves estimates of distant fish catches. *ICES Journal of Marine Science*, 71: 450-454.
- Anderson, S.C., Flemming, J.M., Watson, R. and H.K. Lotze. 2011. Serial exploitation of global sea cucumber fisheries. *Fish and Fisheries*, 12: 317-339.
- Anticamara, J.A., Watson, R., Gelchu, A. and D. Pauly. 2011. Global fishing effort (1950–2010): trends, gaps, and implications. *Fisheries Research*, 107: 131-136.
- Armstrong, J., Armstrong, D. and R. Hilborn. 1998. Crustacean resources are vulnerable to serial depletion—the multifaceted decline of crab and shrimp fisheries in the Greater Gulf of Alaska. *Reviews in Fish Biology and Fisheries*, 8: 117-176.
- Astuti, Rita (1991) *Learning to be Vezo: the construction of the person among fishing people of western Madagascar*. PhD thesis, The London School of Economics and Political Science (LSE).
- Babcock, E.A., Pikitch, E.K., McAllister, M.K., Apostolaki, P. and C. Santora. 2005. A perspective on the use of spatialized indicators for ecosystem-based fishery management through spatial zoning. *ICES Journal of Marine Science*, 62: 469-476.
- Barnes, D.K. and K.A. Rawlinson. 2009. Traditional coastal invertebrate fisheries in south-western Madagascar. *Journal of the Marine Biological Association of the United Kingdom*, 89: 1589-1596.
- Barnes-Mauthe, M., Oleson, K.L. and B. Zafindrasilivonona. 2013. The total economic value of small-scale fisheries with a characterization of post-landing trends: An application in Madagascar with global relevance. *Fisheries Research*, 147: 175-185.
- Bastardie, F., Nielsen, J.R., Ulrich, C., Egekvist, J. and H. Degel. 2010. Detailed mapping of fishing effort and landings by coupling fishing logbooks with satellite-recorded vessel geo-location. *Fisheries Research*, 106: 41-53.
- Batista, V.S., Fabr e, N.N., Malhado, A.C. and R.J. Ladle. 2014. Tropical artisanal coastal fisheries: challenges and future directions. *Reviews in Fisheries Science & Aquaculture*, 22: 1-15.

- Bell, J.D., Watson, R.A. and Y. Ye. 2017. Global fishing capacity and fishing effort from 1950 to 2012. *Fish and Fisheries*, 18: 489-505.
- Booth, A.J., 2000. Incorporating the spatial component of fisheries data into stock assessment models. *ICES Journal of Marine Science*, 57: 858-865.
- Bordalo-Machado, P. 2006. Fishing effort analysis and its potential to evaluate stock size. *Reviews in Fisheries Science*, 14: 369-393.
- Breen, P., Vanstaen, K. and R.W. Clark. 2014. Mapping inshore fishing activity using aerial, land, and vessel-based sighting information. *ICES Journal of Marine Science*, 72: 467-479.
- Brenier, A., Ferraris, J. and J. Mahafina. 2011. Participatory assessment of the Toliara Bay reef fishery, southwest Madagascar. *Madagascar Conservation & Development*, 6: 60-67.
- Bush, E.R., Short, R.E., Milner-Gulland, E.J., Lennox, K., Samoily, M. and N. Hill. 2017. Mosquito net use in an artisanal East African fishery. *Conservation Letters*, 10: 451-459.
- Cardinale, M., Nugroho, D. and P. Jonson. 2011. Serial depletion of fishing grounds in an unregulated, open access fishery. *Fisheries Research*, 108: 106-111.
- Chambers, G.K. 2001. Genetics and the origins of the Polynesians. *e LS*.
- Chassot, E., Bonhommeau, S., Dulvy, N.K., Mélin, F., Watson, R., Gascuel, D. and O. Le Pape. 2010. Global marine primary production constrains fisheries catches. *Ecology letters*, 13: 495-505.
- Davies, T.E., Beanjara, N. and T. Tregenza. 2009. A socio-economic perspective on gear-based management in an artisanal fishery in south-west Madagascar. *Fisheries Management and Ecology*, 16: 279-289.
- de la Torre-Castro, M.D. and P. Rönnbäck. 2004. Links between humans and seagrasses—an example from tropical East Africa. *Ocean & Coastal Management*, 47: 361-387.
- Doukakis, P., Jonahson, M., Ramahery, V., de Dieu Randriamanantsoa, B.J. and Harding, S., 2008. Traditional fisheries of antongil bay, Madagascar. *Western Indian Ocean Journal of Marine Science*, 6: 175-181.
- Doumbouya, A., Camara, O.T., Mamie, J., Intchama, J.F., Jarra, A., Ceesay, S., Guèye, A., Ndiaye, D., Beibou, E., Padilla, A. and D. Belhabib. 2017. Assessing the effectiveness of monitoring control and surveillance of illegal fishing: The case of West Africa. *Frontiers in Marine Science*, 4: 50.

- Dunn, D.C., Stewart, K., Bjorkland, R.H., Haughton, M., Singh-Renton, S., Lewison, R., Thorne, L. and P.N. Halpin. 2010. A regional analysis of coastal and domestic fishing effort in the wider Caribbean. *Fisheries Research*, 102: 60-68.
- Flothmann, S., von Kistowski, K., Dolan, E., Lee, E., Meere, F. and G. Album. 2010. Closing loopholes: getting illegal fishing under control. *Science*, 328: 1235-1236.
- Gerritsen, H. and C. Lordan. 2010. Integrating vessel monitoring systems (VMS) data with daily catch data from logbooks to explore the spatial distribution of catch and effort at high resolution. *ICES Journal of Marine Science*, 68: 245-252.
- Guan, W., Cao, J., Chen, Y. and M. Cieri. 2013. Impacts of population and fishery spatial structures on fishery stock assessment. *Canadian Journal of Fisheries and Aquatic Sciences*, 70: 1178-1189.
- Halim, A., Wiryawan, B., Loneragan, N.R., Hordyk, A., Sondita, M.F.A., White, A.T., Koeshendrajana, S., Ruchimat, T., Pomeroy, R.S. and C. Yuni. 2019. Developing a functional definition of small-scale fisheries in support of marine capture fisheries management in Indonesia. *Marine Policy*, 100: 238-248.
- Humber, F., Godley, B.J., Ramahery, V. and A.C. Broderick. 2011. Using community members to assess artisanal fisheries: the marine turtle fishery in Madagascar. *Animal conservation*, 14: 175-185.
- Johnson, A.F., Moreno-Báez, M., Giron-Nava, A., Corominas, J., Erisman, B., Ezcurra, E. and O. Aburto-Oropeza. 2017. A spatial method to calculate small-scale fisheries effort in data poor scenarios. *PloS one*, 12: p.e0174064.
- Joo, R., Salcedo, O., Gutierrez, M., Fablet, R. and S. Bertrand. 2015. Defining fishing spatial strategies from VMS data: Insights from the world's largest monospecific fishery. *Fisheries Research*, 164: 223-230.
- Junior, J.G.C.O., Silva, L.P., Malhado, A.C., Batista, V.S., Fabr e, N.N. and R.J. Ladle. 2016. Artisanal fisheries research: a need for globalization? *PloS one*, 11: p.e0150689.
- Karpov, K., Haaker, P., Taniguchi, I. and L. Rogers-Bennett. 2000. Serial depletion and the collapse of the California abalone (*Haliotis* spp.) fishery. *Canadian Special Publication of Fisheries and Aquatic Sciences*, pp.11-24.
- Kolding, J., B en e, C. and M. Bavinck. 2014. Small-scale fisheries: Importance, vulnerability and deficient knowledge. *Governance of marine fisheries and biodiversity conservation*, pp.317-331.
- Kroodsma DA, Mayorga J, Hochberg T, Miller NA, Boerder K, Ferretti F, Wilson A, Bergman B, White TD, Block BA, and P. Woods. 2018. Tracking the global footprint of fisheries. *Science*, 359: 904-908.

- Laroche, J. and N. Ramananarivo. 1995. A preliminary survey of the artisanal fishery on coral reefs of the Tulear Region (southwest Madagascar). *Coral Reefs*, 14: 193-200.
- Laroche, J., Razanoelisoa, J., Fauroux, E. and M.W. Rabenevanana. 1997. The reef fisheries surrounding the south-west coastal cities of Madagascar. *Fisheries management and ecology*, 4: 285-299.
- Le Manach, F., Gough, C., Harris, A., Humber, F., Harper, S. and D. Zeller. 2012. Unreported fishing, hungry people and political turmoil: the recipe for a food security crisis in Madagascar? *Marine policy*, 36: 218-225.
- Le Manach, F., Andriamahefazafy, M., Harper, S., Harris, A., Hosch, G., Lange, G.M., Zeller, D. and U.R. Sumaila. 2013. Who gets what? Developing a more equitable framework for EU fishing agreements. *Marine Policy*, 38: 257-266.
- Mahdi, W. 1999. The dispersal of Austronesian boat forms in the Indian Ocean. *Archaeology and language III: Artefacts, languages and texts*, pp.144-179.
- McVean, A.R., Hemery, G., Walker, R.C.J., Ralisaona, B.L.R. and E. Fanning. 2005. Traditional sea cucumber fisheries in southwest Madagascar: A case-study of two villages in 2002. *SPC Beche-de-mer Information Bulletin*, 21: 15-18.
- McVean, A.R., Walker, R.C. and E. Fanning. 2006. The traditional shark fisheries of southwest Madagascar: A study in the Toliara region. *Fisheries Research*, 82: 280-289.
- Mills, D.J., Westlund, L., de Graaf, G., Kura, Y., Willman, R. and K. Kelleher. 2011. Under-reported and undervalued: small-scale fisheries in the developing world. *Small-scale fisheries management: frameworks and approaches for the developing world*, pp.1-15.
- Natale, F., Gibin, M., Alessandrini, A., Vespe, M. and A. Paulrud. 2015. Mapping fishing effort through AIS data. *PloS one*, 10: p.e0130746.
- Narozanski, A.J., Belle, E.M. and M.D. Steer. 2011. Understanding local differences in small-scale fisheries: a comparison of two fishing settlements in Antsiranana Bay, northern Madagascar. *Madagascar Conservation & Development*, 6: 68-77.
- Pascual, M., Borja, A., Galparsoro, I., Ruiz, J., Mugerza, E., Quincoces, I., Murillas, A. and L. Arregi. 2013. Total fishing pressure produced by artisanal fisheries, from a Marine Spatial Planning perspective: A case study from the Basque Country (Bay of Biscay). *Fisheries research*, 147: 240-252.
- Pauly, D., Watson, R. and J. Alder. 2005. Global trends in world fisheries: impacts on marine ecosystems and food security. *Philosophical Transactions of the Royal Society B: Biological Sciences*, 360: 5-12.

- Pauly, D. 2006. Major trends in small-scale marine fisheries, with emphasis on developing countries, and some implications for the social sciences.
- Pauly, D. and D. Zeller. 2016. Catch reconstructions reveal that global marine fisheries catches are higher than reported and declining. *Nature communications*, 7: 10244.
- Pollock, K.H., Hoenig, J.M., Jones, C.M., Robson, D.S. and C.J. Greene. 1997. Catch rate estimation for roving and access point surveys. *North American Journal of Fisheries Management*, 17: 11-19.
- Purcell, S.W., Mercier, A., Conand, C., Hamel, J.F., Toral-Granda, M.V., Lovatelli, A. and S. Uthicke. 2013. Sea cucumber fisheries: global analysis of stocks, management measures and drivers of overfishing. *Fish and fisheries*, 14: 34-59.
- Purcell, S.W. and R.S. Pomeroy. 2015. Driving small-scale fisheries in developing countries. *Frontiers in Marine Science*, 2: p.44.
- Rakotonirina, B. and A. Cooke. 1994. Sea turtles of Madagascar—their status, exploitation and conservation. *Oryx*, 28: 51-61.
- Robinson, L. and W.H.H. Sauer. 2013. A first description of the artisanal shark fishery in northern Madagascar: implications for management. *African Journal of Marine Science*, 35: 9-15.
- Salas, S., Chuenpagdee, R., Seijo, J.C. and A. Charles. 2007. Challenges in the assessment and management of small-scale fisheries in Latin America and the Caribbean. *Fisheries Research*, 87: 5-16.
- Selgrath, J.C., Gergel, S.E. and A.C. Vincent. 2017. Incorporating spatial dynamics greatly increases estimates of long-term fishing effort: a participatory mapping approach. *ICES Journal of Marine Science*, 75: 210-220.
- Short, R., Gurung, R., Rowcliffe, M., Hill, N. and E.J. Milner-Gulland. 2018. The use of mosquito nets in fisheries: A global perspective. *PloS one*, 13: p.e0191519.
- Smallwood, C.B., Pollock, K.H., Wise, B.S., Hall, N.G. and D.J. Gaughan. 2012. Expanding aerial-roving surveys to include counts of shore-based recreational fishers from remotely operated cameras: benefits, limitations, and cost effectiveness. *North American Journal of Fisheries Management*, 32: 1265-1276.
- Smith, H. and X. Basurto. 2019. Defining small-scale fisheries and examining the role of science in shaping perceptions of who and what counts: A systematic review. *Frontiers in Marine Science*, 6: 236.
- Srinivasan, U.T., Watson, R. and U.R. Sumaila. 2012. Global fisheries losses at the exclusive economic zone level, 1950 to present. *Marine Policy*, 36: 544-549.

- Stamatopoulos, C. 2002. *Sample-based fishery surveys. A technical handbook*. FAO.
- Stewart, K.R., Lewison, R.L., Dunn, D.C., Bjorkland, R.H., Kelez, S., Halpin, P.N. and L.B. Crowder. 2010. Characterizing fishing effort and spatial extent of coastal fisheries. *PloS one*, 5: p.e14451.
- Swartz, W., Sala, E., Tracey, S., Watson, R. and D. Pauly. 2010. The spatial expansion and ecological footprint of fisheries (1950 to present). *PloS one*, 5: p.e15143.
- Swartzman, G., Huang, C. and S. Kaluzny. 1992. Spatial analysis of Bering Sea groundfish survey data using generalized additive models. *Canadian Journal of Fisheries and Aquatic Sciences*, 49: 1366-1378.
- Thiault, L., Collin, A., Chlous, F., Gelcich, S. and J. Claudet. 2017. Combining participatory and socioeconomic approaches to map fishing effort in small-scale fisheries. *PloS one*, 12: p.e0176862.
- Tian, S., Chen, Y., Chen, X., Xu, L. and X. Dai. 2010. Impacts of spatial scales of fisheries and environmental data on catch per unit effort standardisation. *Marine and Freshwater Research*, 60: 1273-1284.
- Tickler, D., Meeuwig, J.J., Palomares, M.L., Pauly, D. and D. Zeller. 2018. Far from home: Distance patterns of global fishing fleets. *Science advances*, 4: 3279.
- Tinsman, J.C. and W.H. Whitmore. 2006. Aerial flight methodology to estimate and monitor trends in fishing effort on Delaware artificial reef sites. *Bulletin of Marine Science*, 78: 167-176.
- Turner, R.A., Polunin, N.V. and S.M. Stead. 2015. Mapping inshore fisheries: comparing observed and perceived distributions of pot fishing activity in Northumberland. *Marine Policy*, 51: 173-181.
- Van der Elst, R., Everett, B., Jiddawi, N., Mwatha, G., Afonso, P.S. and D. Boule. 2005. Fish, fishers and fisheries of the Western Indian Ocean: their diversity and status. A preliminary assessment. *Philosophical Transactions of the Royal Society A: Mathematical, Physical and Engineering Sciences*, 363: 263-284.
- Van der Elst, R.P., Groeneveld, J.C., Baloi, A.P., Marsac, F., Katonda, K.I., Ruwa, R.K. and W.L. Lane. 2009. Nine nations, one ocean: A benchmark appraisal of the South Western Indian Ocean Fisheries Project (2008–2012). *Ocean & Coastal Management*, 52: 258-267.
- Walker, R.C. and E. Roberts. 2005. Notes on the status and incidental capture of marine turtles by the subsistence fishing communities of South West Madagascar. *Western Indian Ocean Journal of Marine Science*, 4: 219-226.

- Walters, C. 2000. Impacts of dispersal, ecological interactions, and fishing effort dynamics on efficacy of marine protected areas: how large should protected areas be?. *Bulletin of marine science*, 66: 745-757.
- Walters, C. 2003. Folly and fantasy in the analysis of spatial catch rate data. *Canadian Journal of Fisheries and Aquatic Sciences*, 60: 1433-1436.
- Watson, R., Kitchingman, A., Gelchu, A. and D. Pauly. 2004. Mapping global fisheries: sharpening our focus. *Fish and fisheries*, 5: 168-177.
- Watson, R.A., Cheung, W.W., Anticamara, J.A., Sumaila, R.U., Zeller, D. and D. Pauly. 2013. Global marine yield halved as fishing intensity redoubles. *Fish and Fisheries*, 14: 493-503.
- Watson, R.A. and D. Pauly. 2013. The changing face of global fisheries—The 1950s vs. the 2000s. *Marine Policy*, 42: 1-4.
- Watson, R., Zeller, D. and D. Pauly. 2014. Primary productivity demands of global fishing fleets. *Fish and Fisheries*, 15: 231-241.
- Wilens, J.E. 2004. Spatial management of fisheries. *Marine Resource Economics*, 19: 7-19.
- Witt, M.J. and B.J. Godley. 2007. A step towards seascape scale conservation: using vessel monitoring systems (VMS) to map fishing activity. *PloS one*, 2: p.e1111.
- World Bank/FAO/WorldFish. 2010. The Hidden Harvests: the global contribution of capture fisheries. Agriculture and Rural Development, Sustainable Development Network. World Bank, Washington, D.C.
- Ying, Y., Chen, Y., Lin, L. and T. Gao. 2011. Risks of ignoring fish population spatial structure in fisheries management. *Canadian Journal of Fisheries and Aquatic Sciences*, 68: 2101-2120.

Appendix

April 2014

Dim	Lun	Mar	Mer	Jeu	Ven	Sam
		1	2	3	4	5
		And				
6	7	8	9	10	11	12
	Ifaty	Ifaty	Ifaty	Ifaty	Ifaty	Ber
13	14	15	16	17	18	19
	Ber	Ber	Ber	Ber		
20	21	22	23	24	25	26
	And	And	And	And	And	
27	28	29	30			
Amb	Amb	Amb	Amb			

May 2014

Dim	Lun	Mar	Mer	Jeu	Ven	Sam
				1	2	3
				Amb		
4	5	6	7	8	9	10
	Ber	Ber	Ber	Ber	Ber	
11	12	13	14	15	16	17
	And	And	And	And	And	
18	19	20	21	22	23	24
	Amb	Amb	Amb	Amb	Amb	
25	26	27	28	29	30	31
	Ifaty	Ifaty	Ifaty	Ifaty	Ifaty	

Appendix 3.1. Excerpt from the data collection schedule designed for the fisheries surveys; abbreviated village names indicate location of the survey relative to the full moon (green date) and new moon (red date)

Village: _____ Ticket #: _____ Pirogue #: _____ Date: _____ Departure Time: _____ Return Time: _____

Fisheries Landings Datasheet: Fishing effort survey

Survey ID _____

Fishermen / Pirogues				Gear #1		Gear # _____		Gear # _____	
# pers:	date (-1)	date (-2)	date (-3)	Type:	Length: _____ m	Type:	Length: _____ m	Type:	Length: _____ m
Activity				Gillnet	Width: _____ m	Gillnet	Width: _____ m	Gillnet	Width: _____ m
Reason				Boat seine	Mesh: _____ cm	Boat seine	Mesh: _____ cm	Boat seine	Mesh: _____ cm
				Beach seine	# Lines: _____	Beach seine	# Lines: _____	Beach seine	# Lines: _____
				Mosquito net	# Hooks: _____	Mosquito net	# Hooks: _____	Mosquito net	# Hooks: _____
Pirogue Length: _____				Hook-Line	Depth: Bot / mid / sur	Hook-Line	Depth: Bot / mid / sur	Hook-Line	Depth: Bot / mid / sur
Fishing grounds: _____				Spear gun		Spear gun		Spear gun	
				Harpoon	# Sets	Harpoon	# Sets	Harpoon	# Sets

Village: _____ Ticket #: _____ Pirogue #: _____ Date: _____ Departure Time: _____ Return Time: _____

Survey ID _____

Fishermen / Pirogues				Gear #1		Gear # _____		Gear # _____	
# pers:	date (-1)	date (-2)	date (-3)	Type:	Length: _____ m	Type:	Length: _____ m	Type:	Length: _____ m
Activity				Gillnet	Width: _____ m	Gillnet	Width: _____ m	Gillnet	Width: _____ m
Reason				Boat seine	Mesh: _____ cm	Boat seine	Mesh: _____ cm	Boat seine	Mesh: _____ cm
				Beach seine	# Lines: _____	Beach seine	# Lines: _____	Beach seine	# Lines: _____
				Mosquito net	# Hooks: _____	Mosquito net	# Hooks: _____	Mosquito net	# Hooks: _____
Pirogue Length: _____				Hook-Line	Depth: Bot / mid / sur	Hook-Line	Depth: Bot / mid / sur	Hook-Line	Depth: Bot / mid / sur
Fishing grounds: _____				Spear gun		Spear gun		Spear gun	
				Harpoon	# Sets	Harpoon	# Sets	Harpoon	# Sets

Village: _____ Ticket #: _____ Pirogue #: _____ Date: _____ Departure Time: _____ Return Time: _____

Survey ID _____

Fishermen / Pirogues				Gear #1		Gear # _____		Gear # _____	
# pers:	date (-1)	date (-2)	date (-3)	Type:	Length: _____ m	Type:	Length: _____ m	Type:	Length: _____ m
Activity				Gillnet	Width: _____ m	Gillnet	Width: _____ m	Gillnet	Width: _____ m
Reason				Boat seine	Mesh: _____ cm	Boat seine	Mesh: _____ cm	Boat seine	Mesh: _____ cm
				Beach seine	# Lines: _____	Beach seine	# Lines: _____	Beach seine	# Lines: _____
				Mosquito net	# Hooks: _____	Mosquito net	# Hooks: _____	Mosquito net	# Hooks: _____
Pirogue Length: _____				Hook-Line	Depth: Bot / mid / sur	Hook-Line	Depth: Bot / mid / sur	Hook-Line	Depth: Bot / mid / sur
Fishing grounds: _____				Spear gun		Spear gun		Spear gun	
				Harpoon	# Sets	Harpoon	# Sets	Harpoon	# Sets

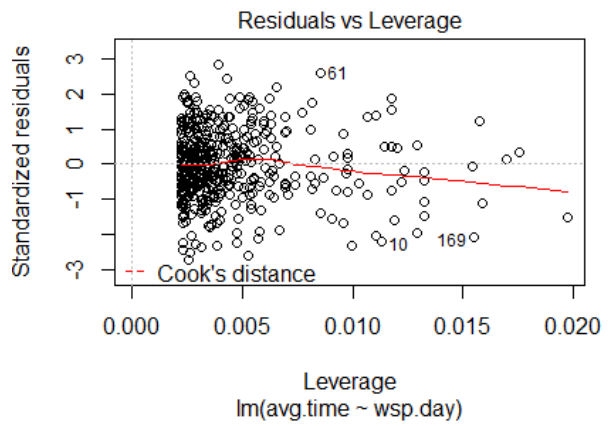
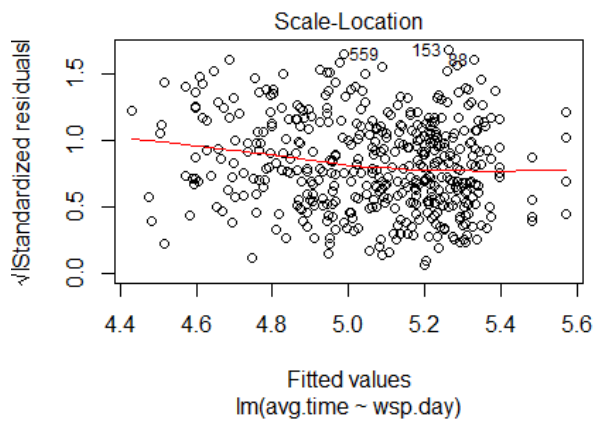
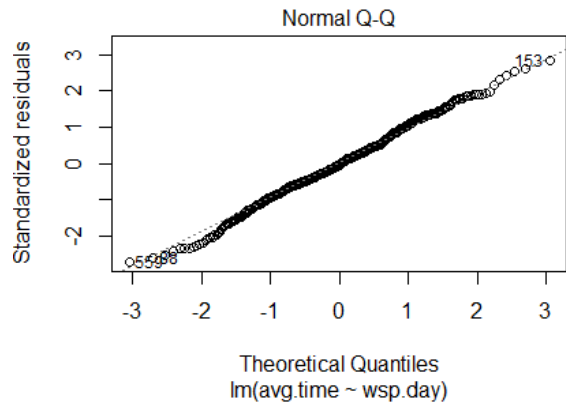
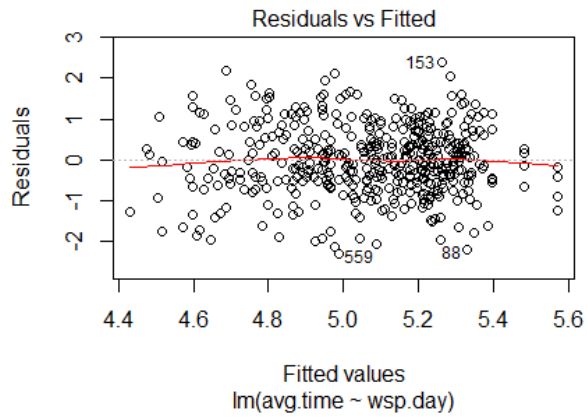
Appendix 3.3. Fishing Effort survey data sheet

Length Bin	Fitsi.	Andre.	Ambolo.	Betsi.	Madio.	Amboa.	Mangily	Ifaty	Ambala.	Beravy	Tsong.	Ambot.
2.50	0	0	0	0	0	0	0	0	0	0	0	0
3.00	0	0	0	0	0	0	0	0	0	1	0	0
3.50	11	6	2	2	3	4	5	13	2	13	4	4
4.00	55	74	16	11	14	21	24	51	8	26	20	18
4.50	67	92	17	14	17	26	30	68	9	27	25	23
5.00	50	52	27	10	13	19	22	45	7	26	18	17
5.50	39	29	24	8	10	15	17	28	5	36	14	13
6.00	32	50	9	7	8	12	14	18	4	21	12	11
6.50	24	25	20	5	6	9	11	20	3	7	9	8
7.00	26	17	33	6	7	10	12	20	4	6	10	9
7.50	24	12	43	5	6	10	11	14	3	0	9	8
8.00	20	4	42	4	5	8	9	9	3	0	7	7
8.50	10	3	22	2	3	4	5	4	1	0	4	4
9.00	3	0	7	1	1	1	1	0	0	1	1	1
9.50	0	0	1	0	0	0	0	0	0	0	0	0
10.00	0	0	0	0	0	0	0	0	0	0	0	0
<i>Total</i>	<i>363</i>	<i>364</i>	<i>263</i>	<i>76</i>	<i>92</i>	<i>141</i>	<i>161</i>	<i>290</i>	<i>50</i>	<i>164</i>	<i>133</i>	<i>122</i>

Appendix 3.4. Pirogue counts per length class, with actual data for surveyed villages highlighted in gray, where estimates for villages not surveyed were generated from the generic density profile

Length Bin	Fitsi.	Andre.	Ambolo.	Betsi.	Madio.	Amboa.	Mangily	Ifaty	Ambala.	Beravy	Tsong.	Ambot.
2.50	0.0	0.0	0.0	0.0	0.0	0.0	0.0	0.0	0.0	0.0	0.0	0.0
3.00	1.4	0.0	0.0	0.3	0.3	0.5	0.6	0.0	0.2	4.3	0.5	0.5
3.50	39.7	20.4	8.6	8.3	10.0	15.4	17.6	45.9	5.5	44.9	14.5	13.3
4.00	219.3	297.0	63.6	45.9	55.6	85.2	97.3	204.7	30.2	102.7	80.4	73.7
4.50	301.8	412.8	77.1	63.2	76.5	117.2	133.9	307.1	41.6	121.9	110.6	101.4
5.00	249.3	262.1	134.6	52.2	63.2	96.8	110.5	223.1	34.3	128.3	91.3	83.8
5.50	214.4	160.2	134.6	44.9	54.3	83.3	95.1	151.6	29.5	196.1	78.5	72.0
6.00	190.3	297.0	51.4	39.9	48.2	73.9	84.4	110.2	26.2	128.3	69.7	64.0
6.50	156.1	160.9	127.2	32.7	39.6	60.6	69.2	127.9	21.5	46.3	57.2	52.5
7.00	184.0	122.3	231.2	38.5	46.6	71.5	81.6	137.8	25.3	39.9	67.4	61.8
7.50	183.5	87.4	321.1	38.4	46.5	71.3	81.4	108.3	25.3	0.0	67.2	61.7
8.00	159.5	34.9	332.7	33.4	40.4	62.0	70.8	73.5	22.0	0.0	58.4	53.6
8.50	88.6	24.8	187.2	18.5	22.5	34.4	39.3	33.5	12.2	0.0	32.5	29.8
9.00	28.6	0.0	66.1	6.0	7.2	11.1	12.7	0.0	3.9	12.8	10.5	9.6
9.50	4.3	0.0	11.6	0.9	1.1	1.7	1.9	0.0	0.6	0.0	1.6	1.4
10.00	0.0	0.0	0.0	0.0	0.0	0.0	0.0	0.0	0.0	0.0	0.0	0.0
<i>Total</i>	2020.7	1879.7	1746.8	423.1	512.1	784.9	896.3	1523.5	278.3	825.7	740.4	679.1

Appendix 3.5. Pirogue total length per length class, with actual data for surveyed villages highlighted in gray, where estimates for villages not surveyed were generated from the generic density profile



Appendix 3.6. Regression diagnostic plots for the time-lagged regression model of average time spent fishing as predicted by wind speed

Vezo Artisanal Fisheries: Characterization of landings and economic valuation of the daytime, boat-based coral reef fisheries of the Bay of Ranobe

4.1 Introduction

Coral reef ecosystems: A global crisis

Coral reef ecosystems (*i.e.*, corals, seagrasses and mangroves) have been steadily declining for millennia, with the earliest declines being attributed to human exploitation at the time of hunter-gatherers (Jackson *et al.*, 2001; Pandolfi *et al.*, 2003). In modern times, the rising demand on marine resources, pollution (*i.e.*, sediment, chemical and nutrient), disease, sea-surface temperature rise, ocean acidification, and other climate-related phenomena have accelerated the degradation of these tropical coastal habitats, resulting in the loss of abundance, biodiversity, and habitat structure (Knowlton, 2001; Hughes *et al.*, 2003; Jones *et al.*, 2004; Alvarez-Filip *et al.*, 2009; Veron *et al.*, 2009). A growing body of research has illustrated that many of these stressors have cumulative effects and may interact non-linearly, resulting in even greater losses of biodiversity and productivity than may be predicted (Harvell *et al.*, 1999; Knowlton, 2001; Jackson *et al.*, 2001; Nugues and Roberts, 2003; Hoegh-Guldberg, 2007; Veron *et al.*, 2009).

Although quantifying the rate at which coral reef ecosystems, *i.e.* coral reef, seagrass, and mangrove habitats, are declining globally has proven difficult (Jenkins *et al.*, 2003), particularly for coral reefs themselves, Pandolfi *et al.* (2003) estimate that all coral reef ecosystems are 20-80% degraded relative to pristine, pre-human conditions. At the current rate of loss, by 2030 nearly 60% of all coral reefs may be destroyed (Hughes *et al.*, 2003), where reefs in certain

regions of the world may have already suffered irrevocable damage, for example the Caribbean reefs (Gardner *et al.*, 2003). In the Indo-Pacific, which contains 75% of the world's coral reefs, the average annual rate of decline of live coral cover is approximately 1% yr⁻¹ (1500 km²) for the period of 1980-2003 (Bruno and Selig, 2007). In the case of seagrasses, a recent comprehensive global assessment, including 215 studies, found that seagrass habitat loss is occurring at a rate of 110 km² yr⁻¹, and since 1980, 29% of the global seagrass cover has disappeared (Waycott *et al.*, 2009). Moreover, this rate of decline has accelerated from a pre-1940 rate of 0.9% yr⁻¹ to a post-1990 rate of 7% yr⁻¹ (Waycott *et al.*, 2009). Similarly, 20-35% of the global coverage of mangrove habitat has been lost since 1980, with estimates for the annual rate of loss varying from 1-2.5% yr⁻¹ (Jenkins *et al.*, 2003; Polidoro *et al.*, 2010). When compared to the 0.5% yr⁻¹ rate of loss for tropical forests (Waycott *et al.*, 2009), the rate at which coral reef ecosystems are being destroyed becomes all that more alarming, especially when considering the contribution of each of these habitats to the productivity of the greater ecosystem (de la Torre-Castro *et al.*, 2014).

Effects of overfishing on coral reef ecosystems

Overfishing has been one of the principle driving forces in coral reef ecosystem deterioration since the beginning of human civilization to the present (Pandolfi *et al.*, 2003; Halpern *et al.*, 2008). Coral reef decline attributed to overfishing may directly result from structural damage, as a result of destructive fishing practices and gear entanglement, or may arise indirectly through disruption of community structure by the removal of ecologically important species. Removal of key species, or functional groups, may impair ecosystem functioning through the modification of reef fish assemblages. Often, the first sign of overfishing is the disappearance of the upper trophic level—large-bodied, predatory fish species (*e.g.*, Stallings,

2009 and references therein). Loss of reef predators, then leads to the targeting by fishermen of the next lower level, with the process continuing sequentially as the preceding trophic levels are depleted, known as “fishing down the food web” (Pauly *et al.*, 1998). However, most coral reef ecosystems are located in the territorial waters of developing countries, which are characterized by low-tech, artisanal fisheries, and high human population densities. In such cases, organisms representing all trophic levels are often targeted and consumed, a phenomenon akin to “fishing through the food web” (Essington *et al.*, 2006). Regardless, both processes inevitably lead to the disruption of key functional relationships required to maintain coral health, in particular the relationship between herbivores, algae, and coral.

On reefs, coral and algae compete for space to grow and substrate suitable for colonization (McCook *et al.*, 2001). By minimizing algal population growth, herbivores play a central role in reducing stress on coral caused by potential algal overgrowth (Mumby *et al.*, 2007). If the role of herbivores is compromised, for example through overfishing, algae may rapidly colonize dead or moribund corals, thereby inducing a shift from a coral-dominated to an algae-dominated system, known as a phase shift (McCook *et al.*, 1999; Hughes *et al.*, 2005). If multiple stressors are present (*e.g.*, overfishing, elevated sea-surface temperature, high sedimentation, *etc.*), given their cumulative effects, coral death becomes more probable and the likelihood of a phase shift occurring increases.

Small-scale fisheries: Artisanal fisheries

Of the 120 million people that are directly dependent on capture fisheries, 90% work in the small-scale fisheries (SSF) sector, whose catch represents more than 50% of the global total (World Bank/FAO/WorldFish, 2010; Mills *et al.*, 2011). Most SSF may be classified as IUU fisheries, as there is little to no data being systematically collected on, ostensibly, the largest sub-

sector of fisheries. Unlike commercial fisheries, research into SSF has substantially lagged, gaining some attention over the past decade (Purcell and Pomeroy, 2015). In part, the lack of research in the SSF sector may be explained by the difficult situational, socio-political, and/or environmental contexts in which SSFs are embedded, and the unique nature of the unorganized and spatially dispersed landings along potentially hundreds of kilometers of shoreline (Salas *et al.*, 2007). Moreover, the multi-species catches taken with multiple gears, which are often modified, complicates data analyses once surveys are completed. The very definition of small-scale fishery is rather ill-defined, and is sometimes used interchangeably with the term artisanal fisheries (Halim *et al.*, 2019; Smith and Basurto, 2019). Although the definition remains vague and has been applied to fisheries ranging from a one-man canoe to a 20m trawler, for the present study emphasis is placed on the low-tech / high-artisanality end of the spectrum, as described by Batista *et al.* (2014), in characterizing the fisheries of the Vezo communities of southwest Madagascar.

Fisheries of Madagascar

In Madagascar, the legal commercial fisheries sector is limited to shrimp trawling operations that have occurred mainly along the west coast since the 1960's (Van der Elst *et al.*, 2009; Le Manach *et al.*, 2012), and through a series of fishing agreements with the European Union dating back to 1986 (Le Manach *et al.*, 2013a), fishing rights to the country's tuna resources are permitted for the seining and longlining fleets of Spain, Portugal, Italy, and France. Commercial harvests are almost entirely exported along with most of their economic and nutritional value. At a smaller scale, an artisanal fishery exists for sea cucumbers that are exported both legally and illegally (McVean *et al.*, 2005; Purcell *et al.*, 2013) to supply the demands of Chinese markets, as well as other targeted invertebrates (Barnes and Rawlinson,

2009). Similarly, the legal artisanal shark fishery has been commandeered to support the illegal international trade in shark fins (McVean *et al.*, 2006; Robinson and Sauer, 2013). At a national level, a ban was placed on the marine turtle fishery through presidential decree in 2006, however the fishery still persists largely unencumbered (Rakotonirina and Cooke, 1994; Walker and Roberts, 2005; Humber *et al.*, 2011). Artisanal finfish fisheries are likely the single most important fishery in terms of biomass productivity and economic benefits provided to the Malagasy people, yet comparatively have received little research attention (Van der Elst *et al.*, 2005). In a comparison of marine fisheries publications originating from nine Western Indian Ocean countries, only 1.4% of the research publications addressed the marine fisheries of Madagascar (Van der Elst *et al.*, 2005), *e.g.* Laroche and Ramananarivo (1995) and Laroche *et al.* (1997). Since, a few studies have been published, documenting the artisanal finfish fisheries catch and effort, either through direct observation (Doukakis *et al.*, 2008; Davies *et al.*, 2009; Brenier *et al.*, 2011) or fishermen interviews (Barnes-Mauthe *et al.*, 2013), with study sites located in the southwest (Davies *et al.*, 2009; Brenier *et al.*, 2011; Barnes-Mauthe *et al.*, 2013) and in the north of the country (Doukakis *et al.*, 2008). One of the published studies from southwest Madagascar (Davies *et al.*, 2009) was conducted in the Bay of Ranobe, which is the location of the present study.

In the present study, a two-year continuous time-series of fisheries landings sampled throughout the Bay of Ranobe, representing to the author's knowledge, the longest fisheries time-series collected in Madagascar, is used to:

1. provide the first representative characterization of the landings of the Bay by weight at various levels of taxonomic classification;

2. create species profiles for the 10 most abundant species in the landings, including landings, standardized CPUE indices, and various length-based indices;
3. determine an economic valuation of landings per annum and per fishermen.

4.2 Methodology

Study Site

The Bay of Ranobe (23°05'S, 43°33'E) is a coastal lagoon situated along the southwestern coast of Madagascar, approximately 20 km northwest of the provincial capital city, Toliara. The Bay of Ranobe (BoR) region may be geographically defined by the Manombo River and Fiherenana River that form the northern and southern borders, respectively. The lagoon system extends *ca.* 32 km along its southeast-northwest axis, measures *ca.* 8 km at the widest point, covering *ca.* 163 km² with maximum depths approaching 12 m within the lagoon. The lagoon experiences a semi-diurnal tidal regime with a spring tidal range of ± 2.3 m. The system is characterized by an inner reef flat composed of: patch reefs, sand, seagrass, macroalgae, and mangrove habitats, with a barrier reef forming the seaward boundary. The 32 km section of barrier reef that delimits the lagoon from the Mozambique Channel forms part of the greater Toliara Barrier Reef complex. Two passes naturally divide the lagoon into three zones (see Chapter 1 for further description of the environment).

The greater Bay of Ranobe community, as defined in the present study, is composed of the 21 villages bounded by the escarpment of the Mahafaly Plateau in the east, the coastline to the west, and the Manombo River and Fiherenana River to the north and south, respectively. Of the 21 villages within the greater Bay of Ranobe community, there are 12 Vezo villages located

along the coast. The 12 Vezo villages, representing the Vezo fishing community of the Bay of Ranobe, are the subject of the research presented here, and include, from south to north (see Chapter 2 for further discussion):

- | | |
|-------------------|-------------------|
| 1. Ambotsibotsike | 7. Amboaboaka |
| 2. Tsongeritelo | 8. Madiorano |
| 3. Beravy | 9. Betsibaroka |
| 4. Ambalaboy | 10. Ambolomailaka |
| 5. Ifaty | 11. Andrevo |
| 6. Mangily | 12. Fitsitke. |

Lifestyles of the inhabitants of the 12 villages of the Bay of Ranobe are quite similar in that they are inextricably linked to the sea and marine resources. However, some differences do exist between the villages, relative to fishing activities, that are likely attributable to the location of the village along the shore of the Bay and access to fishing grounds. Villages located near the mangroves in the north and south of the Bay tend to fish with seine nets to capture smaller fish and invertebrates, such as juvenile fish, mangrove crabs, and shrimp. Moving along the coast from the northern and southern extremes, the villages closest to the two principle passes in the barrier reef tend to fish the passes, without venturing too far outside the pass to fish deeper waters. Villages located more centrally along the coast have the farthest to travel to the barrier reef, thus tend to fish the patch reefs of the lagoon, but will travel to the backreef slope of the barrier reef. Although these tendencies are gross generalizations, and in reality, fishermen travel widely with ranges overlapping substantially, accessibility to fishing grounds affects the size of

fish and species caught, which in turn, has ecological and economic repercussions (see Chapter 3 for further discussion).

Fisheries landing surveys

Fisheries landing surveys were conducted from 3 April 2013 – 18 December 2015 in the villages of Andrevo, Ambolomailaka, Ifaty, and Beravy. From the landings dataset, 2 full years of data were selected for the analyses presented below, where year-1 is defined by the period of 1 July 2013 – 30 June 2014 and year-2 as the period of 1 July 2014 – 30 June 2015. Selection of villages participating in the fisheries study were based on three criteria: 1) villages with the largest pirogue-based fisheries, as identified from the 2013 Annual Pirogue Count dataset, 2) adequate geographic representativity to characterize the fisheries of the entire lagoon system, and 3) accessibility of the villages to the fisheries survey team. Surveys were conducted on a monthly basis, with 5 days of fisheries data collection per village per month, totaling 20 days of surveys per month throughout the study period. Scheduling of monthly surveys were based on lunar cycles, ensuring surveys were conducted over full moon and new moon phases, with villages alternating monthly. For example, in April 2014, Beravy was surveyed for 5 days centered on the date of the full moon and Ambolomailaka for 5 days of the new moon, while the other villages were surveyed in the intervening weeks. In the following month, Andrevo and Ifaty were surveyed during the full moon and new moon, respectively, while Ambolomailaka and Beravy were surveyed during intervening weeks. Alternating village and lunar phases ensured balanced sampling relative to lunar phases and tidal stages, and constituted the first-stage sampling frame of the fisheries survey design. (See Appendix 3.1 for extract of survey schedule)

From a spatial perspective, villages often have a focal point, where the frequency of landings and density of beached pirogues are greatest. The landing zone, as designated for the present study, extended out from the focal point of landings in both directions along the shore far enough to include >90% of pirogues owned by the fishermen of the targeted villages. Another important point worth noting, in a village setting such as this, fishermen and their landing sites are not randomly distributed along the coast (pers. obs.). Often, the more senior members of the village, and their family groups, occupy the more favorable areas of the beach, *e.g.* more sheltered, easier access to markets, etc., which are usually at, or near, the focal point of landing sites for the village. Implications of the structured organization of landing sites extends beyond simple family affiliations, given that the more senior families of fishermen may be more experienced / skilled fishermen, and potentially, favor specific fishing gears. Moving further-and-further out from the focal point of landings, families that have arrived more recently to the village, and likely have less fishing experience, find a place along the shore to land their pirogue. Consequently, a gradient exists of fishing gears and experience that radiates out from the focal point to the margins of the village, where less experienced fishermen have established themselves. In this region, the less experienced fishermen are known to use gears that require less skill and that are less discriminating, such as beach seines and mosquito nets. In order to obtain an unbiased and representative sample across the spectrum of gear-use and skill-level, village landing zones were divided into three sub-zones to ensure a balanced distribution of survey effort (Figure 4.1). Sub-zones represent a subsample of the primary sampling units, the four targeted villages, which are fully sampled on a monthly basis.

Following an access-point creel survey approach (Pollock, 1997) fishing effort and catch surveys were conducted within the designated villages and landing sub-zones, according to the

pre-determined monthly sampling schedule, following a sampling in space and time approach (Stamatopoulos, 2002). As daytime fishermen returned, which occurred over a relatively small window of time, the fisheries survey team initiated contact with fishermen as they landed in a haphazard manner. While one member of the survey team conducted the effort survey (see Chapter 3), the other members of the team characterized the catch. For the year-1 dataset, July 2013 – July 2014, the characterization of landings included the collection of species-specific weights and counts for the entire catch. In year-2, following the same sampling framework, data collection efforts were expanded to include the collection of species-specific fork length (cm) and individual weights (grams). Length measurements were collected with a standard metric measuring tape to the nearest centimeter, while weight measurements were collected using one of several precision, spring hand-scales (Pesola 1000 g x 10g, 2500 g x 20 g, and 20 kg x 200 g). To maintain good-will and continued participation in the fisheries survey, incentives were provided to fishermen in the form of coffee, snacks, and tobacco products to offset the inconvenience of the data collection process, and to compensate for any delays that may have been caused in getting their products to the market.

In the initial months of the catch surveys, April – July 2013, a data collection sheet was used by surveyors that provided a list of 133 species of finfish and targeted invertebrates (Appendix 4.1). Space provided on the datasheet allowed for the addition of species not included. After several months, the data were compiled, with additional species that occurred frequently in the catch being added to the list of targeted species. This initial 3-month period of the survey is considered a “training period”. Data collected during the training period were not included in the analyses presented in the present chapter.

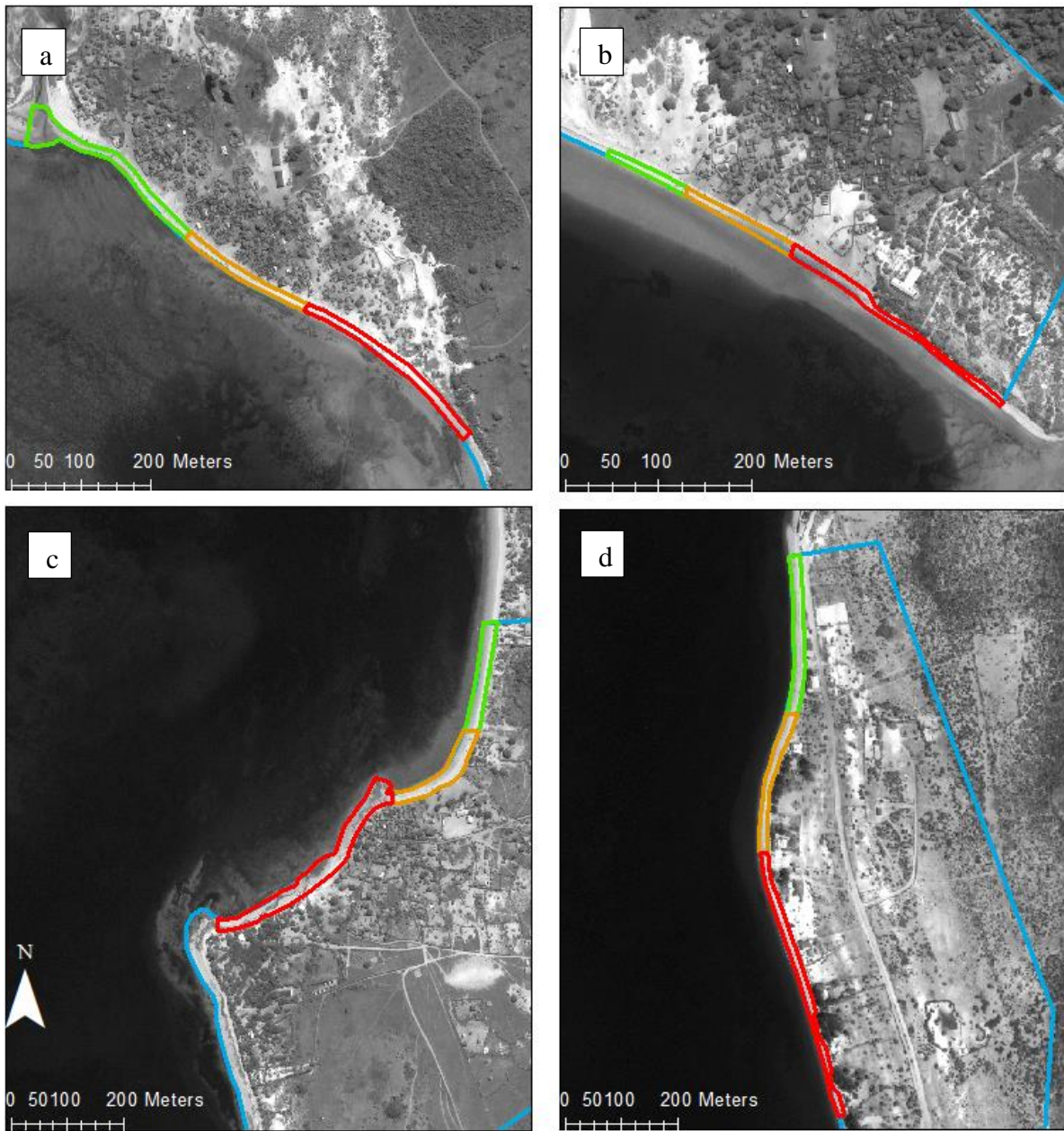


Figure 4.1. Village landing zones (LZ) divided into sub-zones (green, orange, and red) for surveying purposes: a) Andrevo (LZ = 785m), b) Ambolomailaka (LZ= 500m), c) Ifaty (LZ= 620m), and d) Beravy (LZ= 1025m)

4.3 Results

Results of the Bay of the Ranobe angler-intercept surveys, including summaries and analyses of landings, catch-per-unit-effort (CPUE), and an economic evaluation of landings, are presented in the sub-sections below for selected gear types, *e.g.* boat seine, gillnet, harpoon, hook-and-line, and spear gun (Figure 4.2a-f). Data used in the present analyses were collected during the course of 453 survey-days over the period of July 2013 - July 2015, with 228 days sampled in year-1 and 225 days in year-2, representing 62.0% coverage of the calendar days. Unique identifiers assigned to individual surveyed catches per daytrip indicate a survey coverage totaling 9,735 trips, with 4,880 and 4,855 trips surveyed in year-1 and year-2, respectively, averaging 21.5 landing surveys per survey-day.

Total landings

Over the course of the 2-year survey period, data collected for all gear types totaled 38,529 kg of fisheries products, with 20,685 kg in year-1 and 17,844 in year-2 (\bar{x} = 19,264 kg/year). Total landings were classified into 8 basic groups, accounting for 100% of the landings: finfish (69.5%), sea cucumbers (11.4%), unknown mix of juvenile / larval species usually associated with seine netting activities (10.2%), octopus (7.4%), squid (3.5%), morays (2.1%), rays (1.6%), and miscellaneous species (1.0%) (Table 4.1). Miscellaneous species include: lobster, cuttlefish, seahorses, crabs, and turtles. A time-series plot illustrating changes in landings for the top four groups, comprising 91.9% of the landed biomass, is presented in figure 4.3. Remaining analyses presented in the subsections, below, are focused on the finfish species component of the landings.



Figure 4.2. Commonly-used fishing gears by the Vezo of the Bay of Ranobe: gillnets (a-b), harpoons (c), spearguns (d), small mesh nets / mosquito netting used in boat seining (e-f)

Table 4.1. Landings by fisheries categories by total weight and percent

Group	Total Wt (kg)		Percent		Avg. %
	Year-1	Year-2	Year-1	Year-2	
Finfish	14,369	10,057	69.5	56.3	62.9
Sea cucumber	2,320	2,811	11.2	11.6	11.4
Unknown	957	1,413	4.6	15.7	10.2
Octopus	1,438	2,075	6.9	7.9	7.4
Squid	682	661	3.3	3.7	3.5
Moray	463	339	2.2	1.9	2.1
Ray	265	346	1.3	1.9	1.6
Miscellaneous	191	142	1.0	1.0	1.0
<i>Total</i>	<i>20,685</i>	<i>17,844</i>			<i>100.0</i>

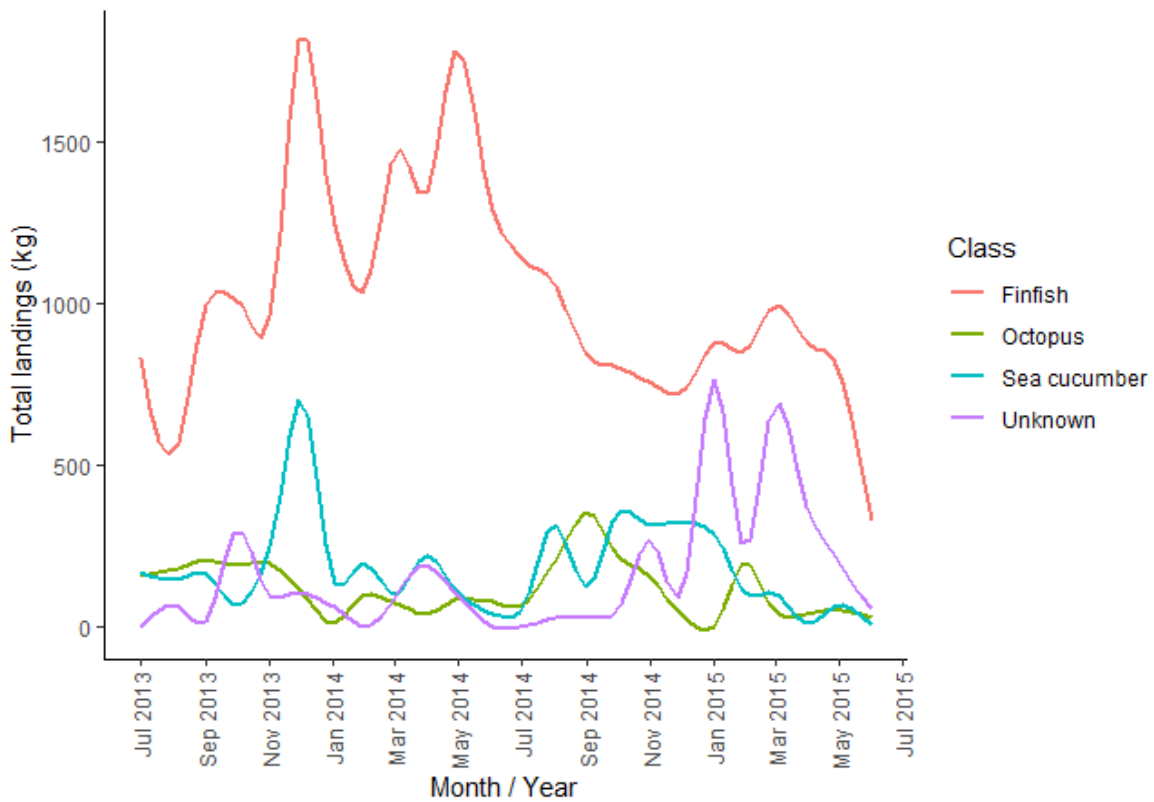


Figure 4.3. Landings time-series for the 4 most abundant fisheries groups: finfish, octopus, sea cucumber, and unknown, representing 91.9% of landings by weight

Landings by finfish species

In addition to quantities of fish landed, the species composition of landings serve as an important ecological indicator for fisheries management (Nash and Graham, 2016). Finfish surveyed during the course of the present 2-year study were comprised of 248 identified species (see Appendix 4.2 for complete species list), representing 61 families and totaling 24,426 kg. Relative abundance, as a percentage of the total landed weight, was calculated at the family and species levels. At the family level, the 5 families representing the greatest percentage of the biomass of surveyed landings include, in descending order: Scaridae (10.8%), Clupeidae (9.6%), Siganidae (8.8%), Lethrinidae (6.9%), and Acanthuridae (6.10%) (Figure 4.4a). At the species level, the 5 identified species representing the greatest percentage of the biomass, include: *Siganus sutor* (13.01%), *Herklotsichthys quadrimaculatus* (10.0%), *Plotosus lineatus* (8.1%), *Leptoscarus vaigiensis* (7.6%), and *Lethrinus harak* (5.6%) (Figure 4.4b).

Although biomass-based relative abundance of species is an important consideration in the characterization of a multi-species coral reef fishery, in order to assess the potential impacts of fisheries on reef fish communities and/or coral reef ecosystems, other metrics of abundance may also be instructive. Frequency may be considered a measure of “abundance in time” that better captures, or characterizes, a coral reef fishery in which high biodiversity and low species richness are the normal state. Daily occurrence, or the frequency of sampled days in which a species occurred in the catch, were calculated and ranked. Results indicated that the 5 most frequently occurring species landed include: *Siganus sutor* (89.5%), *Leptoscarus vaigiensis* (79.7%), *Lethrinus harak* (78.0%), *Cheilinus trilobatus* (74.7%), and *Scarus ghobban* (70.6%) (Figure 4.5).

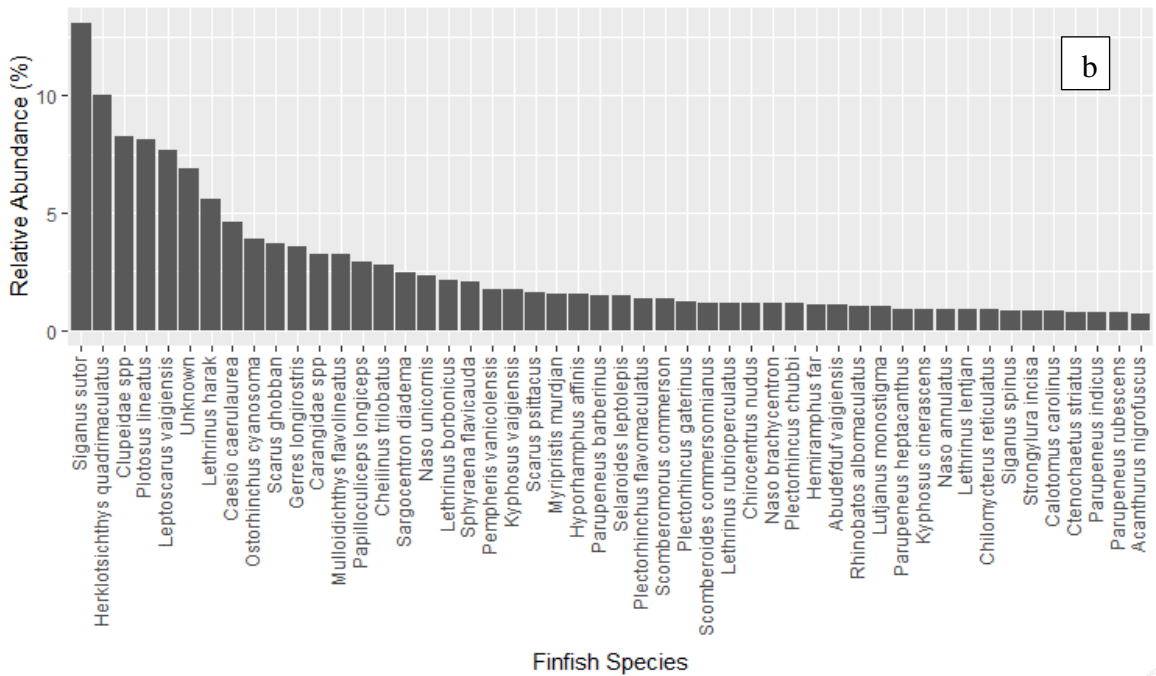
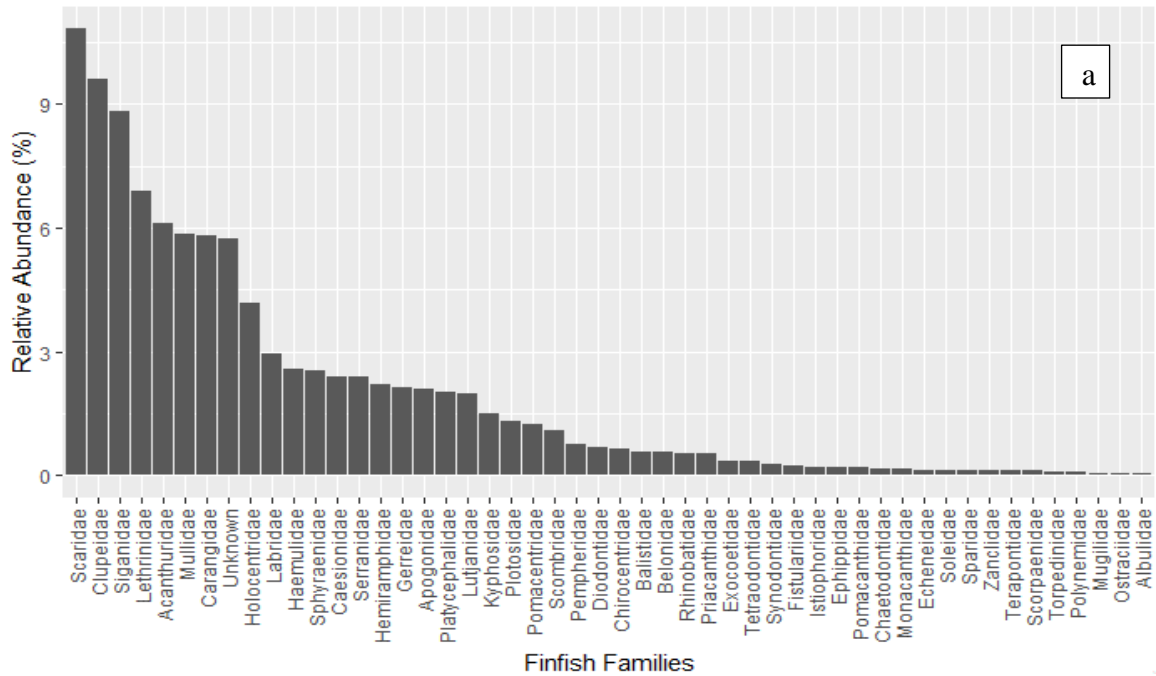


Figure 4.4. Relative abundance as a percentage of total surveyed finfish landings (24,426 kg) of the 50 most abundant groups ranked in descending order by a) family and b) species

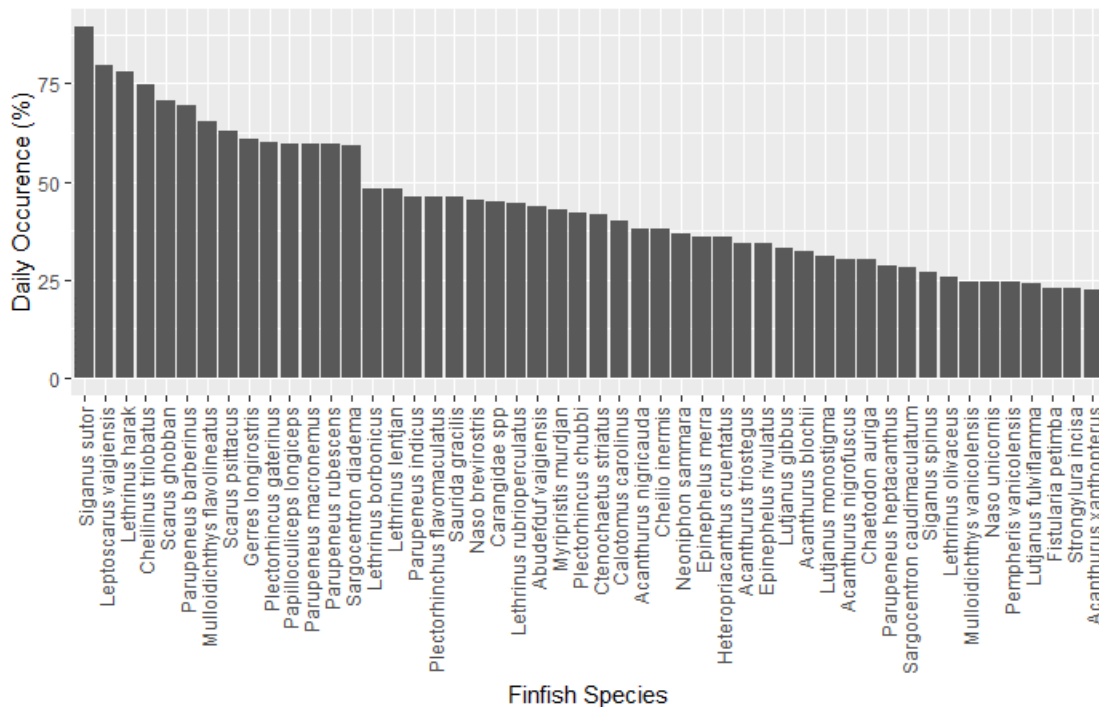


Figure 4.5. Frequency of occurrence in daily landings: 50 most frequently occurring species in landing 296 sampling days

Dominant species in the landings, with respect to village, vary ostensibly as a result of village-specific gear compositions and local environments (Figure 4.6). Total landed weights of finfish surveyed by village equaled, in descending order: 8,161 kg (Ambolomailaka), 6,217 kg (Andrevo), 5,237 kg (Ifaty), and 4,811 kg (Beravy). Again, a comparison was conducted to highlight the differences in the landings between the northern villages (Andrevo and Ambolomailaka) and the southern villages (Ifaty and Beravy). Of the 20 most abundant species from each group, 10 species / groups were commonly present amongst the ranked groups (Figure 4.7):

1. *Siganus sutor*
2. *Leptoscarus vaigiensis*
3. *Herklotsichthys quadrimaculatus*
4. *Lethrinus harak*
5. *Clupeidae spp*
6. *Caesio caeruleaurea*
7. *Carangidae spp*
8. *Gerres longirostris*
9. *Sargocentron diadema*
10. *Papilloculiceps longiceps*.

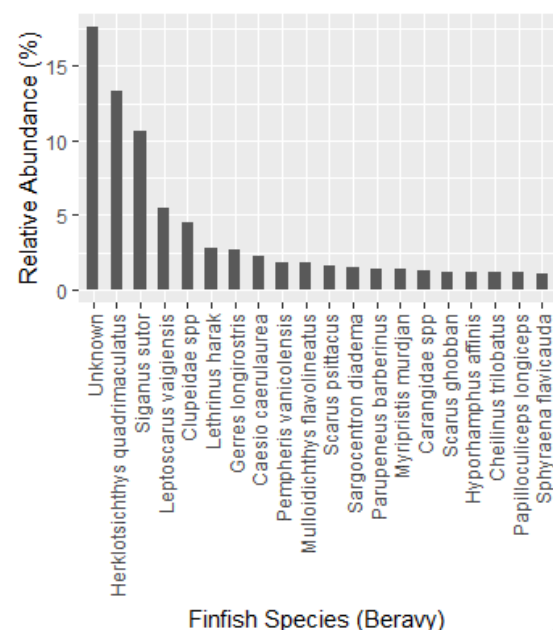
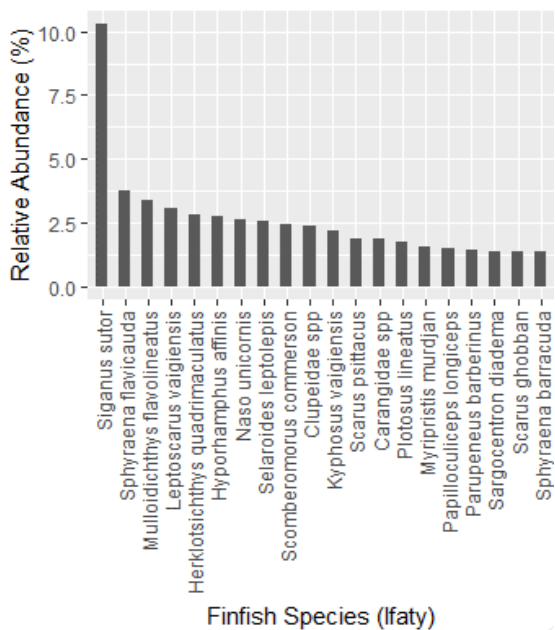
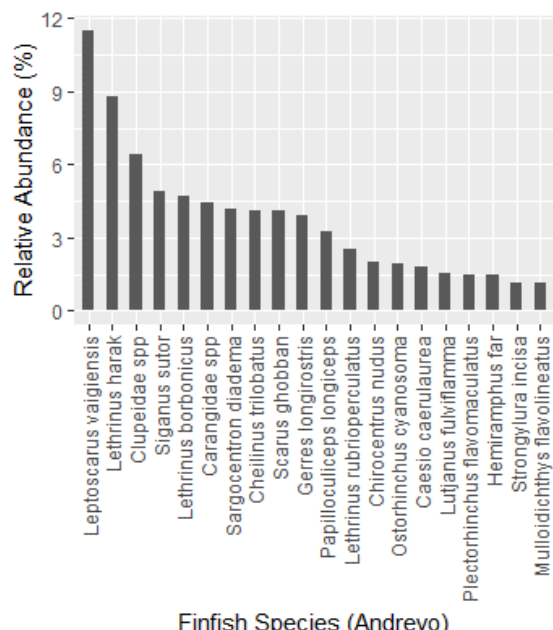
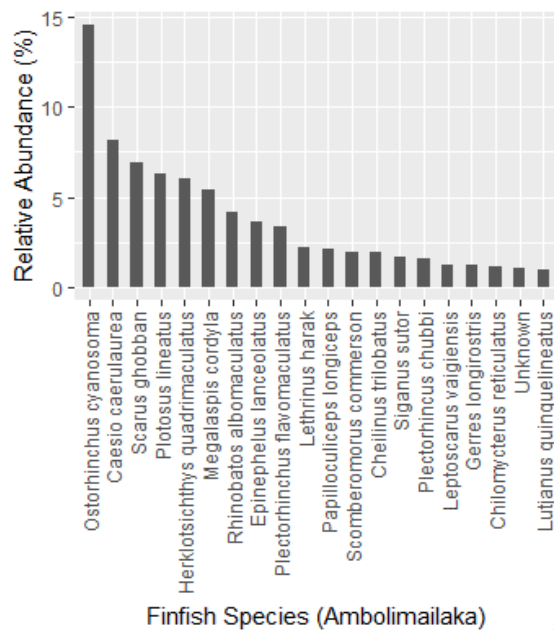


Figure 4.6. Relative abundance of species in landings w.r.t. village, with percentages calculated as a function of total landings per village: Ambolomailaka (8,161 kg), Andrevo (6,217 kg), Ifaty (5,237 kg), and Beravy (4,811 kg)

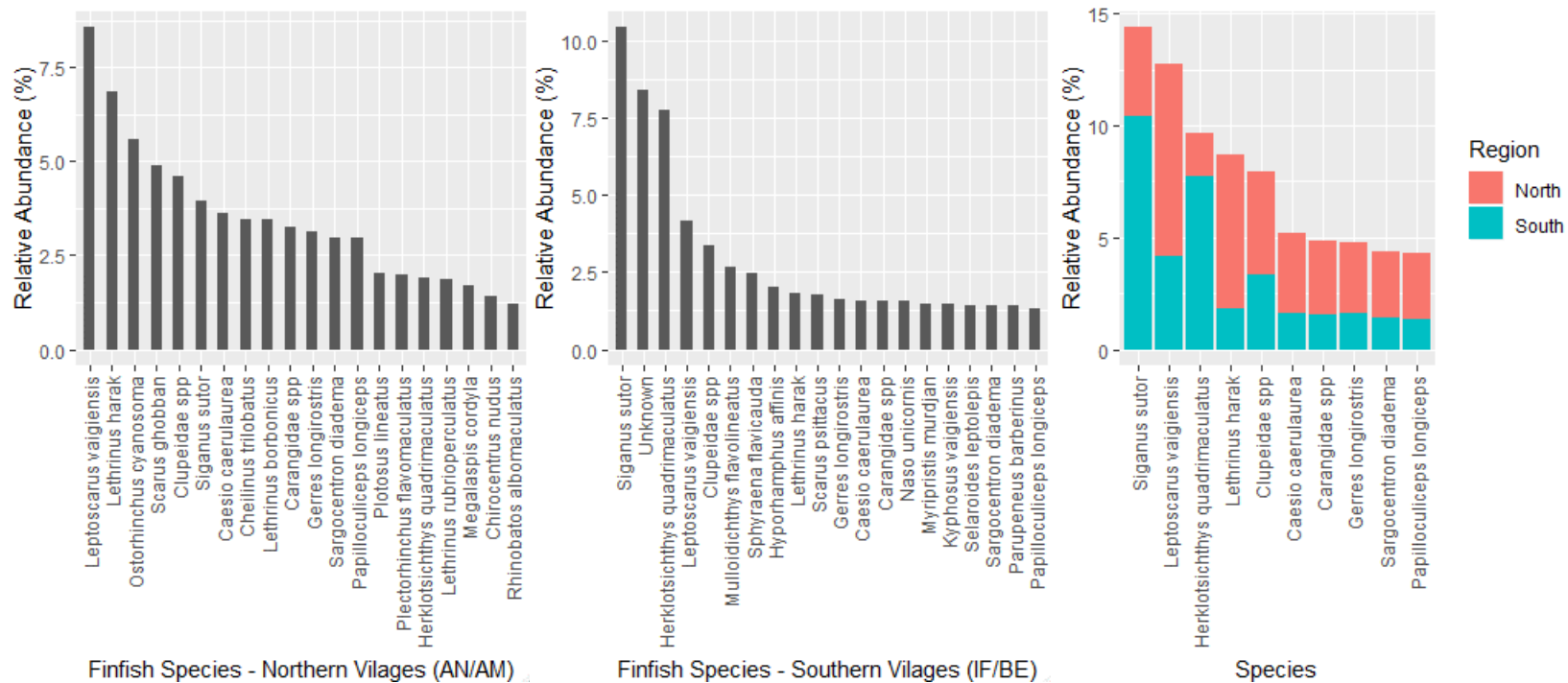


Figure 4.7. Relative abundance as a percentage of total surveyed finfish landings (24,426 kg) of the 20 most abundant groups ranked in descending order by (a) northern and (b) southern villages; (c) of the 20 most abundant species in northern/southern, the relative abundance of the 10 species with overlapping distributions

Nominal CPUE - Finfish

A daily nominal CPUE (nCPUE) for finfish, kilograms per trip, was calculated by summing finfish landings (kg) per day, irrespective of gear, and dividing by the total number of surveyed trips for each survey-day, as follows:

$$nCPUE_{fish} (kg * trip^{-1}) = \frac{\sum (Landings | Finfish) day^{-1}}{(Total\ number\ of\ surveyed\ trips) day^{-1}}$$

For year-1 and year-2 of the survey, annual averages were calculated based on the daily nCPUE_{fish} values, \bar{x} = 3.06 kg/trip (sd= 2.23) and \bar{x} = 2.19 kg/trip (sd= 1.90), respectively, with an overall 2-year average of \bar{x} = 2.63 kg/trip (sd= 0.62 kg/trip). Daily nCPUE values were log-transformed to approximate normality and a Fisher's F-test was used to test for homoscedasticity of variance between year-1 and year-2 groups ($F_{(227,223)}=0.84$, $p= 0.19$). A comparison of annual means indicated nCPUE values significantly differed between years ($t= 5.58$, $df= 445.1$, $p<0.001$). On a monthly basis, nCPUE_{fish} varied from 2.06 kg/trip to 3.14 kg/trip (Figure 4.8).

A comparison of the average nCPUE with respect to surveyed villages demonstrates the differences that exist in the quantities of finfish landed, from north to south: Andrevo (\bar{x} = 2.13 kg/trip, $sd= 1.19$), Ambolomailaka (\bar{x} = 3.51 kg/trip, $sd= 2.77$), Ifaty (\bar{x} = 1.70 kg/trip, $sd= 1.12$), and Beravy (\bar{x} = 3.18 kg/trip, $sd= 2.32$) (Table 4.2). Differences in the village-based nCPUE averaged values may be attributable in part to the differences in fishing gear profiles (Chapter 3), local water depth, and environmental differences (Chapter 1). Differences detected in the formal comparison of northern versus southern villages ($t= 2.59$, $df= 443$, $p= 0.01$; Figure 4.9) may be less attributable to differences in fishing gear compositions, as village-specific data is aggregated, and the environmental factors presumably become more important, specifically

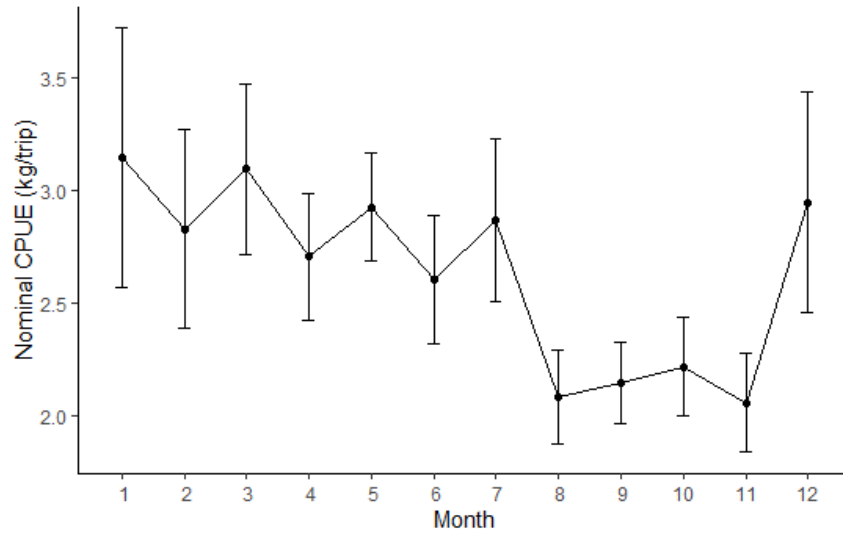


Figure 4.8. Monthly average nCPUE for finfish (\pm se)

Table 4.2. Average nCPUE by village and by region, northern versus southern villages

Village	Landings (kg/trip)	SD	Count (n)
Andrevo	2.13	1.19	114
Ambolomailaka	3.51	2.77	116
<i>Avg. Northern villages</i>	2.82*		
Ifaty	1.70	1.12	113
Beravy	3.18	2.32	109
<i>Avg. Southern villages</i>	2.44*		

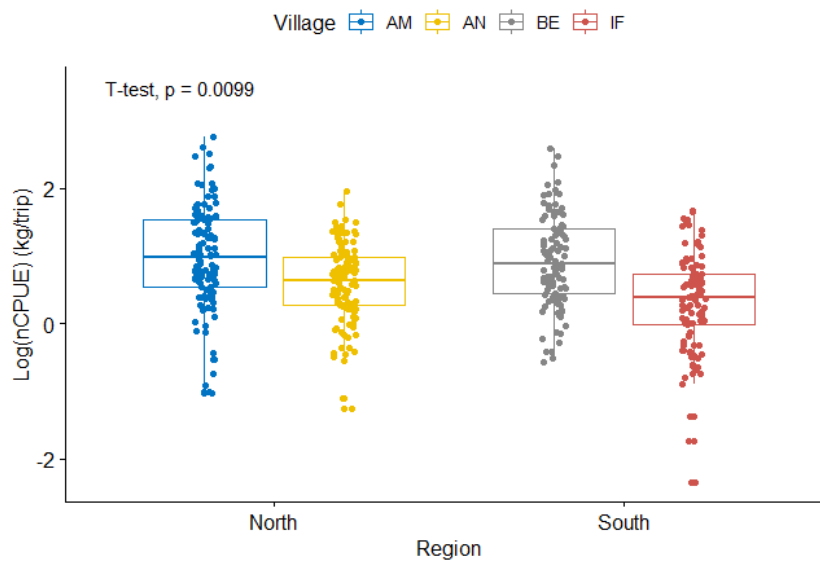


Figure 4.9. Comparison of log(nCPUE) values for villages of the north versus south

differences in extent of seagrass meadows and the width/depth of the northern versus southern reef passes.

Comparisons of nCPUE, with respect to gear types, were used to determine the gear-specific catch rates, with $nCPUE_{fish*gear}$ based on the following formula:

$$nCPUE_{fish*gear} (kg * trip_{gear}^{-1}) = \frac{\sum (Landings | Finfish | Gear) day^{-1}}{\sum (Surveyed trips | Gear) day^{-1}}$$

Average nCPUE values summarized by gear type indicate that the boat seining method produced the greatest quantities of fish (\bar{x} = 15.35 kg/trip, SD= 20.30), followed by: gillnet (\bar{x} = 4.34 kg/trip, SD = 3.70), spear gun (\bar{x} = 3.26, SD= 2.43), hook-and-line (\bar{x} = 2.76, SD= 2.57), and the harpoon (\bar{x} = 0.82 kg/trip, SD= 1.05) (Table 4.3). Significant differences were detected between gear types ($F_{(4, 1306)} = 223.9$, $p < 0.001$) of log-transformed nCPUE values using an ANOVA, with pairwise comparisons indicating differences between all gear types (Figure 4.10). A month-year time series of nCPUE per gear type illustrates variability inherent in the relative efficiencies of the principle gear types used in the Bay of Ranobe fisheries (Figure 4.11).

Table 4.3. Average nCPUE per gear type and percentage of surveys reporting gear-type

Gear type	nCPUE (kg/trip)	SD	% Usage
Boat seine	15.35	20.30	13.15
Gillnet	4.34	3.70	34.96
Spear gun	3.26	2.43	22.94
Hook-line	2.76	2.57	15.22
Harpoon	0.82	1.05	9.81

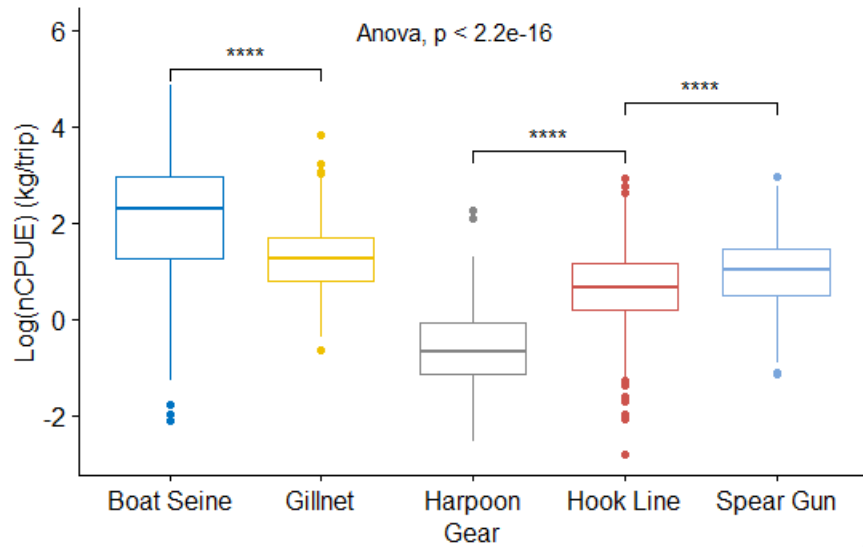


Figure 4.10. Pair-wise comparisons of log(nCPUE) between gear types; significant differences indicated by global ANOVA ($p < 0.001$) and between gear-type groups

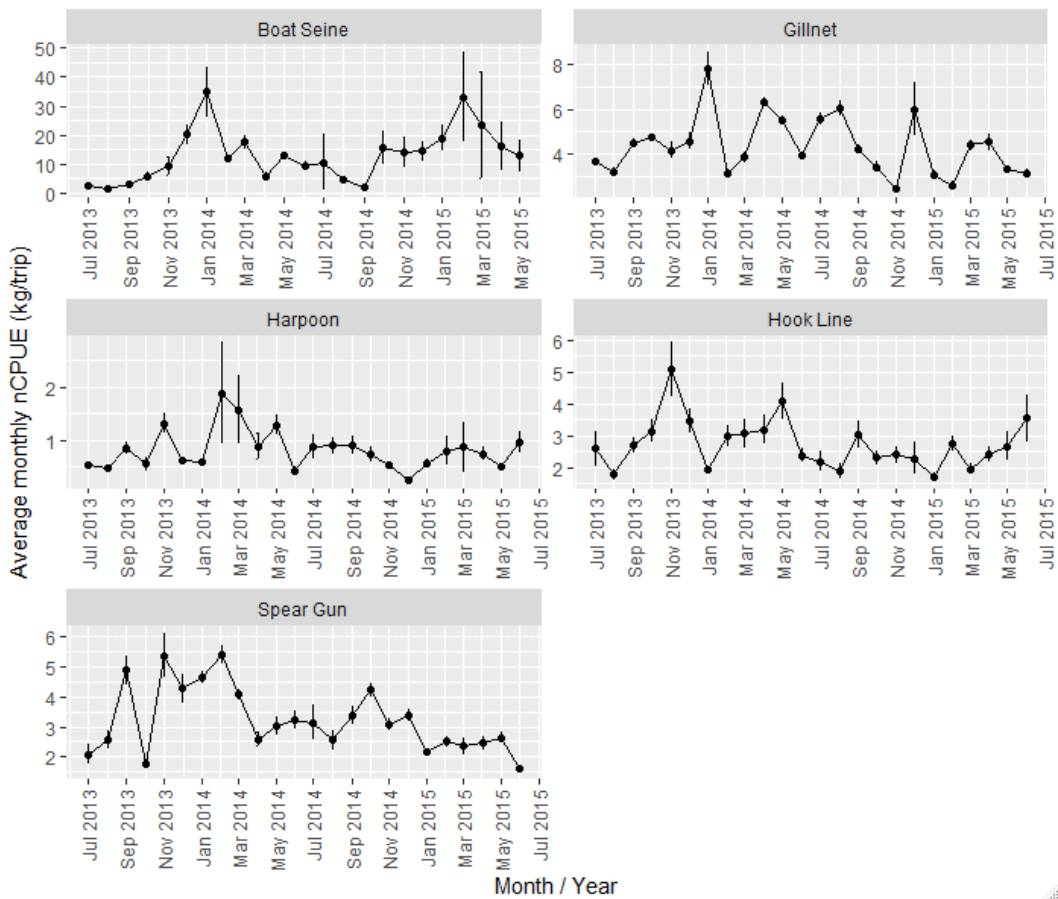


Figure 4.11. Average monthly nCPUE by gear type

Species profiles

Profiles were created for each of the 10 most abundant species / family groups identified in the landings, according to total weight (kg), as depicted in figure 4.4, including, in descending order:

1. *Siganus sutor*
2. *Herklotsichthys quadrimaculatus*
3. Clupeidae spp
4. *Plotosus lineatus*
5. *Leptoscarus vaigiensis*
6. *Lethrinus harak*
7. *Caesio caeruleaurea*
8. *Ostorhinchus cyanosoma*
9. *Scarus ghobban*
10. *Gerres longirostris*.

Each species profile is comprised of multiple plots: a) an image, b) landings per month, c) standardized CPUE year indices, d) length-frequency histogram, e) changes in length over month-year, and f) length per gear type. Standardization of CPUE was achieved using the generalized linear modelling (GLM) approach, where a Gaussian GLM was fitted to log-transformed CPUE data for each of the 10 species listed, above. The catch-rate response variable was calculated from catch (kg/trip) associated with gillnet gear usage, normalized by time spent fishing per trip, Δt . Predictor variables for each of the species-specific models included sample-year, month, and gillnet length, width, and mesh size, as follows:

$$\frac{(Catch_{species|gillnet})}{\Delta t} = sample.yr + month + g.length + g.width + g.mesh.$$

Results of the GLMs are presented in Table 4.3 and model coefficients are plotted in Figures 4.12 - 4.13 for ease of comparison, with standardized year-effect plots included in the species profiles (Figures 4.14 – 4.23). Term plots for the full model, and model diagnostic plots may be found in Appendices 4.4 - 4.14 and 4.15 - 4.25, respectively.

Table 4.4. GLM results for the standardization of log(CPUE) for the 10 most abundant species

	<i>Dependent variable:</i>									
	Log (CPUE)									
	<i>S.sutor</i>	<i>H.quad</i>	<i>Clupeid</i>	<i>P.line</i>	<i>L.vaig</i>	<i>L.harak</i>	<i>C.caer</i>	<i>O.cyan</i>	<i>S.gbob</i>	<i>G.long</i>
Year 2	-0.398*** (0.109)	-2.116*** (0.443)	-1.162*** (0.401)	1.510 (0.893)	-0.299*** (0.096)	-0.616*** (0.102)	-0.062 (0.209)	-2.254*** (0.502)	-0.026 (0.115)	-0.438*** (0.152)
Month 2	0.699** (0.311)				0.070 (0.247)	-0.162 (0.291)			0.094 (0.270)	0.040 (0.398)
Month 3	0.234 (0.257)		1.549* (0.813)		0.713*** (0.194)	-1.061*** (0.224)			-0.426* (0.221)	-0.347 (0.319)
Month 4	0.544** (0.236)	-2.034*** (0.738)	-0.029 (0.652)	-0.744 (1.621)	0.806*** (0.179)	-0.946*** (0.220)	-4.585*** (0.798)		-0.405* (0.214)	0.410 (0.298)
Month 5	0.612*** (0.232)	-2.780*** (0.717)	-0.154 (0.616)	2.413 (1.404)	0.271 (0.177)	-1.518*** (0.205)	-3.627*** (0.760)		-0.335 (0.223)	-0.121 (0.297)
Month 6	0.791*** (0.264)	-3.632*** (0.933)	-1.545** (0.643)	-1.924 (1.305)	-0.210 (0.221)	-1.639*** (0.241)	-4.171*** (0.749)	-1.570* (0.780)	-0.508* (0.265)	0.068 (0.311)
Month 7	0.556** (0.242)	-1.941** (0.822)	-1.961** (0.886)	-2.446* (1.258)	-0.071 (0.203)	-1.487*** (0.202)	-4.190*** (0.757)	-1.393 (1.240)	-0.405* (0.221)	0.135 (0.308)
Month 8	0.667*** (0.256)	-2.962*** (0.776)			-0.366 (0.267)	-1.408*** (0.219)	-3.747*** (0.743)	0.767 (0.753)	-0.136 (0.235)	0.337 (0.319)
Month 9	0.349 (0.295)	-2.533 (1.862)	2.157*** (0.596)		-0.093 (0.269)	-1.201*** (0.221)	-3.358*** (0.794)		-0.580** (0.255)	0.064 (0.351)
Month 10	0.943*** (0.242)	-2.236** (0.986)	0.632 (0.671)	-0.860 (1.335)	-0.207 (0.227)	-0.835*** (0.191)	-3.131*** (0.726)		-0.003 (0.212)	0.378 (0.282)
Month 11	0.838*** (0.276)		-0.146 (0.560)		0.035 (0.219)	-0.290 (0.199)	-3.417*** (0.756)		0.112 (0.223)	0.535* (0.319)
Month 12	0.733*** (0.279)		-1.078 (0.664)	1.074 (1.491)	-0.071 (0.241)	-0.428** (0.217)			-0.297 (0.241)	0.288 (0.301)

Table 4.4 cont. GLM results for the standardization of log(CPUE) for the 10 most abundant species

Gear length	-0.001*** (0.0001)	0.002** (0.001)	-0.002*** (0.001)	0.001 (0.001)	0.0004*** (0.0001)	-0.0003*** (0.0001)	-0.001** (0.0003)	-0.002** (0.001)	-0.0002** (0.0001)	-0.0001 (0.0001)
Gear width	0.168** (0.074)	-1.179 (0.757)	0.212 (0.170)	2.396 (1.407)	-0.276 (0.231)	0.432* (0.247)	0.169 (0.147)	4.635*** (0.876)	2.223 (1.846)	0.412 (0.351)
Gear mesh	0.375*** (0.043)	-0.014 (0.099)	-0.395* (0.199)	0.804* (0.419)	0.163** (0.066)	0.193*** (0.055)	-0.428*** (0.087)	-0.058 (0.223)	0.286*** (0.082)	0.208** (0.086)
Constant	1.895*** (0.406)	12.881*** (2.410)	6.917*** (1.054)	-6.163 (6.165)	4.155*** (0.844)	3.375*** (0.853)	9.176*** (0.879)	-9.227*** (2.784)	-3.743 (5.548)	1.904 (1.246)
Observations	667	85	61	22	588	595	144	26	396	376
Log Likelihood	-1,086.422	-155.958	-85.154	-27.010	-829.875	-835.348	-190.554	-31.348	-512.058	-612.189
Akaike Inf. Crit.	2,204.844	335.915	198.309	76.020	1,691.750	1,702.696	407.108	78.695	1,056.116	1,256.379

Note:

* p < 0.05
 ** p < 0.01
 *** p < 0.001

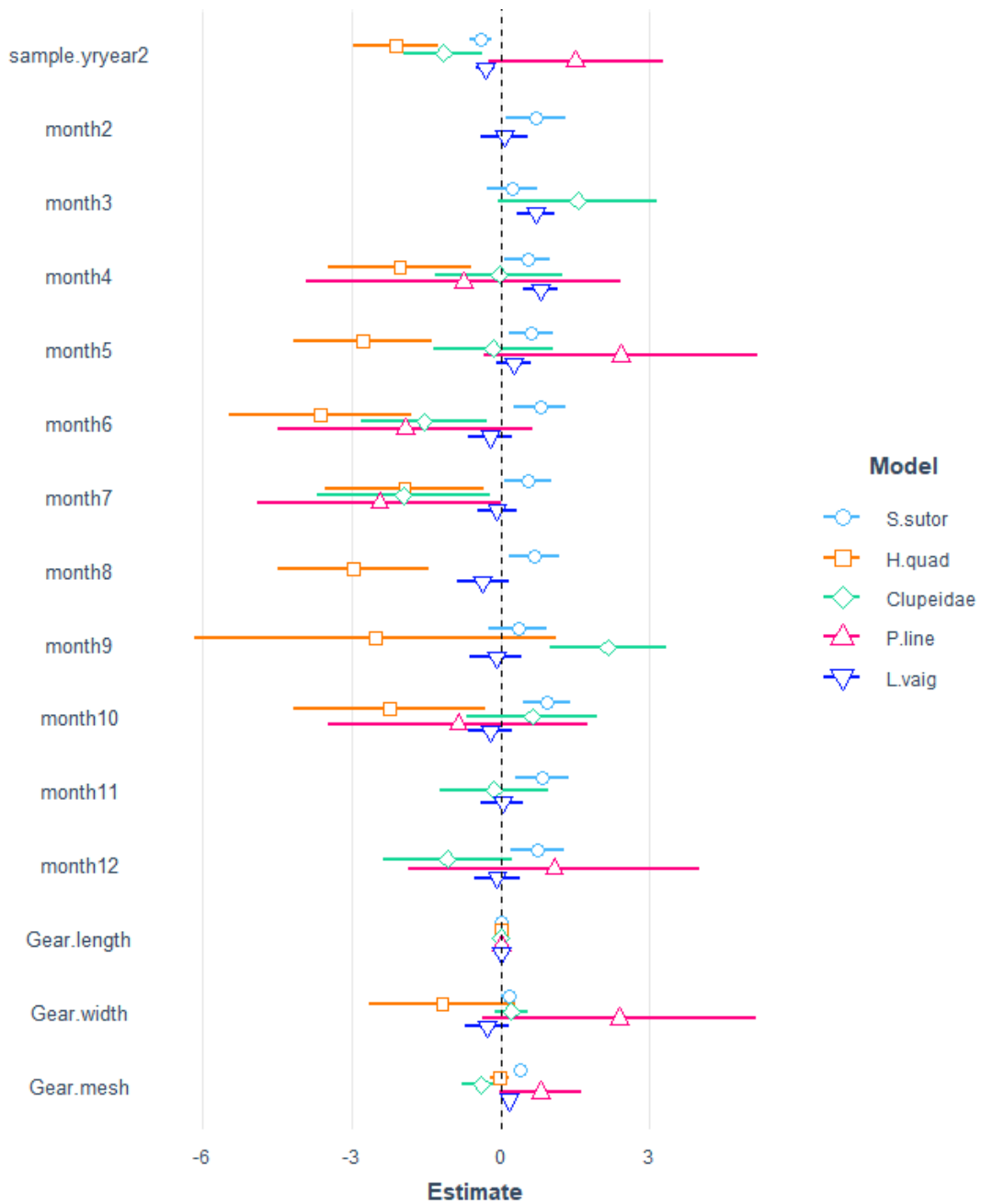


Figure 4.12. GLM regression coefficients from CPUE standardization models (Table 4.3) for species 1-5

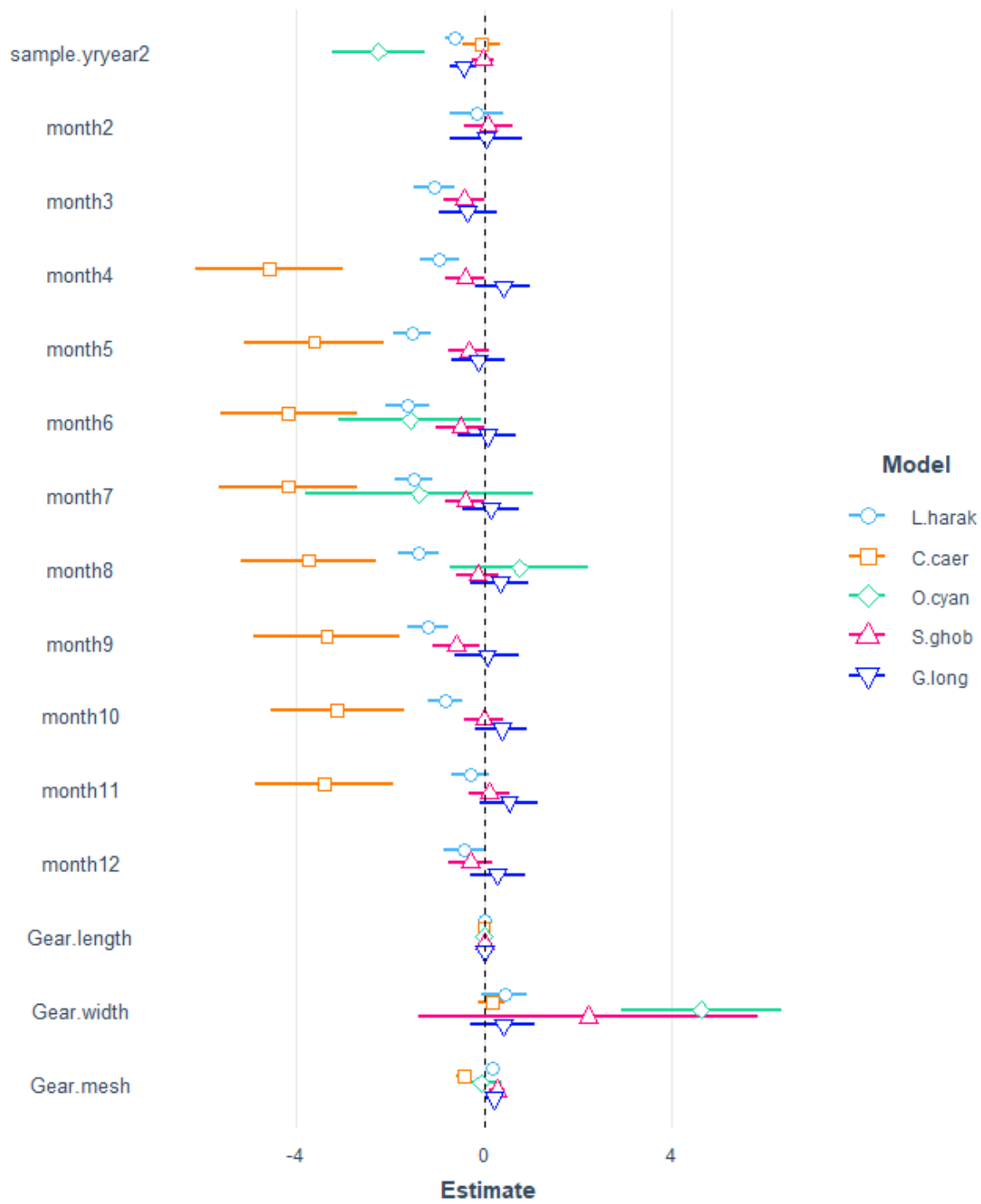


Figure 4.13. GLM regression coefficients from CPUE standardization models (Table 4.3) for species 6-10

Siganus sutor, Shoemaker spinefoot (a.k.a African white-spotted rabbitfish)

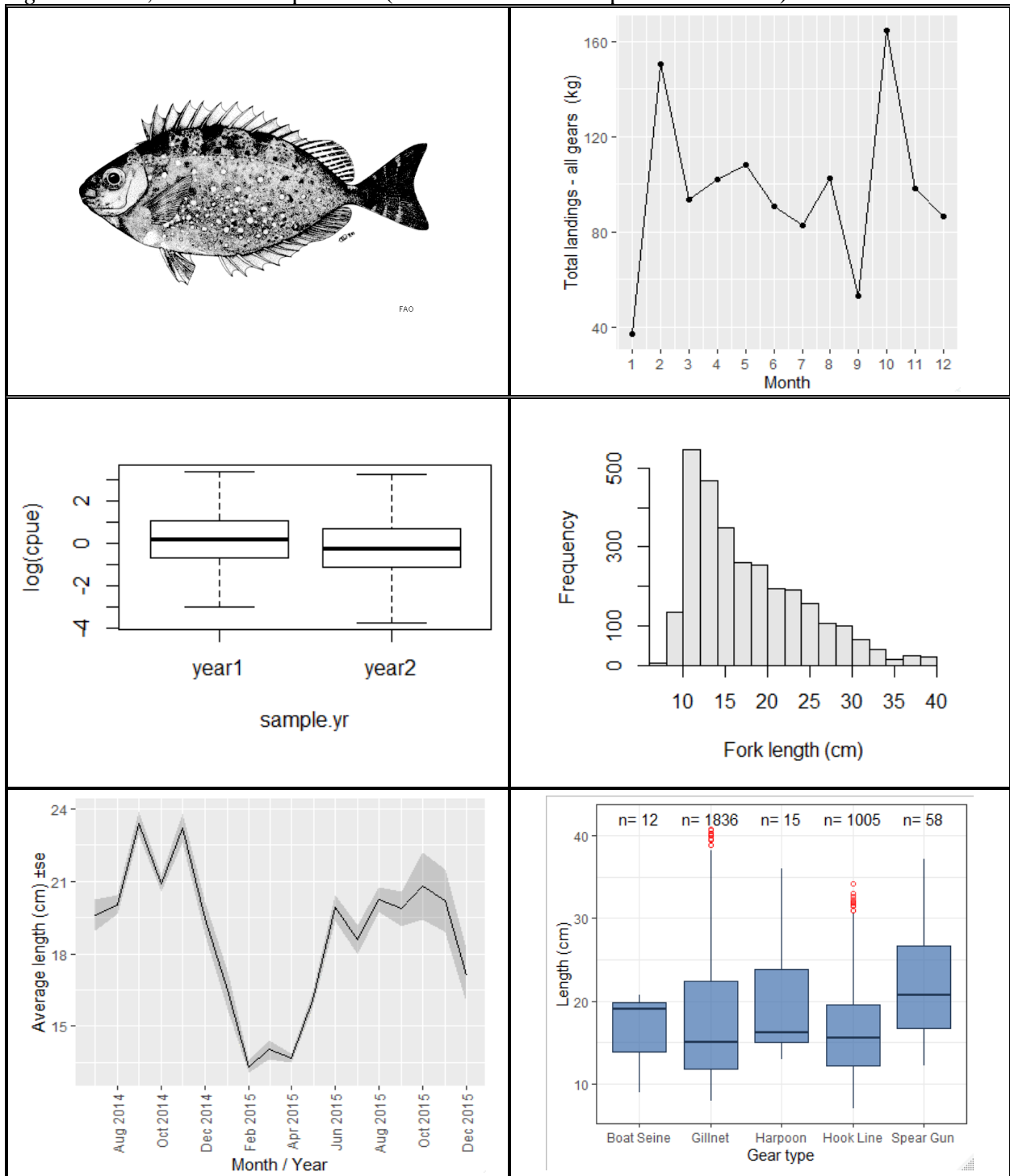


Figure 4.14. Species profile – *Siganus sutor*: image, total landings by month (top row), standardized CPUE year-index (gillnet), length frequency histogram (middle row), changes in average length over study period, and length by gear type (bottom row); length-at maturity, L_m = unknown, L_{max} = 45.0 cm SL (Froese and Pauly, 2019; FishBase)

Herklotsichthys quadrimaculatus, Bluestripe herring

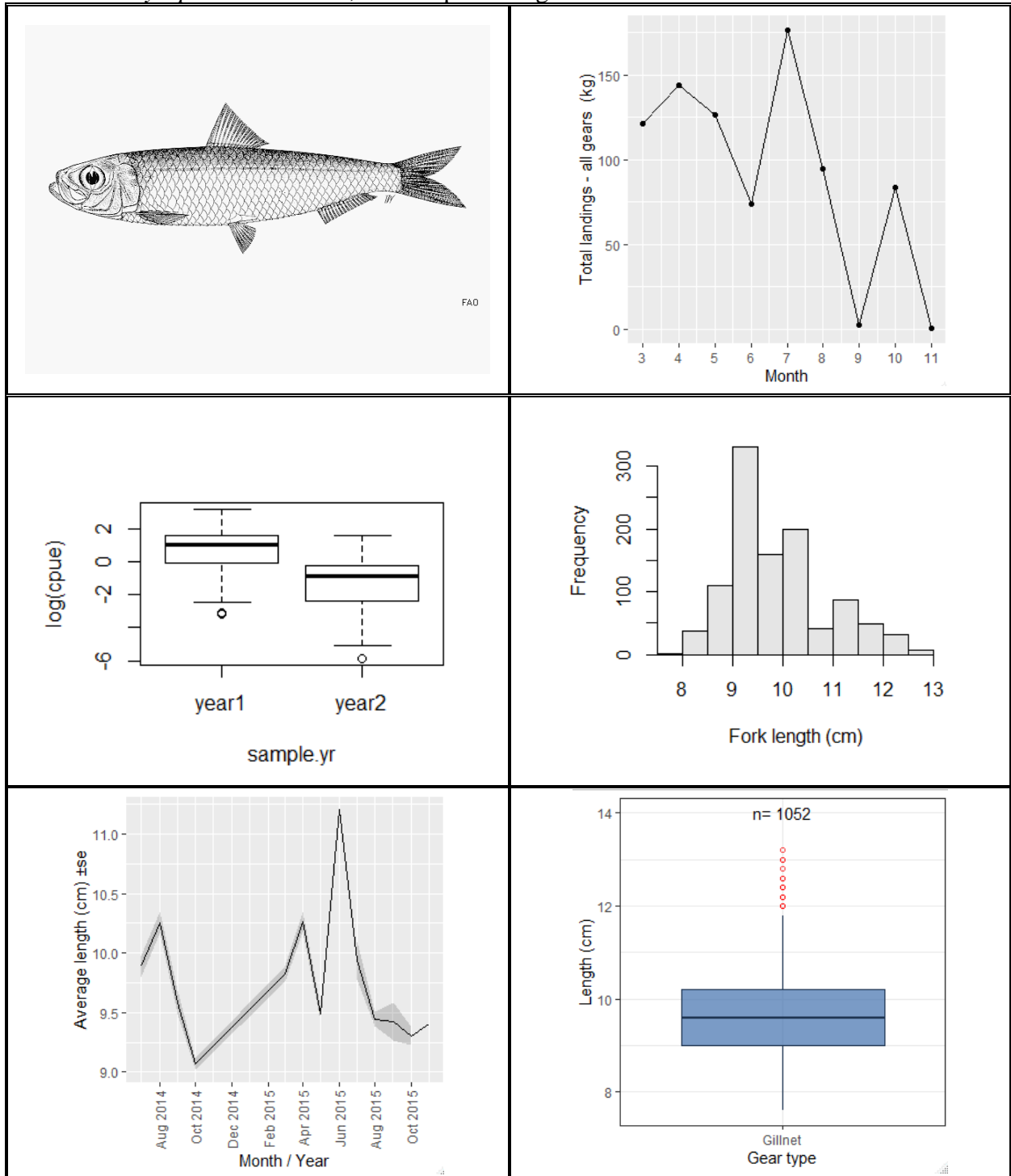


Figure 4.15. Species profile – *Herklotsichthys quadrimaculatus*: image, total landings by month (top row), standardized CPUE year-index (gillnet), length frequency histogram (middle row), changes in average length over study period, and length by gear type (bottom row); $L_m = 10.1$ cm, $L_{max} = 25.0$ cm SL (Froese and Pauly, 2019; FishBase)

Clupeidae spp

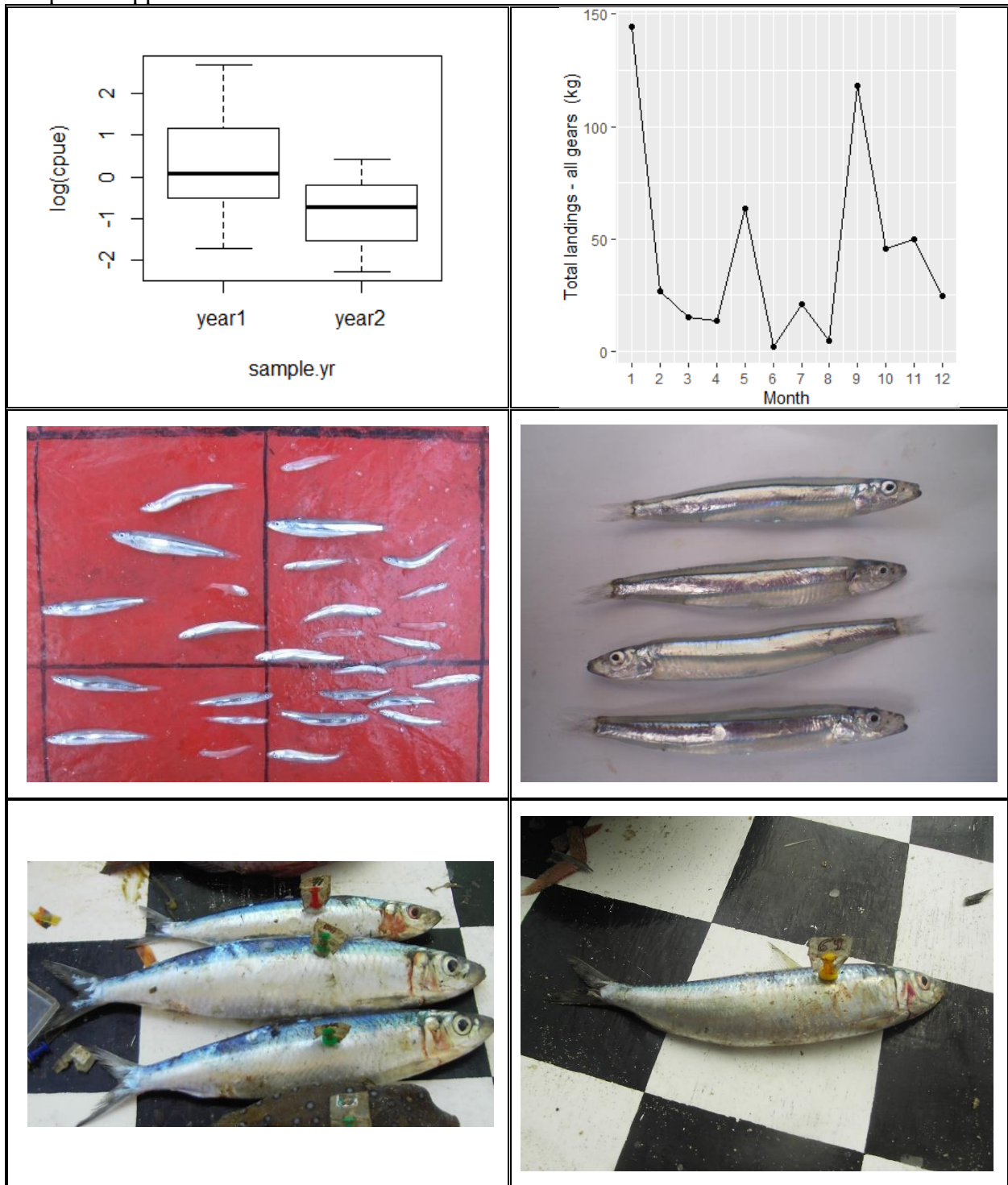


Figure 4.16. Clupeidae spp: Silver-stripe round herring, *Spratelloides gracilis* (middle row), and the Goldstripe sardinella, *Sardinella gibbosa* (bottom row); length-based analyses not performed due to insufficient data (grid squares = 10 cm)

Plotosus lineatus, Striped eel catfish

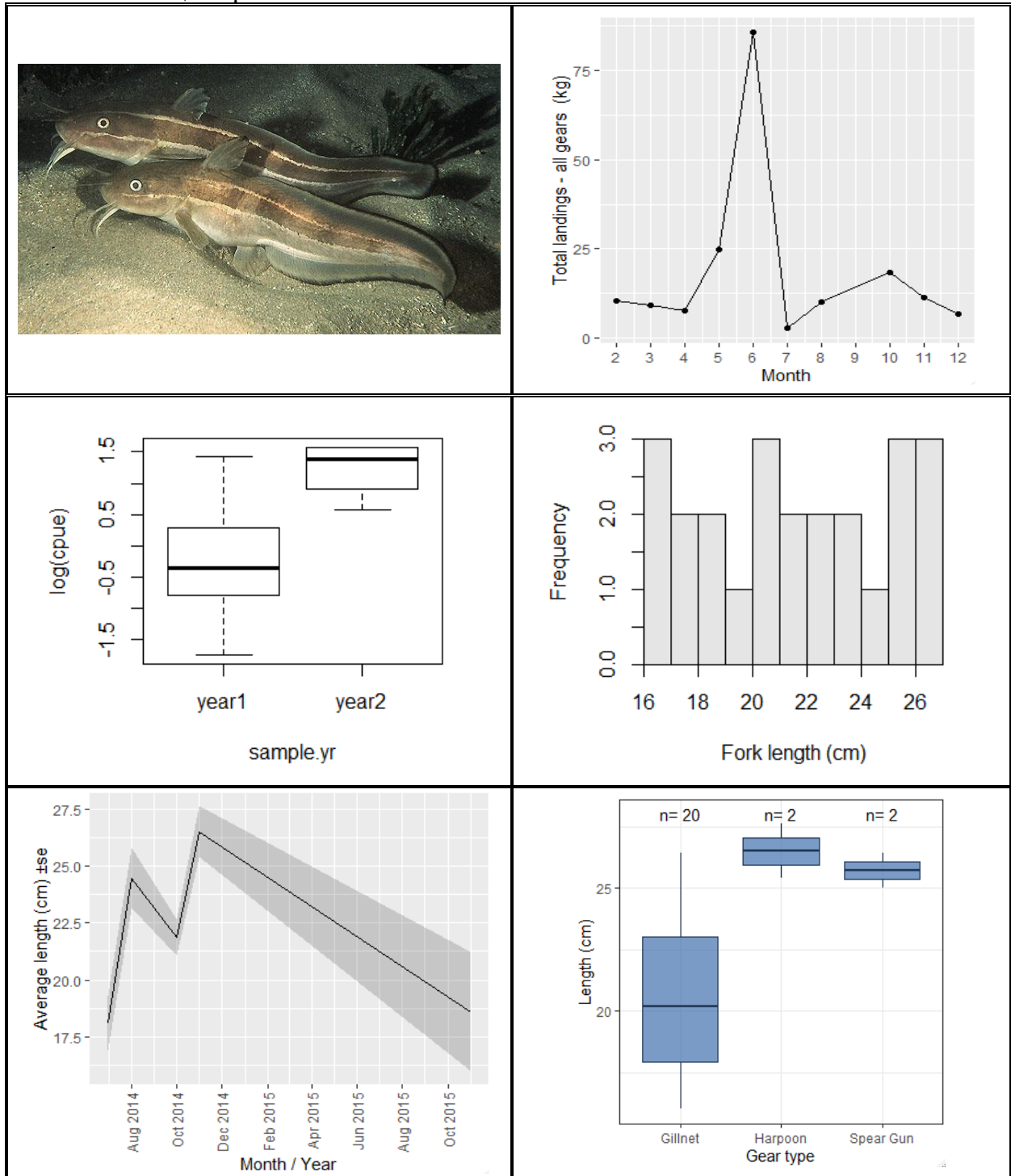


Figure 4.17. Species profile – *Plotosus lineatus*: image, total landings by month (top row), standardized CPUE year-index (gillnet), length frequency histogram (middle row), changes in average length over study period, and length by gear type (bottom row); $L_m = 14.0$ cm, $L_{max} = 32.0$ cm TL (Froese and Pauly, 2019; FishBase)

Leptoscarus vaigiensis, Marbled parrotfish (a.k.a. Seagrass parrotfish)

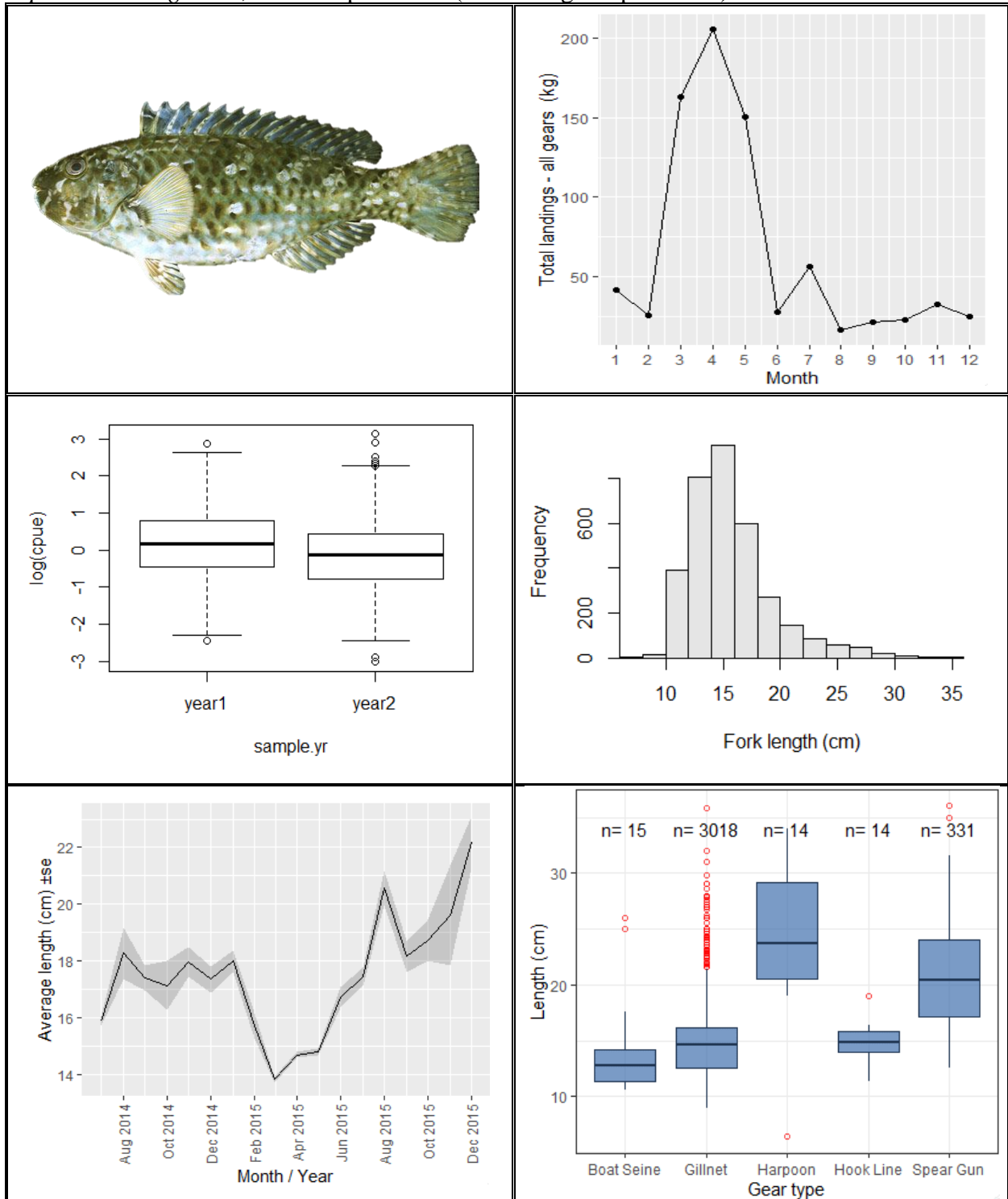


Figure 4.18. Species profile – *Leptoscarus vaigiensis*: image, total landings by month (top row), standardized CPUE year-index (gillnet), length frequency histogram (middle row), changes in average length over study period, and length by gear type (bottom row); L_m = unknown, L_{max} = 35.0 cm TL (Froese and Pauly, 2019; FishBase)

Lethrinus harak, Thumbprint emperor (a.k.a. Blackspot emperor)

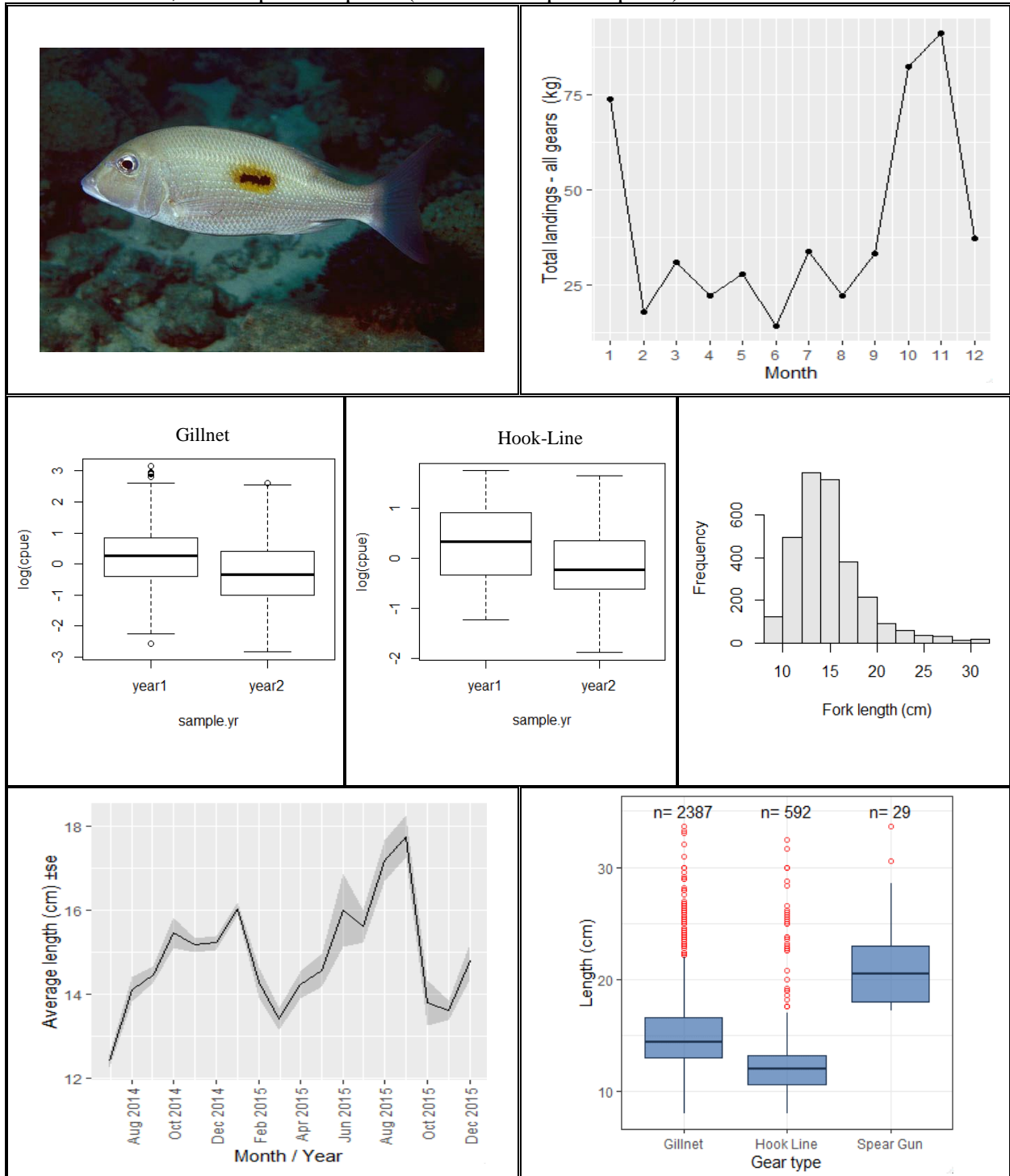


Figure 4.19. Species profile – *Lethrinus harak*: image, total landings by month (top row), standardized CPUE year-index (gillnet), CPUE year-index (hook-line), length frequency histogram (middle row), changes in average length over study period, and length by gear type (bottom row); $L_m = 19.5$, $L_{max} = 50.0$ cm TL (Froese and Pauly, 2019; FishBase)

Caesio caerulaurea, Blue and gold fusilier

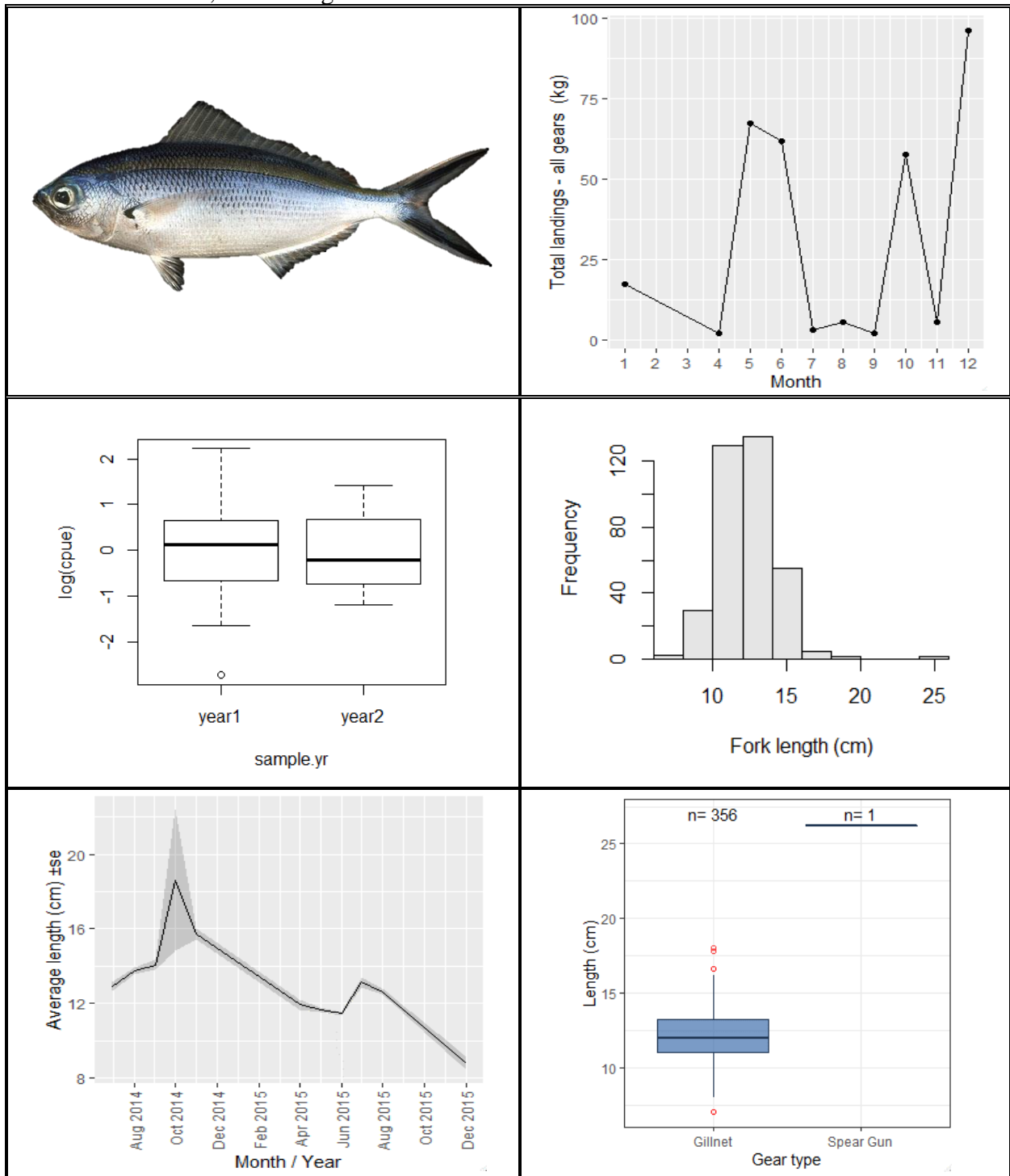


Figure 4.20. Species profile – *Caesio caerulaurea*: image, total landings by month (top row), standardized CPUE year-index (gillnet), length frequency histogram (middle row), changes in average length over study period, and length by gear type (bottom row); L_m = unknown, L_{max} = 35.0 cm TL (Froese and Pauly, 2019; FishBase)

Ostorhinchus cyanosoma, Yellowstriped cardinalfish

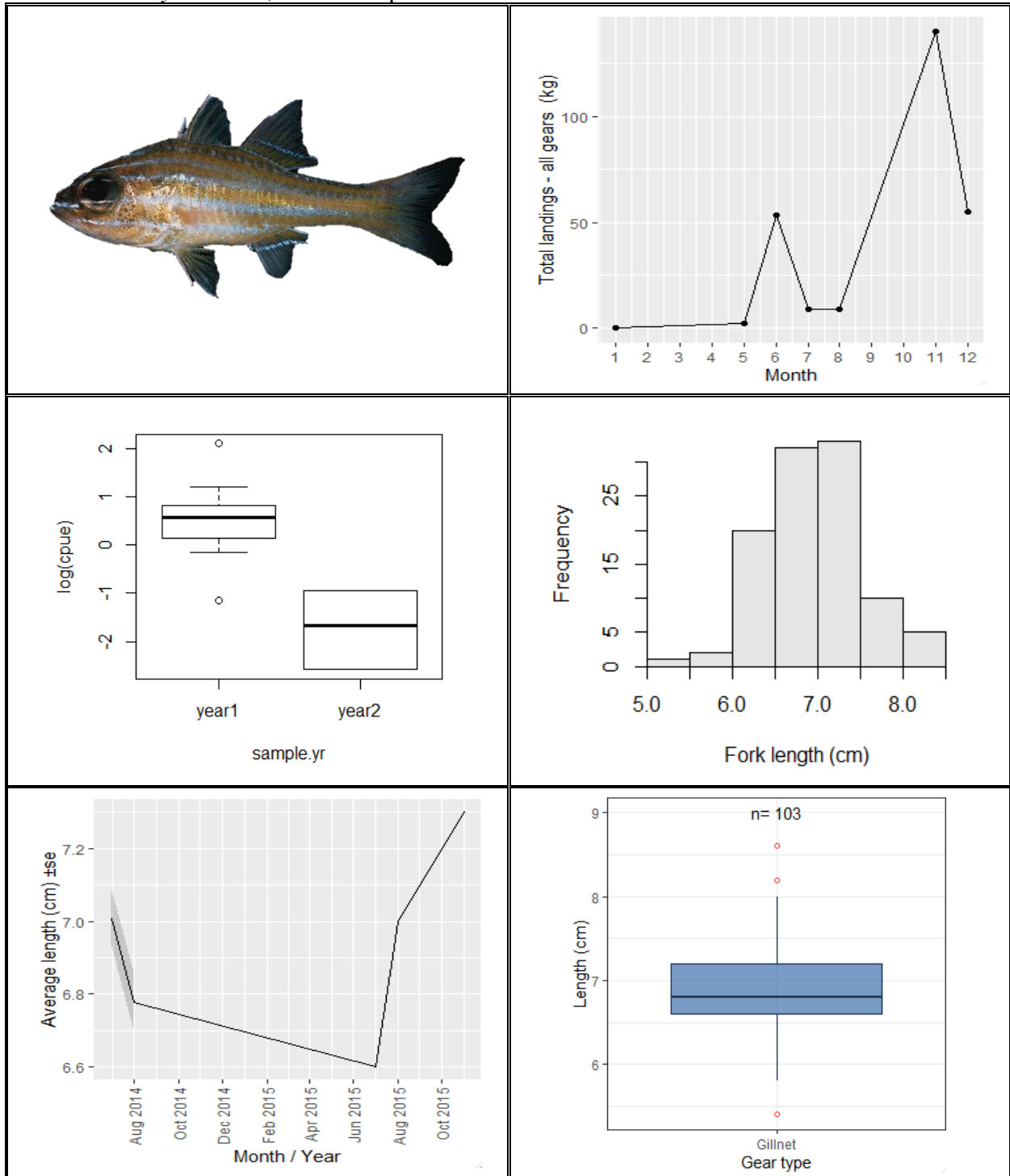


Figure 4.21. Species profile – *Ostorhinchus cyanosoma*: image, total landings by month (top row), standardized CPUE year-index (gillnet), length frequency histogram (middle row), changes in average length over study period, and length by gear type (bottom row); L_m = unknown, L_{max} = 8.0 cm TL (Froese and Pauly, 2019; FishBase)

Scarus ghobban, Blue-barred parrotfish

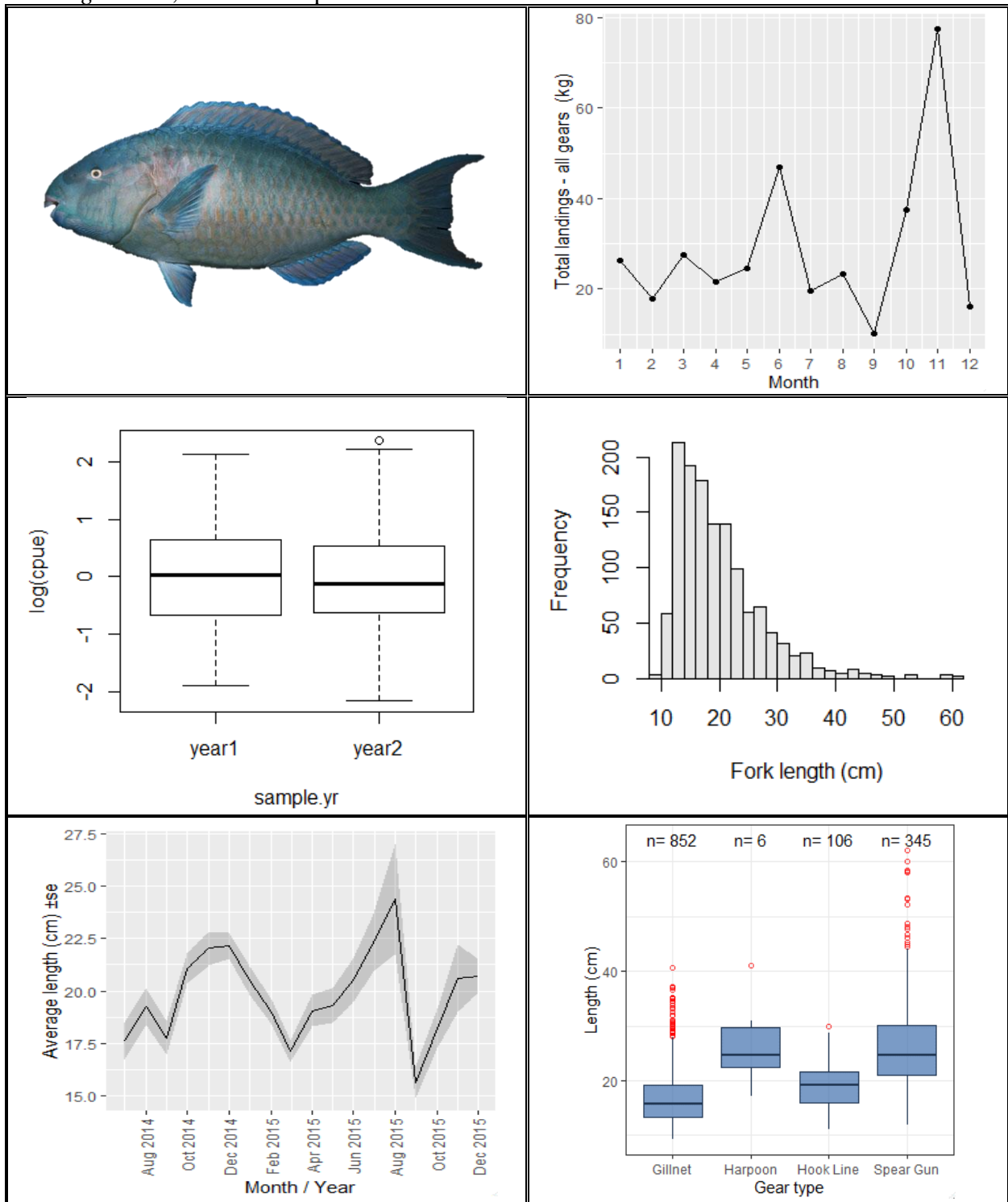


Figure 4.22. Species profile – *Scarus ghobban*: image, total landings by month (top row), standardized CPUE year-index (gillnet), length frequency histogram (middle row), changes in average length over study period, and length by gear type (bottom row); L_m = unknown, L_{max} = 75.0 cm TL (Froese and Pauly, 2019; FishBase)

Gerres longirostris, Strongspine silver-biddy

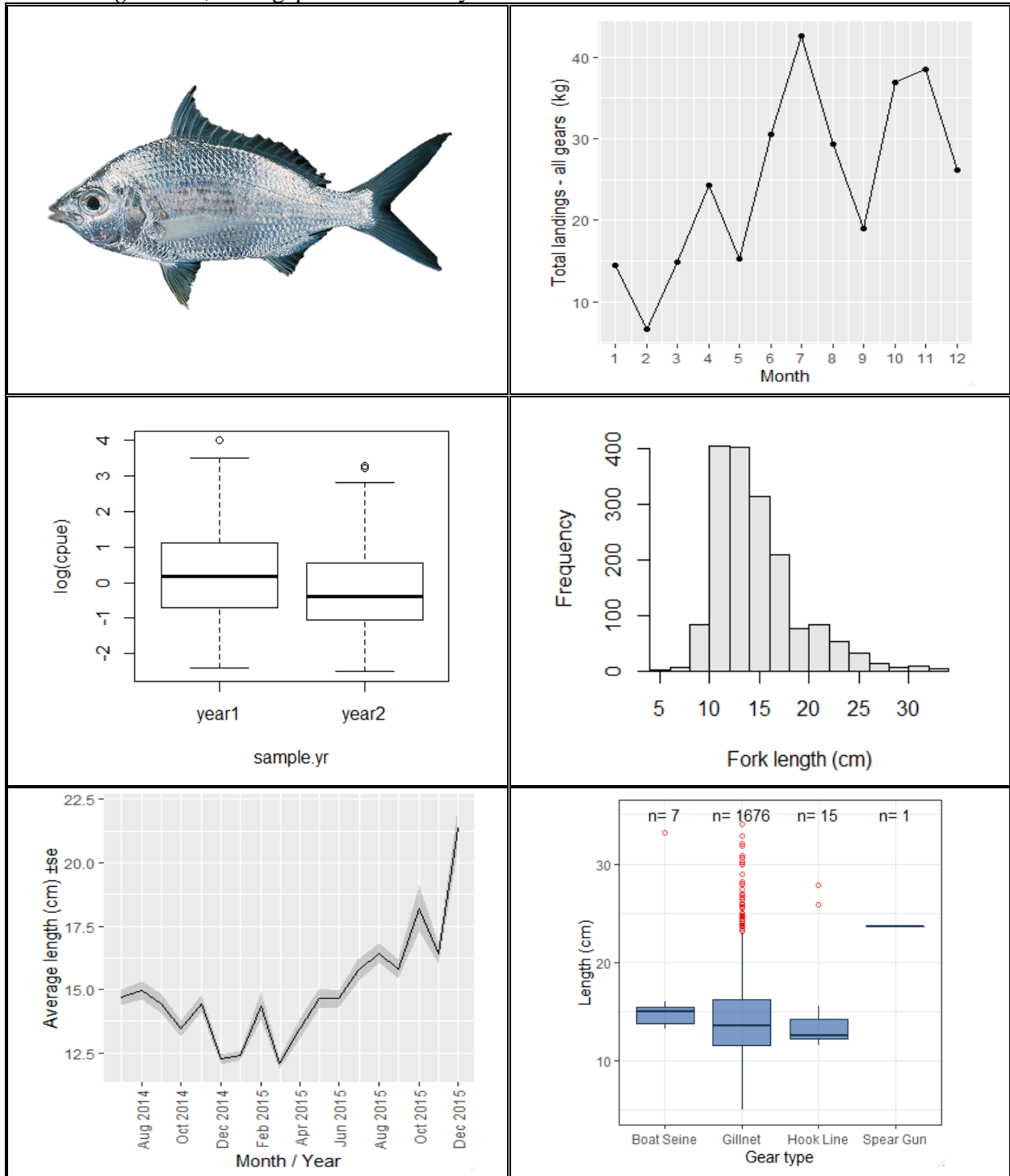


Figure 4.23. Species profile – *Gerres longirostris*: image, total landings by month (top row), standardized CPUE year-index (gillnet), length frequency histogram (middle row), changes in average length over study period, and length by gear type (bottom row); $L_m = 20.6$ cm, $L_{max} = 44.5$ cm TL (Froese and Pauly, 2019; FishBase)

Fisheries productivity and economic valuation

Data collected on all fisheries resources during the course of the landings surveys were classified into 8 basic categories of fisheries and economic importance: finfish, sea cucumbers, octopus, unknown (*i.e.* organisms too small to identify), squid, moray, ray, and miscellaneous (*i.e.* low-abundance, incidental catch comprised of organisms of significant consumptive or economic value, for example: shrimp, crab, lobster, marine turtles, seahorses, etc.). Annual averages for each category were calculated based on the 2 years of data: finfish (\bar{x} = 12,213 kg), sea cucumber (\bar{x} = 2,565 kg), octopus (\bar{x} = 1,756 kg), unknown (\bar{x} = 1,185 kg), squid (\bar{x} = 671 kg), moray (\bar{x} = 401 kg), ray (\bar{x} = 305 kg), and miscellaneous (\bar{x} = 166 kg), resulting in an overall average of \bar{x} = 19,264 kg year⁻¹. The nominal CPUE (nCPUE) was calculated for each category by dividing the averaged landings by the average number of trips surveyed (\bar{x} = 48,673.5). Lagoon-wide pirogue counts (Chapter 3) conducted in 2013 and 2015 were averaged (\bar{x} = 2156) and used in the expansion calculation for the determination of expanded fishing effort, *Effort**, (trips/year) and the estimation of bay-wide landings per year, according to the following formula:

$$\begin{aligned} \text{Effort}^* &= \text{Pirogue Ct (2156)} * \text{BAC (0.628)} * \text{fishing frequency (0.966)} * 365 \text{ days} = \\ &= 477,396 \text{ pirogue*days year}^{-1} = \text{trips year}^{-1}, \end{aligned}$$

where the boating activity coefficient, *BAC*, and fishing frequency were calculated included in the analyses of fishing effort in Chapter 3. Fisheries landing data collected in the 4 target villages of the Bay of Ranboe were expanded to estimate the lagoon-wide annual landings by multiplying the nCPUE values by the expanded effort. Results indicated the annual averaged,

lagoon-wide landings for the 2013-2015 study period totaled 1,885.8 metric tons per year (see Table 4.5 for details). Fisheries productivity per unit area was calculated from the results of the expanded landings ($1,885.7 \text{ mt year}^{-1} / 163 \text{ km}^2$ or $1,885,700 \text{ kg} / 16,300 \text{ ha}$) and found to equal $11.6 \text{ mt year}^{-1} \text{ km}^{-2}$ or $115.7 \text{ kg year}^{-1} \text{ ha}^{-1}$.

Based on market surveys conducted in year-1 of the study, and described in Chapter 3, the average price for fisheries resources were calculated, using the 2-year averaged exchange rate (2013= 2,222 MGA: 1USD; 2015= 3,333 MGA: 1USD; \bar{x} = 2,777.5) according to the eight-category classification system described previously in this section. Average values varied from \bar{x} = 3729 MGA/kg (1.34 USD/kg) for squid to \bar{x} = 1000 MGA/kg (0.36 USD/kg) for the various species of rays. Expanded landings per group, which were based on the 2-year averaged landings, were multiplied by the average exchange rate to determine the average value of the lagoon-wide fisheries per category and overall (\bar{x} = 1,644,678 USD year⁻¹) (Table 4.6). Economic productivity per unit area of the Bay of Ranobe fisheries are estimated at a wholesale value of $10,090 \text{ USD year}^{-1} \text{ km}^{-2}$ ($1,644,678 \text{ USD year}^{-1} / 163 \text{ km}^2$) or $101 \text{ USD year}^{-1} \text{ ha}^{-1}$.

Lastly, results of surveys and analyses of fishing effort described in Chapter 3 were used to estimate the daily revenue of the Vezo fishermen of the Bay of Ranobe. Annual pirogue count values from 2013 and 2015 per village were used to establish the average fleet size for the study period (Chapter 3). The regression analyses of the number of fishermen per length of pirogue (m) was used to predict the number of fishermen (Chapter 3) per the adjusted number of pirogues by multiplying by the boat-activity coefficient, *BAC*. Annual average landings and economic values of landings were attributed to each village based on the representation of the number of pirogues as a percentage of the lagoon-wide fleet. The economic value of landings per village were divided by a full year (365 days) rather than the discounted value (*i.e.* 365 days*0.966

Table 4.5. Expansion of surveyed landings to lagoon-wide estimates of annual yield per fisheries class

Group	Survey Values					Expanded	
	Total wt (kg)		Avg wt	Avg trips	nCPUE	Effort*	Yield
	Year-1	Year-2	year ⁻¹	year ⁻¹	kg/trip	trips/yr	mt/yr
Finfish	14,369	10,057	12,213	4,867.5	2.51	477,396	1,198.3
Sea cucumber	2,320	2,811	2,565	4,867.5	0.53	477,396	253.0
Octopus	1,438	2,075	1,756	4,867.5	0.36	477,396	171.9
Unknown	957	1,413	1,185	4,867.5	0.24	477,396	114.6
Squid	682	661	671	4,867.5	0.14	477,396	66.8
Moray	463	339	401	4,867.5	0.08	477,396	38.2
Ray	265	346	305	4,867.5	0.06	477,396	28.6
Miscellaneous	191	142	166	4,867.5	0.03	477,396	14.3
<i>Total</i>	<i>20,685</i>	<i>17,844</i>	<i>19,264</i>		<i>3.95</i>		<i>1,885.7</i>

Table 4.6. Economic valuation of expanded landings per fisheries class

Group	Landings <i>mt / yr</i>	Economic Value (MGA)			Value <i>(USD*)</i>
		<i>MGA/kg</i>	<i>n</i>	<i>SD</i>	
Finfish	1,198.3	2492	598	1463	1,119,925
Sea cucumber	253.0	2132	52	2176	202,246
Octopus	172.0	2101	323	1859	135,412
Unknown	114.6	1064	6	479	45,706
Squid	66.8	3729	94	1014	93,451
Moray	38.2	1811	2	843	25,935
Ray	28.6	1000	1	-	10,741
Miscellaneous	14.3	2097	102	2399	11,263
<i>Total</i>	<i>1,885.8</i>				<i>1,644,678</i>

*Exchange rate: 2013 – 2015 average, \bar{x} = 2,777.5 MGA: 1 USD

(fishing frequency) = 352.6 days) to determine the value of fisheries products per day per trip, as opposed to the average value per fished-day. Village-specific daily values of fisheries products ranged from 1.17 USD per trip for the village of Ambolomailaka to 1.79 USD per trip for the village of Beravy, with an overall average of \bar{x} = 1.55 USD day⁻¹ (SD= 0.15) (Table 4.7).

4.4 Discussion

Landings

During the 2-year study period, total annual landings surveyed declined in biomass by 13.7% from 20,685 kg in year-1 to 17,844 in year-2, while the number of trips surveyed differed by less than 1%, 4,880 and 4,855 trips, respectively. Of the fisheries classes, finfish represent the bulk of the landings (\bar{x} = 62.9 %) and experienced the greatest decline from year-1 (69.5%) to year-2 (56.3%). Declining landings of finfish were offset to some extent by a substantial increase (+47.6%) in the “unknown” class, and classes of invertebrate species (*i.e.* sea cucumber, octopus, squid, and rays). A substantial increase in the unknown-class, which represents masses of juvenile / larval species, where many are difficult to identify (see image, Appendix 4.26), is generally congruent with personal observations of the growing use of small mesh gear, namely mosquito net / seine nets. With 2 years of data from this study alone, observed declines in annual landings could be attributed to environmental stochasticity, and no conclusions can be drawn at this time.

Relative abundances of landed finfish were examined by family and species to illustrate the diversity found within the fisheries of the Bay of Ranobe, and the significant contributions made by coral reef species. At the family level, in descending order, Scaridae (parrotfish), Clupeidae (sardines and herrings amongst others), Siganidae (rabbitfish), Lethrinidae (emperors),

Table 4.7. Landings (metric tons year⁻¹) and value (USD year⁻¹) of fisheries products per village and per fishermen (USD day*trip⁻¹)

Village	<i>Actual</i>		<i>Predicted</i>	<i>Adjusted</i>			Value (USD/yr)	USD/day (365 d)	Value (USD) fishermen/day *trip
	Avg Pirogue Ct (2013-2015)	% Fleet	Fishermen Count ₁	Pirogue Count ₂	Fishermen Count ²	Landings (mt/yr)			
Fitsitke	376	17.4	820	236	515	328	286,446	785	1.52
Andrevo	351	16.3	680	220	427	307	267,756	734	1.72
Ambolomailaka	274	12.7	778	172	488	239	208,636	572	1.17
Betsibaroka	77	3.6	168	48	106	67	58,739	161	1.52
Madiorano	92	4.2	200	57	126	80	69,800	191	1.52
Amboaboaka	138	6.4	300	86	189	120	104,890	287	1.52
Mangily	171	7.9	373	107	234	149	130,064	356	1.52
Ifaty	267	12.4	532	168	334	234	203,678	558	1.67
Ambalaboy	41	1.9	89	26	56	36	31,276	86	1.53
Beravy	152	7.0	282	95	177	133	115,570	317	1.79
Tsongeritelo	111	5.1	241	69	151	97	84,294	231	1.53
Ambotsibotsike	110	5.1	239	69	150	96	83,531	229	1.53
<i>Total</i>	<i>2156</i>	<i>100.0</i>	<i>4702</i>	<i>1354</i>	<i>2953</i>	<i>1,886</i>	<i>1,644,678</i>	<i>4,506</i>	

1. Prediction of the regression model of the relationship between the number of fishermen and pirogue length (m) (Chapter 3) based on village profiles of pirogue length for the 4 targeted villages (Andrevo, Amobolomailaka, Ifaty, and Beravy) and the averaged, “generic” profile for the other 8 villages
2. Average number of pirogues for the study period (column 2) multiplied by the BAC, with a proportional adjustment to the number of fishermen

Acanthuridae (surgeonfish and unicornfish) were the five most abundant families (Figure 4.4a). At the species / species complex level, *Siganus sutor* (Shoemaker spinefoot; rabbitfish), *Herklotsichthys quadrimaculatus* (Bluestripe herring), other Clupeidae spp, *Plotossus lineatus* (Striped eel catfish), and *Leptoscarus vaigiensis* (Marbled parrotfish; a.k.a. Seagrass parrotfish) ranked amongst the top 5 most abundant species (Figure 4.4b). It is interesting to note that, when species were ranked by the percent occurrence in daily landings, ranks differed substantially. The first two species that were found in landings in over 75% of the survey days, *Siganus sutor* and *Leptoscarus vaigiensis*, were similarly amongst the top 5 species in terms of biomass, however the species that followed in the ranks differed markedly: *Lethrinus harak* (Thumbprint emperor), *Cheilinus trilobatus* (Tripletail wrasse), *Scarus ghobban* (Blue-barred parrotfish) (Figure 4.5).

Given that there are multiple approaches to characterizing landings, in terms of the relative abundances of species / families, it seems to raise questions as to how, in particular, fishermen would perceive and characterize their catch. For fisheries management, biomass is obviously an important criterion. However, for fishermen, the most *natural* approach in describing catches from recollections of the past could be according to fishes encountered most frequently, *i.e.* frequency of occurrence. Recollections of past catches according to the frequency of occurrence combined with an imperfect knowledge of species identification may result in recollections based on a cognitive function that is a blend of any, or all, of the approaches presented here, *i.e.* family-based, species-based, and frequency of occurrence in daily landings. While participatory fisheries management is a very broad term that can imply the beneficial participation of fishermen at numerous levels of the management process (Neiss *et al.*, 1999; Rockmann *et al.*, 2012; Ommer *et al.*, 2012; Stephenson *et al.*, 2016), there has been a

growing trend in the “data poor” fisheries research community to reconstruct landings based on interviews probing the recent, and sometimes distant, past to obtain information on annual landings, effort, and/or CPUE (Kuster *et al.*, 2005; Barnes-Mauthe *et al.*, 2013). Unsurprisingly, estimates obtained through interviews are biased, often resulting in inflated CPUE estimates, with the inflation rate increasing with the passage of time (Kuster *et al.*, 2006; Daw, 2010; Daw *et al.*, 2011; O’Donnell *et al.*, 2011; Damasio *et al.*, 2015; Aylesworth and Kuo, 2018). This point is discussed further, below, relative the CPUE values determined from the present study.

Results of landing surveys were presented by family, species, village and gear types (Figures 4.4 – 4.6; Appendix 4.3) in order to facilitate comparisons with the only published study of the Bay of Ranobe fisheries, Davies *et al.* (2009). In the Davies *et al.* (2009) study, landing surveys were conducted on the daytime, pirogue-based fishery in 3 of the southern villages of the Bay (*i.e.* Beravy, Ifaty, and Mangily). In terms of geographic representativity, the Davies *et al.* (2009) study focuses entirely on the southern half of the Bay, with sampling occurring in the 2 largest fishing villages in the south, Beravy and Ifaty, and in the village of Mangily. Generally, Mangily would not be considered to be representative of a *typical* fishing village of the region, given that the village is known nationally and internationally as the tourist destination in the Bay of Ranobe area. From results of the present study, significant differences were found in comparisons of species composition and nominal CPUE between the northern villages (Andrevo and Ambolomailaka) and the southern villages (Ifaty and Beravy) (Figures 4.7 and 4.9), demonstrating that indeed sampling the southern lagoon is inadequate in characterizing the fisheries of the Bay of Ranobe not to mention the entire southwest region of Madagascar.

The study period for the Davies *et al.* (2009) study is not entirely clear, with the initial statement of the study period in the publication being 1 March to 21 May 2008, then later it is

stated that catches were sampled 7 January to 5 June 2008. Regardless, whether 3 or 5 months of the year were sampled, the brief study period does not capture a full annual cycle. The lack of temporal and spatial representativity likely explain the results of the Davies et al. (2009) study that suggest that 65% of the finfish landings can be attributed to 2 species, *Spratelloides delicatulus* (Blue sprat) and *Herklotsichthys quadrimaculatus* (Bluestripe herring). Generally, clupeids would not be considered a coral reef resident species, but rather a “windfall” harvest for low-tech, artisanal fishermen, where pulses of various species of clupeids would episodically enhance landings. Species profiles developed in the present study indicate that pulses of *Herklotsichthys quadrimaculatus* and other species of clupeids do indeed occur (Figures 4.15 – 4.16; see image, Appendix 4.27), and represent a substantial proportion of the landings by weight (*i.e.* 17% -18%) (Figures 4.4a-b), however at levels that are significantly less than the 65% of total landings, as reported by Davies *et al* (2009). Laroche *et al.*, (1997) documented clupeids comprising 10.9% of the catch in Bay of Toliara, which is the embayment just south of the Bay of Ranobe. The only plausible explanation for the Davies *et al.* (2009) results would be that a strong pulse of *Spratelloides delicatulus* and *Herklotsichthys quadrimaculatus* occurred during the few months of the study, to an extent that over-shadowed the landings of the other 200+ species, and that many of the local fishermen from the 3 targeted villages took advantage of the windfall harvest. In addition to data, over the course of the present study, an extensive photo library of catches has been compiled by the author that clearly illustrates that it would be a gross mischaracterization to consider the Bay of Ranobe fisheries as a “sardine fishery” (see images Appendix 4.28 – 4.31).

Catch per unit effort

Nominal CPUE (nCPUE) values were calculated for finfish species as an aggregate of the multi-species, multi-gear fisheries of the Bay to allow for comparisons between years, months, villages, and gear types. Although the use of aggregate CPUE values for management purposes may be problematic (Maunder et al., 2006; Kleiber and Maunder, 2008), unlike simple landings, nominal CPUE values account for fishing effort and survey effort. Results of the present study indicated that the annual average nCPUE for finfish equaled $\bar{x} = 2.63 \text{ kg trip}^{-1}$, with significant declines from year-1 to year-2, and varied from 2.06 – 3.14 kg trip^{-1} on a monthly basis. Village-specific nCPUE values indicated that Ambolomailaka landings produced the greatest weight per trip ($\bar{x} = 3.51 \text{ kg/trip}$), followed by Beravy ($\bar{x} = 3.18 \text{ kg/trip}$), Andrevo ($\bar{x} = 2.13 \text{ kg/trip}$), and Ifaty ($\bar{x} = 1.70 \text{ kg/trip}$). In chapter 3, gear profiles for each village (Figure 3.16) indicated a proportionately heavier reliance on net gears in Ambolomailaka and Beravy, particularly small mesh nets (*i.e.* seine nets, mosquito net, gillnet), which likely explains the elevated nCPUE values, as large quantities of small fish are more generally targeted. Average nCPUE values per gear type (Table 4.3) are supportive of this assertion in that net gears produce CPUE values significantly greater than the other gears, which is especially pronounced in the case of the boat seine gear-type (boat seine CPUE, $\bar{x} = 15.35 \text{ kg/trip}$; gillnet CPUE, $\bar{x} = 4.34 \text{ kg/trip}$).

Species profiles were developed for the 10 most abundant species, according to total weight in landings (Figures 4.14 – 4.23). Species-specific profiles included plots of total landings by month, year indices from standardized CPUE, catch-at-length histograms, changes in average length by month/year, and length by gear types. Year indices from the standardized CPUEs indicated that the catch per unit effort for 7 of the 10 species significantly declined from year-1 to year-2, while a positive, yet insignificant, change was indicated for the striped eel

catfish, *Plotosus lineatus*. For most of the species, the length-at-maturity (L_m) is unknown, according to the FishBase database. However, for those species of known L_m , such as *Herklotsichthys quadrimaculatus*, *Plotosus lineatus*, *Lethrinus harak*, and *Gerres longirostris*, length-at-catch histograms indicated that the majority of the catch consisted of sexually immature fish, except for *Plotosus lineatus*, which was the only species to exhibit positive change from the standardized year indices.

Fisheries productivity and economic valuation

Landings expanded to lagoon-wide estimates indicate that the Bay of Ranobe fisheries yield 1,885.7 metric tons per year of fisheries products, with a wholesale value of \$1.6 million. Annual yield estimates were attributed to each village relative to the percentage of pirogues contributed by each village to the greater Bay of Ranobe fleet ($n= 2156$ pirogues). Villages with the highest annual yields did not necessarily correspond to the greatest incomes earned by fishermen, given that economic valuations are divided by all fishermen. For example, fishermen from the village with the highest yield, Fitsitke (328 mt year^{-1}), earned a below-average income of $\$1.52 \text{ day}^{-1}$ ($\bar{x}= \$1.55 \text{ day}^{-1}$) due to the total value being divided by a high number of fishermen ($n= 820$). Although no other economic valuation studies have been conducted on the Bay of Ranobe fisheries, estimates provided here correspond well to the numerous socioeconomic and poverty studies that have been conducted in Madagascar, as discussed in Chapter 2, which have found that $\approx 90\%$ of the population live on less than \$2 per day. Barnes-Mauthe *et al.* (2013) estimated CPUE and conducted an economic valuation of landings in a number of villages along a stretch of coastline approximately 100 km north of the Bay of Ranobe. However, the study followed an interview-based, participatory approach, which is known to suffer from inflated estimates, as discussed earlier in this section. According to the

Mauthe et al. (2013) study, total annual finfish landings were estimated at 4,045 mt year⁻¹, whereas the present study documented 1,198.3 mt year⁻¹ based on 2 years of actual data. Moreover, CPUE estimates (13.6 kg per fishermen per day) were 2-3 times greater than other studies in the region (Laroche and Ramananarivo, 1995; Doukakis *et al.*, 2007; Davies *et al.*, 2009; Brenier *et al.*, 2011; Samoily *et al.*, 2017), resulting in an estimated income of \$10.85 per fishermen per day. Logically, if there was a stretch of coast in which fishermen were earning \$10.85 per day, it is likely that all the fishermen in the region would have migrated to this hypothetical location. Indeed, it is not coincidental that the Bay of Ranobe is known to be the most heavily fished area in the country (Figure 4.24).

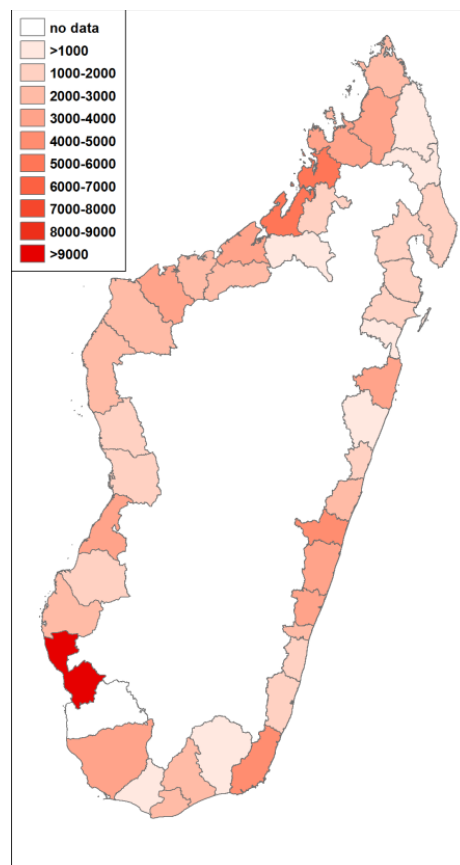


Figure 4.24. Distribution of coastal fishers; data collected by the Ministry of Fisheries (2011), *Ministère de la Pêche et des Ressources Halieutiques*; graphic reproduced from Le Manach *et al.* (2013b)

Works Cited

- Alvarez-Filip, Lorenzo, Nicholas K. Dulvey, Jennifer A. Gill, Isabelle M. Cote and Andrew R. Watkinson. 2009. Flattening the Caribbean coral reefs: region-wide declines in architectural complexity. *Proc. R. Soc. B*, 276: 3019-3025.
- Aylesworth, L. and T.C. Kuo. 2018. Reporting time period matters: quantifying catch rates and exploring recall bias from fisher interviews in Thailand. *Canadian Journal of Fisheries and Aquatic Sciences*, 75: 2114-2122.
- Barnes, D.K. and K.A. Rawlinson. 2009. Traditional coastal invertebrate fisheries in southwestern Madagascar. *Journal of the Marine Biological Association of the United Kingdom*, 89: 1589-1596
- Barnes-Mauthe, M., Oleson, K.L. and B. Zafindrasilivonona. 2013. The total economic value of small-scale fisheries with a characterization of post-landing trends: An application in Madagascar with global relevance. *Fisheries Research*, 147: 175-185.
- Batista, V.S., Fabr e, N.N., Malhado, A.C. and R.J. Ladle. 2014. Tropical artisanal coastal fisheries: challenges and future directions. *Reviews in Fisheries Science & Aquaculture*, 22: 1-15.
- Brenier, A., Ferraris, J. and J. Mahafina. 2011. Participatory assessment of the Toliara Bay reef fishery, southwest Madagascar. *Madagascar Conservation & Development*, 6: 60-67.
- Bruno, J.F. and E.R. Selig. 2007. Regional decline of coral cover in the Indo-Pacific: timing, extent, and subregional comparisons. *PLoS one*, 2: p.e711.
- Damasio, L.D.M.A., Lopes, P.F., Guariento, R.D. and A.R. Carvalho. 2015. Matching fishers' knowledge and landing data to overcome data missing in small-scale fisheries. *PLoS One*, 10: p.e0133122.
- Davies, T.E., Beanjara, N. and T. Tregenza. 2009. A socio-economic perspective on gear-based management in an artisanal fishery in south-west Madagascar. *Fisheries Management and Ecology*, 16: 279-289.
- Daw, T., 2010. Shifting baselines and memory illusions: what should we worry about when inferring trends from resource user interviews? *Animal Conservation*, 13: 534-535.
- Daw, T.M., Robinson, J.A.N. and N.A. Graham. 2011. Perceptions of trends in Seychelles artisanal trap fisheries: comparing catch monitoring, underwater visual census and fishers' knowledge. *Environmental Conservation*, 38: 75-88.
- de la Torre-Castro, M., Di Carlo, G. and N.S. Jiddawi. 2014. Seagrass importance for a small-scale fishery in the tropics: the need for seascape management. *Marine Pollution Bulletin*, 83: 398-407.

- Doukakis, P., Jonahson, M., Ramahery, V., de Dieu Randriamanantsoa, B.J. and S. Harding. 2008. Traditional fisheries of antongil bay, Madagascar. *Western Indian Ocean Journal of Marine Science*, 6: 175-181.
- Essington, Timothy E., Anne H. Beaudreau and John Wiedenmann. 2006. Fishing through marine food webs. *Proc. Natl. Acad. Sci.*, 103: 3171-3175.
- Froese, R. and D. Pauly. Editors. 2019. FishBase. World Wide Web electronic publication. www.fishbase.org, version (04/2019).
- Gardner, Toby A., Isabelle M. Cote, Jennifer A. Gill, Alastair Grant and Andrew R. Watkinson. 2003. Long-term region-wide declines in Caribbean corals. *Science*, 301: 958-960.
- Halim, A., Wiryawan, B., Loneragan, N.R., Hordyk, A., Sondita, M.F.A., White, A.T., Koeshendrajana, S., Ruchimat, T., Pomeroy, R.S. and Yuni, C., 2019. Developing a functional definition of small-scale fisheries in support of marine capture fisheries management in Indonesia. *Marine Policy*, 100: 238-248.
- Halpern, Benjamin S., Shaun Walbridge, Kimberly A. Selkoe, Carrie V. Kappel, Fiorenza Micheli, Caterina D'Agrosa, John f. Bruno, Kenneth S. Casey, Colin Ebert, Helen E. Fox, Rod Fujita, dennis Heinemann, Hunter S. Lenihan, Elizabeth M.P. Madin, Mathew T. Perry, Elizabeth R. Selig, Mark Spaulding, Robert Steneck and Reg Watson. 2008. A global map of human impact on marine ecosystems. *Science*, 319: 948-952.
- Harvell, C.D., K. Kim, J.M. Burkholder, R.R. Colwell, P.R. Epstein, D.J. Grimes, E.E. Hofmann, E.K. Lipp, A.D.M.E. Osterhaus, R.M. Overstreet, J.W. Porter, G.W. Smith and G.R. Vasta. 1999. Emerging marine diseases—Climate links and anthropogenic factors. *Science*, 285: 1505-1510.
- Hoegh-Guldberg, O., P.J. Mumby, A.J. Hooten, R.S. Steneck, P. Greenfield, E. Gomez, C.D. Harvell, P.F. Sale, A.J. Edwards, K. Caldeira, N. Knowlton, C.M. Eakin, R. Iglesias-Prieto, N. Muthiga, R.H. Bradbury, A. Dubi and M.E. Hatzioolos. 2007. Coral reefs under rapid climate change and ocean acidification. *Science*, 18: 1737-1742.
- Hughes, T.P., A.H. Baird, D.R. Bellwood, M. Card, S.R. Connolly, C. Folke, R. Grosberg, O. Hoegh-Guldberg, J.B.C. Jackson, J. Kleypas, J.M. Lough, P. Marshall, M. Nystrom, S.R. Palumbi, J.M. Pandolfi, B. Rosen, J. Roughgarden. 2003. Climate change, human impacts, and the resilience of coral reefs. *Science*, 301: 929-933.
- Hughes, Terence P., David R. Bellwood, Carl Folke, Robert S. Steneck and James Wilson. 2005. New paradigms for supporting the resilience of marine ecosystems. *Trends in Ecology and Evolution*, 20: 380-386.

- Humber, F., Godley, B.J., Ramahery, V. and A.C. Broderick. 2011. Using community members to assess artisanal fisheries: the marine turtle fishery in Madagascar. *Animal conservation*, 14: 175-185.
- Jackson, Jeremy B.C., Michael X. Kirby, Wolfgang H. Berger, Karen A. Bjorndal, Louis W. Botsford, Bruce J. Bourque, Roger H. Bradbury, Richard Cooke, Jon Erlandson, James A. Estes, Terence P. Hughes, Susan Kidwell, Carina B. Lange, Hunter S. Lenihan, John M. Pandolfi, Charles H. Peterson, Robert S. Steneck, Mia J. Tegner and Robert R. Warner. 2001. Historical overfishing and the recent collapse of coastal ecosystems. *Science*, 293: 629-638.
- Jenkins, Martin, Rhys E. Green and Joah Madden. 2003. The challenge of measuring global change in wild nature: Are things getting better or worse? *Conservation Biology*, 17: 20-23.
- Jones, Geoffrey P., Mark I. McCormick, Maya Srinivasan and Janelle V. Eagle. 2004. Coral decline threatens fish biodiversity in marine reserves. *Proc. Nat. Acad. Sci.*, 101: 8251-8253.
- Kleiber, P. and M.N. Maunder. 2008. Inherent bias in using aggregate CPUE to characterize abundance of fish species assemblages. *Fisheries Research*, 93: 140-145.
- Kuster, C., Vuki, V.C. and L.P. Zann. 2005. Long-term trends in subsistence fishing patterns and coral reef fisheries yield from a remote Fijian island. *Fisheries Research*, 76: 221-228.
- Kuster, C., Vuki, V.C. and L.P. Zann. 2006. Validation of the accuracy of household reporting of subsistence fishing catch and effort: a Fijian case study. *Fisheries Management and Ecology*, 13: 177-184.
- Knowlton, Nancy. 2001. The future of coral reefs. *Proc. Nat. Acad. Sci.*, 98: 5419-5425.
- Laroche, J. and Ramanananarivo, N., 1995. A preliminary survey of the artisanal fishery on coral reefs of the Tulear Region (southwest Madagascar). *Coral Reefs*, 14: 193-200.
- Laroche, J. and N. Ramanananarivo. 1995. A preliminary survey of the artisanal fishery on coral reefs of the Tulear Region (southwest Madagascar). *Coral Reefs*, 14: 193-200.
- Laroche, J., Razanoelisoa, J., Fauroux, E. and M.W. Rabenevanana. 1997. The reef fisheries surrounding the south-west coastal cities of Madagascar. *Fisheries management and ecology*, 4: 285-299.
- Le Manach, F., Gough, C., Harris, A., Humber, F., Harper, S. and D. Zeller. 2012. Unreported fishing, hungry people and political turmoil: the recipe for a food security crisis in Madagascar? 2012. *Marine policy*, 36: 218-225.

- Le Manach, F., Andriamahefazafy, M., Harper, S., Harris, A., Hosch, G., Lange, G.M., Zeller, D. and U.R. Sumaila. 2013a. Who gets what? Developing a more equitable framework for EU fishing agreements. *Marine Policy*, 38: 257-266.
- Le Manach, F., Andrianaivojaona, C., Oleson, K., Clausen, A. and G.M. Lange. 2013b. A technical case study for the WAVES Global Partnership in Madagascar.
- Maunder, M.N., Sibert, J.R., Fonteneau, A., Hampton, J., Kleiber, P. and S.J. Harley. 2006. Interpreting catch per unit effort data to assess the status of individual stocks and communities. *ICES Journal of Marine Science*, 63: 1373-1385.
- McCook, L.J. 1999. Macroalgae, nutrients and phase shifts on coral reefs: scientific issues and management consequences for the Great Barrier Reef. *Coral Reefs*, 18: 357-367.
- McCook, L.J., J. Jompa and G. Diaz-Pulido. 2001. Competition between corals and algae on coral reefs: a review of evidence and mechanisms. *Coral Reefs*, 19: 400-417.
- McVean, A.R., Hemery, G., Walker, R.C.J., Ralisaona, B.L.R. and E. Fanning. 2005. Traditional sea cucumber fisheries in southwest Madagascar: A case-study of two villages in 2002. *SPC Beche-de-mer Information Bulletin*, 21: 15-18.
- McVean, A.R., Walker, R.C. and E. Fanning. 2006. The traditional shark fisheries of southwest Madagascar: A study in the Toliara region. *Fisheries Research*, 82: 280-289.
- Mills, D.J., Westlund, L., de Graaf, G., Kura, Y., Willman, R. and K. Kelleher. 2011. Under-reported and undervalued: small-scale fisheries in the developing world. *Small-scale fisheries management: frameworks and approaches for the developing world*, pp.1-15.
- Ministère de la Pêche et des Ressources Halieutiques (MPRH), Enquête cadre nationale – Méthodologie. 2011, Secrétariat Général de la Direction Générale de la Pêche et des Ressources Halieutiques, Ministère de la Pêche et des Ressources Halieutiques: Antananarivo, Madagascar.
- Mumby, Peter J., Alastair R. Harborne, Jodene Williams, Carrie V. Kappel, Daniel R. Brumbaugh, Fiorenza Micheli, Katherine E. Holmes, Craig P. Dahlgren, Claire B. Paris and Paul Blackwell. 2007. Trophic cascade facilitates coral recruitment in a marine reserve. *Proc. Natl. Acad. Sci.*, 104: 8362-8367.
- Nash, K.L. and N.A. Graham. 2016. Ecological indicators for coral reef fisheries management. *Fish and Fisheries*, 17(4), pp.1029-1054.
- Neis, B., Schneider, D.C., Felt, L., Haedrich, R.L., Fischer, J. and J.A. Hutchings. 1999. Fisheries assessment: what can be learned from interviewing resource users? *Canadian Journal of Fisheries and Aquatic Sciences*, 56: 1949-1963.
- Nugues, M.M. and C.M. Roberts. 2003. Coral mortality and interaction with algae in relation to sedimentation. *Coral Reefs*, 22: 507-516.

- O'Donnell, K.P., Molloy, P.P. and A.C. Vincent. 2012. Comparing fisher interviews, logbooks, and catch landings estimates of extraction rates in a small-scale fishery. *Coastal Management*, 40: 594-611.
- Ommer, R.E., Perry, R.I., Murray, G. and B. Neis. 2012. Social–ecological dynamism, knowledge, and sustainable coastal marine fisheries. *Current Opinion in Environmental Sustainability*, 4: 316-322.
- Pauly D., V. Christensen, J. Dalsgaard, R. Froese and F. Torres. 1998. Fishing down marine food webs. *Science*, 279: 860-863.
- Pandolfi, John M., Roger H. Bradbury, Enric Sala, Terence P. Hughes, Karen A. Bjorndal, Richard G. Cooke, Deborah McArdle, Loren McClenachan, Marah J. H. Newman, Gustavo Paredes, Robert R. Warner, Jeremy B. C. Jackson. 2003. Global trajectories of the long-term decline of coral reef ecosystems. *Science*, 301: 955-958.
- Polidoro Beth A., Kent E. Carpenter, Lorna Collins, Norman C. Duke, Aaron M. Ellison, Joanna C. Ellison, Elizabeth J. Farnsworth, Edwino S. Fernando, Kandasamy Kathiresan, Nico E. Koedam, Suzanne R. Livingstone, Toyohiko Miyagi, Gregg E. Moore, Vien Ngoc Nam, Jin Eong Ong, Jurgenne H. Preimavera, Severino G. Salmo, III, Jonnell C. Sanciangco, Sukristijono Sukardjo, Yamin Wang and Jean Wan Hong Yong. 2010. The loss of species: Mangrove extinction risk and geographic areas of global concern. *PLoS ONE*, 5: e10095.
- Pollock, K.H., Hoenig, J.M., Jones, C.M., Robson, D.S. and C.J. Greene. 1997. Catch rate estimation for roving and access point surveys. *North American Journal of Fisheries Management*, 17: 11-19.
- Purcell, S.W., Mercier, A., Conand, C., Hamel, J.F., Toral-Granda, M.V., Lovatelli, A. and S. Uthicke. 2013. Sea cucumber fisheries: global analysis of stocks, management measures and drivers of overfishing. *Fish and fisheries*, 14: 34-59.
- Purcell, S.W. and R.S. Pomeroy. 2015. Driving small-scale fisheries in developing countries. *Frontiers in Marine Science*, 2: p.44.
- Rakotonirina, B. and A. Cooke. 1994. Sea turtles of Madagascar—their status, exploitation and conservation. *Oryx*, 28: 51-61.
- Robinson, L. and W.H.H. Sauer. 2013. A first description of the artisanal shark fishery in northern Madagascar: implications for management. *African Journal of Marine Science*, 35: 9-15.
- Röckmann, C., Ulrich, C., Dreyer, M., Bell, E., Borodzicz, E., Haapasaari, P., Hauge, K.H., Howell, D., Mäntyniemi, S., Miller, D. and G. Tserpes. 2012. The added value of participatory modelling in fisheries management—what has been learnt? *Marine Policy*, 36: 1072-1085.

- Samoilys, M.A., Osuka, K., Maina, G.W. and D.O. Obura. 2017. Artisanal fisheries on Kenya's coral reefs: Decadal trends reveal management needs. *Fisheries research*, 186: 177-191.
- Salas, S., Chuenpagdee, R., Seijo, J.C. and Charles, A., 2007. Challenges in the assessment and management of small-scale fisheries in Latin America and the Caribbean. *Fisheries Research*, 87: 5-16.
- Smith, H. and X. Basurto. 2019. Defining small-scale fisheries and examining the role of science in shaping perceptions of who and what counts: A systematic review. *Frontiers in Marine Science*, 6: 236.
- Stallings, Christopher D. 2009. Fishery-independent data reveal negative effect of human population density on Caribbean predatory fish communities. *PLoS ONE*, 4: e5333.
- Stamatopoulos, C. 2002. Sample-based fishery surveys. A technical handbook. FAO.
- Stephenson, R.L., Paul, S., Pastoors, M.A., Kraan, M., Holm, P., Wiber, M., Mackinson, S., Dankel, D.J., Brooks, K. and A. Benson. 2016. Integrating fishers' knowledge research in science and management. *ICES Journal of Marine Science*, 73: 1459-1465.
- Van der Elst, R., Everett, B., Jiddawi, N., Mwatha, G., Afonso, P.S. and D. Boulle. 2005. Fish, fishers and fisheries of the Western Indian Ocean: their diversity and status. A preliminary assessment. *Philosophical Transactions of the Royal Society A: Mathematical, Physical and Engineering Sciences*, 363: 263-284.
- Van der Elst, R.P., Groeneveld, J.C., Baloi, A.P., Marsac, F., Katonda, K.I., Ruwa, R.K. and W.L. Lane. 2009. Nine nations, one ocean: A benchmark appraisal of the South Western Indian Ocean Fisheries Project (2008–2012). *Ocean & Coastal Management*, 52: 258-267.
- Veron, J.E.N., O. Hoegh-Guldberg, T.M. Lenton, J.M. Lough, D.O. Obura, P. Pearce-Kelly, C.R.C. Sheppard, M. Spalding, M.G. Stafford-Smith, A.D. Rogers. 2009. The coral reef crisis: The critical importance of <350 ppm CO₂. *Marine Pollution Bulletin*, 58: 1428-1436.
- Walker, R.C. and E. Roberts. 2005. Notes on the status and incidental capture of marine turtles by the subsistence fishing communities of South West Madagascar. *Western Indian Ocean Journal of Marine Science*, 4: 219-226.
- Waycott, Michelle, Carlos M. Duarte, Tim J. B. Carruthers, Robert J. Orth, William C. Dennison, Suzanne Olyarnik, Ainsley Calladine, James W. Fourqurean, Kenneth L. Heck, Jr., A. Randall Hughes, Gary A. Kendrick, W. Judson Kenworthy, Frederick T. Short, and Susan L. Williams. 2009. Accelerating loss of seagrass across the globe threatens coastal ecosystems. *Proc. Nat. Acad. Sci.*, 106: 12377-12381.

World Bank/FAO/WorldFish. 2010. The Hidden Harvests: the global contribution of capture fisheries. Agriculture and Rural Development, Sustainable Development Network. World Bank, Washington, D.C.

Appendix

Village: _____ Ticket #: _____

Fisheries Landings Datasheet: Catch survey

Date: _____

Species	Nb	W(g)	Gear	Species	Nb	W(g)	Gear	Species	Nb	W(g)	Gear	Species	Nb	W(g)	Gear
Ear-spot angelfish				Bicolour parrotfish				Dusky surgeonfish				Slingjaw wrasse			
Emperor angelfish				Blue-barred parrotfish				Blckstreak surgeonfish				Tripletail wrasse			
Manyspined angelfish				Bullethead parrotfish				Thompson's surgnfish				Yellowbreasted wrasse			
Midnight angelfish				Dusky parrotfish				Yellowfin surgeonfish				Zigzag wrasse			
Regal angelfish				Dusky-cappd parrotfish				Convict surgeonfish				Green jobfish			
Semicircle angelfish				Greenthroat parrotfish				Brushtail tang				Indian threadfin			
Chevroned butterflyfish				I.O. longnose parrotfish				Sailfin tang				Talang queenfish			
Klein's butterflyfish				Palenose parrotfish				Desjardin's sailfin tang				Trevally spp			
Saddleback butterflyfish				Redlip parrotfish				Orngestripe triggerfish				Graceful lizardfish			
Spotted butterflyfish				Russell's parrotfish				Picasso triggerfish				I.O. crocodilefish			
Threadfin butterflyfish				Seagrass parrotfish				Moustache triggerfish				Cornetfish			
Vagabond butterflyfish				Stareye parrotfish				Bignose unicornfish				Reef needlfish			
Bigeye emperor				Afr. W. spot rabbitfish				Blcktongue unicornfish				Spotted halfbeak			
Blackspace emperor				Scribbled rabbitfish				Bluespine unicornfish				Insular halfbeak			
Longface emperor				Squaretail rabbitfish				Humpback unicornfish				Slenderspine mojarra			
Pink-ear emperor				Stellete rabbitfish				Orang spine unicornfish				Vanikoro sweeper			
Redgill emperor				Scissor-tail sergeant				Spotted unicornfish				Low fin rudderfish			
Sky emperor				Indo-pacific sergeant				White marg unicornfish				Goggle-eye bigeye			
Snubnose emperor				False-eye sergeant				African coris				Glasseye bigeye			
Yellowlip emperor				White-belly damsel				Barred thicklip wrasse				Striped catfish			
Lunar fusilier				Three-spot dascyllus				Blck-edge thcklip wrase				Moorish idol			
Scissor-tail fusilier				Bronze soldierfish				Blue-spotted wrasse				Buccaneer anchovy			
Yellowtop fusilier				Red soldierfish				Checkerboard wrasse				Delicate round herring			
Dash-and-dot goatfish				Tailspot squirrelfish				Cigar wrasse				Gold spot herring			
Indian goatfish				Bloodspot squirrelfish				Crescent wrasse				Squid			
Longbarbel goatfish				Crown squirrelfish				Dragon wrasse				Octopus			
Red spot goatfish				Long-jawed squirrelfish				Goldbar wrasse				Sea cucumber			
Rosy goatfish				Onespot snapper				Longface wrasse				Moray			
Sidespot goatfish				Black-spot snapper				Sixbar wrasse				Lobster			
Two-barred goatfish				Blue-lined snapper				Species				Nb	Wt(g)		
Yellowfin goatfish				Flametail snapper											
Yellowstripe goatfish				Humpback snapper											
Blacktip grouper				Black sweetlips											
Halfmoon grouper				Blck-spotted sweetlips											
Honeycomb grouper				Dusky sweetlips											
Longspined grouper				Gold-spotted sweetlips											
Yellow-edged lyretail				White-barred sweetlips											
Peacock grouper				Goldring bristletooth											
Redmouth grouper				Two spot bristletooth											
Saddleback grouper				Striped bristletooth											

Appendix 4.1. Initial landings survey datasheet, including 133 species + morays + invertebrate groups (squid, lobster, octopus, and sea cucumber)

	Scientific name	Common name
1	<i>Abudefduf sexfasciatus</i>	Scissortail sergeant
2	<i>Abudefduf sparoides</i>	False-eye sergeant
3	<i>Abudefduf vaigiensis</i>	Indo-pacific sergeant
	<i>Acanthuridae spp</i>	<i>Acanthuridae spp</i>
4	<i>Acanthurus blochii</i>	Ringtail surgeonfish
5	<i>Acanthurus dussumieri</i>	Eyestripe surgeonfish
6	<i>Acanthurus lineatus</i>	Lined surgeonfish
7	<i>Acanthurus mata</i>	Elongate surgeonfish
8	<i>Acanthurus nigricauda</i>	Epaulette surgeonfish
9	<i>Acanthurus nigrofuscus</i>	Brown surgeonfish
10	<i>Acanthurus tennentii</i>	Doubleband surgeonfish
11	<i>Acanthurus triostegus</i>	Convict surgeonfish
12	<i>Acanthurus xanthopterus</i>	Yellowfin surgeonfish
13	<i>Aeoliscus strigatus</i>	Razorfish
14	<i>Aethaloperca rogae</i>	Redmouth grouper
15	<i>Albula glossodonta</i>	Roundjaw bonefish
16	<i>Aluterus scriptus</i>	Scribbled leatherjacket filefish
17	<i>Amblyglyphidodon leucogaster</i>	Yellowbelly damselfish
18	<i>Amblygobius semicinctus</i>	Halfbarred goby
19	<i>Anampses caeruleopunctatus</i>	Bluespotted wrasse
20	<i>Anampses twistii</i>	Yellowbreasted wrasse
	<i>Apogonidae spp</i>	<i>Apogonidae spp</i>
21	<i>Aprion virescens</i>	Green jobfish
22	<i>Arothron hispidus</i>	White-spotted puffer
23	<i>Arothron mappa</i>	Map puffer
24	<i>Arothron nigropunctatus</i>	Blackspotted puffer
25	<i>Arothron stellatus</i>	Stellate puffer
26	<i>Balistapus undulatus</i>	Orange-lined triggerfish
	<i>Balistidae spp</i>	<i>Balistidae spp</i>
27	<i>Balistoides conspicillum</i>	Clown triggerfish
28	<i>Balistoides viridescens</i>	Titan triggerfish
29	<i>Bodianus diana</i>	Diana's hogfish
30	<i>Bolbometopon muricatum</i>	Green humphead parrotfish
31	<i>Caesio caeruleaurea</i>	Blue and gold fusilier
32	<i>Caesio lunaris</i>	Lunar fusilier
33	<i>Caesio xanthonota</i>	Yellowback fusilier
34	<i>Calotomus carolinus</i>	Carolines parrotfish
35	<i>Calotomus spinidens</i>	Spinytooth parrotfish
36	<i>Cantherhines pardalis</i>	Honeycomb filefish
	<i>Carangidae spp</i>	<i>Carangidae spp</i>
37	<i>Carangoides fulvoguttatus</i>	Yellowspotted trevally
38	<i>Carangoides gymnostethus</i>	Bludger

Appendix 4.2. Species and species groups occurring in landings dataset

39	<i>Caranx ignobilis</i>	Giant trevally
40	<i>Caranx melampygu</i>	Bluefin trevally
41	<i>Centropyge multispinis</i>	Dusky angelfish
42	<i>Cephalopholis argus</i>	Peacock hind
43	<i>Cephalopholis miniata</i>	Coral hind
44	<i>Cephalopholis urodeta</i>	Darkfin hind
45	<i>Cetoscarus ocellatus</i>	Spotted parrotfish
46	<i>Chaetodon auriga</i>	Threadfin butterflyfish
47	<i>Chaetodon blackburnii</i>	Blackburn's butterflyfish
48	<i>Chaetodon falcula</i>	Blackwedged butterflyfish
49	<i>Chaetodon guttatissimus</i>	Peppered butterflyfish
50	<i>Chaetodon kleinii</i>	Sunburst butterflyfish
51	<i>Chaetodon lineolatus</i>	Lined butterflyfish
52	<i>Chaetodon lunula</i>	Raccoon butterflyfish
53	<i>Chaetodon madagaskariensis</i>	Seychelles butterflyfish
54	<i>Chaetodon trifascialis</i>	Chevron butterflyfish
55	<i>Chaetodon trifasciatus</i>	Melon butterflyfish
56	<i>Chaetodon vagabundus</i>	Vagabond butterflyfish
57	<i>Chaetodon xanthocephalus</i>	Yellowhead butterflyfish
	<i>Chaetodontidae spp</i>	<i>Chaetodontidae spp</i>
58	<i>Cheilinus chlorourus</i>	Floral wrasse
59	<i>Cheilinus oxycephalus</i>	Snooty wrasse
60	<i>Cheilinus trilobatus</i>	Tripletail wrasse
61	<i>Cheilinus undulatus</i>	Humphead wrasse
62	<i>Cheilio inermis</i>	Cigar wrasse
63	<i>Cheilodipterus macrodon</i>	Large toothed cardinalfish
64	<i>Cheilodipterus quinquelineatus</i>	Five-lined cardinalfish
65	<i>Cheilopogon abei</i>	Abe's flyingfish
66	<i>Chilomycterus reticulatus</i>	Spotfin burrfish
67	<i>Chirocentrus nudus</i>	Whitefin wolf-herring
68	<i>Chlorurus sordidus</i>	Daisy parrotfish
69	<i>Chromis weberi</i>	Weber's chromis
70	<i>Chrysiptera annulata</i>	Footballer demoiselle
	<i>Cirrhitidae spp</i>	<i>Cirrhitidae spp</i>
71	<i>Cirrhitus pinnulatus</i>	Stocky hawkfish
	<i>Clupeidae spp</i>	<i>Clupeidae spp</i>
72	<i>Coris caudimacula</i>	Spottail coris
73	<i>Coris cuvieri</i>	African Coris
74	<i>Crenimugil crenilabis</i>	Fringelip mullet
75	<i>Ctenochaetus binotatus</i>	Twospot surgeonfish
76	<i>Ctenochaetus striatus</i>	Striated surgeonfish
77	<i>Ctenochaetus strigosus</i>	Spotted surgeonfish
78	<i>Cymolutes praetextatus</i>	Knife razorfish

Appendix 4.2 cont. Species and species groups occurring in landings dataset

79	<i>Dactyloptena orientalis</i>	Oriental flying gurnard
80	<i>Dascyllus aruanus</i>	Whitetail dascyllus
81	<i>Dascyllus trimaculatus</i>	Threespot dascyllus
82	<i>Dendrochirus brachypterus</i>	Dwarf lionfish
83	<i>Diagramma pictum</i>	Painted sweetlips
	<i>Diodontidae spp</i>	Diodontidae spp
84	<i>Echeneis naucrates</i>	Live sharksucker
85	<i>Epibulus insidiator</i>	Sling-jaw wrasse
86	<i>Epinephelus coeruleopunctatus</i>	Whitespotted grouper
87	<i>Epinephelus fasciatus</i>	Blacktip grouper
88	<i>Epinephelus flavocaeruleus</i>	Blue-and-yellow grouper
89	<i>Epinephelus hexagonatus</i>	Starspotted grouper
90	<i>Epinephelus lanceolatus</i>	Giant grouper
91	<i>Epinephelus longispinis</i>	Longspine grouper
92	<i>Epinephelus macrospilos</i>	Snubnose grouper
93	<i>Epinephelus malabaricus</i>	Malabar grouper
94	<i>Epinephelus melanostigma</i>	One-blotch grouper
95	<i>Epinephelus merra</i>	Honeycomb grouper
96	<i>Epinephelus polyphkadion</i>	Camouflage grouper
97	<i>Epinephelus rivulatus</i>	Halfmoon grouper
98	<i>Epinephelus spilotoceps</i>	Foursaddle grouper
99	<i>Epinephelus tukula</i>	Potato grouper
	<i>Exocoetidae spp</i>	Exocoetidae spp
100	<i>Fistularia petimba</i>	Red cornetfish
101	<i>Fowleria marmorata</i>	Marbled cardinalfish
	<i>Gerreidae spp</i>	Gerreidae spp
102	<i>Gerres longirostris</i>	Strongspine silver-biddy
103	<i>Gnathanodon speciosus</i>	Golden trevally
104	<i>Gnathodentex aureolineatus</i>	Striped large-eye bream
	<i>Gobiidae spp</i>	Gobiidae spp
105	<i>Gomphosus caeruleus</i>	Green birdmouth wrasse
	<i>Haemulidae spp</i>	Haemulidae spp
106	<i>Halichoeres hortulanus</i>	Checkerboard wrasse
107	<i>Halichoeres marginatus</i>	Dusky wrasse
108	<i>Halichoeres scapularis</i>	Zigzag wrasse
109	<i>Hemigymnus melapterus</i>	Blackeye thicklip
110	<i>Hemigymnus fasciatus</i>	Barred thicklip wrasse
111	<i>Hemiramphus far</i>	Black-barred halfbeak
112	<i>Heniochus acuminatus</i>	Pennant coralfish
113	<i>Heniochus monoceros</i>	Masked bannerfish
114	<i>Herklotsichthys quadrimaculatus</i>	Bluestripe herring
115	<i>Heteropriacanthus cruentatus</i>	Glasseye
116	<i>Hipposcarus harid</i>	Candelamoia parrotfish

Appendix 4.2 cont. Species and species groups occurring in landings dataset

	<i>Holocentridae spp</i>	Holocentridae spp
117	<i>Hyporhamphus affinis</i>	Tropical halfbeak
118	<i>Istiompax indica</i>	Black marlin
119	<i>Kyphosus cinerascens</i>	Blue sea chub
120	<i>Kyphosus vaigiensis</i>	Brassy chub
	<i>Labridae spp</i>	Labridae spp
121	<i>Lactoria cornuta</i>	Longhorn cowfish
122	<i>Leptomelanosoma indicum</i>	Indian threadfin
123	<i>Leptoscarus vaigiensis</i>	Marbled parrotfish
	<i>Lethrinidae spp</i>	Lethrinidae spp
124	<i>Lethrinus borbonicus</i>	Snubnose emperor
125	<i>Lethrinus harak</i>	Thumbprint emperor
126	<i>Lethrinus lentjan</i>	Pink ear emperor
127	<i>Lethrinus mahsena</i>	Sky emperor
128	<i>Lethrinus nebulosus</i>	Spangled emperor
129	<i>Lethrinus olivaceus</i>	Longface emperor
130	<i>Lethrinus rubrioperculatus</i>	Spotcheek emperor
131	<i>Lethrinus xanthochilus</i>	Yellowlip emperor
	<i>Lutjanidae spp</i>	Lutjanidae spp
132	<i>Lutjanus argentimaculatus</i>	Mangrove red snapper
133	<i>Lutjanus bohar</i>	Two-spot red snapper
134	<i>Lutjanus fulviflamma</i>	Dory snapper
135	<i>Lutjanus fulvus</i>	Blacktail snapper
136	<i>Lutjanus gibbus</i>	Humpback red snapper
137	<i>Lutjanus kasmira</i>	Common bluestripe snapper
138	<i>Lutjanus monostigma</i>	One-spot snapper
139	<i>Lutjanus quinquelineatus</i>	Five-lined snapper
140	<i>Lutjanus rivulatus</i>	Blubberlip snapper
141	<i>Macolor niger</i>	Black and white snapper
142	<i>Megalaspis cordyla</i>	Torpedo scad
	<i>Monacanthidae spp</i>	Monacanthidae spp
143	<i>Monotaxis grandoculis</i>	Humpnose big-eye bream
	<i>Mugilidae spp</i>	Mugilidae spp
144	<i>Mulloidichthys flavolineatus</i>	Yellowstripe goatfish
145	<i>Mulloidichthys vanicolensis</i>	Yellowfin goatfish
146	<i>Myripristis adusta</i>	Shadowfin soldierfish
147	<i>Myripristis murdjan</i>	Pinecone soldierfish
148	<i>Naso annulatus</i>	Whitemargin unicornfish
149	<i>Naso brachycentron</i>	Humpback unicornfish
150	<i>Naso brevirostris</i>	Spotted unicornfish
151	<i>Naso fageni</i>	Horseface unicornfish
152	<i>Naso hexacanthus</i>	Sleek unicornfish
153	<i>Naso lituratus</i>	Orangespine unicornfish

Appendix 4.2 cont. Species and species groups occurring in landings dataset

154	<i>Naso unicornis</i>	Bluespine unicornfish
155	<i>Neoniphon sammara</i>	Sammara squirrelfish
156	<i>Novaculichthys taeniourus</i>	Rockmover wrasse
157	<i>Novaculoides macrolepidotus</i>	Seagrass wrasse
158	<i>Ostorhinchus aureus</i>	Ring-tailed cardinalfish
159	<i>Ostorhinchus cyanosoma</i>	Yellowstriped cardinalfish
160	<i>Ostorhinchus nigrofasciatus</i>	Blackstripe cardinalfish
	<i>Ostraciidae spp</i>	Ostraciidae spp
161	<i>Ostracion cubicus</i>	Yellow boxfish
162	<i>Ostracion meleagris</i>	Whitespotted boxfish
163	<i>Papilloculiceps longiceps</i>	Tentacled flathead
164	<i>Parapercis hexophthalma</i>	Speckled sandperch
165	<i>Pardachirus pavoninus</i>	Peacock sole
166	<i>Parupeneus barberinus</i>	Dash-and-dot goatfish
167	<i>Parupeneus cyclostomus</i>	Gold-saddle goatfish
168	<i>Parupeneus heptacanthus</i>	Cinnabar goatfish
169	<i>Parupeneus indicus</i>	Indian goatfish
170	<i>Parupeneus macronemus</i>	Long-barbel goatfish
171	<i>Parupeneus pleurostigma</i>	Sidespot goatfish
172	<i>Parupeneus rubescens</i>	Rosy goatfish
173	<i>Parupeneus trifasciatus</i>	Doublebar goatfish
174	<i>Pempheris vanicolensis</i>	Vanikoro sweeper
175	<i>Platax orbicularis</i>	Orbicular batfish
176	<i>Platycephalus indicus</i>	Bartail flathead
177	<i>Plectorhinchus flavomaculatus</i>	Lemonfish
178	<i>Plectorhincus chubbi</i>	Dusky rubberlip
179	<i>Plectorhincus gaterinus</i>	Blackspotted rubberlip
180	<i>Plectorhincus gibbosus</i>	Harry hotlips
181	<i>Plectroglyphidodon lacrymatus</i>	Whitespotted devil
182	<i>Plectropomus pessuliferus</i>	Roving coralgroupier
183	<i>Plectropomus punctatus</i>	Marbled coralgroupier
184	<i>Plotosus lineatus</i>	Striped eel catfish
185	<i>Pomacanthus chrysurus</i>	Goldtail angelfish
186	<i>Pomacanthus imperator</i>	Emperor angelfish
187	<i>Pomacanthus semicirculatus</i>	Semicircle angelfish
	<i>Pomacentridae spp</i>	Pomacentridae spp
188	<i>Pomacentrus aquilus</i>	Dark damselfish
189	<i>Priacanthus blochii</i>	Paeony bulleye
190	<i>Priacanthus hamrur</i>	Moontail bullseye
191	<i>Pristiapogon kallopterus</i>	Iridescent cardinalfish
192	<i>Pseudobalistes flavimarginatus</i>	Yellowmargin triggerfish
	<i>Pseudoginglymostoma</i>	
193	<i>brevicaudatum</i>	Short-tail nurse shark
194	<i>Pteragogus flagellifer</i>	Cocktail wrasse

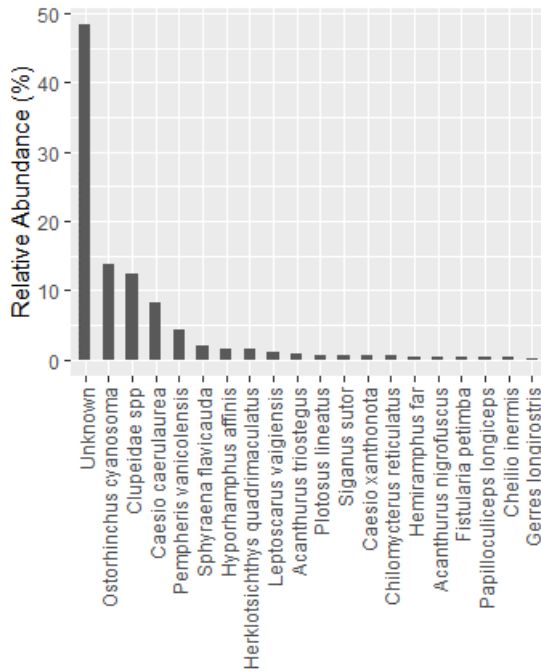
Appendix 4.2 cont. Species and species groups occurring in landings dataset

195	<i>Pterois antennata</i>	Broadbarred firefish
196	<i>Pterois volitans</i>	Red lionfish
197	<i>Pygoplites diacanthus</i>	Regal angelfish
198	<i>Remora remora</i>	Shark sucker
199	<i>Rhabdosargus sarba</i>	Goldlined seabream
200	<i>Rhinecanthus aculeatus</i>	White-banded triggerfish
201	<i>Rhinobatos albomaculatus</i>	Whitespotted guitarfish
202	<i>Sargocentron caudimaculatum</i>	Silverspot squirrelfish
203	<i>Sargocentron diadema</i>	Crown squirrelfish
204	<i>Sargocentron praslin</i>	Dark-striped squirrelfish
205	<i>Sargocentron punctatissimum</i>	Speckled squirrelfish
206	<i>Sargocentron spiniferum</i>	Sabre squirrelfish
207	<i>Saurida gracilis</i>	Gracile lizardfish
	<i>Scaridae spp</i>	Scaridae spp
208	<i>Scarus falcipinnis</i>	Sicklefin parrotfish
209	<i>Scarus ghobban</i>	Blue-barred parrotfish
210	<i>Scarus niger</i>	Dusky parrotfish
211	<i>Scarus psittacus</i>	Common parrotfish
212	<i>Scarus rubroviolaceus</i>	Ember parrotfish
213	<i>Scarus russelii</i>	Eclipse parrotfish
214	<i>Scarus scaber</i>	Fivesaddle parrotfish
215	<i>Scolopsis bimaculata</i>	Thumbprint monocle bream
216	<i>Scolopsis ghanam</i>	Arabian monocle bream
217	<i>Scomberoides commersonianus</i>	Talang queenfish
		Narrow-barred Spanish mackerel
218	<i>Scomberomorus commerson</i>	
	<i>Scombridae spp</i>	Scombridae spp
	<i>Scorpaenidae spp</i>	Scorpaenidae spp
219	<i>Scorpaenopsis venosa</i>	Raggy scorpionfish
220	<i>Selaroides leptolepis</i>	Yellowstripe scad
	<i>Serranidae spp</i>	Serranidae spp
221	<i>Siganus argenteus</i>	Streamlined spinefoot
222	<i>Siganus luridus</i>	Dusky spinefoot
223	<i>Siganus spinus</i>	Little spinefoot
224	<i>Siganus stellatus</i>	Brown-spotted spinefoot
225	<i>Siganus sutor</i>	A.W.Rabbitfish
	<i>Soleidae spp</i>	Soleidae spp
226	<i>Sphyraena barracuda</i>	Great barracuda
227	<i>Sphyraena flavicauda</i>	Yellowtail barracuda
228	<i>Sphyraena jello</i>	Pickhandle barracuda
	<i>Sphyraenidae spp</i>	Sphyraenidae spp
229	<i>Stegastes fasciolatus</i>	Pacific gregory
230	<i>Stethojulis albovittata</i>	Bluelined wrasse

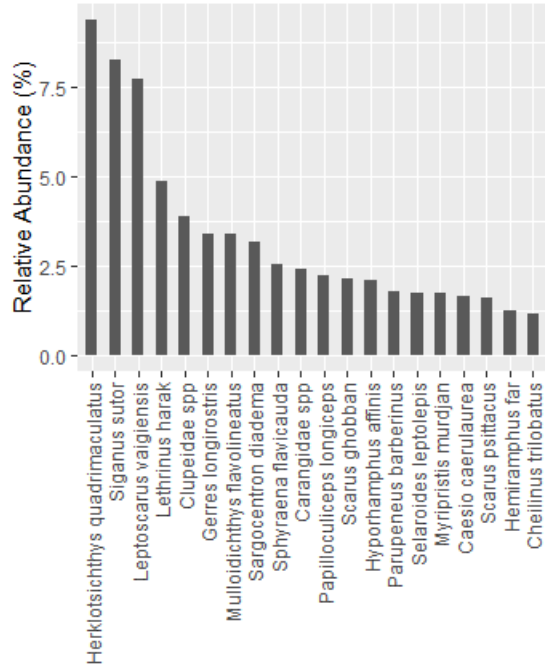
Appendix 4.2 cont. Species and species groups occurring in landings dataset

231	<i>Stethojulis bandanensis</i>	Red shoulder wrasse
232	<i>Stethojulis strigiventer</i>	Three-ribbon wrasse
233	<i>Strongylura incisa</i>	Reef needlfish
234	<i>Sufflamen chrysopterum</i>	Halfmoon triggerfish
235	<i>Sunagocia arenicola</i>	Broadhead flathead
	<i>Synanceiidae spp</i>	Synanceiidae spp
	<i>Synodontidae spp</i>	Synodontidae spp
236	<i>Terapon jarbua</i>	Jarbua terapon
	<i>Tetradontidae spp</i>	Tetradontidae spp
237	<i>Thalassoma hardwicke</i>	Sixbar wrasse
238	<i>Thalassoma hebraicum</i>	Goldbar wrasse
239	<i>Thalassoma lunare</i>	Moon wrasse
240	<i>Thalassoma trilobatum</i>	Christmas wrasse
241	<i>Torpedo sinuspersici</i>	Variable torpedo ray
242	<i>Trachinotus blochii</i>	Snubnose pompano
	<i>Unknown</i>	Mixed spp
243	<i>Upeneus vittatus</i>	Yellowstriped goatfish
244	<i>Variola louti</i>	Yellow-edged lyretail
245	<i>Zanclus cornutus</i>	Moorish idol
246	<i>Zebrasoma desjardini</i>	Indian sail-fin surgeonfish
247	<i>Zebrasoma scopas</i>	Twotone tang
248	<i>Zebrasoma velifer</i>	Sailfin tang

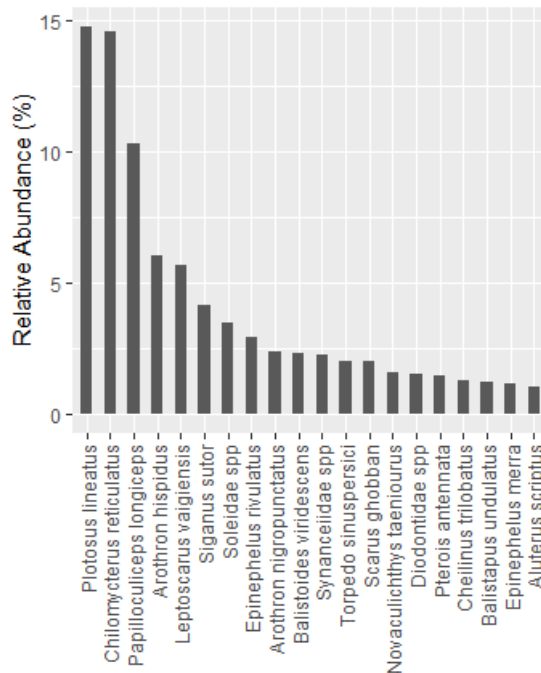
Appendix 4.2 cont. Species and species groups occurring in landings dataset



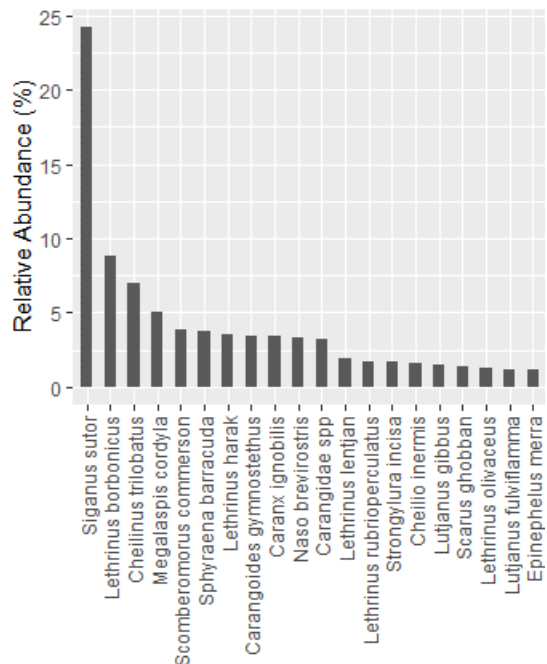
Finfish Species (Boat Seine)



Finfish Species (Gillnet)

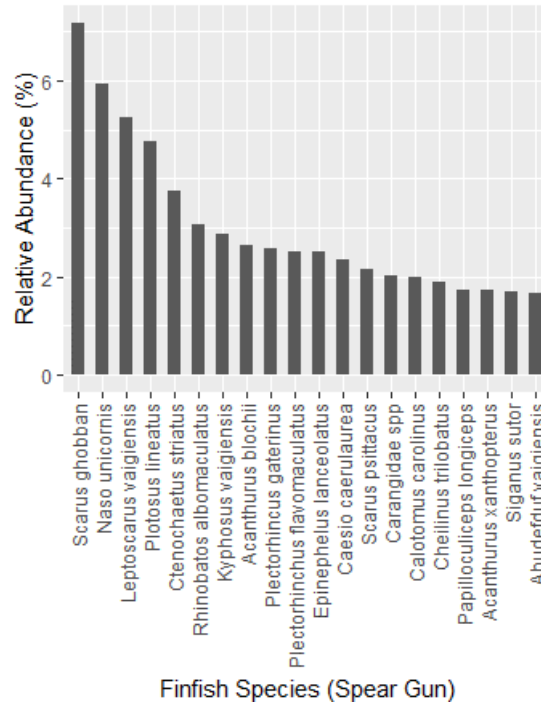


Finfish Species (Harpoon)



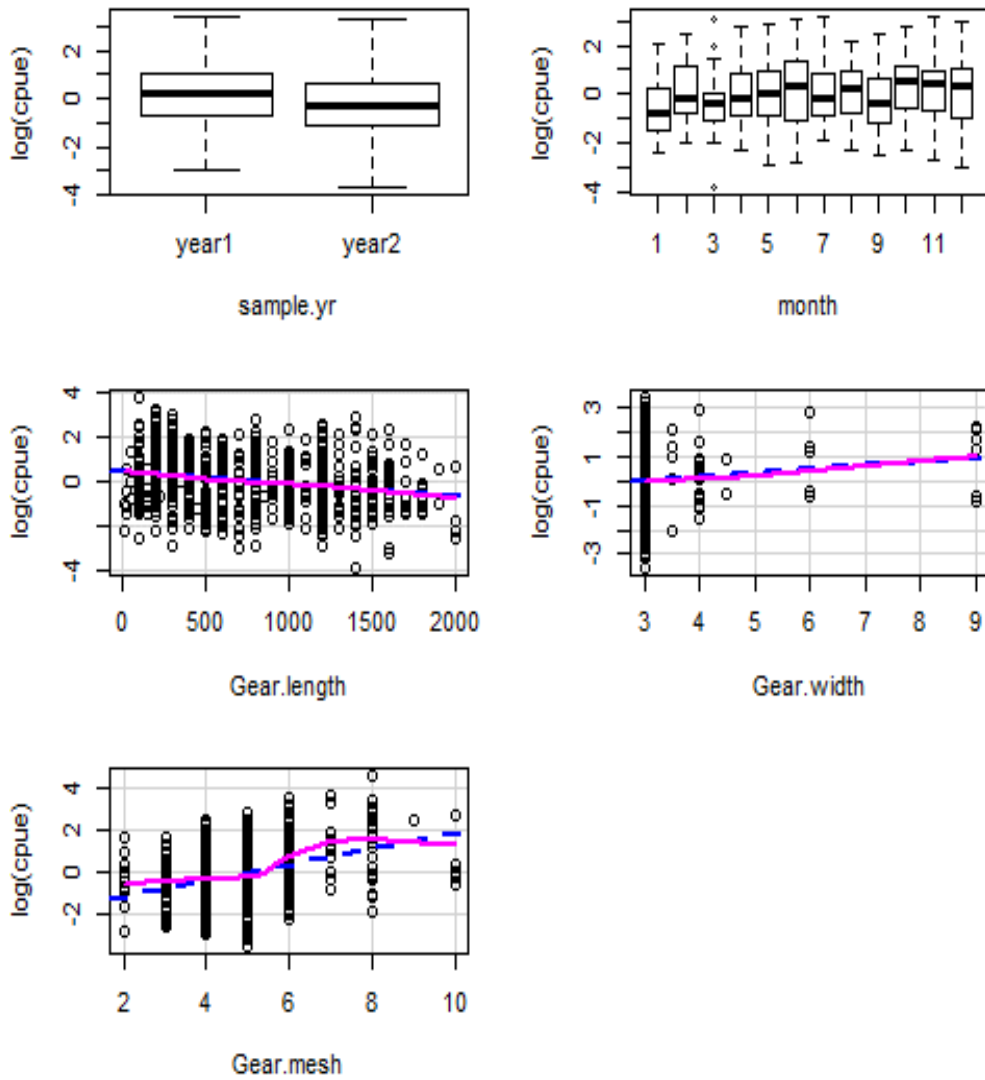
Finfish Species (Hook-Line)

Appendix 4.3. Relative abundance of species by gear type for the 20 most abundant species



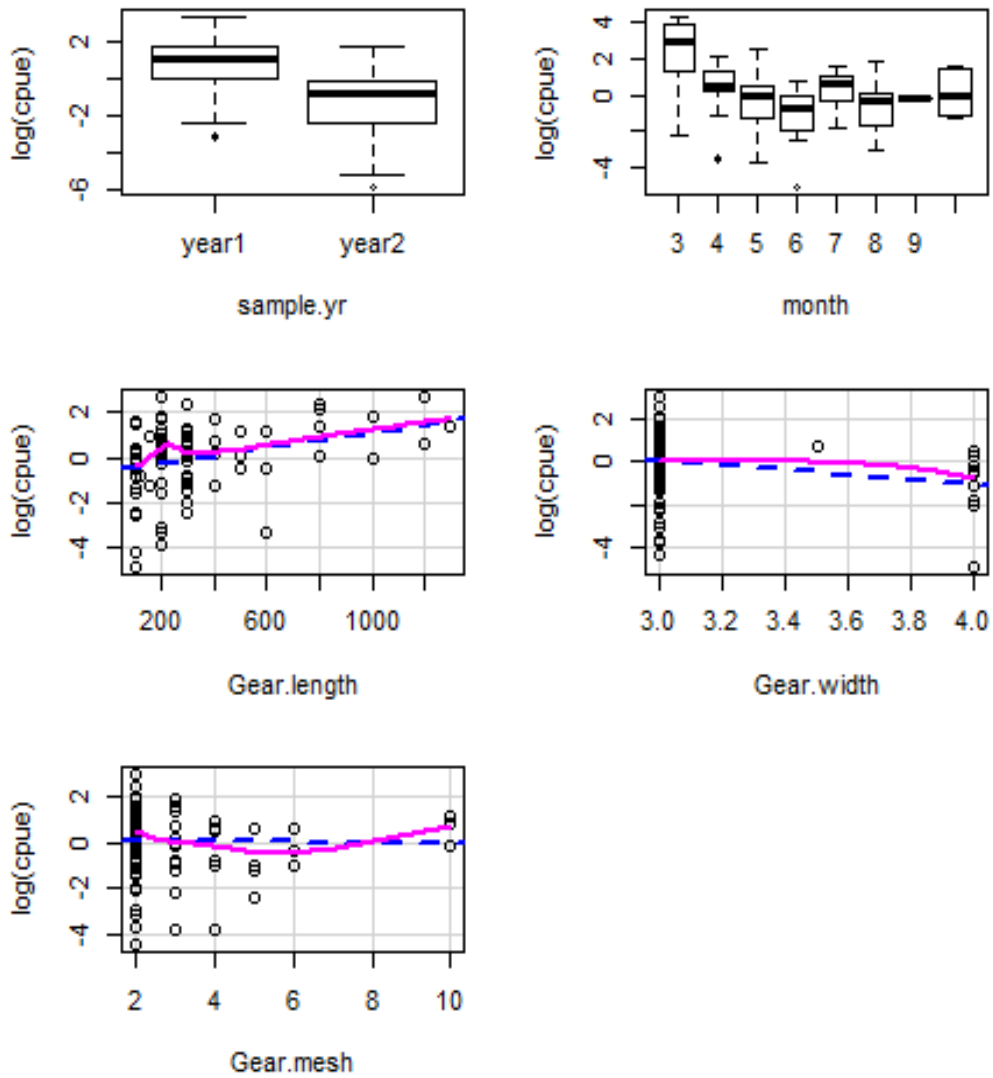
Appendix 4.3 cont. Relative abundance of species by gear type for the 20 most abundant species

Siganus sutor Gillnet Fishery



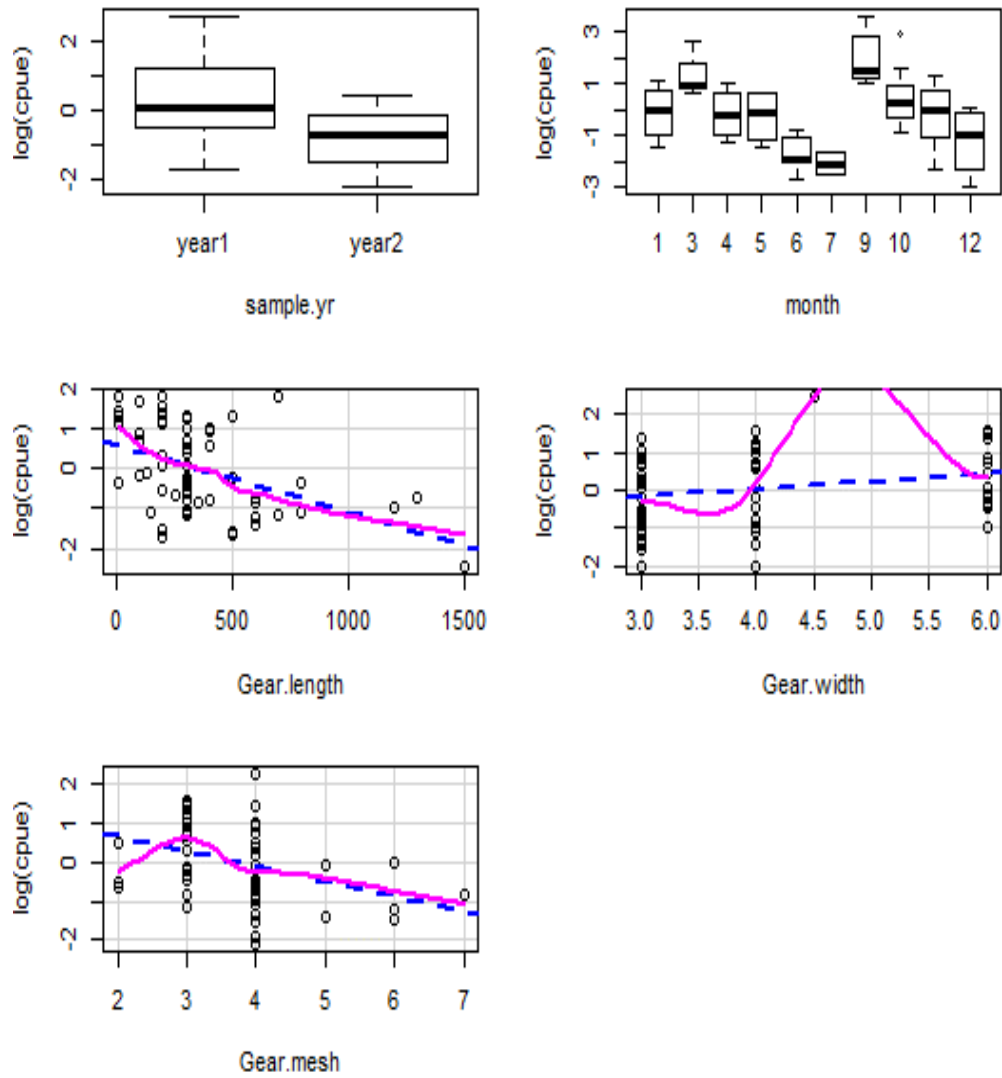
Appendix 4.4. Term plots, component plus residual plots, for GLM model used in the standardization of *S. sutor* after removal of $n=3$ outliers (pseudo- $R^2=0.24$)

Herklotsichthys quadrimaculatus Gillnet Fishery



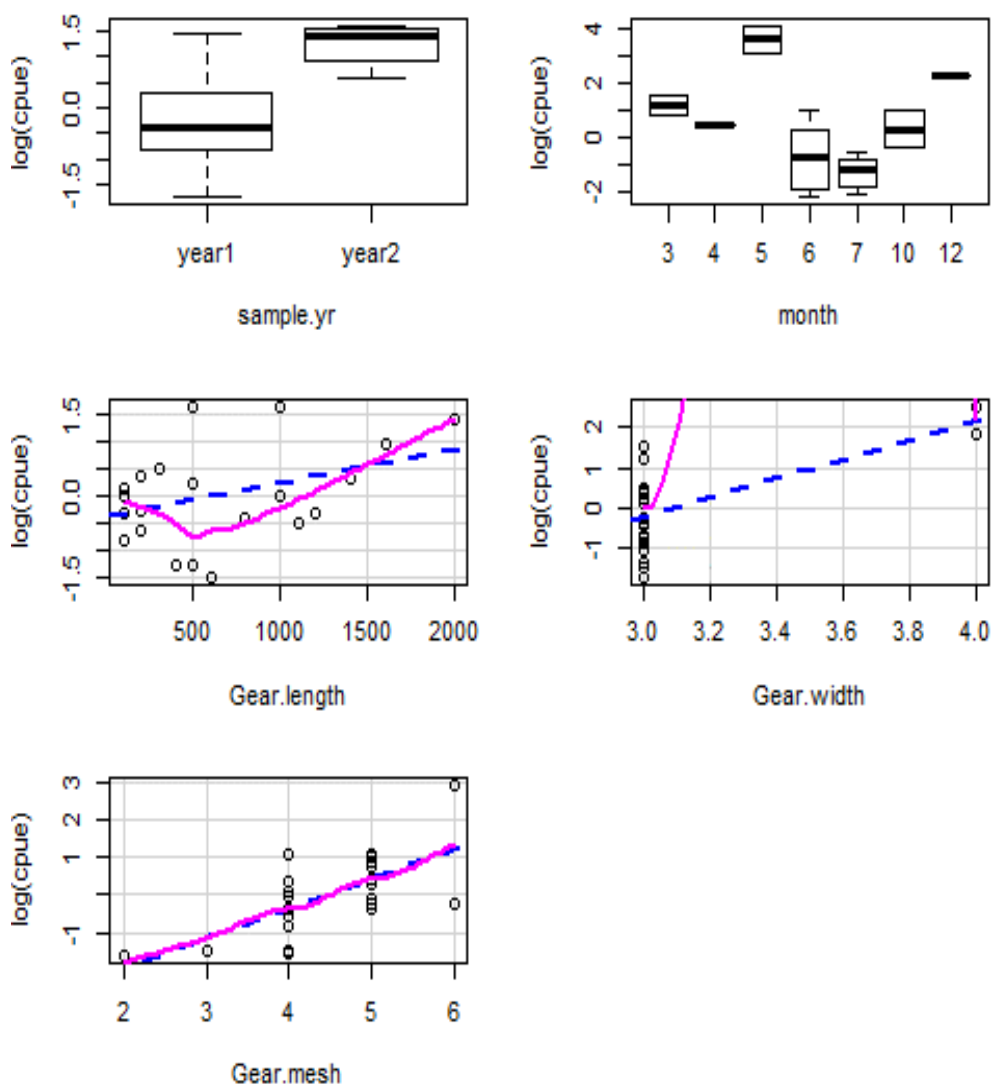
Appendix 4.5. Term plots, component plus residual plots, for GLM model used in the standardization of *H. quadrimaculatus* after removal of $n=4$ outliers (pseudo- $R^2=0.36$)

Clupeidae spp Gillnet Fishery



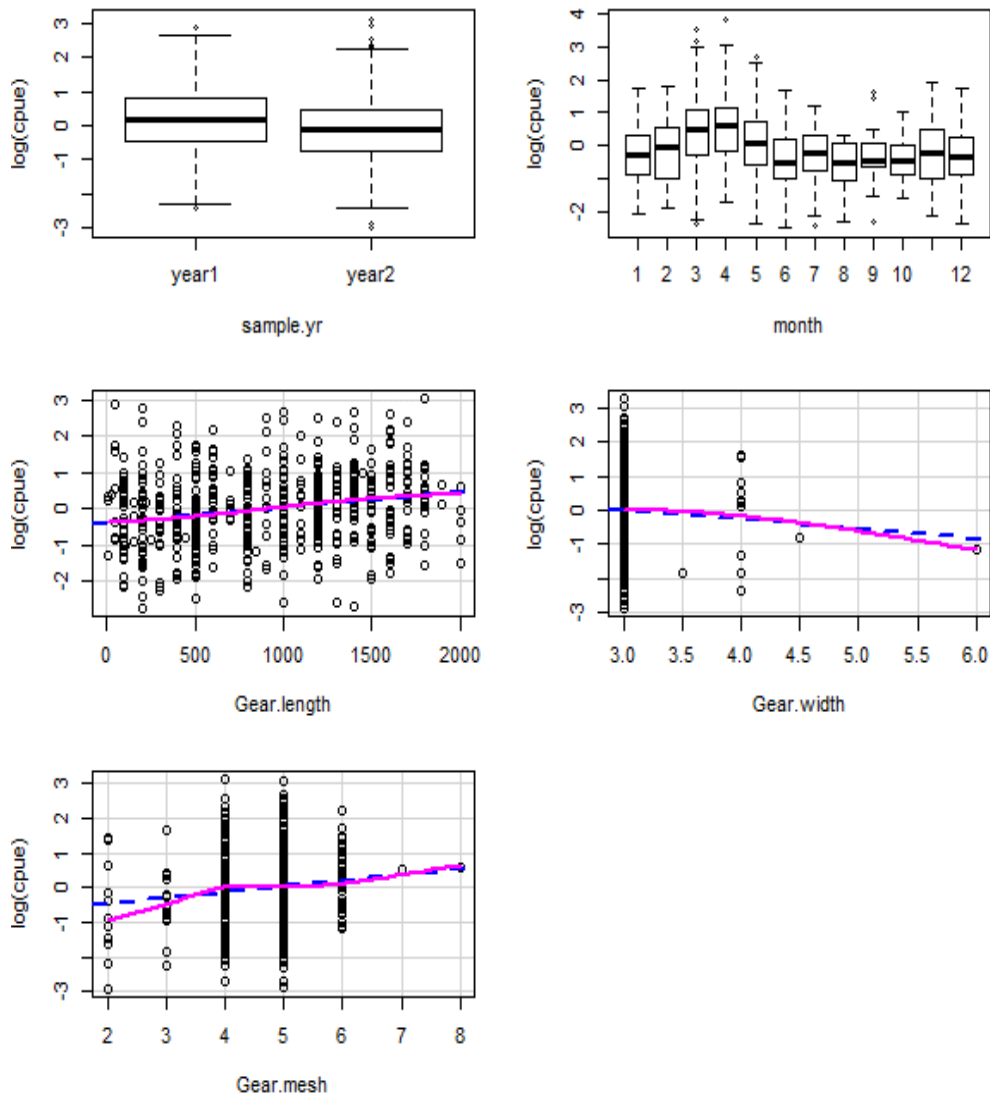
Appendix 4.6. Term plots, component plus residual plots, for GLM model used in the standardization of Clupeidae spp after removal of $n=5$ outliers ($\text{pseudo-R}^2=0.71$)

Plotosus lineatus Gillnet Fishery



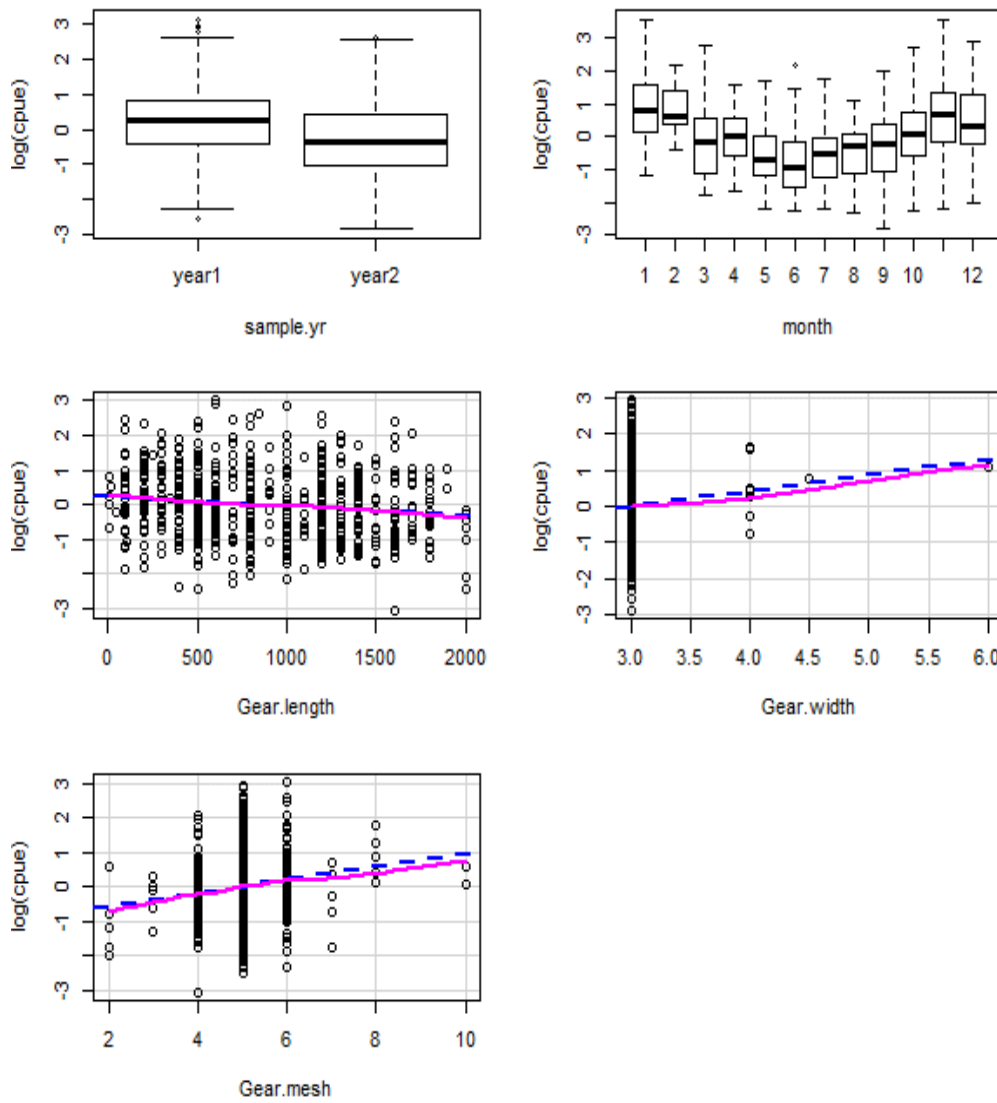
Appendix 4.7. Term plots, component plus residual plots, for GLM model used in the standardization of *P. lineatus* after removal of $n=1$ outlier ($\text{pseudo-R}^2=0.81$)

Leptoscarus vaigiensis Gillnet Fishery



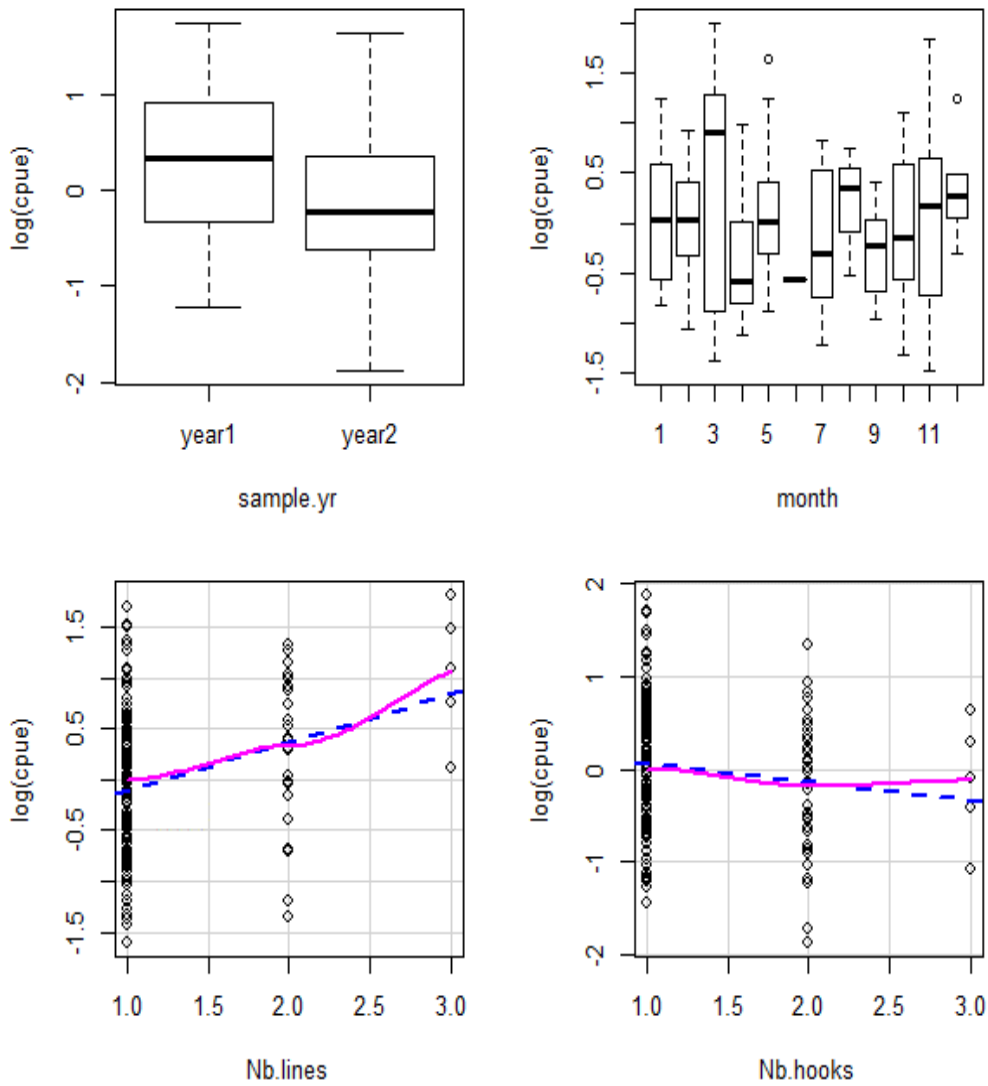
Appendix 4.8. Term plots, component plus residual plots, for GLM model used in the standardization of *L. vaigiensis* after removal of $n=4$ outliers (pseudo- $R^2=0.21$)

Lethrinus harak Gillnet Fishery



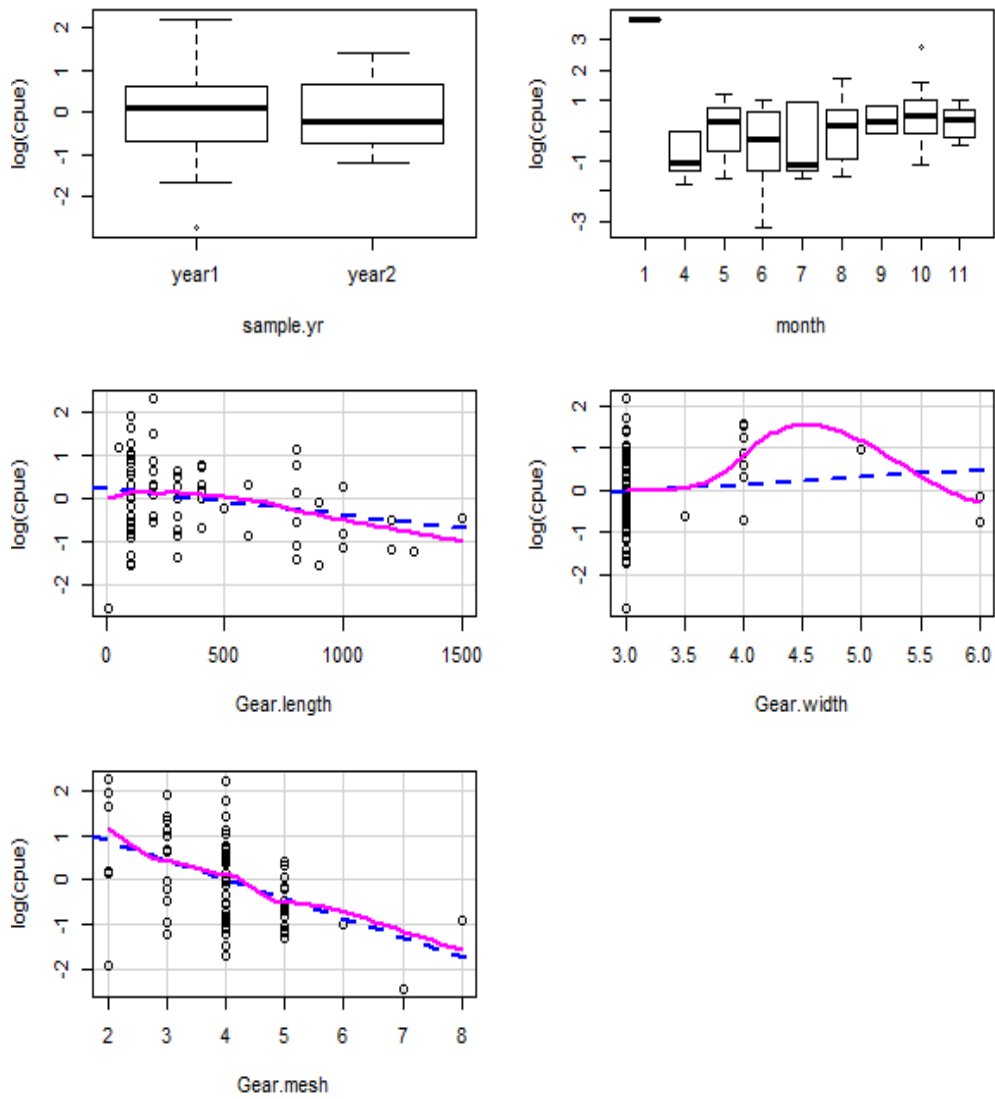
Appendix 4.9. Term plots, component plus residual plots, for GLM model used in the standardization of *L. harak* (gillnet) after removal of $n=6$ outliers (pseudo- $R^2=0.30$)

Lethrinus harak Hook-Line Fishery



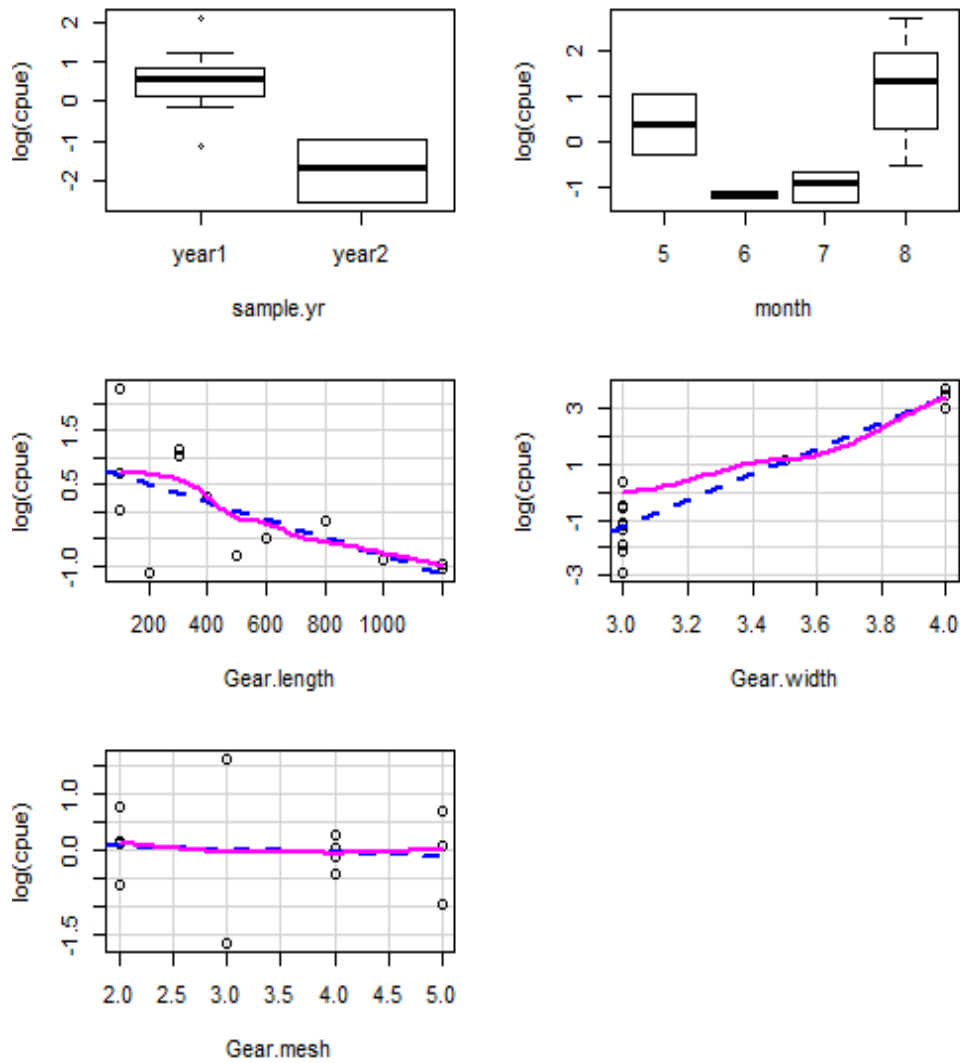
Appendix 4.10. Term plots, component plus residual plots, for GLM model used in the standardization of *L. harak* (hook-line) after removal of $n=4$ outliers (pseudo- $R^2=0.18$)

Caesio caerulea Gillnet Fishery



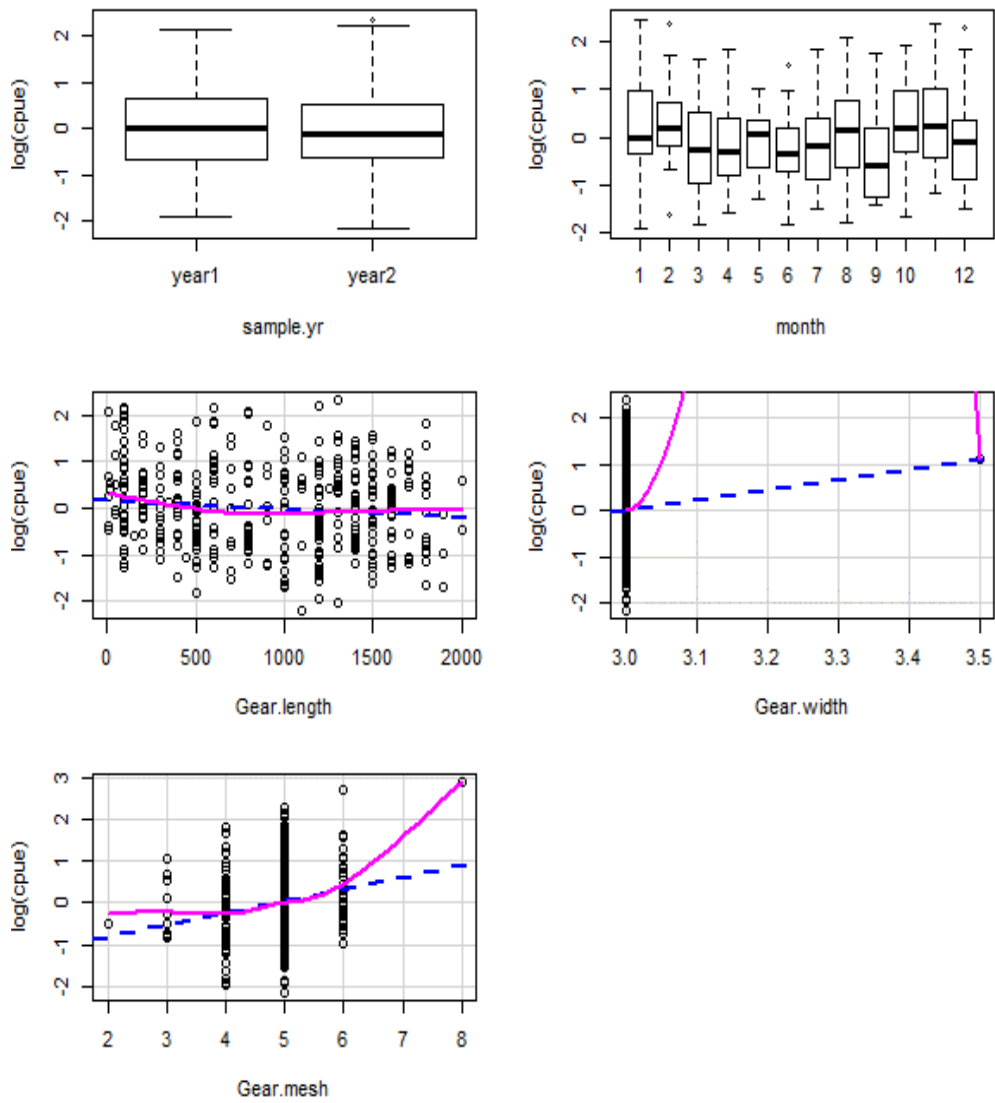
Appendix 4.11. Term plots, component plus residual plots, for GLM model used in the standardization of *C. caerulea* after removal of $n=6$ outliers (pseudo- $R^2=0.44$)

Ostorhinchus cyanosoma Gillnet Fishery



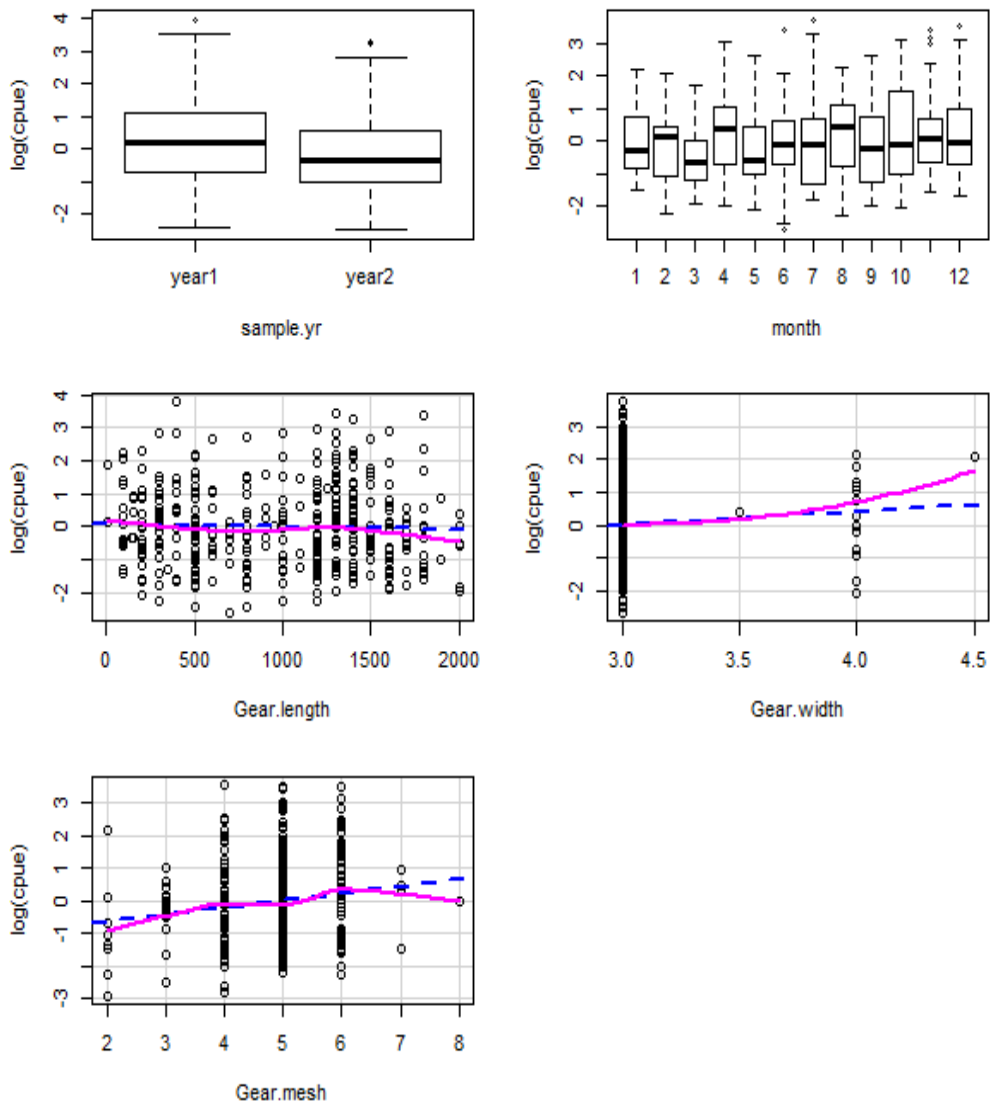
Appendix 4.12. Term plots, component plus residual plots, for GLM model used in the standardization of *S. gobban* after removal of $n=0$ outliers (pseudo- $R^2=0.87$)

Scarus ghobban Gillnet Fishery

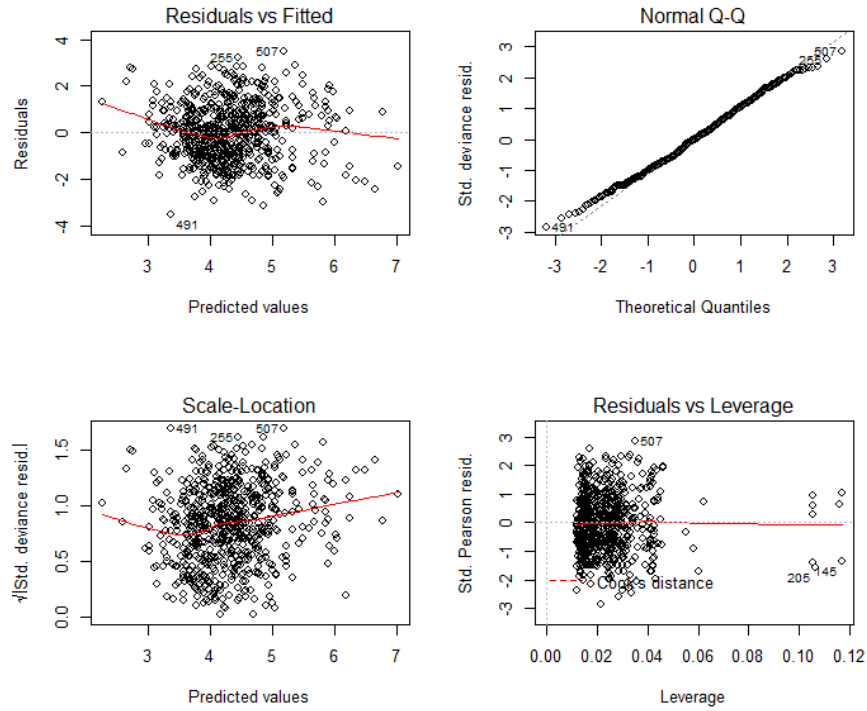


Appendix 4.13. Term plots, component plus residual plots, for GLM model used in the standardization of *S. ghobban* after removal of $n=1$ outlier ($\text{pseudo-}R^2=0.13$)

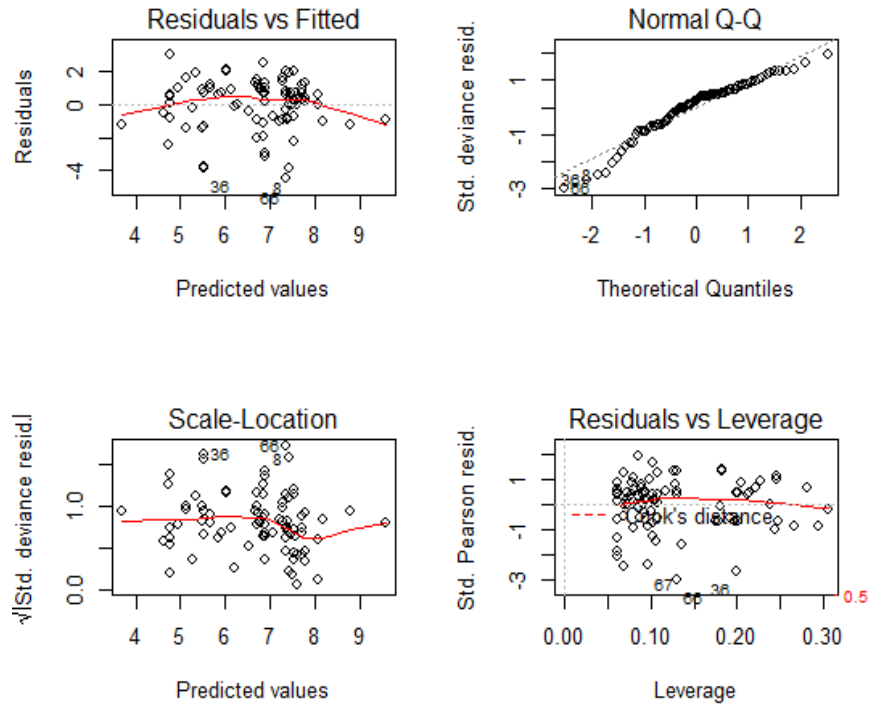
Gerres longirostris Gillnet Fishery



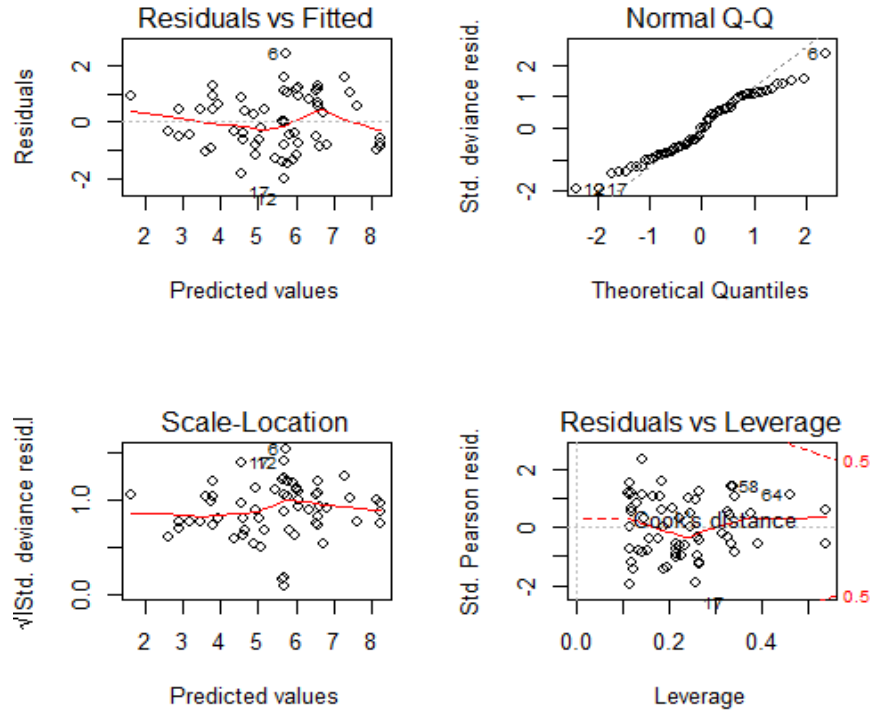
Appendix 4.14. Term plots, component plus residual plots, for GLM model used in the standardization of *G. longirostris* after removal of $n=2$ outliers (pseudo- $R^2=0.10$)



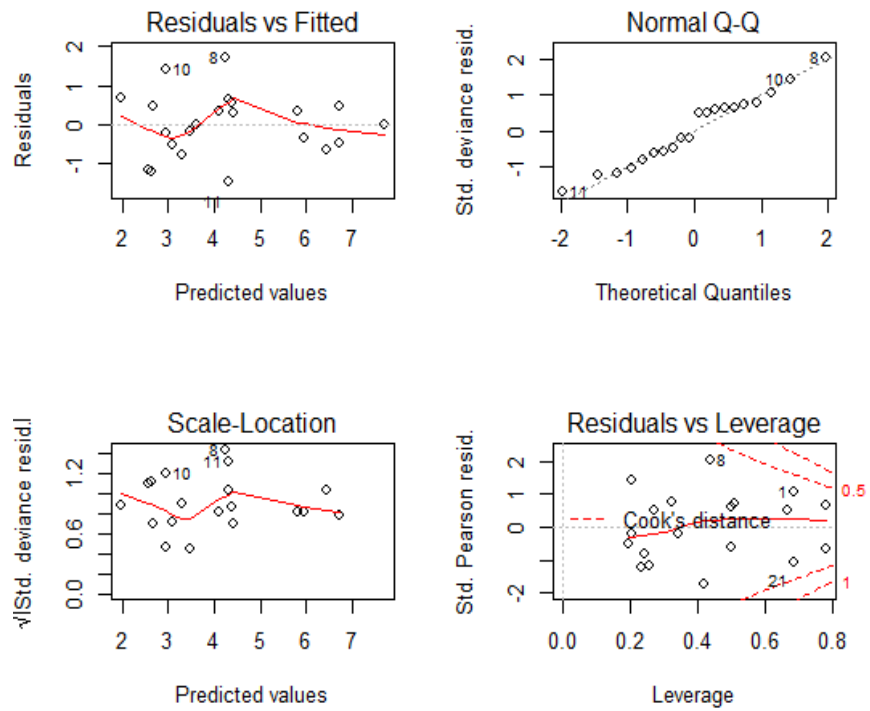
Appendix 4.15. GLM regression diagnostic plots for *S. sutor* CPUE standardization



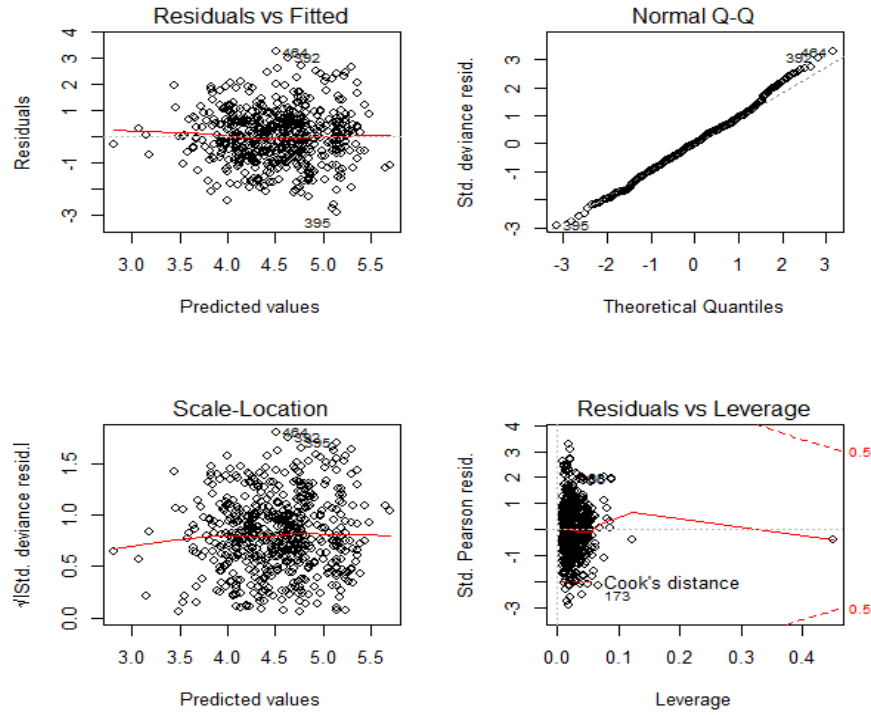
Appendix 4.16. GLM regression diagnostic plots for *H. quadrimaculatus* CPUE standardization



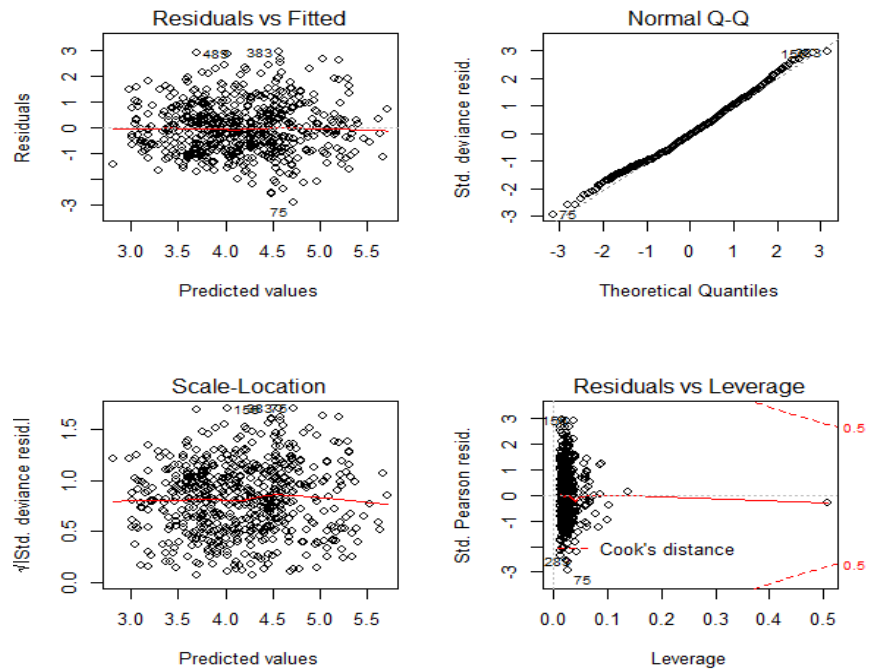
Appendix 4.17. GLM regression diagnostic plots for Clupeidae spp CPUE standardization



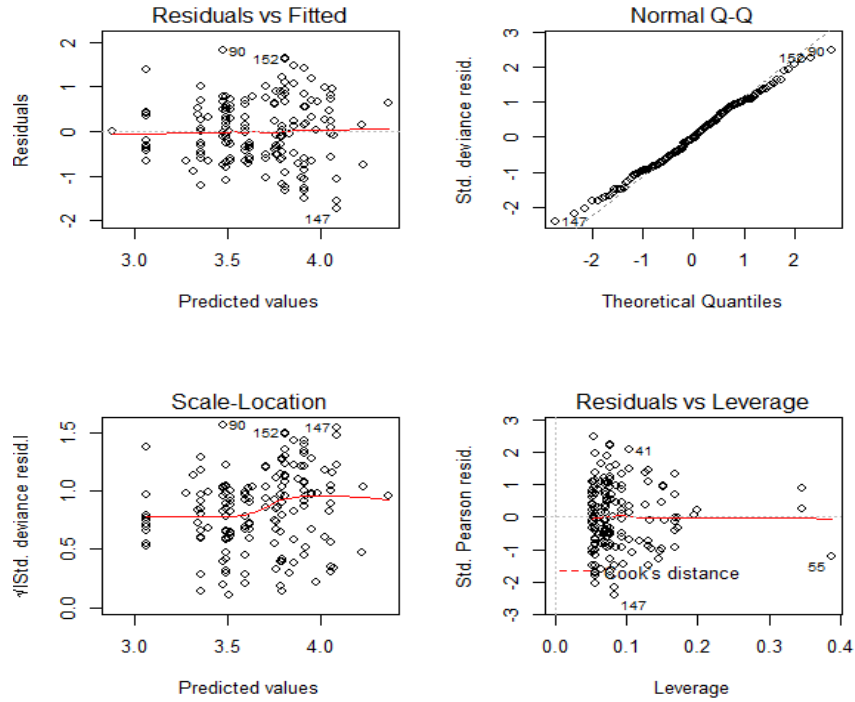
Appendix 4.18. GLM regression diagnostic plots for *P. lineatus* CPUE standardization



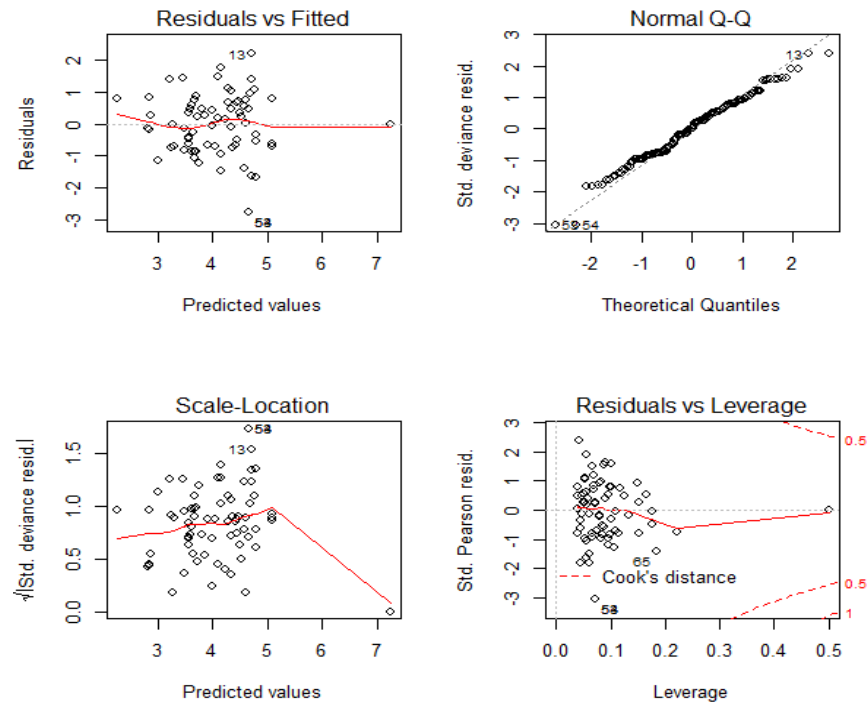
Appendix 4.19. GLM regression diagnostic plots for *L. vaigiensis* CPUE standardization



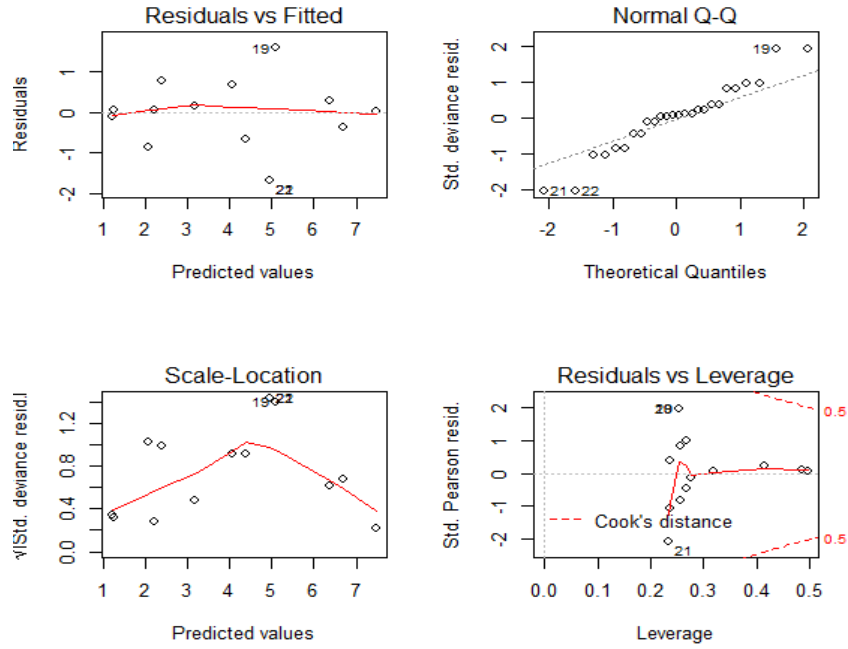
Appendix 4.20. GLM regression diagnostic plots for *L. harak* (gillnet) CPUE standardization



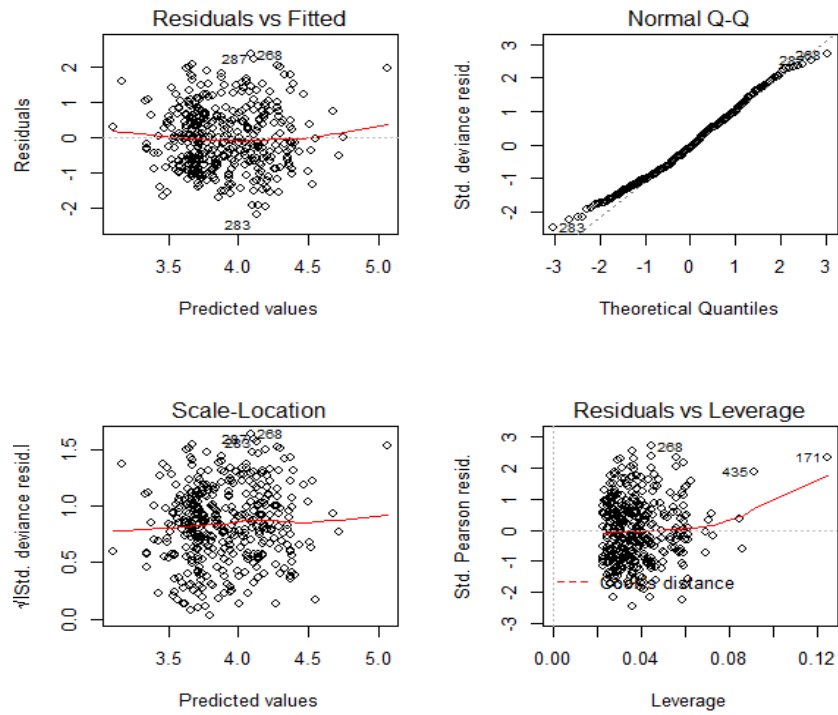
Appendix 4.21. GLM regression diagnostic plots for *L. harak* (hook-line) CPUE standardization



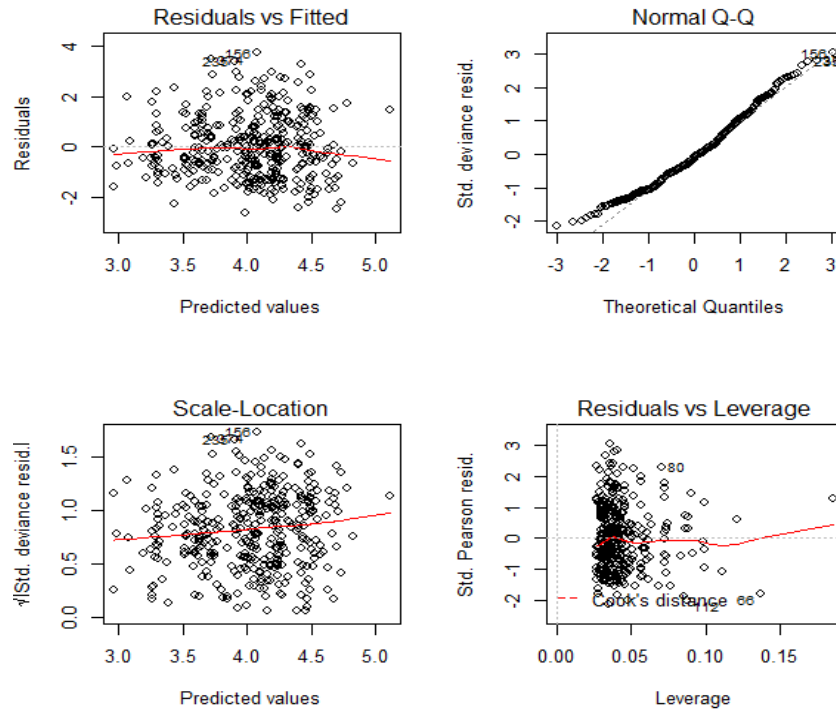
Appendix 4.22. GLM regression diagnostic plots for *C. caerulea* CPUE standardization



Appendix 4.23. GLM regression diagnostic plots for *O. cyanosoma* CPUE standardization



Appendix 4.24. GLM regression diagnostic plots for *S. gobban* CPUE standardization



Appendix 4.25. GLM regression diagnostic plots for *G. longirostris* CPUE standardization



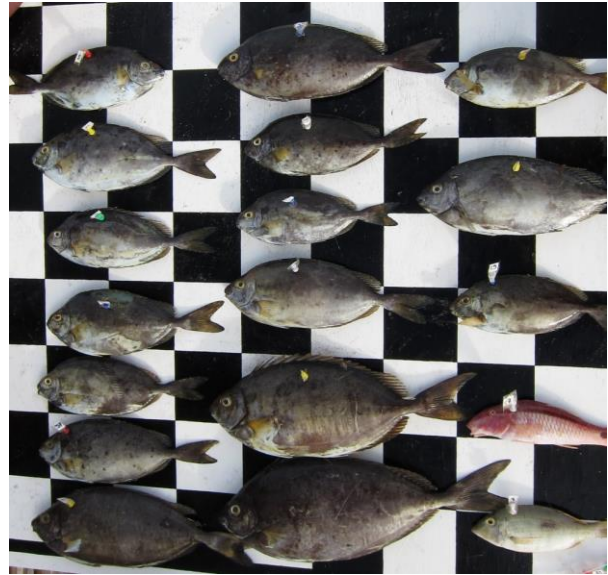
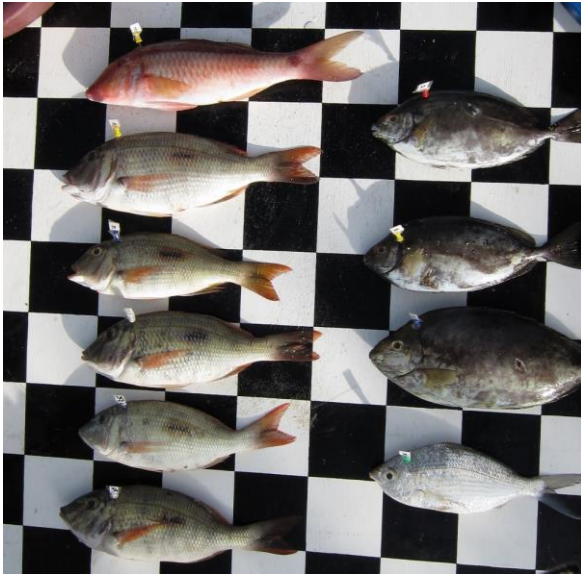
Appendix 4.26. A mixed catch from a seine net haul typically composed of juvenile length classes, and often larval stages; dominant species here are the Three-ribbon wrasse, *Stethojulis strigiventer*, Cigar wrasse, *Cheilio inermis*, and Marbled (seagrass) parrotfish, *Leptoscarus vaigiensis*



Appendix 4.27. Bluestripe herring, *Herklotsichthys quadrimaculatus* November 2011



Appendix 4.28. Examples of complete catches sampled in Ifaty, November 2011, illustrating the range of fish sizes, species diversity, and range of landed biomass (10 cm grid)



Appendix 4.29. Catches sampled in Ifaty between September – December 2012; (top-left) Dash-and-dot goatfish (*Parupeneus barberinus*), thumbprint emperors (*Lethrinus harak*), shoemaker spinfoot (*Siganus sutor*), and strongspine silver-biddy (*Gerres longirostris*) (top-left); same species with *Siganus sutor* dominant in catch (top-right); same species with *Gerres longirostris* and *Lethrinus harak* dominant in catch (bottom-left); *Myripristis spp*, sammara squirrelfish (*Neoniphon sammara*), and crown squirrelfish (*Sargocentron diadema*)



Appendix 4.30. Shoemaker spinefoot (*Siganus sutor*) and brown-spotted spinefoot (*Siganus stellatus*) (top row); ember parrotfish (*Scarus rubroviolaceus*), yellow-edged lyretail (*Variola louti*), giant moray (*Gymnothorax javanicus*) (left middle); green turtle (*Chelonia mydas*) (left bottom); tomato hind (*Cephalopholis sonnerati*) and *Variola louti* (right)



Appendix 4.31. Scalloped hammerhead (*Sphyrna lewini*) (first row); malabar grouper (*Epinephelus malabaricus*) (August 2013) and humphead wrasse (*Cheilinus undulatus*) (September 2013) (second row); stonefish (*Syanecia verrucosa*) (10 cm grid; November 2011), and weedy scorpionfish (*Rhinopias frondosa*) (third row)

Vita



Shane M. Abeare was born in Flint, Michigan, where he obtained his Bachelor of Science in biology, minoring in chemistry, from the University of Michigan. As an undergraduate student, Shane participated in field research with professors in the Amazonian rainforests of Peru, the rainforests of Papua New Guinea, and in Queensland, Australia. He also participated in an NSF-funded Research Experience for Undergraduates (REU) program at Eastern Illinois University.

After graduating, Shane enrolled in the Peace Corps in Togo, West Africa, and thus began the 10-year long chapter of his life spent on the African continent. From West to Central Africa to South Africa, and Madagascar, he worked for the conservation of African wildlife in national parks, and with communities managing local reserves. His interests were, initially, focused on the conservation of terrestrial animals, and after having obtained a Master of Science in African Mammalogy and Conservation at the University of Pretoria, Shane volunteered on a Great White shark research project in South Africa, as his first foray into the realm of marine conservation. Then, shortly thereafter, he accepted a position in the management of a national park in the Republic of Congo.

While working in the Congo, it became apparent that both fish and wildlife conservation were important avenues to pursue in order to provide a holistic approach to the numerous and complex issues of conservation in Africa. After having completed a Master of Science in oceanography, with a minor in statistics, he decided to continue his studies and pursue a PhD at the University of New Orleans, where he would eventually conduct his dissertation research on the artisanal fisheries of the Vezo communities of southwest Madagascar.

Today, Shane is currently employed as the Senior Fisheries Biologist with the Division of Fish and Wildlife in the Commonwealth of the Northern Mariana Islands. Although he is now far from Africa, he does hope to return some day.

